FEW-MODE OPTICAL WAVEGUIDES

AND THEIR STUDY BY THE

FOUR-PHOTON MIXING PROCESS

Stephen John Garth

A thesis submitted for the degree of

Doctor of Philosophy

at the Australian National University

Canberra

February 1987

ERRATA

FEW-MODE OPTICAL WAVEGUIDES AND THEIR STUDY BY THE FOUR-PHOTON MIXING PROCESS

S.J. Garth

1. page 12. Footnote to eqn. (2.14)

   "Eqn. (2.14) is exact, but we note that it was derived by refering th field components to a fixed cartesian coordinate system".

2. page 25. Above eqn. (2.40)

   The relation retween $\ell n\ n^2$ and profile shape should be

   " $\underset{\sim}{\nabla}_t\ \ell n\ n^2 = -\ 2\Delta\ \underset{\sim}{\nabla}_t f$ "

3. page 26. Eqn. (2.42)

   To avoid confusion, ℓ in eqn. (2.42) should be replaced by s, with th following comment:

   "where $ds = \rho\ d\phi$ is an element of arc length of the boundary interface".

4. page 35. Eqn. (2A.3)

   Eqn. (2A.3) should be:

   $$" \left.\frac{y'}{y}\right|_{R=1} = -\frac{W\left(K_{\ell-1}(W) + K_{\ell+1}(W)\right)}{2\ K_\ell(W)}$$

   where the field in the cladding is given by $y = K_\ell(W)$ ".

5. page 43. Addition to last paragraph.

   "(See ref. [7] for a complete discussion of the feasibility of using thi system for local area networks. We are only concerned with dispersic properties in this discussion)."

6. page 44. Eqn. (3.2)

   There should be a minus sign between the 2nd and 3rd terms on the RHS ‹ eqn. (3.2), and the last term should not be there in this approximation.

Declaration

This thesis is an account of research undertaken in the Department of Applied Mathematics within the Research School of Physical Sciences at the Australian National University between February 1983 and March 1986, while I was enrolled for the degree Doctor of Philosophy.

Professor C. Pask supervised the research, but unless specifically disowned, the material presented herein is my own.

None of the work presented here has ever been submitted for any other degree at this or any other institution of learning.

S J Garth

Stephen J. Garth

Publications

[1] S.J. Garth and C. Pask, "Properties of modes on perturbed fibers"
Electron. Letters, 22, pp. 22-28 (1986).

[2] S.J. Garth and C. Pask, "Four-photon mixing and dispersion in single-mode fibers"
Optics Letters, 11, pp. 380-382 (1986).

[3] S.J. Garth, "Modes on a bent optical waveguide"
IEE Proc. Pt. J., (in press)

[4] S.J. Garth, "Birefringence in bent single-mode fibers'
IEEE J. Lightwave Tech., (in press)

[5] S.J. Garth, "Fields in a bent single-mode fiber"
Electron. Letters, (submitted)

Papers in preparation:

[6] C. Pask and S.J. Garth, "Comparison of focal and afocal lens systems in insect eyes"

[7] S.J. Garth, C. Pask and G.E. Rosman, "Four-photon mixing in bent few-mode optical fibers"

[8] S.J. Garth, C. Pask and R.A. Sammut, "Single-mode fibers operating at few-mode wavelengths"

Acknowledgements

Now that the task of writing up this thesis is over I can sit back and get into the really important things in life - such as writing these acknowledgements. They say that a man's worth is the sum of all the people he has known. If so, then over the last four years I have indeed been fortunate.

It's not possible for me to fully express my thanks and gratitude to Colin Pask, except to say no one could have a finer supervisor and friend. Colin has been a constant source of encouragement and guidance. His understanding of, and committment to, research students is without parallel, and he has made my time in a research environment an enjoyable and rewarding experience. I have gained much more than just a degree by my association with Colin.

I owe an enormous debt of gratitude to Barry Ninham, the founding head of the Department. Barry is the driving force behind a dynamic, exciting, and friendly department. He has been a great inspiration to me, and I value his advice and friendship.

The Optics Group at the A.N.U. is a wonderful group to be a part of, with many interesting and diverse personalities. At the top of the tree is Allan Whitenack Snyder, whose frank and witty insights into life, the universe, and optics has always been much appreciated. All the other members of the Department have made my time at the A.N.U. an exciting learning experience. In particular I would like to thank John Love and Adrian Ankiewicz for their willingness to discuss the many problems I approached them with.

For the last year I have been a Teaching Fellow in the Department of Mathematics at the Australian Defence Force Academy. Under Colin's zestful leadership this is a friendly and active Department, and I have enjoyed the year tremendously. I would like to thank Rowland Sammut for many helpful discussions.

I would especially like to thank Gavan Rosman, of the Telecom Research Labs in Melbourne, who introduced me to the problem of four-photon mixing in optical fibers. Later he showed me around the Labs, and allowed me to participate in the re-creation of some of the experimental results that are presented here.

I owe much to my typist, and friend, the lovely Diana. Her dedication, ability and sensational body are without question, and the layout of this thesis is due to her. I thank Julie and Shiu for providing an efficient computer service.

Finally, I'm grateful for financial support from a Commonwealth Post-graduate Research Award, and later a Teaching Fellowship from the University of New South Wales, to undertake this study.

FEW-MODE OPTICAL WAVEGUIDES
and their study by
THE FOUR-PHOTON MIXING PROCESS

The design and use of optical fibers for communications systems or sensing devices requires an understanding of the properties of modal fields. This thesis theoretically examines mode characteristics on optical fibers where the symmetry has been broken, especially in the cases of fibers that are uniformly bent and those that have arbitrary shaped core cross-sections.

In general the higher-order modes of these fibers are strongly affected, as they are dependent on symmetry, and a birefringence in the fundamental mode originates. Corrections to the fields and propagation constants of the unperturbed fiber are found by several perturbation methods. The relation between symmetry and polarization effects is discussed in detail.

In order to examine the modal characteristics of these fibers the theory of stimulated four-photon mixing is employed. This non-linear optics effect generates multiple new output frequencies that are symmetrically shifted above and below the input frequency. The process occurs strongly when it is phase-matched.

A study of the resulting shifts in optical frequencies on few-mode fibers gives information on the symmetry and magnitude of fiber perturbations, and thus the theoretical results are available for confirmation by experiment. Some experimental results that have been performed by other researchers are included.

Four-photon mixing on different single-mode fibers is examined, where material dispersion and fiber design are delicately balanced near the zero-dispersion wavelength. Frequency shifts reveal information about the total dispersion properties of the fiber. Singly-clad and doubly-clad profiles are studied.

Notes on Text

References are labelled within each Chapter by square brackets, i.e. [12]. A list of references is found at the end of each Chapter. Back-references to past Chapters are given by:

See ref. [3-9].

This means see reference [9] of Chapter 3.

Equations are labelled within each Chapter by Chapter and equation numbers, i.e., (6.21) refers to Chapter 6. Equations in the Appendicies are labelled as, for example, (5A.10) meaning the Appendix of Chapter 5. Good luck.

CONTENTS

CHAPTER 1

INTRODUCTION

Optical fibers are used extensively for long- and short-range communication systems, as well as in high-sensitivity measuring devices. In order to fully utilize the potential of such systems one needs to determine and understand the fiber characteristics. This thesis theoretically examines changes to the electromagnetic fields when the fiber is perturbed from the ideal case, and examines the use of a non-linear optics process in order to measure such changes.

We are principally concerned with few-mode optical fibers that are perturbed by (i) uniform bending, and (ii) a non-circular core cross-section. The perturbations can be measured by the stimulated four-photon mixing process, a non-linear effect that reveals information about not only waveguide characteristics, but material characteristics as well. The fiber material properties are very important in the design and application of single-mode fibers for long distance communication systems.

Chapter 2 lays the foundations of few-mode optical waveguide theory, as well as introducing the notation. The "weakly-guiding" approximation is used as a basis for the theoretical description of fiber characteristics, and the conceptual premise of this approximation is discussed. The modal properties of the three different waveguide profiles that are used throughout is presented, as well as a review of the Gaussian approximation, which is used to simplify the description of the modal fields.

In Chapter 3 the dispersion properties of glass fiber waveguides ~~is~~ are examined. The ~~dispersion~~ dispersion consists of material and waveguide contributions, and ~~describes~~ causes pulse spreading due to the modal characteristics as well as the dependence of the refractive index on wavelength. Curves that describe the group delay and chromatic dispersion are presented for the different profiles.

A very important design consideration for single-mode fibers is the zero-dispersion wavelength, where material and waveguide contributions to the dispersion cancel. The design and application of fibers operating at this wavelength is discussed. The practical implications of operating such a fiber at lower wavelengths than they are designed for is investigated.

In Chapter 4 the stimulated four-photon mixing process in optical fibers is reviewed. This non-linear optics effect generates multiple new frequencies at the output of the fiber. These new frequencies are symmetrically shifted below and above the input (or pump) frequency. The process occurs strongly when it is phase-matched.

Chapter 5 deals with this phase-matched condition, and it is shown that the resulting frequency shift reveals information on the material and modal properties of few-mode fibers. Phase-matching on single-mode fibers offers a way to examine the total dispersion characteristics of the fiber.

Chapter 6 examines the modal characteristics on fibers that are perturbed by having a non-circular core cross-section. In this case the symmetry of the waveguide is broken. In general the higher-order modes of these fibers are strongly affected, as they are dependent on symmetry, and a birefringence originates in the fundamental mode. The relation between symmetry and polarization effects is discussed in detail. A study of frequency shifts on these fibers gives information on the symmetry and magnitude of the perturbations.

Profiles that are perturbed by having a depressed refractive index profile (or dip) are also examined. In this case the symmetry is not broken but modal characteristics, such as group delay, are strongly affected. We use the theory of four-photon mixing to study these changes, and compare our results to experimental data.

Chapter 7 examines the modal characteristics on waveguides that are uniformly bent. This form of perturbation also breaks the degeneracy of the higher-order modes and creates a birefringence between the orthogonally polarized fundamental modes. By using the theory of four-photon mixing the theoretical prediction of mode splitting is confirmed by experimental results.

Chapter 8 attempts to simplify the description of mode propagation on bent fibers by using the Gaussian approximation for modal fields. The simple forms of the approximation also allow an investigation of the perturbation theory used to analyse bends. Finally, experimental results showing the shift of the peak intensity of the electric field due to the bend, in regions where the usual perturbation theory breaks down, are explained.

CHAPTER 2

PROPERTIES OF FEW MODE OPTICAL WAVEGUIDES

CHAPTER 2

FEW-MODE OPTICAL WAVEGUIDES

1. Introduction

In this chapter we lay the foundations of the waveguide theory that will be used throughout this work. While parts of this chapter ~~is~~ are essentially a review of standard theory (see reference [1]), we present some results which are not available elsewhere.

Throughout this work we are concerned with three types of waveguide structures; (1) the basic singly-clad step-index (or rectangular-profile) fiber; (2) the singly-clad power-law profile fiber; and (3) the doubly-clad (W-type) step-index fiber. These three profiles are shown in Figure 2.2.

We begin at the beginning: Maxwell's equations and the homogeneous vector wave equations. We then invoke an approximation to solve the wave equations. This approximation, called the "weakly-guiding limit", is the basis of the theoretical analysis of waveguides presented here, and is related to the polarization properties of the waveguide. The details and significance of this approximation are discussed.

In general polarization effects can be ignored, but when dealing with birefringence problems one must take into account the fact that light is polarized in two orthogonal directions, and the "weakly-guiding" approximation is no longer sufficient to describe the mode characteristics. We present a perturbation theory which, when added to the "weakly-guiding" waveguide solutions, gives a complete description of the modes of an optical fiber.

We then present the mode characteristics of the three fiber models we are investigating. We write down the solution to the wave equation, called the modal field, for the solvable cases and detail the numerical solution for the other cases. We present curves which give the eigenvalue and cut-off characteristics of the respective waveguide structures.

We then examine the polarization corrections in more detail, and as an example consider the singly-clad step-profile fiber. We show how the vector fields can be constructed from the scalar fields, and how these corrections describe the polarization properties of the fiber.

In the next section we show how approximations to the "weakly-guiding" waveguide solutions can be made by making use of the fact that the fundamental mode field is Gaussian in shape. Simple analytic solutions result for many waveguide parameters, and the approximation can be extended to describe higher-order modes as well. We examine and discuss the accuracy of the Gaussian approximation in relation to the mode characteristics we will be concerned with.

Finally, we present an outline of useful numerical procedures that are used throughout this work.

2. Basic Theory

(a) The Vector Wave Equation

In this section we quickly review the fundamental equations for an electromagnetic analysis of optical waveguides. Maxwell's equations in non-magnetic, homogeneous and isotropic source-free media are [2]

$$\begin{aligned} \underset{\sim}{\nabla} \times \underset{\sim}{E} + \mu_0\, \partial \underset{\sim}{H}/\partial t &= 0 \\ \underset{\sim}{\nabla} \times \underset{\sim}{H} - \partial \underset{\sim}{D}/\partial t &= 0 \\ \underset{\sim}{\nabla} \cdot \underset{\sim}{D} &= 0 \\ \underset{\sim}{\nabla} \cdot \underset{\sim}{H} &= 0 \end{aligned} \tag{2.1}$$

where $\underset{\sim}{E}$ and $\underset{\sim}{H}$ are the electric and magnetic fields, respectively, μ_0 is the free-space permeability, and the electric displacement, $\underset{\sim}{D}$, is related to the electric field by

$$\underset{\sim}{D} = \varepsilon_0\, \underset{\sim}{E} + \underset{\sim}{P} \tag{2.2}$$

ε_0 is the free-space dielectric constant and $\underset{\sim}{P}$ is the electric polarization, which in linear media is given by

$$\underset{\sim}{P} = \varepsilon_0\, \chi\, \underset{\sim}{E} \tag{2.3}$$

where χ is the electric suscept~~a~~ibility ~~tensor.~~ scalar Combining eqns.(2.2) and (2.3) we have

$$\underset{\sim}{D} = \varepsilon_0\, n^2\, \underset{\sim}{E} \tag{2.4}$$

where the refractive index n(x,y,z) is related to the susceptability tensor χ by

$$n(x,y,z) = (1 + \chi)^{1/2} \tag{2.5}$$

We shall be concerned with electric and magnetic fields that have an implicit time dependence $\exp(-i\omega t)$, so that the time derivatives of eqn.(2.1) can be replaced by factors of $i\omega = ikc$, where $c = (\varepsilon_0 \mu_0)^{-1/2}$ is the speed of light in free space and

$$k = 2\pi/\lambda \tag{2.6}$$

is the free space wavenumber, where λ is the wavelength of light in free space.

If we eliminate either the electric or magnetic fields from eqns. (2.1) we obtain, with the use of eqn.(2.4), the homogeneous vector wave equations;

$$\{\underset{\sim}{\nabla}^2 + n^2k^2\} \underset{\sim}{E} = -\underset{\sim}{\nabla}(\underset{\sim}{E} \cdot \underset{\sim}{\nabla} \ln n^2) \tag{2.7a}$$

$$\{\underset{\sim}{\nabla}^2 + n^2k^2\} \underset{\sim}{H} = (\underset{\sim}{\nabla} \times \underset{\sim}{H}) \times \underset{\sim}{\nabla} \ln n^2 \tag{2.7b}$$

If the refractive index profile does not vary with longitudinal distance z along the waveguide, so that $n = n(x,y)$, then the electric and magnetic fields can be expressed in the separable form

$$\underset{\sim}{E} = (\underset{\sim}{e}_t + e_z \hat{\underset{\sim}{z}}) \exp(i\beta z) \tag{2.8a}$$

$$\underset{\sim}{H} = (\underset{\sim}{h}_t + h_z \hat{\underset{\sim}{z}}) \exp(i\beta z) \tag{2.8b}$$

where β is called the propagation constant, $\hat{\underset{\sim}{z}}$ is the unit vector parallel to the waveguide axis, and subscripts t and z denote the transverse and longitudinal field components. By substituting eqn. (2.8) into eqn. (2.1), and comparing longitudinal and transverse field components, relationships between the field components $\underset{\sim}{e}_t$, e_z, $\underset{\sim}{h}_t$ and h_z are obtained.

The operator $\underset{\sim}{\nabla}^2$ in eqn. (2.7) is a vector operator, and couples the field components in an arbitrary coordinate system, as we shall see in Chapter 7, when we deal with bent optical fibers. However, if the field components are specified relative to fixed cartesian coordinates, ie.,

$$\begin{aligned} \underset{\sim}{e}_t &= e_x \, \hat{\underset{\sim}{x}} + e_y \, \hat{\underset{\sim}{y}} \\ \underset{\sim}{h}_t &= h_x \, \hat{\underset{\sim}{x}} + h_y \, \hat{\underset{\sim}{y}} \end{aligned} \tag{2.9}$$

then this coupling does not occur and the vector operation is replaced by the scalar Laplacian ∇^2 .

Substituting eqn. (2.8) into eqn. (2.7), separating longitudinal and transverse components, then we have the vector wave equation of the transverse electric field [1]

$$\{\nabla_t^2 + n^2k^2 - \beta^2\} \, \underset{\sim}{e}_t = - \underset{\sim}{\nabla}_t\left(\underset{\sim}{e}_t \cdot \underset{\sim}{\nabla}_t \, \ell n \, n^2\right) \tag{2.10}$$

where $\underset{\sim}{e}_t$ are defined by eqn. (2.9), $n = n(x,y)$ and

$$\underset{\sim}{\nabla}_t f = \hat{\underset{\sim}{x}} \frac{\partial f}{\partial x} + \hat{\underset{\sim}{y}} \frac{\partial f}{\partial y}$$

$$\nabla_t^2 f = \frac{\partial^2 f}{\partial x^2} + \frac{\partial^2 f}{\partial y^2}$$

(b) Polarization Properties

There are few exact solutions to eqn. (2.10), and so we must use approximation methods to obtain the field and propagation ~~propagtion~~ constant. The term on the right-side of eqn. (2.10) is called the vector correction term, and describes the polarization properties of the electric field. This correction term is due to the fact that the refractive index varies over the cross-section of the fiber.

In an infinite medium of constant refractive index the electric field would be a plane wave whose initial polarization state would be maintained as it propagates through the medium. The vector correction term changes the electric field so that its polarization state rotates as it propagates along the fiber.

The "weakly-guiding" approximation makes use of the fact that the difference between the refractive index of the core and cladding regions is negligibly small, so that the vector correction term in eqn. (2.10) can be neglected ~~set equal to zero~~ [3,4]. In other words, if the refractive indicies are nearly equal, the slight boundary difference maintains total internal reflection, so light is still guided by the waveguide, but the medium is virtually homogeneous as far as polarization effects are concerned, and the wave is essentially plane polarized. The modes are said to be "linearly-polarized" [4].

If we set the vector-correction term in eqn. (2.10) to zero then we obtain the scalar wave equation [5,6]

$$\left\{\nabla_t^2 + n^2k^2 - \bar{\beta}^2\right\} \bar{\underset{\sim}{e}}_t = 0 \qquad (2.11)$$

where the bar on the propagation constant and field components signifies that these are not the exact $\underset{\sim}{e}_t$ and β that are solutions of the vector wave equation (2.10). ~~If $\bar{e}_t$ is expressed in cartesian coordinates then~~ e_t can be polarized along any arbitrary set of orthogonal axes.

The range of bound mode propagation constants is $kn_{c\ell} < \bar{\beta} < kn_{co}$ where n_{co} and $n_{c\ell}$ are the maximum values of the refractive index in the core and cladding respectively. Thus the variation of $\bar{\beta}$ on weakly-guiding waveguides is very narrow and we set

$$\bar{\beta} \simeq kn_{co} \simeq kn_{c\ell} \tag{2.12}$$

By knowing only $\underset{\sim}{e}_t$ the modal fields are fully specified. The waves are very nearly plane waves and $e_z \simeq 0$, $h_z \simeq 0$.

The scalar wave equation (2.11) will be the basis of our theoretical analysis of mode properties in this work, and later we will see that this equation will be sufficient to describe the higher-order modes of perturbed optical fibers. A solution of the scalar wave equation represents a modal field whose intial state of polarization is maintained over the entire length of the fiber. However, in general polarization properties are important, and describe how the polarization state changes as the mode propagates through the fiber. In particular, we shall see in Capters 6 and 7 that these polarization effects are essential to describe birefringence phenomena. These effects can be included by adding a correction term to the scalar propagation constant [7,8]. The proper modal fields are then given by the scalar solution plus correction term.

We use a standard perturbation technique [7] to derive the difference between the scalar propagation constant $\bar{\beta}$, and the exact propagation constant β given by the vector wave equation. If we dot multiply eqn. (2.10) by $\bar{\underset{\sim}{e}}_t$, and dot multiply eqn. (2.11) by $\underset{\sim}{e}_t$, subtract and integrate over the infinite cross-section A_∞ we obtain

$$\beta^2 - \bar{\beta}^2 = \int_{A_\infty} \bar{\underset{\sim}{e}}_t \cdot \underset{\sim}{\nabla}_t \{\underset{\sim}{e}_t \cdot \nabla_t \ln n^2\} \, dA / \int_{A_\infty} \bar{\underset{\sim}{e}}_t \cdot \underset{\sim}{e}_t \, dA \tag{2.13}$$

The terms involving ∇_t^2 vanish, as we can transform the area integral over these terms into a line integral using Green's theorem:

$$\int_{A_\infty} (\bar{\underset{\sim}{e}}_t \cdot \nabla_t^2 \underset{\sim}{e}_t - \underset{\sim}{e}_t \cdot \nabla_t^2 \bar{\underset{\sim}{e}}_t) \, dA$$

$$= \oint_{\ell_\infty} \{\bar{\underset{\sim}{e}}_t \underset{\sim}{\nabla}_t \cdot \underset{\sim}{e}_t - \underset{\sim}{e}_t \underset{\sim}{\nabla}_t \cdot \bar{\underset{\sim}{e}}_t\} \cdot \hat{\underset{\sim}{n}} \, d\ell$$

where ℓ_∞ is the perimeter of A_∞ and $\hat{\underset{\sim}{n}}$ is the unit outward normal on ℓ_∞ in the plane of A_∞ . Because the fields of bound modes and their derivatives decay exponentially to zero at large distances from the waveguide the line integral vanishes.

Using the vector identity

$$\underset{\sim}{\nabla}_t \cdot (f \underset{\sim}{A}_t) = f \underset{\sim}{\nabla}_t \cdot \underset{\sim}{A}_t + \underset{\sim}{A}_t \cdot \underset{\sim}{\nabla}_t f$$

and noting that the area integral over $f \underset{\sim}{\nabla}_t \cdot \underset{\sim}{e}_t$ can be transformed into a line integral, which will vanish, the integrand in the numerator of eqn. (2.13) can be re-written and we obtain

$$\beta^2 - \bar{\beta}^2 = - \int_{A_\infty} (\underset{\sim}{\nabla}_t \cdot \bar{\underset{\sim}{e}}_t) \underset{\sim}{e}_t \cdot \underset{\sim}{\nabla}_t \ln n^2 \, dA / \int_{A_\infty} \bar{\underset{\sim}{e}}_t \cdot \underset{\sim}{e}_t \, dA \tag{2.14}$$

We use this equation to show the vector corrections for the modes of a singly-clad step-profile fiber in Section 2-4.

(c) Modal Parameters

We now introduce the normalized parameters that we will use throughout this work. The normalized frequency is

$$V = k\rho\, n_{co}(2\Delta)^{1/2} \tag{2.15}$$

where $k = 2\pi/\lambda$, ρ is the fiber radius (or half-width of a rectangular guide) and the profile-height is defined to be

$$\begin{aligned} \Delta &= \frac{1}{2}\left(1 - n_{c\ell}^2/n_{co}^2\right) \\ &\simeq \left(n_{co} - n_{c\ell}\right)/n_{co} \end{aligned} \tag{2.16}$$

Following our discussion in the previous section, the "weakly-guiding" approximation may be described as the $\Delta \to 0$ limit [4]. Throughout this work we assume that the refractive index in the cladding is a constant and extends to infinity, and the variation of refractive index in the core is given by

$$n^2(x,y) = n_{co}^2(1 - 2\Delta\ f) \tag{2.17}$$

where f describes the shape of the profile.

The normalized eigenvalues are defined to be [1]

$$U^2 = \rho^2\left(k^2 n_{co}^2 - \bar{\beta}^2\right) \tag{2.18a}$$

$$W^2 = \rho^2\left(\bar{\beta}^2 - k^2 n_{c\ell}^2\right) \tag{2.18b}$$

so that $U^2 + W^2 = V^2$.

Figure 2.1 is a cylindrical fiber with cartesian coordinates (x,y,z), and polar coordinates (r,ϕ,z) , radius ρ , and refractive indicies $n_{c\ell}$ in the cladding and n(x,y) in the core.

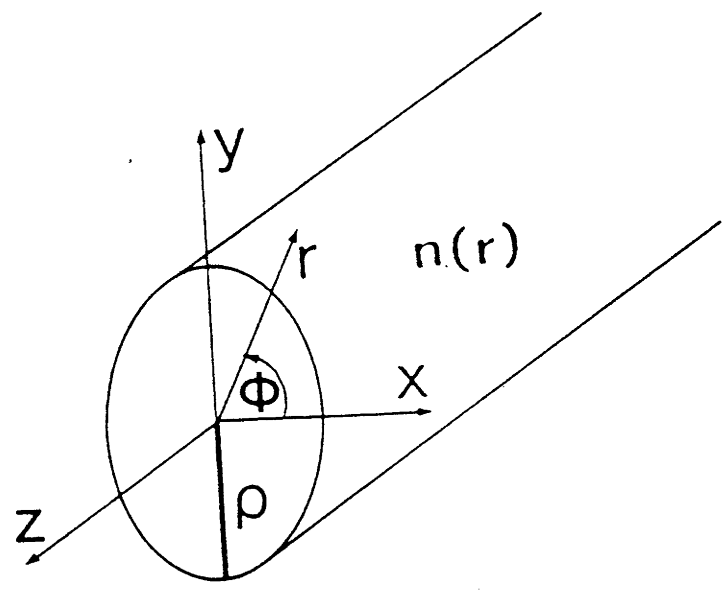

Fig. 2.1 A circularly symmetric fiber, which is unbounded in the r- and z-directions. The core radius is ρ , the normalized radius is $R = r/\rho$, and n(r) is the refractive index profile.

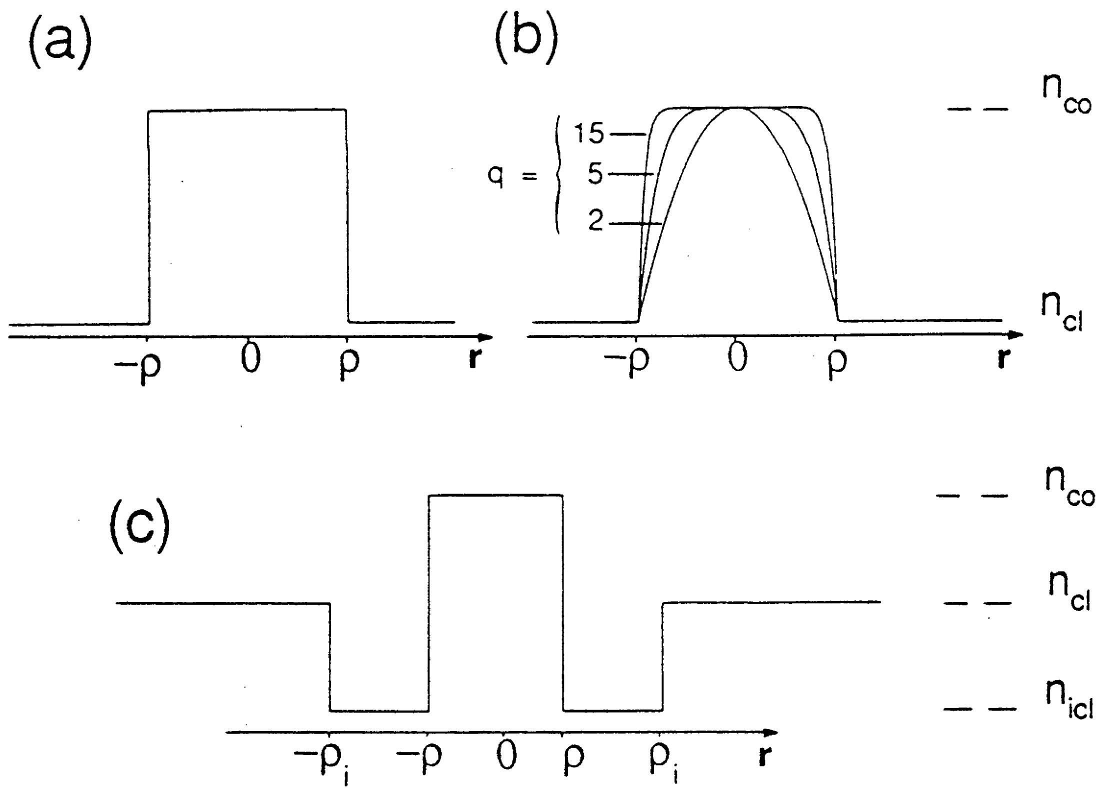

Fig. 2.2 Refractive index profiles for (a) the singly-clad step-profile, (b) the singly-clad power-law profile, and (c) the doubly-clad step-profile.

3. Modal Characteristics

We now have the basic equations necessary to describe the behaviour of light propagating in optical waveguides. The equations are general and apply to waveguides of any profile shape or cross-sectional shape.

Throughout this work we will deal with 3 types of fibers; the singly-clad step- and clad power-law profile fibers, and the doubly-clad step-profile fiber. We will consider a circularly-symmetric cross-section, so that the scalar wave equation (2.11) can be written as

$$\left(\frac{\partial^2}{\partial r^2} + \frac{1}{r}\frac{\partial}{\partial r} + \frac{1}{r^2}\frac{\partial^2}{\partial \phi^2} + k^2n^2 - \bar{\beta}^2\right)\psi = 0 \qquad (2.19)$$

where the scalar Laplacian has been written in cylindrical polar coordinates and $\psi = \bar{e}_x\,\hat{\underset{\sim}{x}}$ or $\bar{e}_y\,\hat{\underset{\sim}{y}}$. ψ can be expressed in the separable form

$$\psi = F_\ell(R)\begin{Bmatrix}\cos \ell\phi\\ \sin \ell\phi\end{Bmatrix} \qquad (2.20)$$

where $\begin{Bmatrix}\cos \ell\phi\\ \sin \ell\phi\end{Bmatrix}$ refer to $\begin{Bmatrix}\text{even}\\ \text{odd}\end{Bmatrix}$ modes, $\ell = 0,1,.....$, and we have introduced the normalized radial coordinate $R = r/\rho$. We will use this normalized coordinate throughout this work. The radial function $F_\ell(R)$ is then the solution to ~~be~~ the differential equation

$$\left(\frac{d^2}{dR^2} + \frac{1}{R}\frac{d}{dR} + \frac{\ell^2}{R^2} + U^2 - V^2 f(R)\right)F_\ell(R) = 0 \qquad (2.21)$$

where we have substituted eqns. (2.17), (2.18) and (2.20) into the scalar wave equation (2.19). The smallest value of U (and hence the largest value of $\bar{\beta}$) occurs for the fundamental ($\ell = 0$) mode. We now examine solutions to eqn. (2.21) for our 3 fiber models.

(a) **Singly-Clad Step-Profile Fiber**

This profile shape, shown in figure 2.2(a) represents a fiber with a constant refractive index in the core and a constant refractive index in the cladding, and with respect to eqn. (2.17) is specified by

$$f(R) = \begin{cases} 0 \ , & 0 \le R \le 1 \\ 1 \ , & R > 1 \end{cases} \tag{2.22}$$

The solution to equation (2.21) is then given by

$$F_\ell(R) = \begin{cases} J_\ell(UR)/J_\ell(U) \ , & 0 \le R \le 1 \\ K_\ell(WR)/K_\ell(W) \ , & R > 1 \end{cases} \tag{2.23}$$

where J and K are the Bessel and modified Bessel functions. The eigenvalues U and W can be determined by matching the field and its first derivative at the fiber boundary R = 1. The result is the eigenvalue equation:

$$U \frac{J_{\ell+1}(U)}{J_\ell(U)} = W \frac{K_{\ell+1}(W)}{K_\ell(W)} \tag{2.24}$$

The m^{th} zero of this equation specifies the (ℓ,m) mode propagating in the fiber. In Section 2-4 we explain that (ℓ,m) modes are designated by the notation $LP_{\ell m}$, unless otherwise specified. The method of numerically determining the zero's of eqn.(2.24) is outlined in the Appendix.

For future reference, the normalization integral for a singly-clad step-profile fiber is

$$\chi_\ell = \int_0^\infty F_\ell^{\,2}(R)\ R\,dR = \frac{V^2}{2U} \frac{K_{\ell-1}(W)\ K_{\ell+1}(W)}{K_\ell^{\,2}(W)} \tag{2.25}$$

The lower limit $\bar{\beta} = kn_{c\ell}$ of permissible values of the bound mode propagation constant is called modal cut-off, and is defined by

$$U = V \quad ; \quad W = 0$$

The fundamental mode will propagate for any positive value of V, but higher-order modes will only propagate when V is greater than the characteristic cut-off value.

For the step-profile fiber the cut-off values are given by

$$J_{\ell-1}(V) = 0 \quad .$$

Figure 2.3 is a plot of the numerical solutions to the eigenvalue equation (2.24) as a function of V. The cut-off values are also given. These curves represent the scalar propagation constant $\bar{\beta}$.

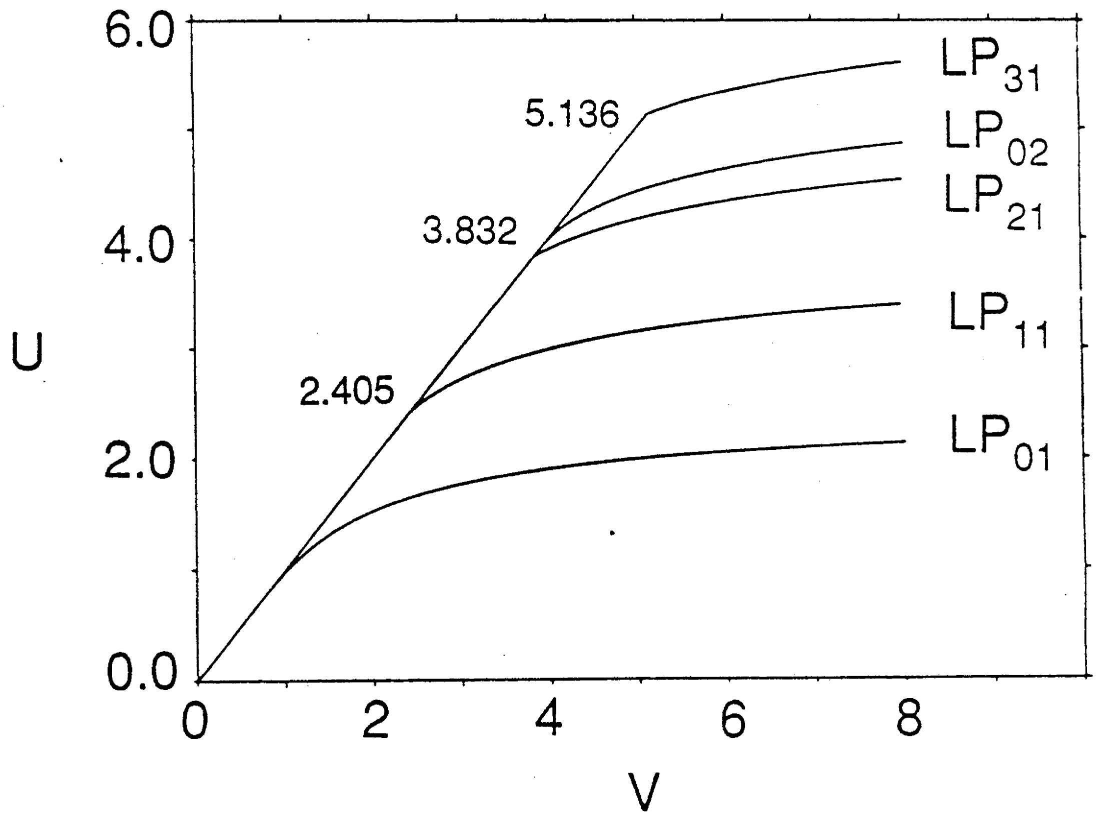

Fig. 2.3 Scalar eigenvalues for the singly-clad step-profile fiber. The numbers along the U = V line are the cut-off values, V_{co}, for the different modes.

(b) **Singly-Clad Power-Law Profile Fibers**

This profile shape, shown in figure 2.2(b) is specified by [9]

$$f(R) = \begin{cases} R^q & , \quad 0 \le R \le 1 \\ 1 & , \quad R > 1 \end{cases} \tag{2.26}$$

where q is a grading parameter. q = 2 is the square-law or parabolic index, and q = ∞ is the step-index.

The solution to eqn.(2.21) in the cladding is the same as that for the singly-clad step-profile. There are no analytic expressions for $F_\ell(R)$ in the core region, but eqn. (2.21) can be solved numerically. In the Appendix we outline a fourth-order Runge-Kutta method to solve this equation. Cut-off values are also found numerically from this equation.

In figure 2.4 the cut-off values, V_{co}, are plotted against q. In figure 2.5(a) we plot the eigenvalue U against V for several values of q, and in figure 2.5(b) we plot U against q for several values of V.

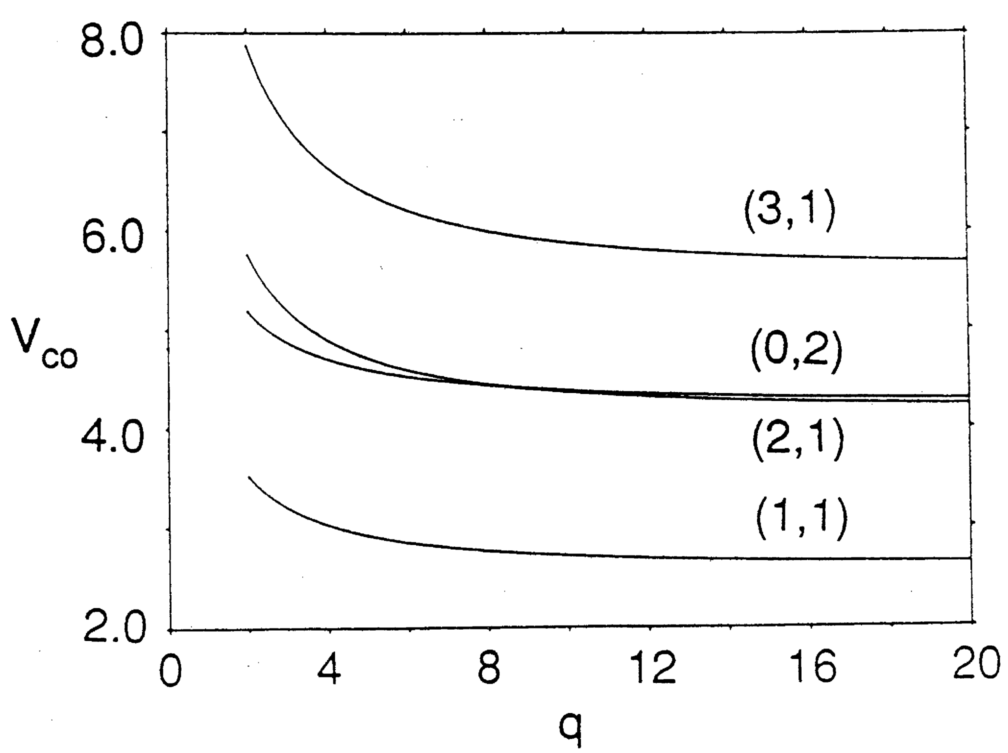

Fig. 2.4 Cut-off values for the power-law profile against grading parameter q.

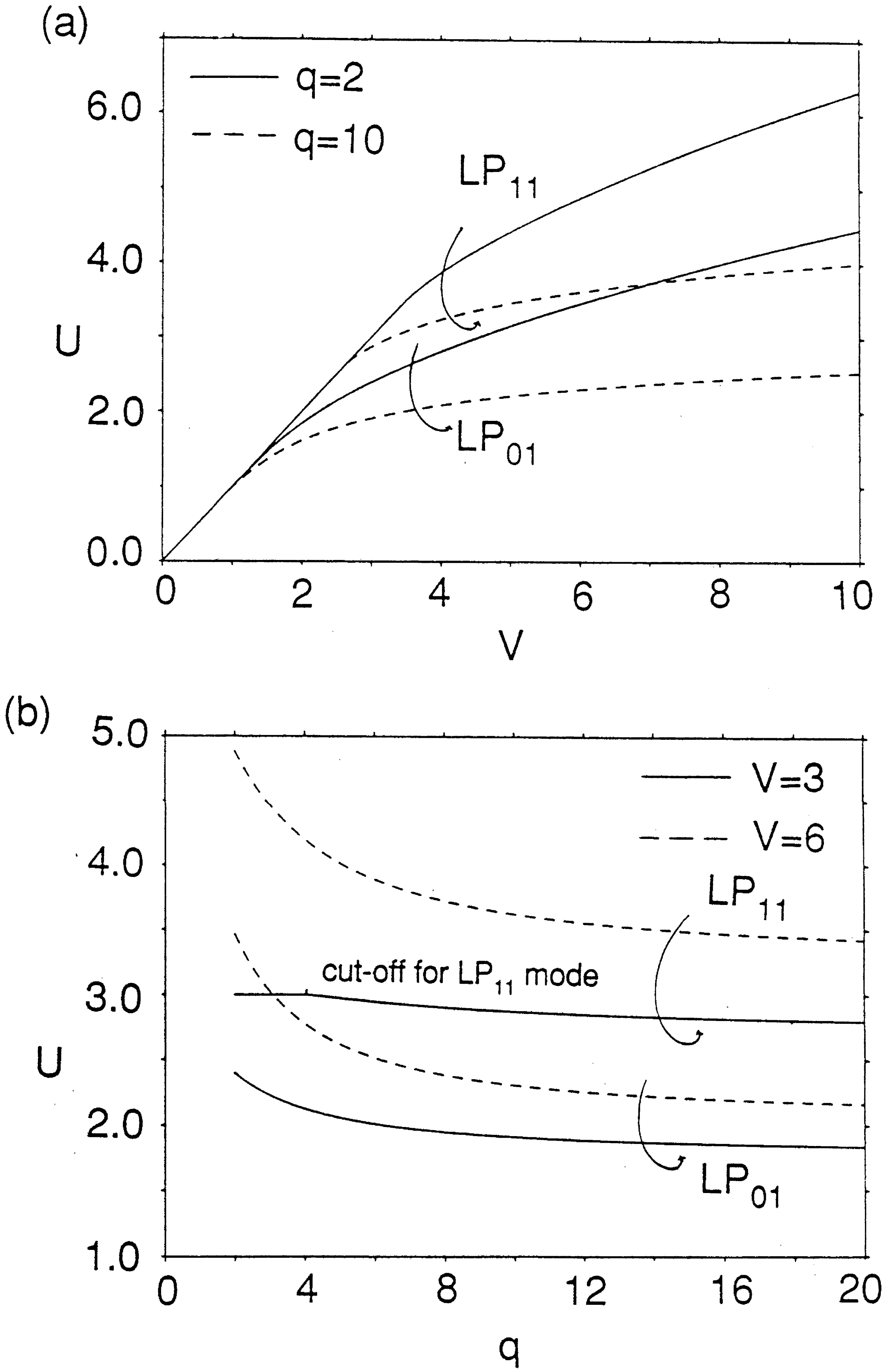

Fig. 2.5 Eigenvalues for the first two modes of the power-law profile fiber. (a) U vs. V for different q, and (b) U vs. q for different values of V.

(c) Doubly-Clad Step-Profile Fiber

This profile is often called the W-fiber, or depressed inner-cladding fiber, and its profile is shown in figure 2.2(c). As we shall see in Chapter 3, this fiber has a shifted zero-dispersion wavelength [10,11], due to its multiple cladding, and can be used for minimum dispersion operation at longer wavelengths (and therefore less loss) than the singly-clad fibers. Following reference [11] we define two profile parameters

$$\Delta = \frac{1}{2}\left(1 - n_{c\ell}^2/n_{co}^2\right)$$
$$\Delta_i = \frac{1}{2}\left(1 - n_{ic\ell}^2/n_{co}^2\right) \tag{2.27}$$

where $n_{ic\ell}$ is the refractive index of the inner cladding. We also define two V's according to eqn. (2.15)

$$V = k\rho n_{co}\,(2\Delta)^{1/2}$$
$$V_i = k\rho n_{co}(2\Delta_i)^{1/2} \tag{2.28}$$

and the mode parameters are

$$U = \rho\left(k^2 n_{co}^2 - \bar{\beta}^2\right)^{1/2}$$
$$W = \rho\left(\bar{\beta}^2 - k^2 n_{c\ell}^2\right)^{1/2} \tag{2.29}$$
$$W_i = \rho\left(\bar{\beta}^2 - k^2\, n_{ic\ell}^2\right)^{1/2}$$

We introduce the two main parameters

$$P = 1 - \frac{\Delta}{\Delta_i} \simeq \left(n_{c\ell} - n_{ic\ell}\right)/\left(n_{co} - n_{ic\ell}\right) \tag{2.30}$$

$$Q = \rho_i/\rho \tag{2.31}$$

For the profile shape we have

$$f(R) = \begin{cases} 0 & , \quad 0 \le R \le 1 \\ \Delta_i/\Delta & , \quad 1 < R \le Q \\ 1 & , \quad R > Q \end{cases} \tag{2.32}$$

The solution to equation (2.21) is then given by [11]

$$F_\ell(R) = \begin{cases} A_0 J_\ell(UR) & , \quad 0 \le R \le 1 \\ A_1 I_\ell(W_i R) + A_2 K_\ell(W_i R) & , \quad 1 < R \le Q \\ A_3 K_\ell(WR) & , \quad R > Q \end{cases} \tag{2.33}$$

where I is the modified Bessel function of the first kind, and the A's are normalized constants which ensure the continuity of $F_\ell(R)$ at the boundary R = 1 and R = Q. Analytic expressions for A's are presented in the Appendix. The eignevalue equation is found by matching the field and its first derivative at the boundaries R = 1 and R = Q:

$$\frac{\left[\hat{J}_\ell(U) - \hat{K}_\ell(W_i)\right]\left[\hat{K}_\ell(WQ) + \hat{I}_\ell(W_i Q)\right]}{\left[\hat{J}_\ell(U) + \hat{I}_\ell(W_i)\right]\left[\hat{K}_\ell(WQ) - \hat{K}_\ell(W_i Q)\right]} = \frac{I_{\ell+1}(W_i)\, K_{\ell+1}(W_i Q)}{I_{\ell+1}(W_i Q)\, K_{\ell+1}(W_i)} \tag{2.34}$$

where

$$\hat{Z}_\ell(x) = \frac{Z_\ell(x)}{x Z_{\ell+1}(x)} \tag{2.35}$$

and Z represents the Bessel functions J,K or I.

The cut-off condition is given by

$$\frac{\hat{J}_\ell(V) - \hat{K}_\ell(\bar{V})}{\hat{J}_\ell(V) + \hat{I}_\ell(\bar{V})} = \frac{I_{\ell+1}(\bar{V})\ K_{\ell-1}(\bar{V}\ Q)}{K_{\ell+1}(\bar{V})\ I_{\ell-1}(\bar{V}\ Q)} \tag{2.36}$$

where $\bar{V} = V\left(\frac{P}{1-P}\right)^{1/2}$.

In figure 2.6 the cut-off curves are plotted against Q for several values of P. In figure 2.7(a) we plot the eigenvalue U against V for a fixed radius ratio Q and several values of profile ratio P, and in figure 2.7(b) we plot U against Q for several values of profile ratio and fixed V.

We mention here that variation of V for a given fiber implies variation of wavelength, and since refractive index is a function of λ (see Chapter 3) then P must also be a function of λ . However, in Chapter 3 we show that variation of P with respect to wavelength is very small, and throughout we regard P as constant.

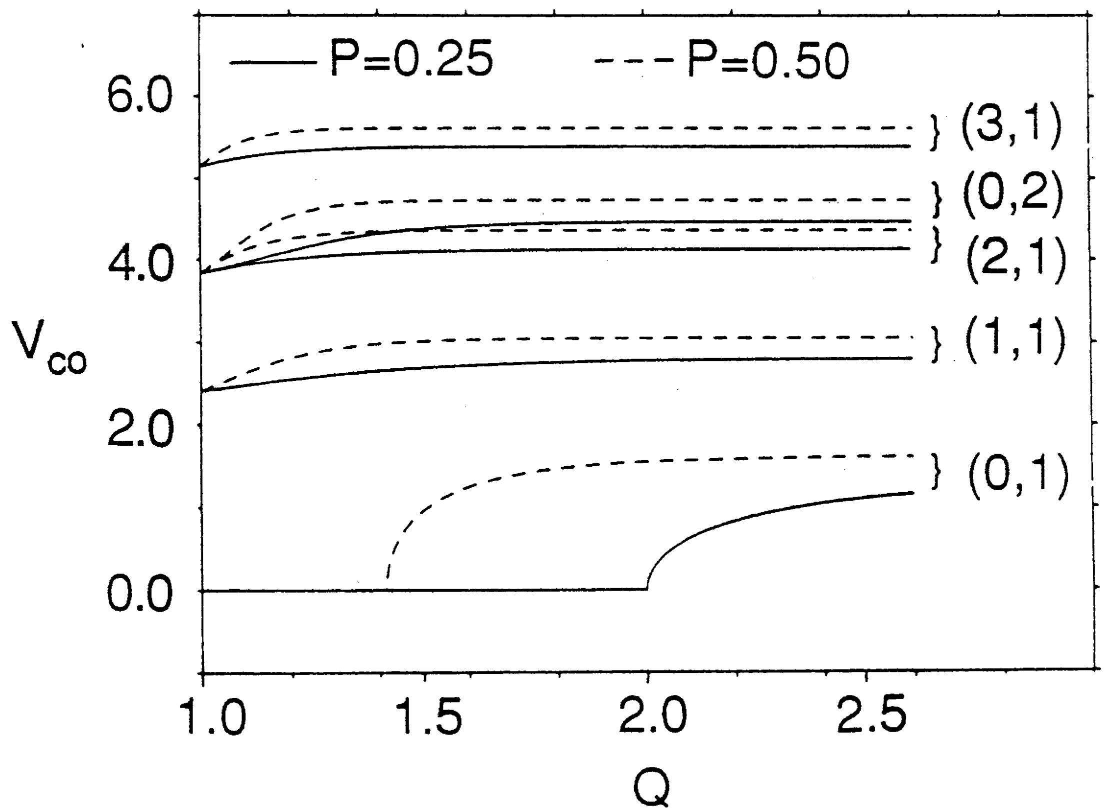

Fig. 2.6 Cut-off values for the W-fiber against radius ratio Q for P = 0.25 and P = 0.50.

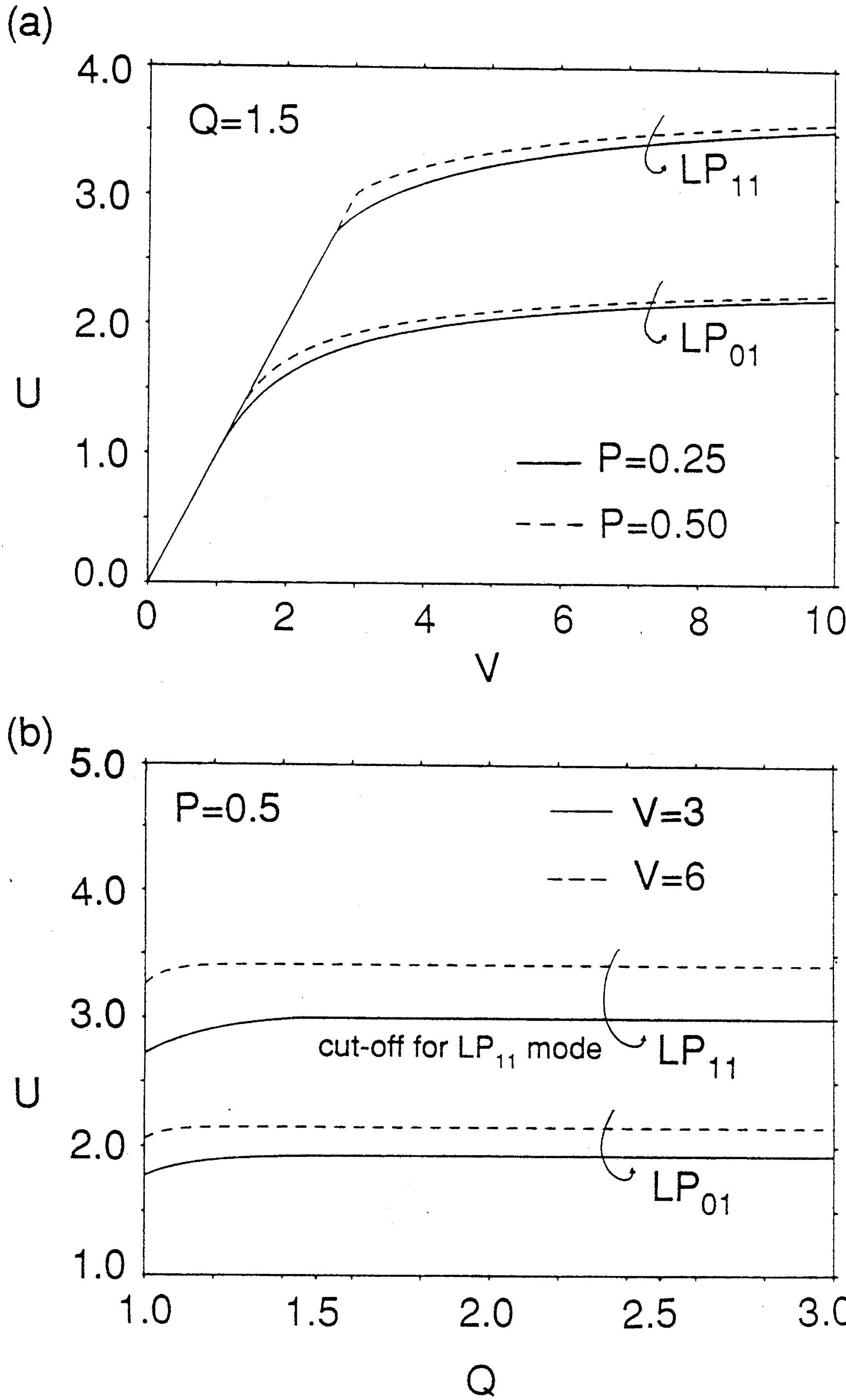

Fi.g 2.7 Eigenvalues for the first two modes of the doubly-clad step-profile (W-) fiber. (a) U vs. V for a fixed Q = 1.5 and different values of P, and (b) U vs. Q for a fixed P = 0.5 and different values of V.

4. Polarization Corrections to the Step-Profile Fiber

In section 2-2(b) we saw that by using the "weakly-guiding", or $\Delta \to 0$, approximation the vector wave equation could be replaced by the scalar wave equation, and the fields can be described by plane waves which are called LP (linearly-polarized) modes.

An (ℓ,m) mode will be designated as $LP_{\ell m}$ throughout this work, unless otherwise specified. We stress that LP modes are not the true modes of the fiber, they are only an approximation in which all polarization properties are ignored. However, we will show in later chapters that in fact the LP modes can be an accurate description of mode propagation if the fiber is perturbed in some manner.

In our study of birefringence in Chapter 6 we will have cause to use the vector properties of the modal field, so here we review the scheme in which vector fields are constructed from scalar fields, and consider a specific example. There are four solutions to the circularly-symmetric form of the scalar wave equation (2.19), which all have the same $\tilde{\beta}$'s :

$$\begin{aligned}
\bar{\underset{\sim}{e}}_{xe} &= F_\ell(R)\cos\ell\phi\,\hat{\underset{\sim}{x}} \\
\bar{\underset{\sim}{e}}_{ye} &= F_\ell(R)\cos\ell\phi\,\hat{\underset{\sim}{y}} \\
\bar{\underset{\sim}{e}}_{xo} &= F_\ell(R)\sin\ell\phi\,\hat{\underset{\sim}{x}} \\
\bar{\underset{\sim}{e}}_{yo} &= F_\ell(R)\sin\ell\phi\,\hat{\underset{\sim}{y}}
\end{aligned} \tag{2.37}$$

where $F_\ell(R)$ is the solution to eqn. (2.21).

Using symmetry methods these scalar solutions can be linearly combined to form the true modes [7];

$$\underset{\sim}{e}_1 = \bar{\underset{\sim}{e}}_{xe} + \bar{\underset{\sim}{e}}_{yo}$$

$$\underset{\sim}{e}_2 = \bar{\underset{\sim}{e}}_{xe} - \bar{\underset{\sim}{e}}_{yo}$$

$$\underset{\sim}{e}_3 = \bar{\underset{\sim}{e}}_{xo} + \bar{\underset{\sim}{e}}_{ye} \tag{2.38}$$

$$\underset{\sim}{e}_4 = \bar{\underset{\sim}{e}}_{xo} - \bar{\underset{\sim}{e}}_{ye}$$

Note that for the two fundamental ($\ell = 0$) modes the exact modes are the same as the scalar modes. The correction to the propagation constant is now given by eqn. (2.14), with $\underset{\sim}{e}_t$ given by any one of eqn. (2.38), and $\bar{\underset{\sim}{e}}_t$ given by either of eqns. (2.37) that make up $\underset{\sim}{e}_t$.

As an example for determining the proper modes of a fiber, we consider the singly-clad step-profile fiber, whose scalar fields are given by eqn. (2.23). The scalar propagation constants are given by eqn. (2.18a):

$$\bar{\beta} = kn_{co}\left(1 - 2\Delta \frac{U^2}{V^2}\right)^{1/2} \tag{2.39}$$

where use has been made of the definition of V, eqn. (2.15), and U is the eigenvalue of the scalar wave eqn. (2.21).

In order to evaluate eqn.(2.14) we use eqn.(2.17) and write $\underset{\sim}{\nabla}_t \ell n\, n^2 \simeq -2\Delta \underset{\sim}{\nabla}_t f$. For a step-profile f is a step-function at the boundary R=1, and we can write

$$-2\Delta\ \underset{\sim}{\nabla}_t f = -2\Delta\ \delta(R-1)\ \hat{\underset{\sim}{n}} \tag{2.40}$$

where δ is the Dirac delta function. The unit outward vector $\hat{\underset{\sim}{n}}$ is on the boundary interface in the waveguide cross-section. Furthermore

$$\beta^2 - \bar{\beta}^2 \simeq 2\bar{\beta}(\beta - \bar{\beta}) \simeq 2kn_{co}(\beta - \bar{\beta}) = \frac{2V}{(2\Delta)^{1/2}\ \rho}\ \delta\beta \tag{2.41}$$

where we have used the approximation eqn. (2.12).

Eqn. (2.14) then reduces to

$$\delta\beta = \frac{\rho(2\Delta)^{3/2}}{2V} \oint_{s} (\underset{\sim}{\nabla}_t \cdot \underset{\sim}{\bar{e}}_t)\, \underset{\sim}{e}_t \cdot \hat{\underset{\sim}{n}}\, ds \Big/ \int_{A_\infty} \underset{\sim}{\bar{e}}_t \cdot \underset{\sim}{e}_t \, dA \qquad (2.42)$$

where $ds = \rho\, d\phi$ is an element of arc length on the boundary interface.

In Table 2.1 we present the corrections to $\bar{\beta}$ for the four exact modes, where the modes are labelled in the standard EH and HE notation (see [1] for a discussion). In figure 2.8 we plot the exact eigenvalue, U_{ex} against V for a fixed $\Delta = 0.01$. U_{ex} is defined as

$$U_{ex}^2 = \rho^2(k^2 n_{co}^2 - \beta^2) = U^2 - \rho^2(\beta^2 - \bar{\beta}^2) \qquad (2.43)$$

where U is the scalar eigenvalue given by eqn. (2.18a). Figure 2.8 thus represents the true modes propagating in a singly-clad step-index fiber, and should be compared to the approximate LP modes of figure 2.3. We note that the fundamental mode does not have a degeneracy split.

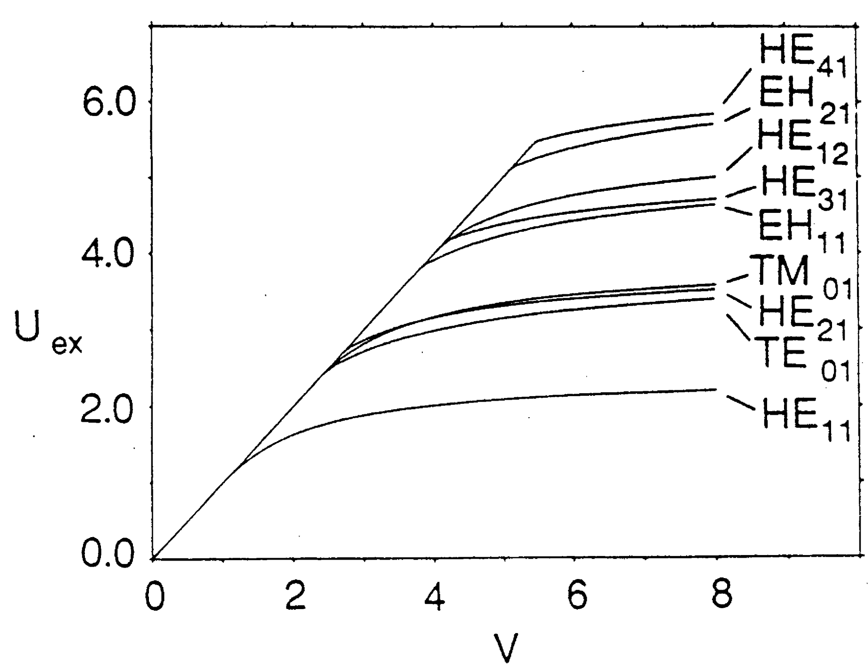

Fig. 2.8 The true modes in a singly-clad step-profile fiber. U_{ex} is given by eqn. (2.43), and the modes are labelled by the HE and EH notation (see text).

TABLE 2.1

Polarization corrections to the step-profile fiber

MODE 1	MODE 2	MODE 3	MODE 4
EVEN $EH_{\ell-1,m}$ (even $EH_{0,m} = TM_{0,m}$)	EVEN $HE_{\ell+1,m}$	ODD $HE_{\ell+1,m}$	ODD $EH_{\ell-1,m}$ (odd $EH_{0,m} = TE_{0,m}$)
$e_1 = \bar{e}_{ex} + \bar{e}_{oy}$	$e_2 = \bar{e}_{ex} - \bar{e}_{oy}$	$e_3 = \bar{e}_{ox} + \bar{e}_{ey}$	$e_4 = \bar{e}_{ox} - \bar{e}_{ey}$
$\beta_1^2 - \bar{\beta}^2$ $= + \frac{(2\Delta)}{\rho^2} \left(\frac{U^2}{V^2}\right) \frac{WK_\ell(W)}{K_{\ell+1}(W)}$ $\ell \neq 1$ $= + \frac{2(2\Delta)}{\rho^2} \left(\frac{U}{V}\right)^2 \frac{WK_1(W)}{K_2(W)}$ $\ell = 1$	$\beta_2^2 - \bar{\beta}^2 = \beta_3^2 - \bar{\beta}^2$ $= + \frac{(2\Delta)}{\rho^2} \left(\frac{U^2}{V^2}\right) \frac{WK_\ell(W)}{K_{\ell-1}(W)}$		$\beta_4^2 - \bar{\beta}^2$ $= + \frac{(2\Delta)}{\rho^2} \left(\frac{U^2}{V^2}\right) \frac{WK_\ell(W)}{K_{\ell+1}(W)}$ $\ell \neq 1$ $= 0$ $\ell = 1$

4. Gaussian Approximation to Modal Fields

The fundamental mode field of an optical fiber is approximately Gaussian in shape, and this fact can be exploited by giving very simple forms for the modal parameters discussed in Section 2-3. The basis of the approximation is that the fundamental mode of an arbitrary profile circularly symmetric fiber can be approximated by some Gaussian function:

$$F_0(R) \simeq \exp\left(-R^2/2R_0^2\right) \tag{2.44}$$

where $R_0 = r_0/\rho$ is called the spot-size. The problem then is to find an R_0 such that eqn. (2.44) gives a good approximation to the exact field. In this work we will only be concerned with approximations to step-profile fibers.

Marcuse [12] has determined the spot-size of the fundamental mode by minimizing the difference between the exact and Gaussian fields:

$$I(R_0) = \int_0^\infty \left[\frac{e^{-R^2/2R_0^2}}{N(R_0)} - \frac{F_0(R)}{\chi_0}\right]^2 R\,dR \tag{2.45}$$

where $N(R_0)$ and χ_0 are normalization factors, with χ_0 given by eqn. (2.25).

The spot-size is then determined by

$$\frac{dI}{dR_0} = 0 \quad . \tag{2.46}$$

For the step-profile fiber we have [12]

$$R_0 = \frac{1}{\sqrt{2}}\left(0.65 + \frac{1.619}{V^{3/2}} + \frac{2.879}{V^6}\right) \quad . \tag{2.47}$$

A second, variational, method for finding R_0 is due to Snyder and Sammut [13]. This method has two advantages: first of all it results in a simple expression for R_0 ; and secondly it can be generalized to describe higher-order modes [14].

The basis for the approximation is that the exact higher order modes of the infinite parabolic profile (i.e. $f = R^2$ in eqn. (2.21)) are given by

$$F_\ell(R) = \left(\frac{R}{R_0}\right)^\ell L_{m-1}^{(\ell)}\left(\frac{R^2}{R_0^2}\right)\exp\left(-R^2/2R_0^2\right) \tag{2.48}$$

with $R_0^2 = 1/V$. $L_{m-1}^{(\ell)}$ is a generalized Laguerre polynomial and is given by [15]

$$L_{m-1}^{(\ell)}\left(\frac{R^2}{R_0^2}\right) = \sum_{n}^{m-1} \frac{(-1)^n}{n!}\,\frac{(m-1+\ell)}{(n+\ell)!\,(m-1-n)!}\left(\frac{R^2}{R_0^2}\right)^n \tag{2.49}$$

It is assumed that the modes of an arbitrary profile fiber are of the same form as eqn. (2.48). The spot-size is then chosen to minimize the variation in $\bar{\beta}$ when eqn (2.48) is substituted into a stationary expression for $\bar{\beta}$. This expression can be obtained by multiplying the scalar wave equation (2.21) by $RF_\ell(R)$ and integrating over the profile:

$$U^2 = \int_0^\infty \left\{\left(\frac{\ell^2}{R^2} + V^2 f\right)F_\ell - \frac{d^2F_\ell}{dR^2} - \frac{1}{R}\frac{dF_\ell}{dR}\right\}F_\ell^2\, R\, dR \Big/ \int_0^\infty F_\ell^2\, R\, dR \tag{2.50}$$

where U^2 is related to $\bar{\beta}^2$ by eqn. (2.18a). Given $f(R)$ for a particular profile, the value of R_0 is found by solving the equation for the extremum value of U [13]

$$\frac{dU^2}{dR_0} = 0 \quad . \tag{2.51}$$

The result is [14]

$$2m + \ell - 1 = \frac{V^2(m-1)!}{(\ell+m-1)!} \int_0^\infty \frac{df}{dR} F_\ell^2 R^2 \, dR \tag{2.52}$$

Given the solution of this equation for R_0 , the corresponding value of U, and hence $\bar{\beta}$, is found by substituting the extremum value of R_0 back into eqn. (2.50).

For the step-profile fiber f(R) is given by eqn. (2.22), and the derivative of f(R) is the Dirac delta function: $df/dR = \delta(R-1)$. For the fundamental $(\ell = 0, m = 1)$ mode eqn. (2.52) reduces to [13,14]

$$R_0 = (1/\ell n V^2)^{1/2} \tag{2.53}$$

In figure 2.9 we compare eqns. (2.47) and (2.53). The two spot-sizes behave similarly over a large range of V, although eqn. (2.53) will break down as $V \to 1$. We discuss this later.

In Table 2.2 we list $F_\ell(R)$, R_0 and U for the first two modes of the step-profile fiber. The relative error of U with its exact value (i.e. the eigenvalue equation (2.24)) is at most only a few percent [14].

Table 2.2: Gaussian Approximation for the Step-profile Fiber

Mode (ℓ,m)	$F_\ell(R)$	R_0	U^2
(0,1)	$e^{-R^2/2R_0^2}$	$\frac{1}{V^2} = e^{-1/R_0^2}$	$\left(1 + \frac{1}{R_0^2}\right)$
(1,1)	$\frac{R}{R_0} e^{-R^2/2R_0^2}$	$\frac{2}{V^2} = \frac{1}{R_0^2} e^{-1/R_0^2}$	$2\left(\frac{1}{R_0^2} + 1 + R_0^2\right)$

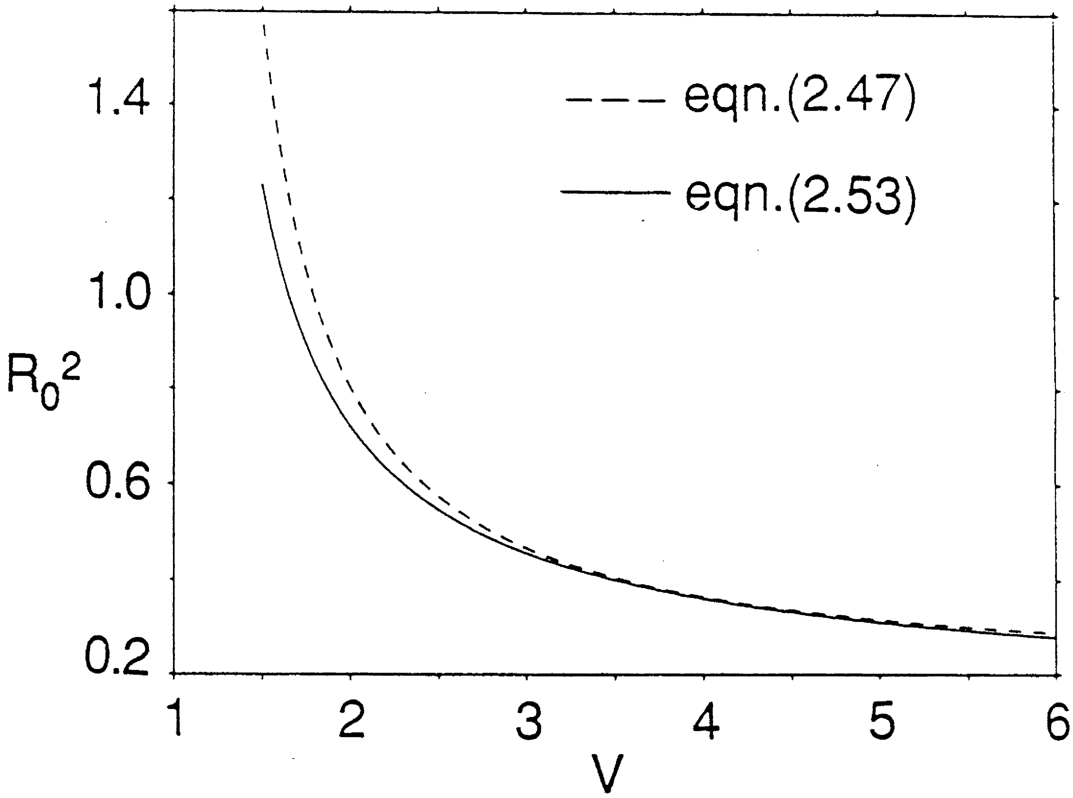

Fig. 2.9 Comparison of spot-size definitions for the Gaussian approximation to the fundamental mode.

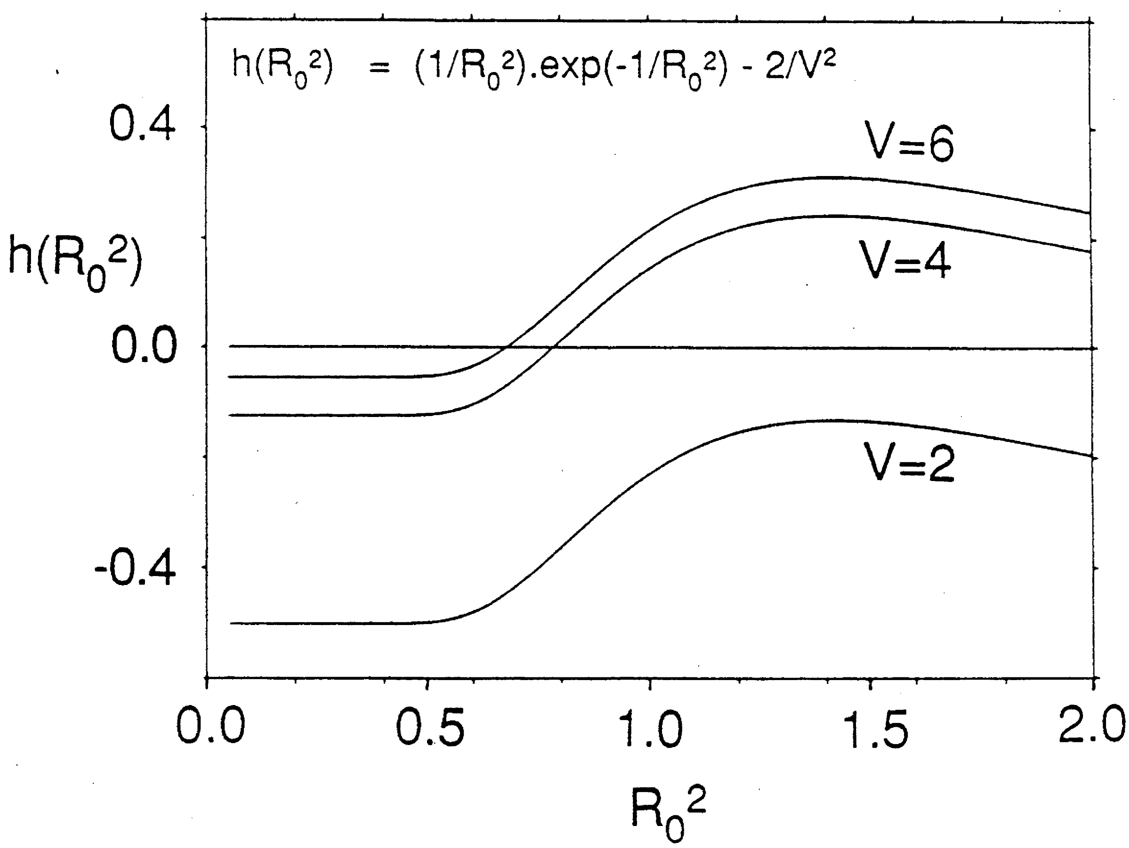

Fig. 2.10 The spot-size equation for the LP_{11} modes vs. R_0^2. The curve that has no roots is below cut-off.

In order to find R_0 for the $\ell \geq 1$ modes one must use a zero finding method as outlined in the Appendix. In general the equation for R_0 for these modes has more than one zero.

As an example for determining the spot-size for some mode we consider the LP_{11} mode (refer to Table 2.2), and in figure 2.10 we plot the function

$$h(R_0^2) = \frac{1}{R_0^2} e^{-1/R_0^2} - \frac{2}{V^2}$$

against R_0 for several values of V. The curves that have no zero's are for V values below cut-off (for the step-profile fiber the LP_{11} modes does not propagate for $V < 2.405$). The other curves may have multiple zero s, and in this case the correct value of R_0 (that value which gives the most accurate value of U) is given by the first zero.

In Table 2.2 R_0 is not the same for different modes, and we may write

$$M_{\ell,m}(V) = R_0 \tag{2.54}$$

In figure. 2.11 we plot the function M against V for the first four modes.

As mentioned previously, eqn.(2.53) will break down as $V \to 1$. Henceforth, when using the Gaussian approximation to describe mode properties on single-mode fibers (i.e., those fibers with $V < 2.4$) we will use the spot-size given by eqn.(2.47). However, when we deal with the more general case of few-mode fibers we will use the spotsize defined by eqn.(2.52) for the (ℓ,m) mode, and represent this spot-size by $M_{\ell,m}$.

Later we will use the results of this section in an effort to simplify the description of mode propagation on bent fibers (Chapter 8).

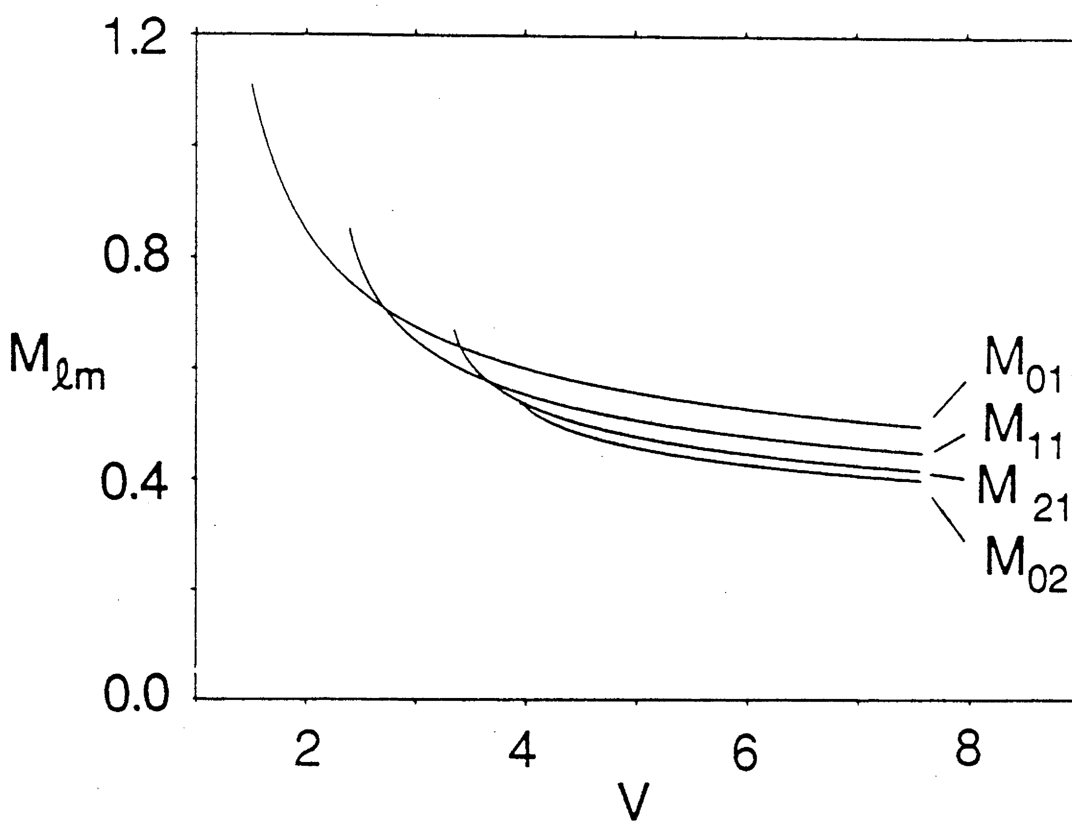

Fig. 2.11 Spot-size $M_{\ell m}$ for different modes vs. V. The spot-sizes are numerically evaluated from the zero's of eqn. (2.52).

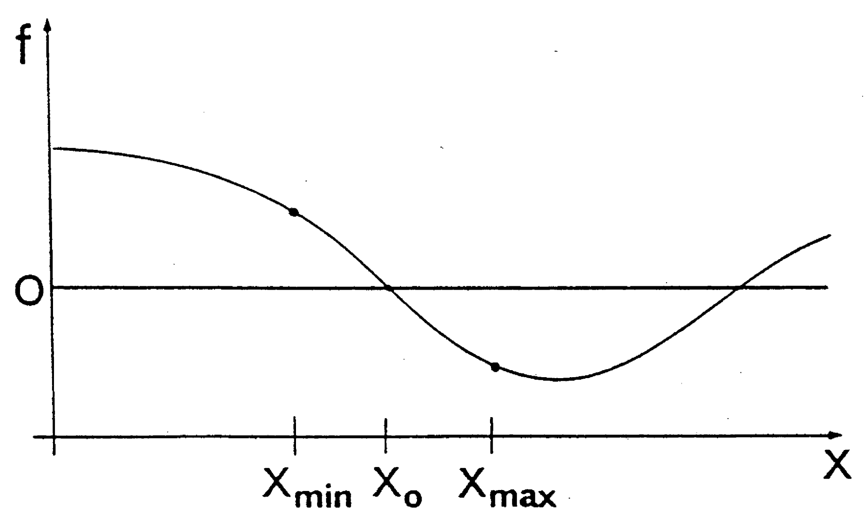

Fig. 2.12 Arbitrary functions f(x) vs. x.

6. Appendix

(i) Zero finding routine for functions

To find the zero, x_0 , of the function f(x) we write g = f(x) and choose minimum and maximum values of x such that

$$x_{min} < x_0 < x_{max}$$

as shown in fig. 2.12. We then determine x_0 by the following routine: (with reference to fig. 2.12)

$$\begin{aligned}
&\text{ROUTINE ZERO } (f,\ x_{min},\ x_{max};\ x_0) \\
&\qquad \text{start:}\quad x = 1/2\ (x_{min} + x_{max}) \\
&\qquad\qquad g = f(x) \\
&\qquad\quad \text{is}\quad |g| \le \varepsilon\ ,\quad g < 0\ ,\quad g > 0\quad ? \\
&\qquad\quad \text{if}\quad g < 0\quad \text{then}\quad x_{max} = x \\
&\qquad\qquad\qquad\qquad \text{return to start} \\
&\qquad\quad \text{if}\quad g > 0\quad \text{then}\quad x_{min} = x \\
&\qquad\qquad\qquad\qquad \text{return to start} \\
&\qquad\quad \text{if}\quad |g| \le \varepsilon\quad \text{then}\quad x_0 = x
\end{aligned} \qquad (2A.1)$$

$\varepsilon << 1$ determines the accuracy of x_0 . x_{min} and x_{max} can be found automatically, and the routine can be generalized to find any zero of a multi-zeroed function.

(ii) Eigenvalues and fields for arbitrary pofiles

The differential equation for the core region is

$$y'' + \frac{1}{R} y' - \frac{\ell^2}{R^2} y + (U^2 - V^2 f)y = 0 \tag{2A.2}$$

where f is the profile shape, eqn.(2.17). y must be continuous and have a continuous derivative y' at the fiber boundary R = 1, giving an eigenvalue equation for U:

$$\left.\frac{y'}{y}\right|_{R=1} = - \frac{W(K_{\ell-1}(W) + K_{\ell+1}(W))}{2\, K_\ell(W)} \tag{2A.3}$$

where the field in the cladding is given by $y = K_\ell(W)$

If we write equation (2A.2) in the form

$$y'' = \bar{f}(R,y,y') \tag{2A.4}$$

then for some value of V,f,ℓ and U y and y' can be found at R = 1 by a fourth-order Runge-Kutta method

ROUTINE R-K($f,\ell,V,U;\ y,y'$)

For n=0,1...,N, do:

$y_a = y_n$

$y'_a = y'_n$

$y''_a = \bar{f}(R_n, y_a, y'_a)$

$y_b = y_n + \frac{1}{2} h\, y'_a$

$y'_b = y'_n + \frac{1}{2} h\, y''_a$

$y''_b = \bar{f}(R_n + \frac{1}{2} h\,,\ y_b,\ y'_b)$

$$y_c = y_n + \frac{1}{2} h\, y'_b$$

$$y'_c = y'_n + \frac{1}{2} h\, y''_b$$

$$y''_c = \bar{f}\left(R_n + \frac{1}{2} h,\ y_c, y'_c\right) \tag{2A.5}$$

$$y_d = y_n + h y'_c$$

$$y'_d - y'_n + h y''_c$$

$$y''_d = \bar{f}\left(R_n + h,\ y_d,\ y'_d\right)$$

$$y_{n+1} = y_n + \frac{h}{6}\left(y'_a + 2y'_b + 2y'_c + y'_d\right)$$

$$y'_{n+1} = y'_n + \frac{h}{6}\left(y''_a + 2y''_b + 2y''_c + y''_d\right)$$

Then y_{n+1} and y'_{n+1} are approximations to y and y', respectively, at $R_{n+1} = R_0 + (n+1)h$. Usually we choose $N = 1/h$ and $h = 0.1$. The intial conditions are

$$\ell = 0: \quad y_0 = 1, \quad y'_0 = 0, \quad y'' = -U^2 + V^2 f$$

$$\ell \geq 1: \quad y_0 = 0, \quad y'_0 = 1, \quad y''_0 = 0 \tag{2A.6}$$

The eigenvalue for an arbitrary profile can then be found by calling the zero-finding routine eqn. (2A.1):

ROUTINE EIG $\left(f,\ell,m,V,U_{min},U_{max};\ U\right)$

CALL ZERO $\left(f(U);\ U_{min},\ U_{max};\ U\right)$

where the function f(U) is the eigenvalue eqn. (2A.3)

$$f(U) = K_{\ell}(W)y' + \frac{1}{2} W \left(K_{\ell-1}(W) + K_{\ell+1}(W)\right)y \qquad (2A.7)$$

and U and y,y' are given by

$$U = \frac{1}{2}\left(U_{min} + U_{max}\right)$$

CALL R-K$\left(f,\ell,m,V,U;\ y,y'\right)$

(iii) Normalization constants for the W-fiber modal fields

The normalization constants of eqn. (2.33) are given by [11]

$$\begin{aligned}
A_0 &= 1/J_{\ell}(U) \\
A_1 &= \left(W_i J_{\ell}(U)\ K_{\ell+1}(W_i) - U\ J_{\ell+1}(U)\ K_{\ell}(W_i)\right)/J_{\ell}(U) \\
A_2 &= \left(W_i J_{\ell}(U)\ I_{\ell+1}(W_i) + U\ J_{\ell+1}(U)\ I_{\ell}(W_i)\right)/J_{\ell}(U) \\
A_3 &= \left(A_1 I_{\ell}(W_i Q) + A_2 K_{\ell}(W_i Q)\right)/K_{\ell}(WQ)
\end{aligned} \qquad (2A.8)$$

References to Chapter 2

[1] A.W. Snyder and J.D. Love, "Optical Waveguide Theory" (Chapman and Hall, New York, 1983)

[2] P. Lorrain and D. Corson, "Electromagnetic Fields and Waves" (W.H. Freeman, San Francisco, 1970)

[3] A.W. Snyder, "Asymptotic expressions for eigenfunctions and eigenvalues of a dielectric or optical waveguide"
IEEE Trans., MTT-17, pp. 1130-1138 (1969)

[4] D. Gloge, "Weakly-guiding fibers"
Applied Optics, 10, pp. 2252-2258 (1971)

[5] J.A. Arnaud, "Transverse coupling in fibre optics part II"
Bell. Syst. Tech. J., 53, pp. 675-696 (1974)
See Appendix

[6] C.N. Kurtz, "Scalar and vector mode relations in gradient index light guides"
J. Opt. Soc. Am., 65, pp. 1235-1240 (1975)

[7] A.W. Snyder and W.R. Young, "Modes of optical waveguides"
J. Opt. Soc. Am., 68, pp. 297-309 (1978)

[8] D.L.A. Tjaden, "First-order correction to weak guidance approximation in fibre optics theory"
Phillips J. Res., 33, pp. 103-112 (1978)

[9] D. Gloge and E.A.J. Marcatili, "Multimode theory of graded-core fibers"
Bell. Syst. Tech. J., 52, pp. 1563-1578 (1973)

[10] S. Kawakami and S. Nishida, "Perturbation theory of a doubly clad optical fiber with a low index inner cladding"
IEEE J. Quantum Electron., QE-11, pp. 130-138 (1975)

[11] M. Monerie, "Propagation in doubly clad single-mode fibers"
IEEE J. Quantum Electron., QE-18, pp. 535-542 (1982)

[12] D. Marcuse, "Loss analysis of single-mode fiber splices"
Bell. Syst. Tech. J., 56, pp. 703-718 (1977)

[13] A.W. Snyder and R.A. Sammut, "Fundamental (HE11) modes of graded optical fibers"
J. Opt. Soc. Am., 69, pp. 1663-1671 (1979)

[14] J.D. Love and C.D. Hussey, "Variational approximations for higher-order modes of weakly guiding fibres"
Opt. Quantum Electron., 16, pp. 41-48 (1984)

[15] M. Abramowitz and I.A. Stegun, "Handbook of Mathematical Functions" (Dover, New York, 1964).

CHAPTER 3

DISPERSION OF LIGHT IN GLASS OPTICAL WAVEGUIDES

CHAPTER 3

DISPERSION OF LIGHT IN GLASS OPTICAL WAVEGUIDES

1. Introduction

In Chapter 5 we will see that phase-matching the stimulated four-photon mixing process is very sensitive to the dispersion properties of the fiber, and an understanding of such properties is essential to explain experimental results which are presented in later Chapters. As well, dispersion effects are the key to the optimum use of practical fiber systems. In this Chapter we present results which will be referred to throughout this work, as well as some results which are of interest for various optical fiber applications.

Dispersion is one of the detrimental factors inherent to light propagation in optical fibers. When a pulse of light propagates along a waveguide several dispersion effects contribute to distort its shape.

Intra-modal dispersion is due to the fact that the group velocity of a pulse of light depends on λ , and there is a small spread $\delta\lambda$ in the bandwidth of the source of light transmission. Intra-modal dispersion deteriorates the shape of the input signal so that information may be lost at the receiving end of the fiber, but the effect can be minimized by choosing an optimum range of parameters, such as operating wavelength and waveguide geometry. The effect consists of a combination of material dispersion, which depends on the bulk material used for the fiber, and waveguide dispersion, which depends on the fiber geometry.

Normally material dispersion dominates, but in the region $\lambda = 1.3\ \mu m$ (where the fiber is usually single-moded) material dispersion is ~~zero~~ small and the waveguide dispersion controls the total dispersion.

Inter-modal dispersion is due to the fact that the modes of an optical fiber propagate with different group velocities, so another dispersive effect is the difference in the group delay between modes. Thus if a pulse is formed by more than one mode it will spread out as it propagates along the fiber. As we shall see in Chapter 5 this inter-modal dispersion effect is the key to phase-matching the stimulated four-photon mixing process in few-mode fibers. This form of dispersion can easily be eliminated by having only one mode propagate - this is why single-mode fibers are the most commonly used for fiber communication systems. None the less, even a few mode fiber can be optimized to reduce this dispersion, as we show later. In figure 3.1 we schematically represent intra- and inter-modal dispersion.

After presenting the dispersion relations we investigate the change in refractive index with respect to wavelength. We are only concerned with fibers that have a ~~refractive index in the~~ cladding that is pure silica, and the ~~refractive index in the~~ core is GeO_2-doped silica. We show the variation of refractive index, material dispersion and profile height with respect to wavelength for several amounts of GeO_2 dopant, and show that there is a linear relation between refractive index and the amount of GeO_2 for any wavelength.

We then give exact expressions for the waveguide dispersion and group delay in a step-profile fiber, and give numerical results for the clad power-law profile and W-fiber. The W-fiber alters the waveguide dispersion so that the zero-dispersion wavelength (i.e., the wavelength at which the total dispersion is zero) is shifted from 1.3μm to the 1.55μm range, where the loss is much lower. We consider some examples of this shifting effect and present numerical results.

As an example of dispersive effects in optical waveguides, we examine the case of a singly-clad step-index fiber designed for single-mode operation at a wavelength of 1.3μm that is then used in the few-mode range of 0.85μm . This is a problem of practical interest, because most single-mode fibers currently being manufactured are designed to achieve optimum performance at $\lambda = 1.3$ μm , but the most inexpensive sources operate at the lower wavelength. In applications such as local area networks, where transmission is required over relatively short distances and large numbers of sources and detectors may be used, the combination of readily available fibers designed for 1.3 μm and sources operating at 0.85 μm is desirable, provided that adequate performance can be achieved. (See ref. [7] for a complete discussion of the feasibility of using this system for local area networks. We are only concerned with dispersion properties in this discussion.)

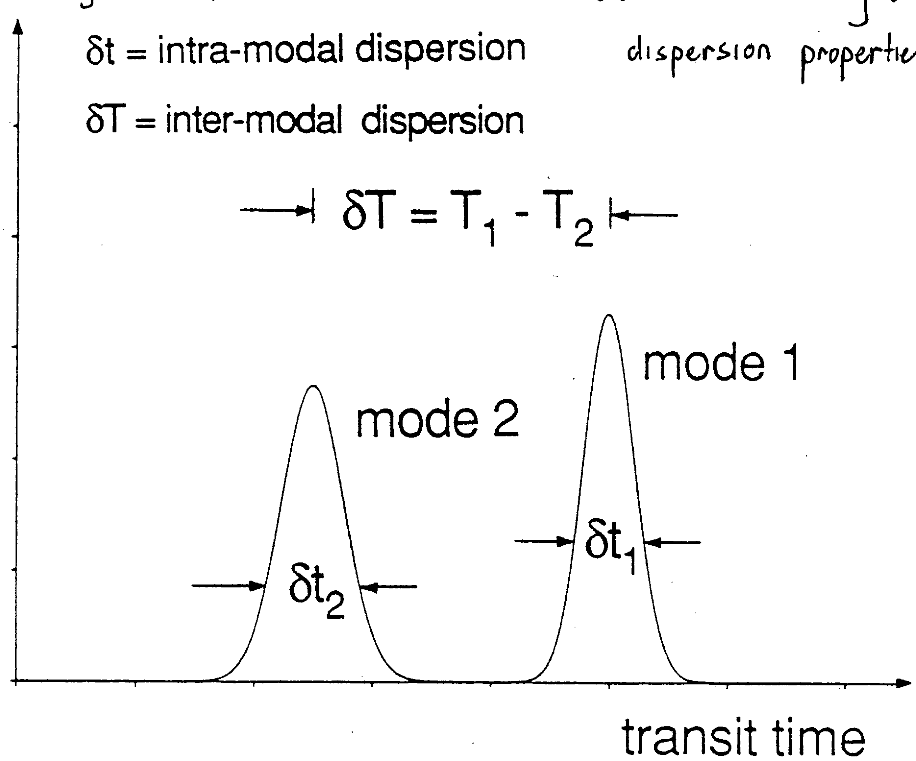

Fig. 3.1 Schematic representation of intra- and inter-modal dispersion for a pulse of light propagating in two modes.

2. The Dispersion Relations

The scalar propagation constant is given by eqn. (2.39). Because we are using the weakly-guiding approximation, so that $\Delta \ll 1$, we may write

$$\bar{\beta} \simeq kn_{co}\left(1 - \Delta \frac{U^2}{V^2}\right) \tag{3.1}$$

We define the dimensionless group delay as

$$\tau = \frac{d\bar{\beta}}{dk} = \left\{n + k\frac{dn}{dk} - \frac{U}{V}\frac{dU}{dV}\left(kn\frac{d\Delta}{dk}\right) + n\Delta\left[\left(\frac{U^2}{V^2} - 2\frac{U}{V}\frac{dU}{dV}\right)\left(1 + \frac{k}{n}\frac{dn}{dk}\right)\right]\right\} \tag{3.2}$$

where we have set $n = n_{co}$ for simplicity. The conversion of eqn. (3.2) to practical units is given in the Appendix.

As we shall see later, we can neglect terms of order $\Delta(k/n)(dn/dk)$ and $(d\Delta/dk)$ and write the group delay for each mode as

$$\tau = N + n\Delta T \tag{3.3}$$

where

$$N \equiv N(\lambda) = n + k\frac{dn}{dk} = n(\lambda) - \lambda\frac{dn(\lambda)}{d\lambda} \tag{3.4}$$

is the group index and

$$T \equiv T(V) = \frac{U^2}{V^2} - 2\frac{U}{V}\frac{dU}{dV} \tag{3.5}$$

is the normalized modal group delay [1]. (The equation for T in reference [1] should be corrected by a term Δ [2], which gives eqn. (3.5).)

The intra-modal dispersion, or total dispersion, of a mode is the spread in the group delay due to the small spread in wavelength of the source of transmission, and here we define it as

$$\delta t = \left(t/\lambda\right)\,\delta\lambda \tag{3.6a}$$

$$t = k\,\frac{d^2\bar{\beta}}{dk^2} = D(\lambda) + n\Delta V\,\frac{dT}{dV} \tag{3.6b}$$

where

$$D(\lambda) = 2k\,\frac{dn}{dk} + k^2\,\frac{d^2n}{dk^2} = \lambda^2\,\frac{d^2n}{d\lambda^2} \tag{3.7}$$

is the material dispersion of the bulk material from which the fiber is made, and $V(dT/dV)$ is the waveguide dispersion, and depends only on the geometry of the guide. The total dispersion can then be expressed as a combination of material and waveguide dispersions:

$$t = t_m + n\Delta\,t_w \tag{3.8}$$

in reference [3] the complete expression for t is derived (i.e., the derivative with respect to k of eqn. (3.2)) where it is shown that profile dispersion, i.e., terms with coefficient $d\Delta/dk$, are small and can be neglected. In the Appendix we compare eqn.(3.8) to the numerical derivative $kd^2\bar{\beta}/dk^2$, with $\bar{\beta}$ given by eqn.(2.39), over a range of wavelengths. The results are given in figure 3.12. We find eqn. (3.6) to be an excellent approximation to the intra-modal dispersion of a fiber.

3. Material Dispersion

In this section we will investigate the variation of the refractive index, profile height, and material dispersion with respect to wavelength. Throughout this thesis we consider an optical fiber in which the refractive index of the cladding, $n_{c\ell}$, is composed of pure silica, and the refractive index of the core, n_{co}, is composed of GeO_2 doped silica. We find that there is a linear relation between n_{co} and the amount (molar percent, m) of GeO_2 for any given wavelength. Throughout this work we will be mainly concerned with the wavelength range $0.5\ \mu m < \lambda < 1.5\ \mu m$.

The experimental variation of refractive index with wavelength can be fitted to a three term Sellmeir dispersion relation of the form

$$n^2 = 1 + \sum_{i=1}^{3} \frac{A_i}{B_i} \qquad B_i = 1 - \ell_i^2/\lambda^2 \tag{3.9}$$

where A_i are constants related to material oscillator strengths and ℓ_i are the oscillator wavelengths. The dispersion can then be found by direct differentiation:

$$\lambda \frac{dn}{d\lambda} = -\frac{\lambda}{n} \sum_{i=1}^{3} \frac{A_i}{B_i^2} \frac{\ell_i^2}{\lambda^3} \tag{3.10a}$$

$$\lambda^2 \frac{d^2n}{d\lambda^2} = \frac{\lambda^2}{n} \left[4 \sum_{i=1}^{3} \frac{A_i}{B_i^3} \frac{\ell_i^4}{\lambda^6} + 3 \sum_{i=1}^{3} \frac{A_i}{B_i^2} \frac{\ell_i^2}{\lambda^4} - \left(\frac{1}{n} \sum_{i=1}^{3} \frac{A_i}{B_i^2} \frac{\ell_i^2}{\lambda^3}\right)^2\right] \tag{3.10b}$$

We use the experimental results of reference [4], in which the values of A_i and ℓ_i are determined for 5 different amounts of GeO_2, including the pure silica case. We define the quantity m to be the molar percent of GeO_2 dopant in the core, and consider m = 0%, 3.1%, 5.8% and 7.9%. Similar data is available for other dopants [5].

In figure 3.2 we use eqns.(3.9) and (3.10) and plot a) $n(\lambda)$, b) $\lambda\, dn/d\lambda$ and c) $\lambda^2\, dn/d\lambda^2$ against wavelength for the different m. In fig. 3.2(d) we plot n, against λ over a large range of wavelengths and find that the Sellmeir equation (3.9) breaks down for $\lambda \lesssim 0.3$ and $\lambda \geq 8.0$. We note that material dispersion (eqn.(3.7)) is zero at around $\lambda = 1.3\ \mu m$.

As mentioned previously, we consider fibers in which the cladding is considered to be pure silica (0 m% GeO_2). Thus the profile height is directly related to the amount of dopant in the core. In fig. 3.3 we plot a) Δ and b) $\lambda\, d\Delta/d\lambda$ against wavelength for different amounts of GeO_2 in the core. We note that fig. 3.2(b) and fig. 3.3(b) justify our approximation of eqn. (3.3) where terms of order $\Delta(k/n)(dn/dk)$ and $k(d\Delta/dk)$ are neglected.

In fig. 3.4 we plot a) n and b) $D(\lambda) = \lambda^2\, d^2n/d\lambda^2$ against the amount of GeO_2 for several values of wavelength. The experimental points are from ref. [4] For a wide range of wavelengths there is a linear relation between n, $D(\lambda)$ and the molar percent of GeO_2 dopant in the core. Thus we can write a simple linear relation to find the value of n, D and Δ at any wavelength λ and any molar percent m of GeO_2 :

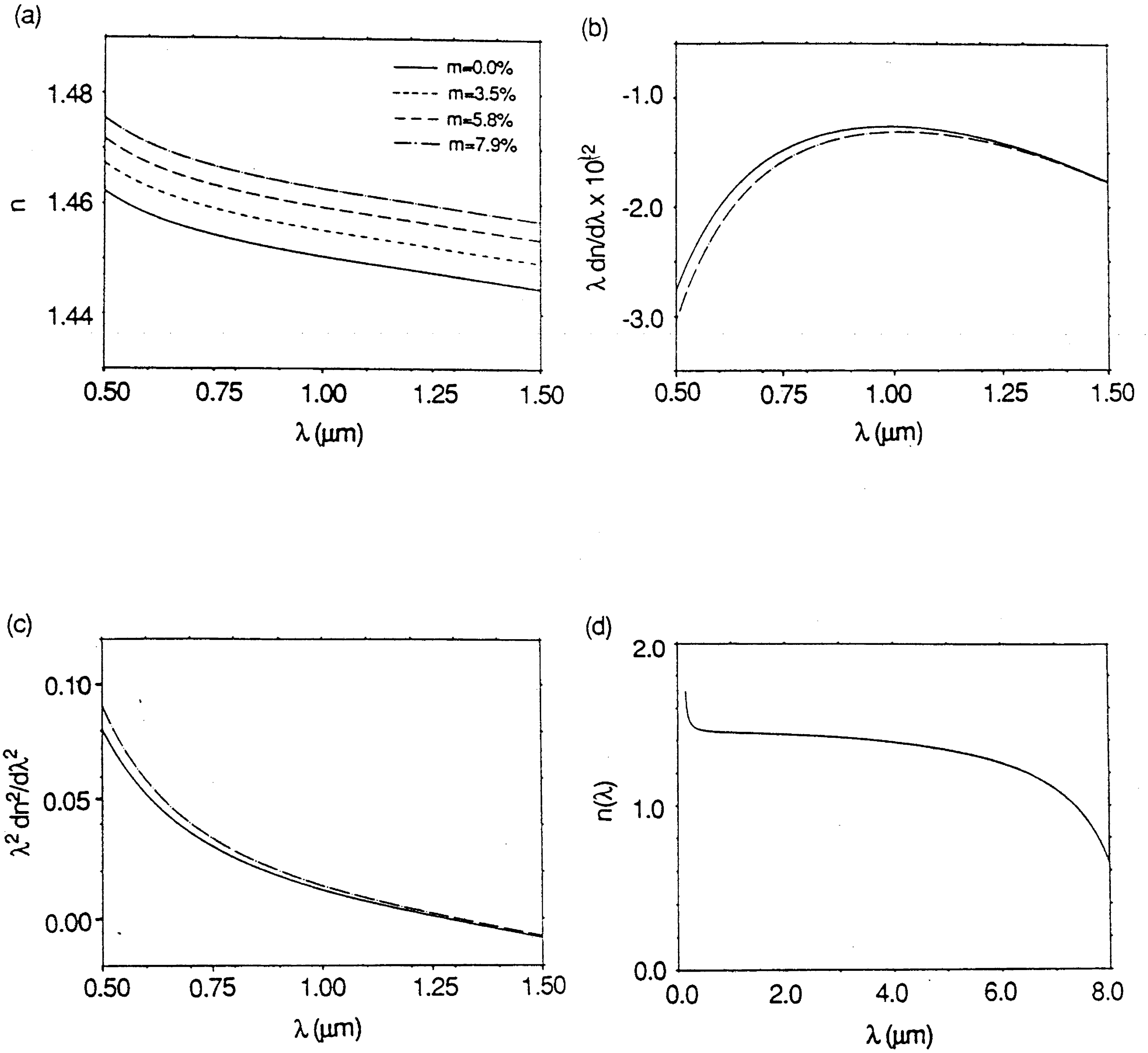

Fig. 3.2 Material dispersion data against wavelength for different concentrations of GeO_2 dopant.

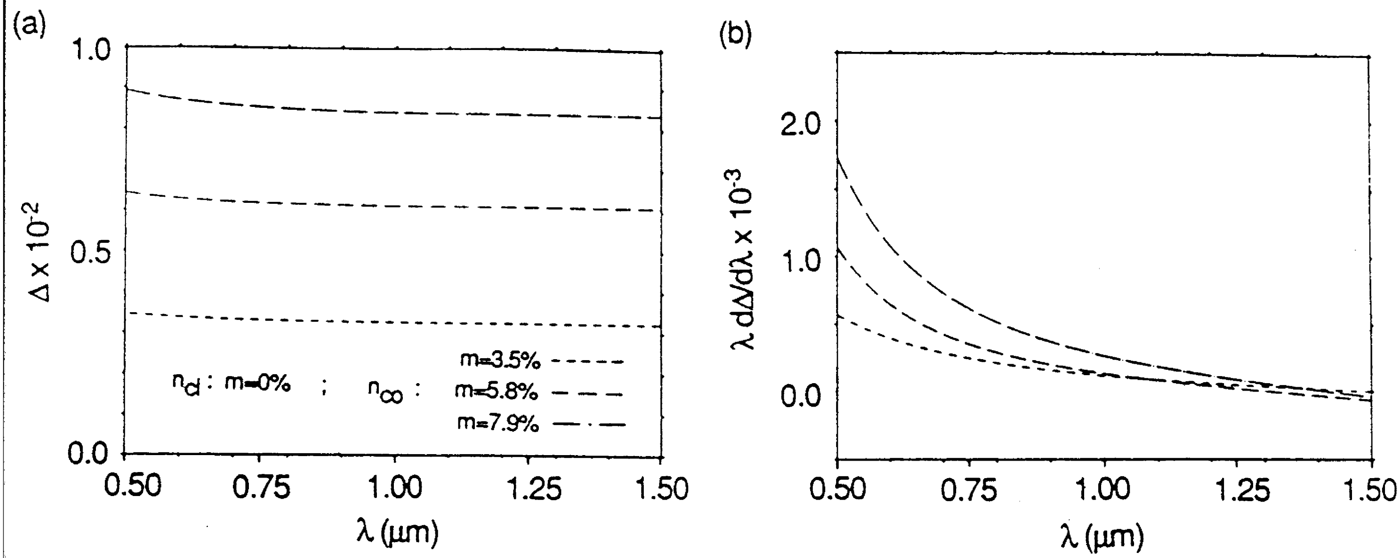

Fig. 3.3 Profile height against wavelength. The cladding is assumed pure silica (m = 0%) and the core has different concentrations of GeO_2 dopant.

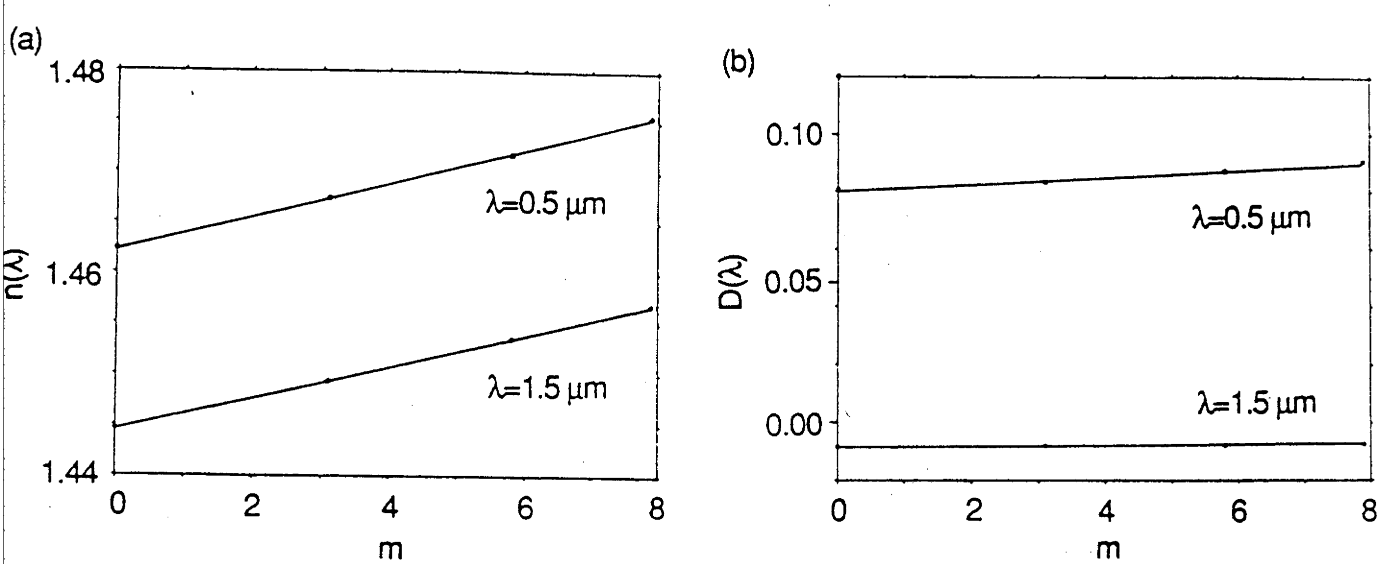

Fig. 3.4 Refractive index and dispersion against m, the amount of GeO_2 dopant in the core. The experimental points are from ref. [4].

$$n(\lambda,m) = n(\lambda,0) + \{n(\lambda,7.9) - n(\lambda,0)\}\ m/7.9 \tag{3.11a}$$

$$D(\lambda,m) = D(\lambda,0) + \{D(\lambda,7.9) - D(\lambda,0)\}\ m/7.9 \tag{3.11b}$$

and hence

$$\Delta(\lambda,m) = \frac{1}{2}\ \{1 - \frac{n^2(\lambda,0)}{n^2(\lambda,m)}\} \quad . \tag{3.11c}$$

Equations (3.11) are the basis for evaluating the theoretical results on four-photon mixing and mode propagation that will be presented later. In the Appendix we express our dimensionless dispersion $D(\lambda)$ in practical units.

4. Waveguide Dispersion

We are interested in the waveguide part of the intra-modal dispersion relation (3.8):

$$t_w = V \frac{d}{dV} \left(\frac{U^2}{V^2} - 2 \frac{U}{V} \frac{dU}{dV}\right) \tag{3.12}$$

For the singly clad step-profile fiber one can differentiate the eigenvalue equation (~~2.19~~ 2.24) with respect to V to obtain

$$\frac{dU}{dV} = \frac{U}{V} \left\{1 - \frac{K_\ell^2(W)}{K_{\ell-1}(W)\ K_{\ell+1}(W)}\right\} \quad . \tag{3.13}$$

After a great deal of algebra we find from eqn. (3.12)

$$t_W = 2\,\frac{U^2}{V^2}\left\{(1-2\kappa)\kappa + \frac{V^2}{W^2}\left(1-\frac{U^2}{V^2}(1-\kappa)\right)\times\right.$$
$$\left.\left(\left(\frac{WK_\ell(W)}{K_{\ell+1}(W)} + \frac{WK_\ell(W)}{K_{\ell-1}(W)}\right)(\kappa-1)+2\kappa\right)\right\} \qquad (3.14)$$

where

$$\kappa = \frac{K_\ell^2(W)}{K_{\ell-1}(W)\,K_{\ell+1}(W)}\,.$$

For the fundamental mode ($\ell=0$) eqn. (3.14) reduces to the result of reference [6]. Usually, only the waveguide dispersion of the fundamental mode is important, because in few-mode fibers the inter-modal and material dispersion will dominate.

For the clad power-law profile and W-fiber the waveguide dispersion t_W is evaluated numerically, with eigenvalue U specified in Section 2-3. In fig. 3.5(a) the fundamental mode waveguide dispersion t_W is plotted against V for the clad power-law profile with several values of profile parameter q. ($q = \infty$ is the step-profile, given by eqn. (3.14)), and in fig. 3.5(b) we plot t_W against q for a fixed value of V = 2.2.

In figure 3.6 we consider the fundamental mode t_W for the W-fiber. Fig. 3.6(a) is a plot of t_W against V for several values of radius ratio Q and fixed profile ratio P = 0.5 (refer to Section 2-3(c) for definitions of P and Q). Fig. 3.6(b) shows t_W against Q for several values of P and fixed V = 2.2. As mentioned earlier, variation of V is really a variation in wavelength, so one may expect the profile ratio P to change with a change in λ. However, as fig. 3.4(b) shows, the variation in the difference between any two Δ's is negligibly small, so the ratio P is effectively a constant.

In Section 3-6 we examine the intra-modal dispersion in the wavelength region where t_m is very small, so that t_w plays a major role in determing the zero-dispersion wavelength.

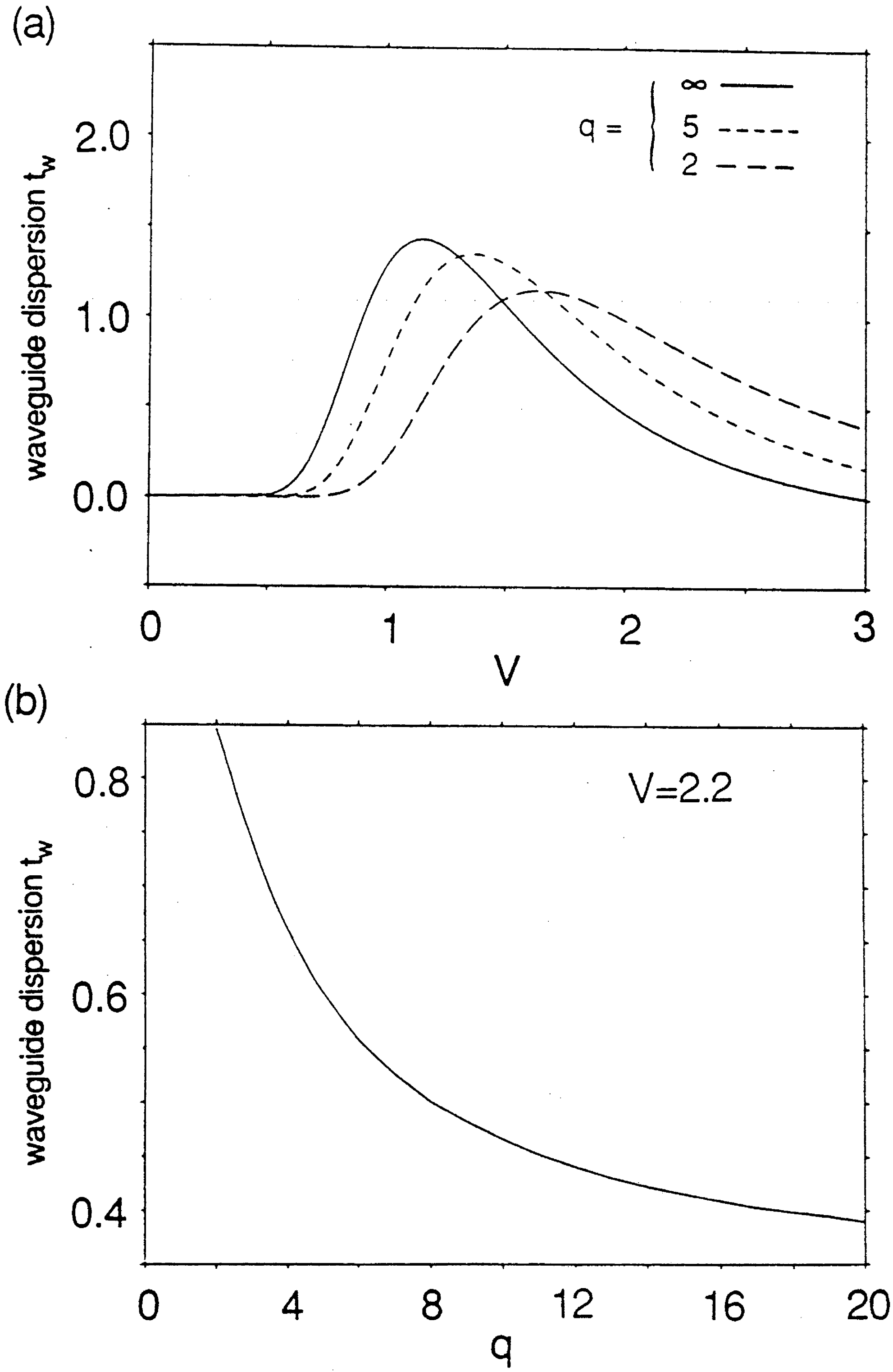

Fig. 3.5 Waveguide dispersion of the fundamental mode for the clad power-law profile. (a) t_w vs. V for different q ($q = \infty$ is the step-profile); and (b) t_w vs. q for a fixed $V = 2.2$.

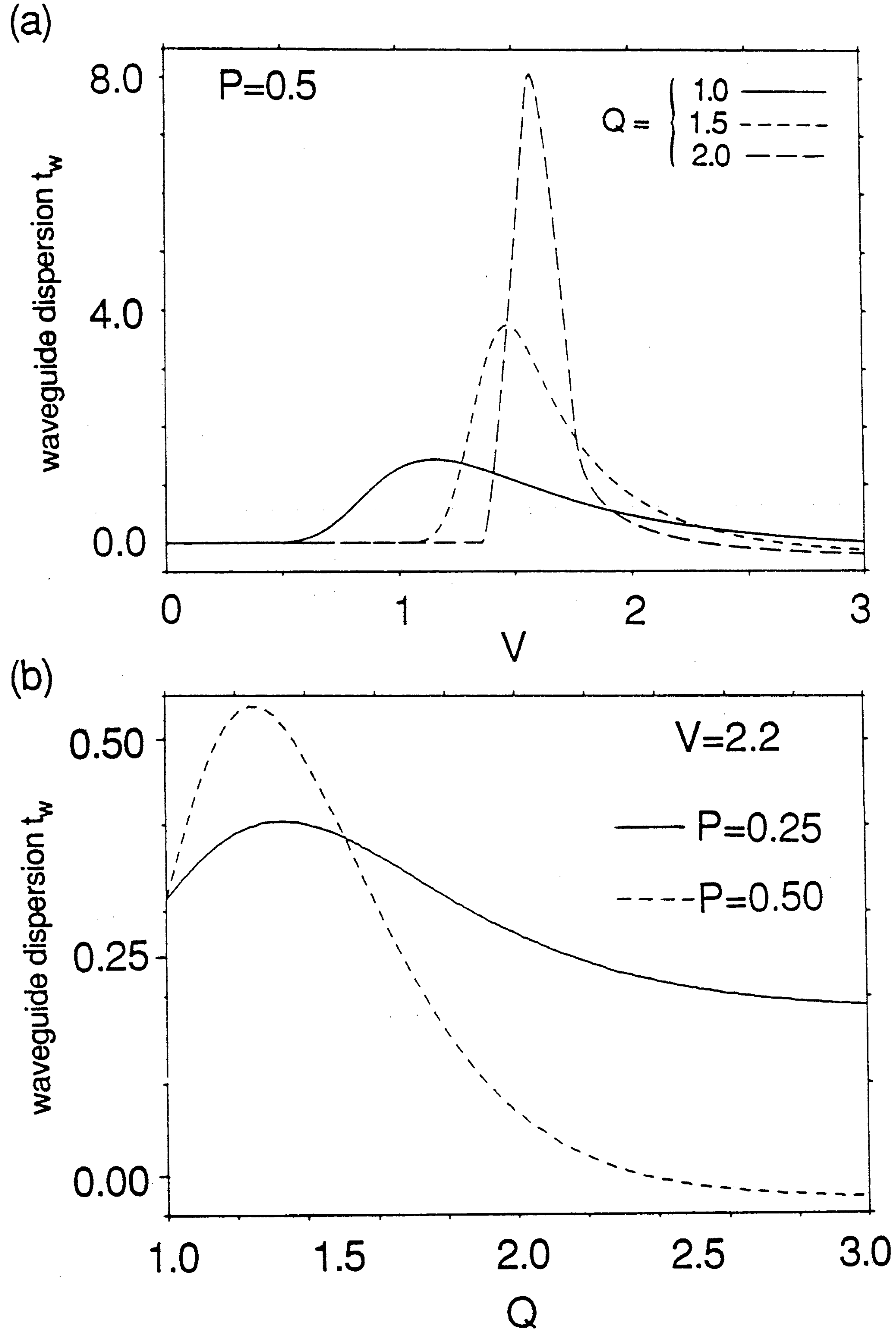

Fig. 3.6 Waveguide dispersion of the fundamental mode for the W-fiber. (a) t_w vs. V for a fixed P and different radius ratio Q; and (b) t_w vs. Q for a fixed V = 2.2 and several values of P.

5. Modal Group delay

We now consider the few mode case in which inter-modal dispersion is the major cause of pulse spreading. Inter-modal dispersion is the difference in group delays of the modes. For the step-profile fiber the modal group delay is

$$T_{\ell m} = \frac{U^2}{V^2} \left(2 \frac{K_\ell^2(W)}{K_{\ell-1}(W)\ K_{\ell+1}(W)} - 1\right) \tag{3.15}$$

where we have substituted eqn. (3.13) into eqn. (3.5). For the clad power-law profile and W-fiber eqn. (3.5) is evaluated numerically.

In figure 3.7 we plot T for the first five modes against normalized frequency V. Figure 3.8(a) is a plot of T against V for the clad-power law profile for several values of q, and fig. 3.8(b) is a plot of T against q for several values of V.

In figure 3.9 we consider the W-fiber, and in (a) we plot T against V for a fixed Q and several values of P, while in (b) we plot T against Q for fixed P and several values of V.

In Chapter 5 we shall see that the difference in modal group delay is the key to phase matching the stimulated four-photon mixing process on few mode optical fibers, and understanding experimental results.

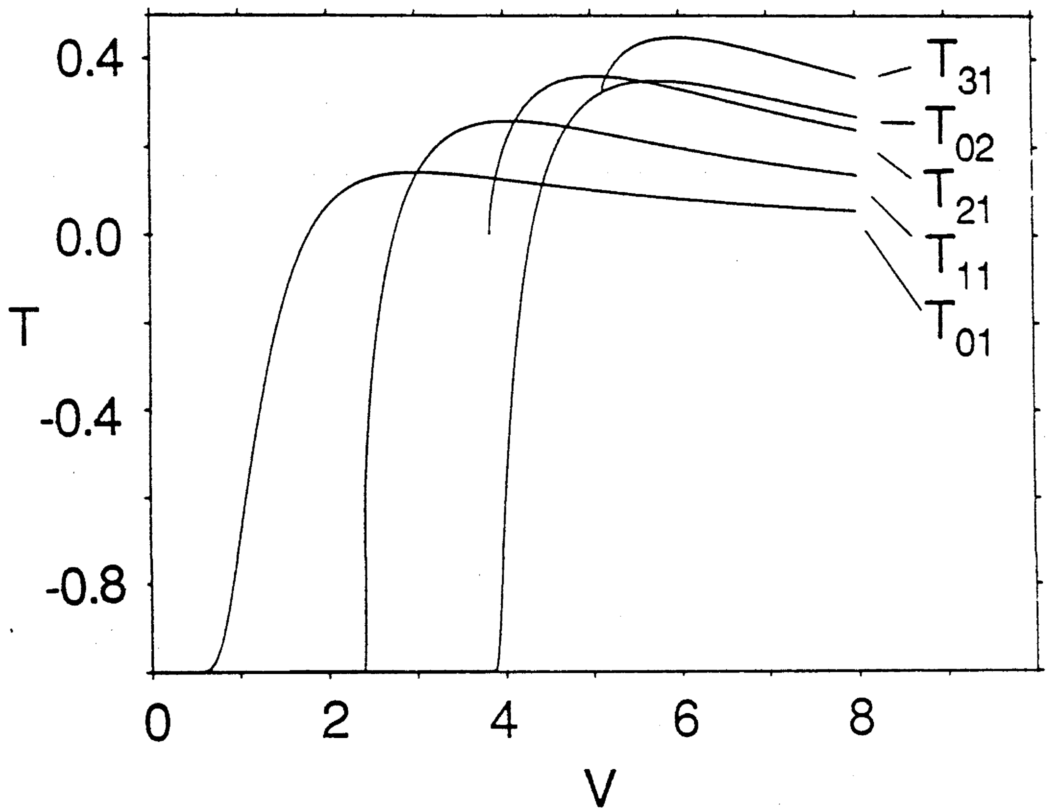

Fig. 3.7 The modal group delay of a step-index fiber against V.

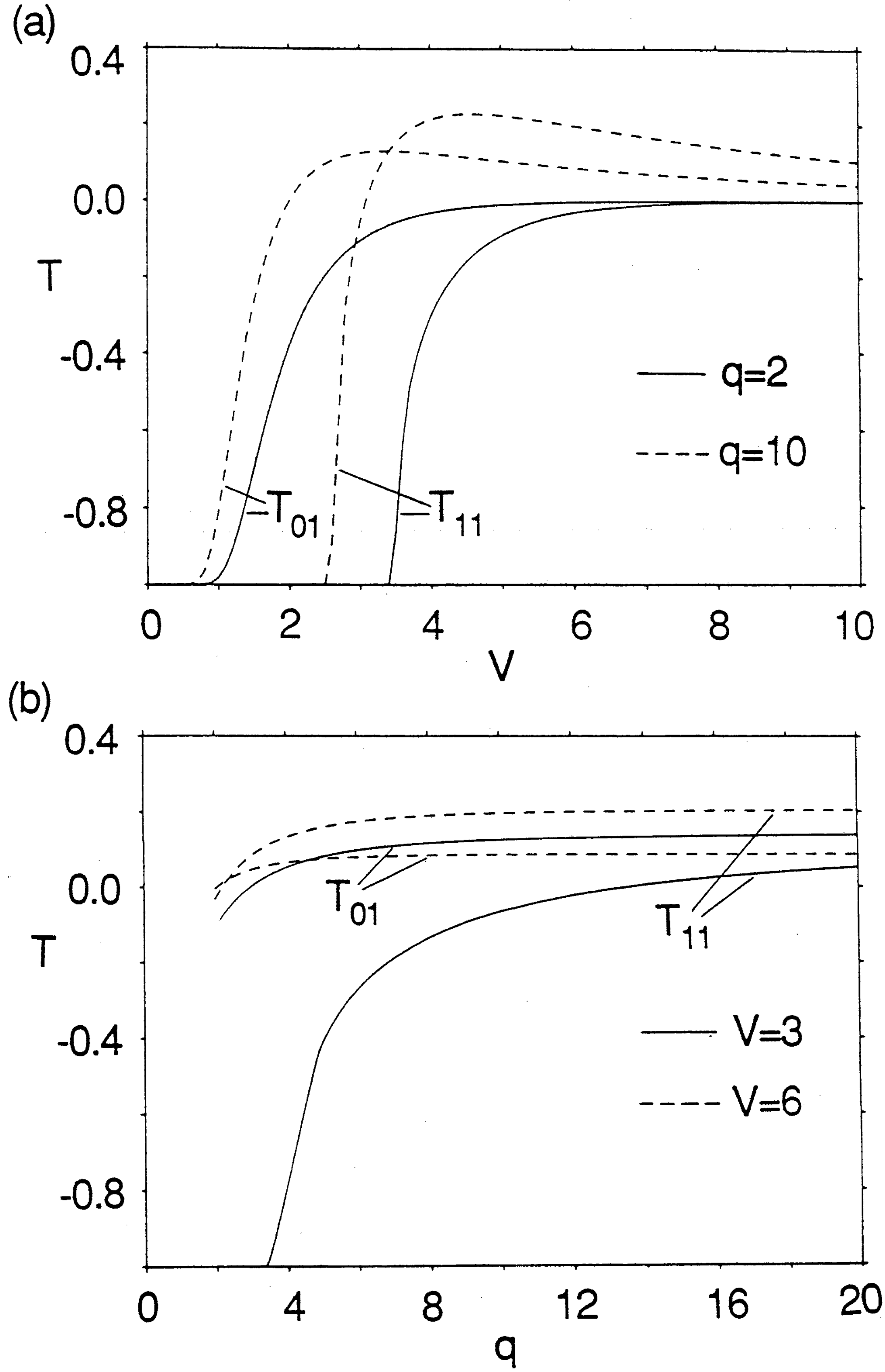

Fig. 3.8 Modal group delay for the clad power-law profile. (a) T vs. V for different q; and (b) T vs. q for different V.

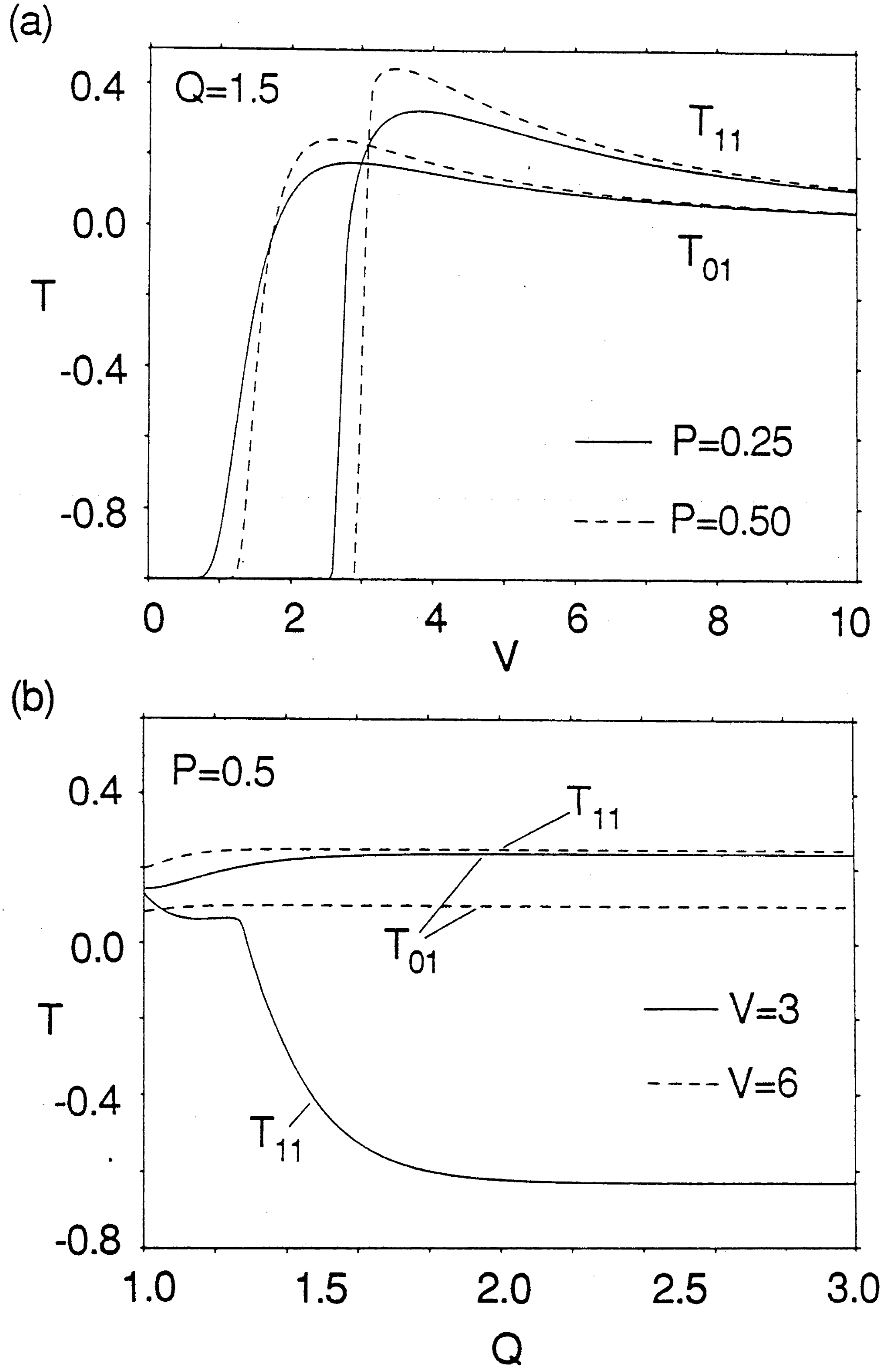

Fig. 3.9 Modal group delay for the W-fiber. (a) T vs. V for different P and fixed Q; and (b) T vs. Q for different V and fixed P.

6. The Zero-Dispersion Wavelength

In Chapter 5 we will see that phase-matching the stimulated four-photon mixing process on single mode fibers depends critically on the zero-dispersion wavelength. In this Section we review the concepts and basic design considerations for achieving zero-dispersion operation on optical fibers.

In Sections 3-3 and 3-4 we looked at material and waveguide dispersion seperately. In this section we examine the total intra-modal dispersion (i.e. eqn. (3.6)) for a single mode fiber in the region where material dispersion t_m is small and the dominant effect is the waveguide dispersion. We consider some specific examples.

In figure 3.10 we give a typical loss curve for a Germanium doped core optical fiber. The peak at $\lambda = 1.4$ μm is due to ~~water~~ OH ions. Thus a fundamental design principle is to operate at longer wavelengths to reduce losses, but avoid the OH peaks. 1.3 μm and 1.55 μm are ideal operating wavelengths.

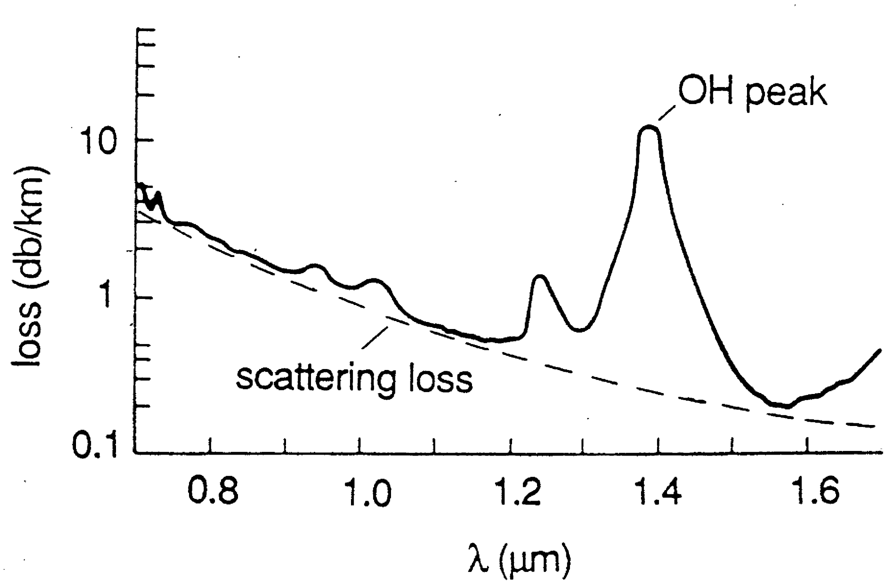

Fig. 3.10 Typical loss curve for a GeO_2-doped silica fiber.

As shown in fig. 3.2(c) material dispersion is zero near 1.3μm , and waveguide dispersion will dictate at which wavelength the total dispersion is zero. When using optical fibers we want minimum loss and dispersion, so one must design a fiber that will have zero dispersion at either 1.3 μm or 1.55 μm .

(a) Singly-Clad Fibers

We require total dispersion, eqn. (3.6), to be zero at some specified wavelength λ_{zd}, so that $\beta''(V) = 0$, where the prime means differentiation with respect to k, and V contains all material and waveguide information. We now consider only the clad power-law profile. If we specify the molar percent of GeO_2 in the core, m, and the wavelength λ_{zd} at which total zero-dispersion is wanted, then the only waveguide variables will be profile shape, q, and core radius, ρ :

$$\bar{\beta}''(m,\lambda_{zd};\ q,\rho_{zd}) = 0 \tag{3.16}$$

If q is specified, then ρ_{zd} , which is the core radius at which $\beta'' = 0$, can be determined by the numerical zero-finding procedure outlined in the Appendix of Chapter 2. $V_{zd} = V(m,\lambda_{zd},\rho_{zd})$ is then also determined.

In fig. 3.11(a) we consider a step-profile fiber and show the variation of V_{zd} with respect to zero-dispersion wavelength λ_{zd} , for several concentration of GeO_2 dopant. (m and λ_{zd} specify n_{co} and Δ , and eqn (3.16) then gives ρ_{zd} and hence V_{zd}). The fiber is multimoded in the shaded region. In fig. 3.11(b) we show variation of V_{zd} with λ_{zd} for a fixed m = 2.0% and several values of q.

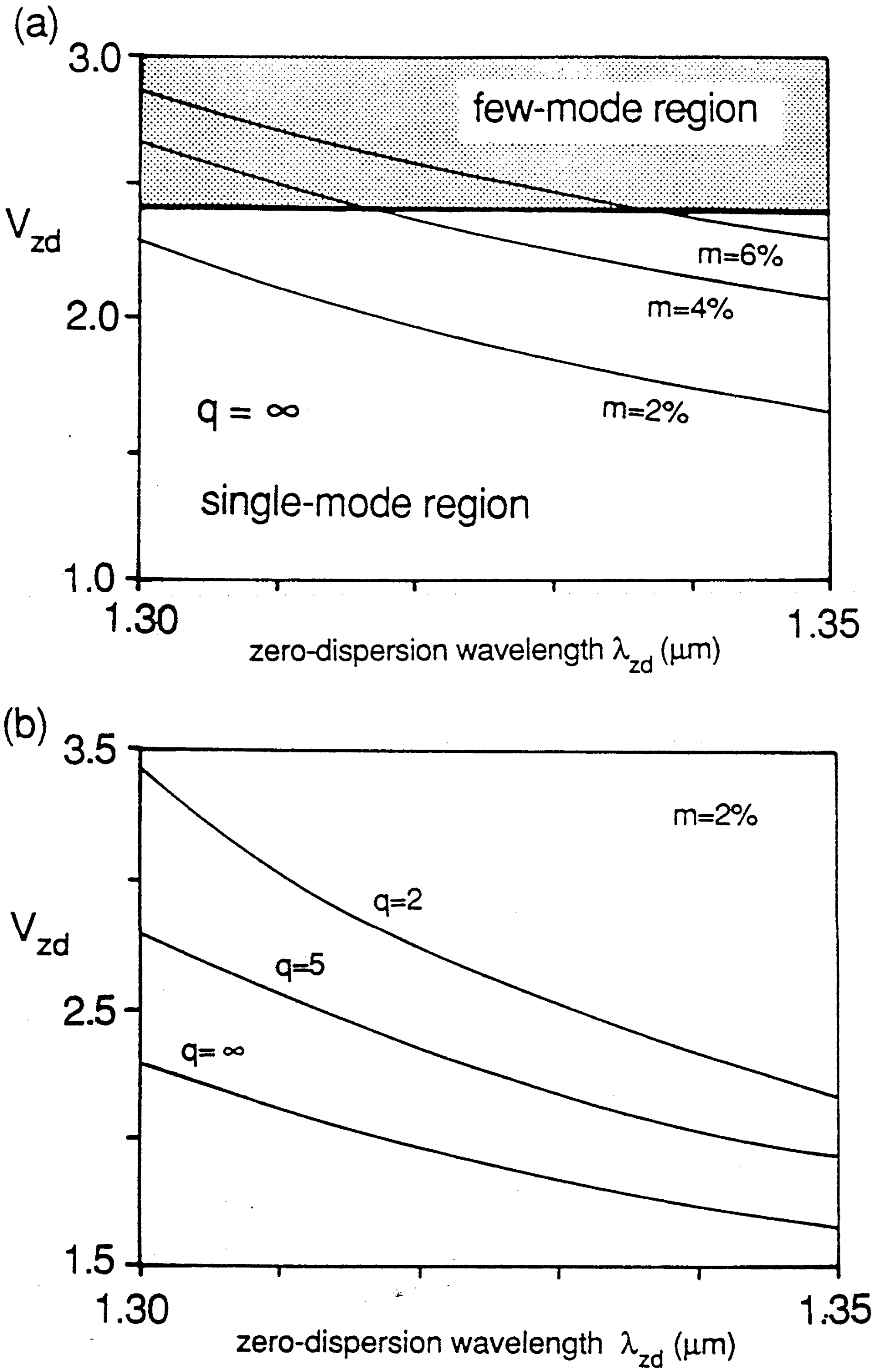

Fig. 3.11 The V value, V_{zd}, for which a clad power-law profile has zero dispersion for some wavelength, λ_{zd} . (a) A step-profile fiber with m = 2, 4 and 6 molar percent of GeO_2 . The corresponding values for the profile height are Δ = 0.0021, 0.0043 and 0.0064 respectively. The shaded region is V > 2.405 where the fiber is multimoded. (b) V_{zd} for different values of grading parameter q, and m = 2%.

In figure 3.12 we plot the material, waveguide and total dispersion of a step-index fiber against λ over the range $1.1\ \mu m < \lambda < 1.9\ \mu m$.

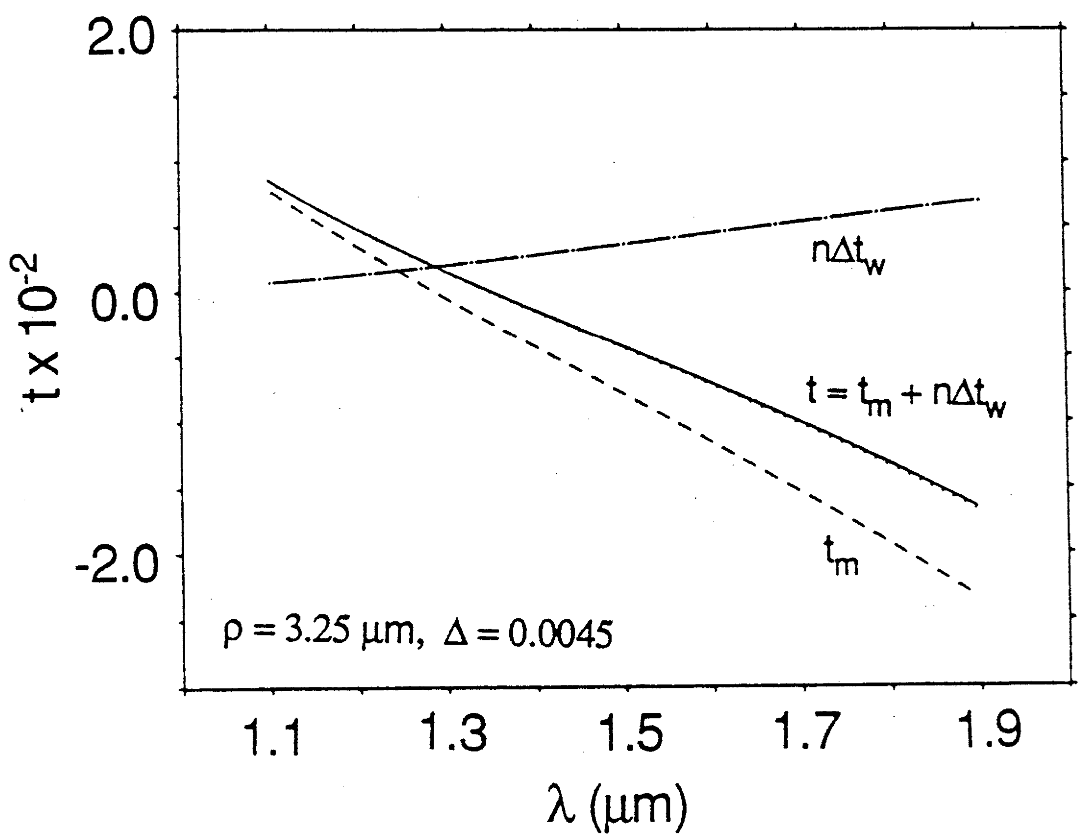

Fig. 3.12 The material, waveguide and total dispersion, t, of a step-index fiber with parameters $\rho = 3.25\ \mu m$ and $\Delta = 0.0045$. The dotted line is the numerical derivative $k\ d^2\bar{\beta}/dk^2$, demonstrating the accuracy of the approximation eqn. (3.8).

(b) Doubly-Clad Fibers

It is relatively easy then to design a fiber that will be single-moded and dispersionless in the 1.3 μm region. As shown in figure 3.10, if we want even lower losses then we must operate at 1.55 μm . To achieve efficient light transmission at this wavelength a more advanced design fiber is favourable.

In figure 3.13 we consider a W-fiber with various values of P, Q ρ and Δ (refer to Section 2-3(c) for definitions), and plot the total disperion t against wavelength λ . We note that there may be several zero-dispersion wavelengths for some W-fibers. Thus, with the correct design parameters, one can have single-mode W-fibers operating over a large range of low-loss zero-dispersion wavelengths.

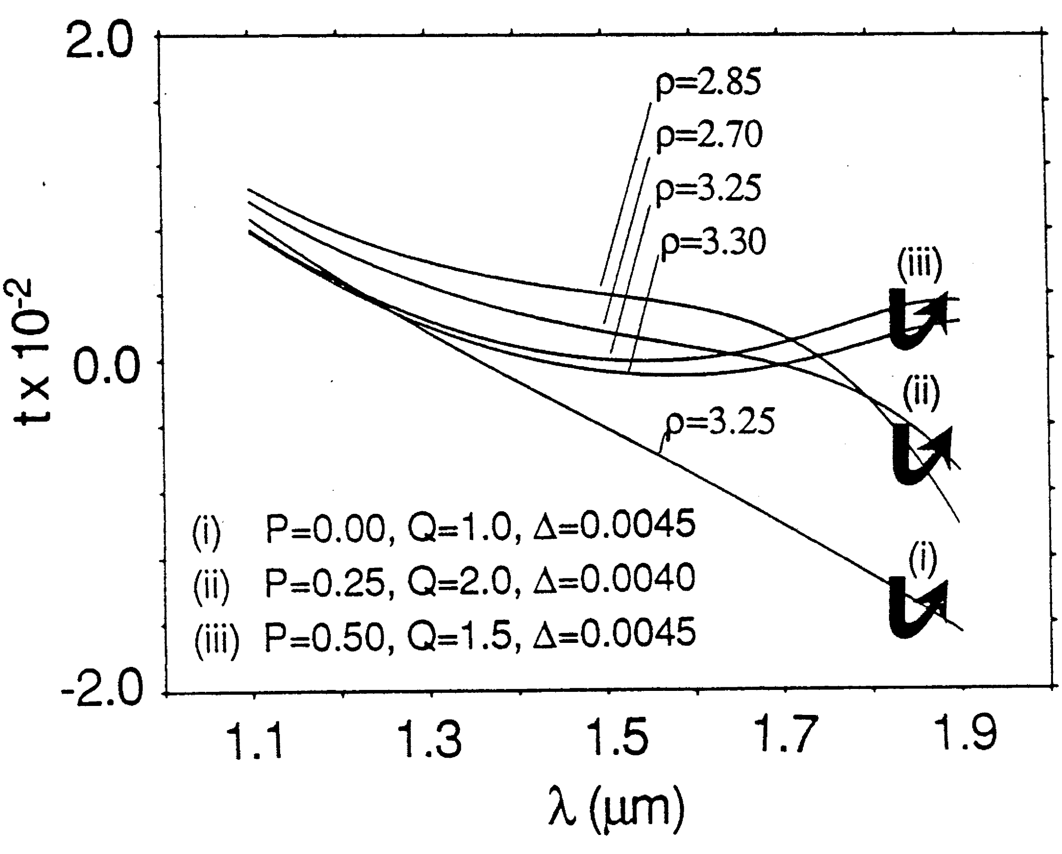

Fig. 3.13 The total dispersion t for a W-fiber with various fiber parameters P, Q and ρ . Profile heights are Δ = 0.0040 (m = 3.8%) and Δ = 0.0045 (m = 4.2%) .

7. Single-Mode Fibers Operating at Few-Mode Wavelengths*

Most single-mode fibers are designed to be used at wavelengths near 1.3 μm , where we have seen loss and total dispersion are small. Thus it is necessary to use sources that emit light near 1.3 μm to take advantage of these fiber properties.

However, in applications such as local area networks where transmission is required over relatively short distances and large numbers of sources and detectors may be needed, the high cost of these long-wavelength sources may not be justifiable. For such applications, a combination of readily available fibers designed for 1.3 μm and sources operating at 0.85 μm may be attractive, provided that adequate performance can be achieved.

From our previous results it is obvious that when wavelength is reduced both loss and dispersion will increase due to material properties of the fiber. However, a system using such a combination would no longer be single-moded, and so the performance may be further degraded. In reference [7], the consequences of having the second mode propagate on fiber loss, dispersion and modal noise are examined, and these factors are used to predict performance limits for a two-mode fiber system operating at 0.85 μm . Here we examine the effect on inter- and intra-modal dispersion.

As an example we consider a singly-clad step-index fiber that has zero-dispersion at $\lambda = 1.32$ μm . If m=3.0%, the fiber parameters are $\rho = 4.0$ μm and $\Delta = 0.0032$ so that $V = 2.21$. In fig. 3.14(a) we plot the total dispersion t, and component material and waveguide dispersions t_m and t_w, of the fundamental mode against λ over the range $0.85\,\mu m < \lambda < 1.32\,\mu m$.

* This section forms part of reference [7]

At 0.85 μm $V = 3.465$ and t is completely dominated by material dispersion.

At $\lambda = 1.32$μm only the single mode propagates, but at $\lambda = 0.85$ μm the fiber is bi-modal. In fig. 3.14(b) we plot t, t_m, and t_w for the $\ell = 1$ mode. The waveguide dispersion for the LP_{11} mode is a factor of 10 greater than the waveguide dispersion for the LP_{01}, but material dispersion still dominates at the shorter wavelength. Fig. 3.14(c) is a comparison of the two waveguide dispersions. The LP_{11} mode becomes very large near cut-off, but in this region the mode is only weakly bound and rapidly radiates away where fiber imperfections are present as in practice.

In fig. 3.14(d) we plot the group delays (eqn. (3.15)) of the two modes against wavelength. The inter-modal dispersion is the difference δT between the two group delays, and we note that this is zero near $V = 3.0$ ($\lambda = 0.98$ μm) .

In conclusion, when a fiber designed for zero-dispersion single-mode operation at 1.3 μm is operated at 0.85 μm , it becomes bi-modal and thus inter-modal dispersion is introduced into the system. Nonetheless, with the right parameters, (and grading considerations) this could be made zero at 0.85 μm . On the other hand, it has been shown that in this close-to-cut off region the LP_{11} is very sensitive to applied pressure and slight bends, and can be easily eliminated [8]. Thus inter-modal dispersion should not be a major course of degradation to the system. However, at wavelengths of 0.85 μm the intra-modal dispersion will be dominated by material dispersion, leading to pulse spreading, and this will degrade the performance (i.e., bit-rate $\times$ length of fiber) of the system.

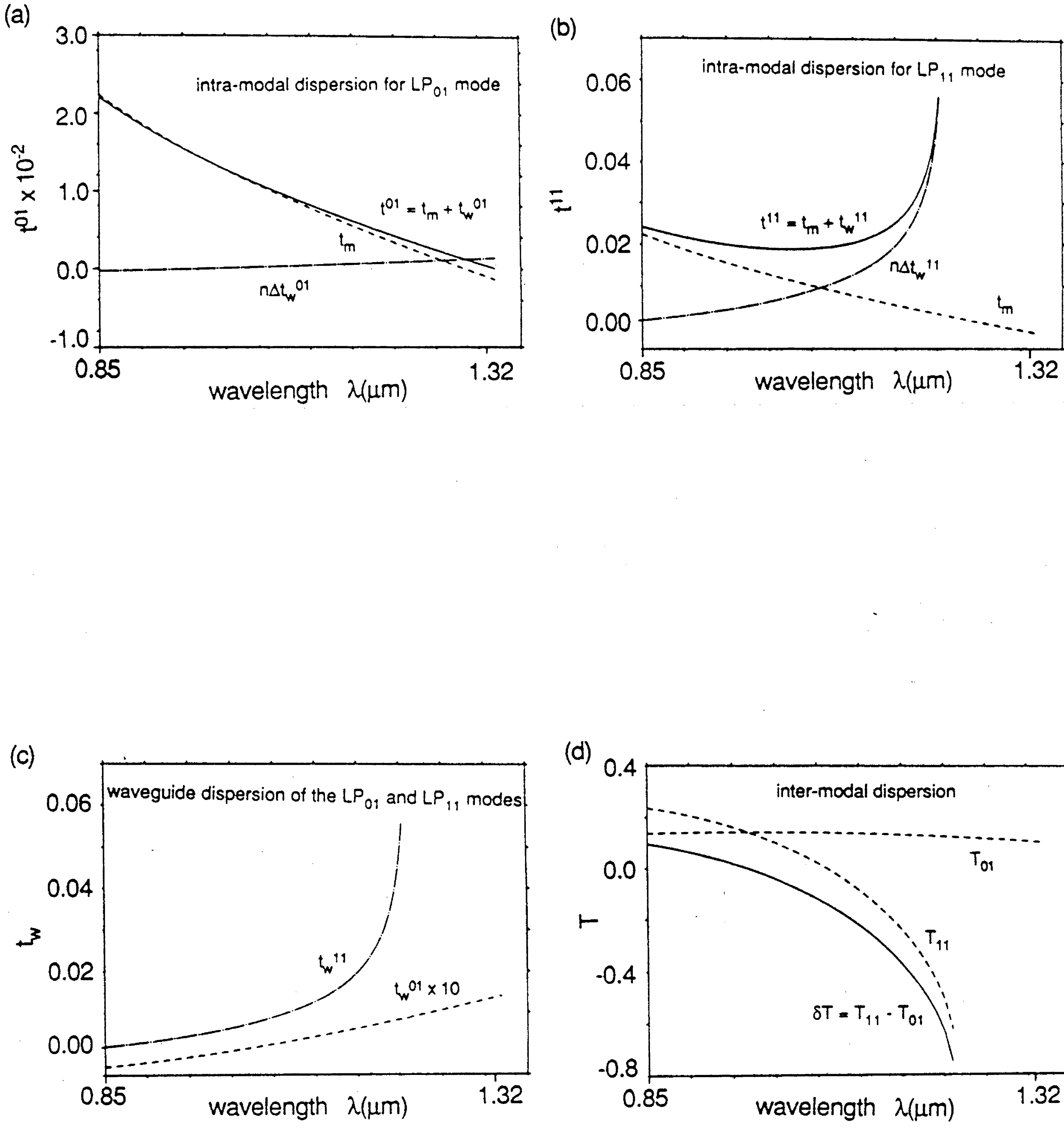

Fig. 3.14 Intra- and inter-modal dispersion curves for a step-index fiber designed to have zero-dispersion at λ_{zd} = 1.32 μm but operating at λ = 0.85 μm .

Appendix

(i) **Practical units for dispersion**

The arrival time of a light pulse transmitted through a fiber of length L due to material dispersion alone is [9]

$$\bar{\tau} = L \frac{d\bar{\beta}}{dw} = \frac{L}{c}\,\tau$$

where τ is our dimensional parameter and is given by eqn. (3.3). $\bar{\tau}/L$ usually has units [ns/km]

The pulse spread per unit length due to a small spread $\delta\lambda$ in the source is

$$\delta\bar{t} = (\bar{t}/L).\delta\lambda, \qquad \bar{t} = d\bar{\tau}/d\lambda$$

where $\bar{t}$ is usually expressed in units of [ps/km.nm]. In terms of our dimensionless dispersion t (eqn. (3.6)) this practical quantity can be expressed as

$$\bar{t} = -\frac{1}{c}\,t/\lambda \quad [\rho s/km.nm] \tag{3A.1}$$

where $c = 3 \times 10^{-7}$ [km/ps] and λ is expressed in [nm].

(ii) **Comparison of exact and approximate results**

In figure 3.12 we compare the approximate dispersion relation eqn.(3.6), which consists of seperate modal and material contributions, with the numerical derivative $t = kd^2\bar{\beta}/dk^2$, where $\bar{\beta}$ is given by eqn.(2.39). The derivative of $\bar{\beta}$ involves using the Sellmeir equation, as well as the modal eigenvalues as a function of V. We observe that eqn. (3.6) is an excellent approximation over a large range of wavelengths, including the intricate zero-dispersion region.

References for Chapter 3

[1] See reference [2-4]

[2] K.F. Barrel, D.J. Carpenter and C. Pask, "Interpretation of optical-fibre base band frequency measurements"
Microwaves, Opt. Acoust., 2, pp. 41-44 (1978)

[3] W.A. Gambling, H. Matsumura and C.M. Ragdale, "Mode dispersion, material dispersion and profile dispersion in graded-index single-mode fibres"
Microwaves, Opt. Acoust., 3, pp. 239-246 (1979)

[4] S. Kobayashi, S. Shibata, N. Shibata and T Izawa, "Refractive-index dispersion of doped fused silica" in Proceedings of first International Conference on Integrated Optics and Optical Fiber Communication (Institute of Electrical Engineers of Japan, Tokyo, 1977)

[5] J.W. Fleming, "Material dispersion in lightguide glasses"
Electron. Letters, 14, pp. 326-328 (1978)

[6] See reference [2-1], p. 313. Waveguide dispersion is given by the distortion parameter $\tilde{D}$. Our waveguide dispersion is $t_w = 2V\tilde{D}$.

[7] S.J. Garth, C. Pask and R.A. Sammut, "Single-mode fibres operating at few-mode wavelengths"
To be published

[8] W.A. Gambling, H. Matsumura and C.M. Ragdale, "Zero-mode dispersion in single mode fibres"
Electron. Letters, 14, pp. 618-620 (1978)

[9] D. Gloge, E.A.J. Marcatili, D. Marcuse and S.D. Personick, "Dispersion Properties of Fibers"
in Optical Fiber Telecommunication, S.E. Miller and A.G. Chynoweth, eds (Academic, New York, 1979).

CHAPTER 4

THE STIMULATED FOUR-PHOTON MIXING PROCESS

CHAPTER 4

THE STIMULATED FOUR-PHOTON MIXING PROCESS

1. Introduction

The theory of electromagnetic wave propagation in optical fibers outlined in Chapter 2 is based on the assumption that there is a linear relation between the electric displacement $\tilde{D}$ and the electric field $\tilde{E}$ (see eqn. (2.4)). In reality the relationship between $\tilde{D}$ and $\tilde{E}$ is a non-linear one, and new optical effects become apparent.

One important feature of this non-linear dependence is the creation of new waves with different frequencies from the incident wave. In this work we are concerned with such a process; one in which two frequencies, one of a higher frequency and the other of a lower frequency than the pump, are fed by the pump wave and are amplified from the noise. This is a stimulated parametric process. In this work we are only concerned with the parametric process of stimulated four-photon mixing.

Non-linear optical effects occur in media when the intensity of light is greater than some threshold value. Because optical fibers have small cross-sections it requires only comparatively small power levels to maintain high intensities over long distances and many non-linear processes have been observed (see [1] for a review). Among these processes are stimulated Raman and Brillouin scattering, self-phase modulation, light-induced refractive index changes and parametric four-photon mixing.

These non-linear effects can be detrimental to communication fibers, and present power transmission limitations [2]. In optical signal transmission frequency conversion can lead to signal loss and signal distortion, as well as cross-talk in wavelength multi-plexed optical fiber systems.

On the other hand, these same effects are potentially useful in fiber-optical amplifiers, oscillators, and modulators [3], and also for investigations of the fiber itself [4]. We are concerned with phase-matching the stimulated four-photon mixing process in order to investigate such fiber characteristics as dispersion and mode properties on perturbed optical fibers.

Four-photon mixing, or three-wave mixing, is the process whereby waves of one frequency combine with waves of a second frequency to produce waves of a third frequency. In stimulated four-photon mixing two photons of one frequency, called the pump frequency, generate photons of higher and lower frequencies, called anti-Stokes and Stokes frequencies respectively. The difference in frequency between the anti-Stokes and pump waves is equal to the difference in frequency between the pump and Stokes waves.

In order that light be efficiently converted to the new frequencies in these parametric processes it is necessary that they be phase-matched. This means that the sum of the wave-vectors involved in the process should equal zero, but because of material dispersion this condition is not automatically satisfied. In Chapter 5 we show that by using various techniques phase-matching can be achieved on single- and few-mode fibers.

We first of all discuss some of the non-linear effects that occur in optical fibers, and introduce the non-linear polarization. We also show that this gives an intensity dependent refractive index. However, because only low intensities are necessary in fibers we will not be concerned with changes to the refractive index due to the non-linear presence.

We then turn to the theory of stimulated four-photon mixing itself, and present a simplified derivation of the coupled wave equations based on the analysis of reference [5]. Solution of the coupled wave equations give expressions for the gain and conversion efficiency of these new frequencies.

The gain is proportional to an overlap integral that involves the modes that participate in the process, and in Section 4-5 we show how these overlap integrals depend on fiber characteristics by using a Gaussian approximation for single- and few-mode fibers. In the next Chapter we show that these overlap integrals impose symmetry restrictions on which modes may participate in the parametric process.

Non-linear optics is a well established branch of optics and there ~~their~~ are many text books on the subject [6-8]. The coupled wave equations describing the interaction of light waves in a non-linear dielectric are well known [6,9], and their application in describing stimulated four-photon mixing in few mode fibers can be found in reference [5]. The theory for three-wave mixing in a single-mode fiber has also been worked out [10].

The first comprehensive study of non-linear optical effects due to the polarization third order in the electric field strength can be found in reference [11]. These effects have been investigated for the case of optical fibers in many review articles [1,3,4,12].

The overlap integrals we use here are common to all non-linear processes on optical fibers that are characterized by the same order of non-linearity, and plots of these integrals against normalized frequency can be found for Gaussian fields [13] and exact weakly-guiding fields [14] for the single-mode case.

2. Non-linear Effects in Optical Fibers

Linear optics in isotropic media is described by assuming the electric susceptibility, χ, is a scalar (see eqn. (2.3)). Anisotropic media can be taken into account by representing χ as a tensor. This linear relation between the polarization and electric field implies that, with respect to an optical waveguide, the output frequency will be the same as the input frequency.

There are many optical effects in which new frequencies are generated from the input pump frequency, and these can only be described by assuming non-linear, or other more general relationships, between $\underset{\sim}{P}$ and $\underset{\sim}{E}$.

The theory of these non-linear effects is based on an expansion of the polarization $\underset{\sim}{P}$ in a general power series in the electric and magnetic fields and the spatial derivatives [6,7]. The polarization is then the linear term (eqn. (2.3)) plus a non-linear correction term, and we write the expansion as

$$\begin{aligned} \underset{\sim}{P} &= \underset{\sim}{P}^{L} + \underset{\sim}{P}^{NL} \\ &= \varepsilon_0 \chi_1 \underset{\sim}{E} + \varepsilon_0 \chi_2 \underset{\sim}{E}\,\underset{\sim}{E} + \varepsilon_0 \chi_3 \underset{\sim}{E}\,\underset{\sim}{E}\,\underset{\sim}{E} + \ldots \end{aligned} \tag{4.1}$$

where the χ's are tensors.

In an isotropic glass optical fiber the third rank tensor χ_2 is zero due to ~~symmettry~~ symmetry [1,5] and optical effects are due to the polarization third order in electric field strength;

$$\underset{\sim}{P}^{NL} = \varepsilon_0 \chi_3 (\underset{\sim}{E} \cdot \underset{\sim}{E}) \underset{\sim}{E} \quad . \tag{4.2}$$

* (See footnote)

The electric susceptibility may then be regarded as

$$\chi = \chi_1 + \chi_3 E^2 \tag{4.3}$$

and from eqn. (2.5) we have a non-linear correction to the refractive index;

$$\bar{n} \simeq n + n_2 E^2 \tag{4.4}$$

where $n_2 = \frac{1}{2} \chi_3 / n$

Before studying the four-photon mixing process in detail we briefly outline some of the non-linear processes that have been observed on optical fibers that are due to the polarization third-order in the electric field strength [11].

Three-wave mixing is a parametric process - incident photons from the laser at frequency ω_p mix with photons at a signal frequency ω_s to create new light waves at an idler frequency ω_a. Energy conservation requires that

$$\omega_a = \omega_p - \omega_s \quad .$$

* The electric susceptibility is a fourth-order tensor with 81 elements which, in general, are functions of four frequencies. Since glass is an isotropic material, symmetry restricts χ_3 to 21 non-zero elements of which only 3 are independent. Furthermore, if there is no Raman contribution to the susceptibility a further reduction to a single coefficient results. [10]

This is the same process as four-photon mixing where two photons at ω_p mix with ω_s to create new waves at ω_a :

$$\omega_a = 2\omega_p - \omega_s \quad .$$

Because the refractive index is a function of frequency there is a phase mismatch between the wave vectors

$$\Delta k = 2k_p - k_s - k_a$$

where $k_i = \omega_i n_i / c$. The above equation represents a momentum conservation law that must be satisfied along with energy conservation. As we shall see in the next section, the parametric processes will occur strongly when the phase-matched condition is satisfied; $\Delta k = 0$. In bulk material phase matching can be achieved by the use of birefringent crystals or by mixing the beams at an angle [7]. There are several ways to achieve phase-matching in optical fibers, as we shall detail in Chapter 5.

The third order susceptibility χ_3 is complex, giving an imaginary component to the non-linear refractive index (see eqn. (4.4)). The real part of χ_3 gives parametric amplification, while the imaginary part gives Raman and Brillouin amplification [5].

Raman scattering can be regarded as due to the mixing of the incident photon with a molecular vibration at ω_ν , leading to scattered light at

$$\omega_a = \omega_p - \omega_\nu$$

Brillouin scattering is similar; the incident light wave mixes with a thermally excited acoustic vibration.

The most important difference between Raman and Brillouin scattering and the parametric processes is that the former are automatically ~~require no~~ phase-matched.

Both the scattering and parametric processes involve the creation of up shifts as well as down shifts in frequency. The latter are called Stokes shifts; a photon of lower energy than the incident wave appears in the scattering light. When a photon of higher energy appears in the scattered light it is called an anti-Stokes shift.

The intensity dependent refractive index (see eqn. (4.4)) leads to self-phase modulation in optical fibers. The phase of a single optical pulse is retarded at the intensity peak with respect to the leading and trailing edges. This phase shift adds up in long fibers and can cause additional pulse changes, limiting the power capacity of single mode fibers.* Another effect due to the intensity dependent refractive index is the optical Kerr effect, in which a birefringence is induced by the incident field.†

We now examine the stimulated four-photon mixing process in detail. In the next Chapter we study phase-matching this process on single- and few-mode optical fibers.

---

* In fact when $k\, d^2\beta/dk^2 >$ (anomalous dispersion) the pulse-narrowing effect of the non-linear refractive index may add to this pulse-spreading to give a stationary pulse shape, called optical solitons. [A. Hasegawa and F. Tappert, Appl. Phys. Lett., 23, pp. 142-144 (1973)]

---

† When applied to pulses the term self-phase modulation encompasses both phase, or intensity-dependent refractive index, type effects and amplitude, or four-photon mixing effects. For a discussion see [C. Pask and A. Vatarescu, J. Opt. Soc. Am., B3, pp. 1018-1024 (1986)]

3. Theory of Stimulated Four-Photon Mixing

(a) Maxwell's Equations with a Non-Linear Polarization

If we express the polarization as $\underset{\sim}{P} = \underset{\sim}{P}_L + \underset{\sim}{P}_{NL}$, then we can write the displacement vector as (see eqn. (2.4))

$$\underset{\sim}{D} = \varepsilon_0 n^2 \underset{\sim}{E} + \underset{\sim}{P}_{NL} \tag{4.5}$$

and the second of eqns. (2.1) becomes

$$\underset{\sim}{\nabla} \times \underset{\sim}{H} = \varepsilon_0 n^2 \frac{\partial \underset{\sim}{E}}{\partial t} + \frac{\partial \underset{\sim}{P}_{NL}}{\partial t} \quad . \tag{4.6}$$

By taking the curl of the third of eqns. (2.1), substituting into eqn. (4.6) and using eqn. (4.2) we have

$$\nabla^2 \underset{\sim}{E} = \frac{n^2}{c^2} \frac{\partial^2 \underset{\sim}{E}}{\partial t^2} + \frac{\chi_3}{c^2} \frac{\partial^2 E^2 \underset{\sim}{E}}{\partial t^2} \quad . \tag{4.7}$$

The dielectric medium is considered to be lossless. So far we have not assumed an implicit time dependence, i.e.

$$\underset{\sim}{E} = \underset{\sim}{E}(r,\phi,z,t)$$

Following [5], the electric field is expanded in frequency and in terms of the waveguide transverse modes. It is assumed that the modes which are solutions of the transverse scalar wave equation (eqn. (2.11)) are not perturbed by the presence of the non-linear polarization. We write the electric field as

$$E(r,\phi,z,t) = \sum_{\nu,\ell} A_{\nu\ell}(z)\ \psi_\ell(r,\phi)\exp\{-i(\bar{\beta}_{\nu\ell}z - \omega_\nu t)\} \tag{4.8}$$

$$+ \text{c.c.}$$

where ν refers to the frequency, ℓ is the mode number, β is the propagation constant, and c.c. stands for complex conjugation. ψ_ℓ represents the transverse modal field, and in the weak-guidance limit is given by eqn. (2.20) and (2.21). The phase is given by

$$A_{\nu\ell} = |A_{\nu\ell}|\ e^{i\theta_{\nu\ell}} \quad . \tag{4.9}$$

We restrict our analysis to only four modes. We assume that the pump wave propagates in either or both of two modes which we label 1 and 2. The Stokes and anti-Stokes wave propagate in modes labelled s and a, respectively. The frequency index ν and mode index ℓ can then be replaced by the single index ℓ , and we write eqn. (4.8) as

$$E = A_1\psi_1 e^{i(\bar{\beta}_1 z - \omega_1 t)} + A_2\psi_2 e^{i(\bar{\beta}_2 z - \omega_2 t)}$$

$$+ A_a\psi_a e^{i(\bar{\beta}_a z - \omega_a t)} + A_s\psi_s e^{i(\bar{\beta}_s z - \omega_s t)} + \text{c.c.} \tag{4.10}$$

(b) The Coupled Wave Equations

The simulated four-photon mixing process occurs when

$$\omega_1 + \omega_2 = \omega_a + \omega_p \quad . \tag{4.11}$$

The wave propagates only in the z-direction, and we use the slowly varying envelope approximation

$$\frac{d^2A}{dz^2} << i\bar{\beta}\,\frac{dA}{dz} \quad .$$

Substituting eqn. (4.10) into the field equation (4.7), then for frequencies that satisfy eqn. (4.11) we have the following coupled wave equations

$$2i\bar{\beta}_1 \frac{dA_1}{dz}\psi_1 = -3\,\frac{\omega_1^2}{c^2}\,\chi_3(0)\left(A_1A_1^*A_1\psi_1^3 + 2A_1A_2^*A_2\psi_1\psi_2^2\right)$$

$$2i\bar{\beta}_2 \frac{dA_2}{dz}\psi_2 = -3\,\frac{\omega_2^2}{c^2}\,\chi_3(0)\left(A_2A_2^*A_2\psi_2^3 + 2A_2A_1^*A_1\psi_2\psi_1^2\right)$$

$$\begin{aligned} 2i\bar{\beta}_s \frac{dA_s}{dz}\psi_s &= -6\,\frac{\omega_s^2}{c^2}\,\chi_3(\Omega)\left(A_sA_1^*A_1\psi_s\psi_1^2 + A_sA_2^*A_2\psi_s\psi_2^2\right) \\ &\quad -6\,\frac{\omega_s^2}{c^2}\,\chi_3(\Omega)\;A_1A_2A_a^*\psi_1\psi_2\psi_a e^{i(\Delta kz)} \end{aligned} \tag{4.12}$$

$$\begin{aligned} 2i\bar{\beta}_a \frac{dA_a}{dz}\psi_a &= -6\,\frac{\omega_a^2}{c^2}\,\chi_3(\Omega)\left(A_aA_1^*A_1\psi_a\psi_1^2 + A_aA_2^*A_2\psi_a\psi_2^2\right) \\ &\quad -6\,\frac{\omega_a^2}{c^2}\,\chi_3(\Omega)\;A_1A_2A_s^*\psi_1\psi_2\psi_s e^{i(\Delta kz)} \end{aligned}$$

Ω is called the modulation frequency, or frequency shift, and is conventionally defined by

$$2\pi c\Omega = \omega_1 - \omega_S = \omega_a - \omega_2 \tag{4.13}$$

and has units [length]$^{-1}$.

Δk is called the phase mis-match

$$\Delta k(\Omega) = \bar{\beta}_a(\omega_a) + \bar{\beta}_S(\omega_S) - \bar{\beta}_1(\omega_1) - \bar{\beta}_2(\omega_2) \tag{4.14}$$

where subscripts on the β's indicate different modes.

The power in a mode is defined to be

$$P_\ell = |A_\ell|^2 \int \psi_\ell^2 \, dA \tag{4.15}$$

and, following reference [5], we introduce a new amplitude

$$F_\ell = [\int \psi_\ell^2 \, dA]^{1/2} A_\ell \tag{4.16}$$

so that $P_\ell = |F_\ell|^2$.

We neglect the differences in $k_i^2/\bar{\beta}_i$, and define the quantity

$$Q = \frac{3\omega_P}{n_{co}c} \quad . \tag{4.17}$$

We substitute eqn. (4.6) into (4.12). The result is then multiplied by an appropriate ψ_ℓ and integrated over the infinite cross-section of the fiber. The coupled wave equations then take the form [5]

$$\frac{\partial F_1}{\partial z} = \frac{i}{2} Q \chi_3(0) \{F_1 F_1^* F_1 \langle 1111 \rangle + 2F_1 F_2^* F_2 \langle 1221 \rangle\}$$

$$\frac{\partial F_2}{\partial z} = \frac{i}{2} Q \chi_3(0) \{F_2 F_2^* F_2 \langle 2222 \rangle + 2F_2 F_1^* F_1 \langle 2112 \rangle\}$$

$$\frac{\partial F_s}{\partial z} = i\, Q \chi_3(\Omega) \{F_s F_1^* F_1 \langle s11s \rangle + F_s F_2^* F_2 \langle s22s \rangle + F_1 F_2 F_a^* \langle s12a \rangle\, e^{i\Delta kz}\} \tag{4.18}$$

$$\frac{\partial F_a}{\partial z} = i\, Q \chi_3(\Omega) \{F_a F_1^* F_1 \langle a11a \rangle + F_a F_2^* F_2 \langle a22a \rangle + F_1 F_2 F_s^* \langle a12s \rangle\, e^{i\Delta kz}\}$$

The overlap integrals, which have units of inverse area, are defined to be

$$\langle s12a \rangle = \frac{\int \psi_s \psi_1 \psi_2 \psi_a \, dA}{[\int \psi_s dA]^{1/2} \, [\int \psi_1 dA]^{1/2} \, [\int \psi_2 dA]^{1/2} \, [\int \psi_a dA]^{1/2}} \tag{4.19}$$

We now simplify the analysis by assuming the pump power does not generate any intensity dependent changes to the refractive index. Further, we assume that depletion of the input waves due to creation of the Stokes and anti-Stokes waves is negligible, so that F_1 and F_2 are constant. Furthermore, we take χ_3 to be real to describe the frequency mixing, as discussed in Section 4-2. These assumptions are appropiate for many non-linear optics experiments. We then have the following coupled wave equations:

$$\frac{\partial F_s}{\partial z} = i\ Q\ \chi_3(\Omega)\ \sqrt{P_1 P_2}\ F_a^{*}\langle s12a\rangle\ e^{i\Delta kz} \tag{4.20a}$$

$$\frac{\partial F_a^{*}}{\partial z} = -i\ Q\ \chi_3(\Omega)\ \sqrt{P_1 P_2}\ F_s\langle a12s\rangle\ e^{-i\Delta kz} \tag{4.20b}$$

where $P_1 = |F_1|^2$, $P_2 = |F_2|^2$ and total pump power is given by $P = P_1 + P_2$. Complete expressions, which include intensity dependent changes to the wavevector at the pump frequency, can be found in reference [5].

4. Frequency Conversion and Gain

The solution to eqns. (4.20) is

$$\begin{aligned} F_s &= \left(c_1 e^{gz} + c_2 e^{-gz}\right) e^{i\Delta kz/2} \\ F_a &= \left(c_3 e^{gz} + c_4 e^{-gz}\right) e^{-i\Delta kz/2} \end{aligned} \tag{4.21}$$

where

$$g = \left(I^2 - \left(\tfrac{1}{2}\ \Delta k\right)^2\right)^{1/2} \tag{4.22a}$$

$$I = Q\ \chi_3(\Omega)\ \sqrt{P_1 P_2}\ \langle s12a\rangle \tag{4.22b}$$

g is the Stokes and anti-Stokes exponential gain coefficient, and I is defined as an effective intensity. The coefficients c_i are given in the Appendix.

In figure 4.1 we plot g against Δk for several values of I. Maximum gain occurs when the phase-matched condition is satisfied:

$$g_{max} = I \quad \text{when} \quad \Delta k = 0 \quad .$$

If we assume that in a fiber of length l we have $I > \pm \frac{1}{2} \Delta k$ so that $gl \gg 1$, then the conversion effeciency for the Stokes wave will be

$$\eta = \frac{P_s}{P} = \frac{|F_s|^2}{P} = |c_1|^2 \, e^{2gl}/P \tag{4.23}$$

c_1 can be found in the Appendix. We have

$$\begin{aligned} |c_1|^2 = \{ & I^2 P_{so} + I^2 P_{ao} + 2I \sqrt{P_{so} P_{ao}} \, (g\sin(\phi_s + \phi_a) \\ & - \frac{\Delta k}{2} \cos(\phi_s + \phi_a))\}/4g^2 \end{aligned} \tag{4.24}$$

where the powers are given by $P_j = F_j F_j^*$. The intial phase of the pump wave was set at $\phi_1 = \phi_2 = 0$, and the phase of the Stokes and anti-Stokes waves are given by eqn. (4.9) and the definition of F_ℓ , eqn. (4.16):

$$F_{so} = |F_{so}| \, e^{i\phi_s}$$

$$F^*_{ao} = |F_{ao}| e^{-i\phi_a}$$

At the phase-matched condition $g = \pm I$, and the conversion efficiency of the Stokes wave will depend on the relative phases of the pump, Stokes and anti-Stokes wave. The efficiency (or amplification) will then be a maximum or minimum for

$$\phi_s + \phi_a = \pm \frac{\pi}{2}$$

where (+,-) refers to (max,min).

Equation (4.23) is then equal to

$$\eta = \frac{P_s}{P} = \frac{1}{4} \left(\sqrt{P_{so}} \pm \sqrt{P_{ao}}\right)^2 e^{2gl}/P \qquad (4.25)$$

with $P = P_1 + P_2$.

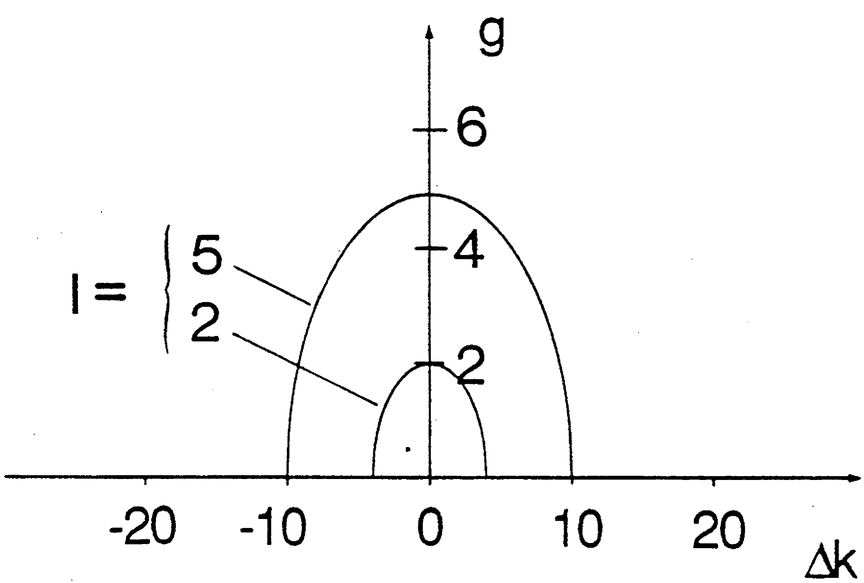

Fig. 4.1 The exponential gain coefficient g against phase mis-match Δk for several values of effective intensity I. (See eqn. (4.22).)

5. The Overlap Integrals

Equations (4.22) tell us that at the phase-matched condition the gain of the Stokes or anti-Stokes waves will depend on the overlap integral <s12a>, defined by eqn. (4.19).

Throughout this work we will mainly be concerned with a "divided-pump process" - the pump waves are divided into two modes that the Stokes and anti-Stokes waves propagate in. We shall explain this process in more detail in the next Chapter. The overlap integral for such a process is then

$$\langle 1|2\rangle = \frac{\int \psi_1^2\ \psi_2^2\ dA}{\int \psi_1^2\ dA \int \psi_2^2\ dA} \tag{4.26}$$

where the subscripts stand for mode 1 and mode 2.

To investigate these overlap integrals, we consider the singly clad step-profile fiber and use the Gaussian approximations to the modal fields given in Table 2.2. We recall that the modal fields within this approximation are specified by the spot-sizes $M_{\ell m}$. We first consider the process in which all waves are in the fundamental mode. The overlap integral for this process is easily evaluated to be

$$\langle 01|01\rangle = \frac{1}{2\pi M_{01}^2} \quad . \tag{4.27}$$

For the process in which pump and Stokes waves are in the LP_{11} mode and pump and anti-Stokes waves are in the LP_{01} mode we have

$$\langle 01|11\rangle = \frac{1}{\pi}\ \frac{M_{01}^2}{\left(M_{01}^2 + M_{11}^2\right)^2} \quad . \tag{4.28}$$

In figure 4.2 we plot eqns. (4.27) and (4.28) against normalized frequency V. The spot-sizes $M_{\ell m}$ as functions of V are defined via eqn.(2.54) and are given in Table 2.2. We also include in this figure the step-profile solutions, which are found by substituting the exact expressions for the LP_{01} and LP_{11} modes (given by eqn. (2.23)) into eqn. (4.26) and evaluating the integrals numerically. We observe that the Gaussian approximation gives simple, accurate expressions for the overlap integrals.

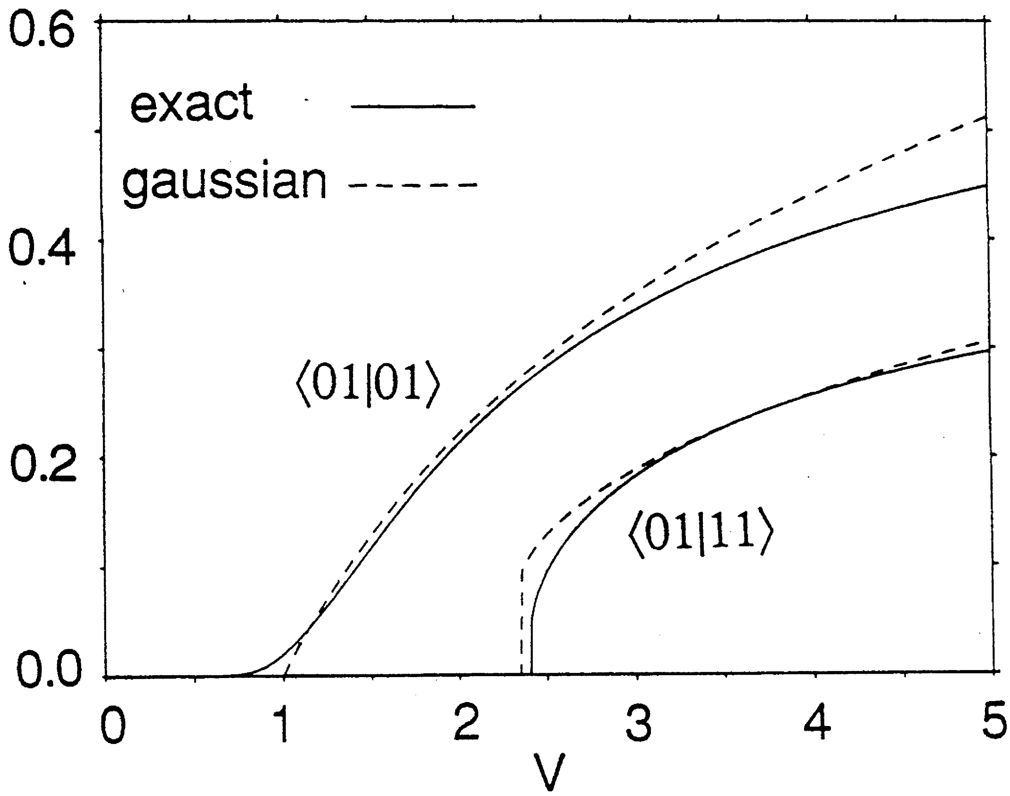

Fig. 4.2 Overlap integrals against normalized frequency V for a single-mode process, in which all four waves are in the (01) mode, and a few-mode divided-pump process. The fiber has a step-index profile.

6. Appendix

(i) Solutions to the coupled wave equations

The general solution to the coupled wave equations (4.20) are given by eqn. (4.21). The coefficients c_i are given by these sets of equations and the intial condition that at $z = 0$ $F_s = F_{so}$ and $F_a^* = F_{ao}^*$, and χ_3 is real.

$$
\begin{aligned}
2gc_1 &= (g - i\,\Delta k/2)F_{so} + i\,I\,F_{ao}^* \\
2gc_2 &= (g + i\,\Delta k/2)F_{so} - i\,I\,F_{ao}^* \\
2gc_3 &= (g + i\,\Delta k/2)F_{ao}^* - i\,I\,F_{so} \\
2gc_4 &= (g - i\,\Delta k/2)F_{ao}^* + i\,I\,F_{so}
\end{aligned}
\qquad (4A.1)
$$

where g and I are defined by eqn. (4.22).

References to Chapter 4

[1] R.H. Stolen, "Non-linear properties of optical fibers" in Optical Fiber Telecommunications, S.E. Miller and A.G. Chynoweth, Eds, Chap. 5 (Academic, New York, 1979)

[2] R.G. Smith, "Optical power-handling capacity of low loss optical fibers as determined by stimulated Raman and Brillouin scattering"
Applied Optics, 11, pp. 2489-2494 (1972).

[3] K.O. Hill, B.S. Kawasaki, D.C. Johnson and Y. Fujii, "Non-linear effects in optical fibers: Application to the fabrication of active and passive devices"
in Fiber Optics - Advances in Research and Development, B. Bendow and S.S. Mitra, Eds. pp.211-240 (Plenum, New York, 1979)

[4] C. Lin, "Non-linear optics in fibers for fiber measurements and special device functions"
IEEE J. Lightwave Tech., LT-4, pp.1062-1072 (1986)

[5] R.H. Stolen and J.E. Bjorkholm, "Parametric amplification and frequency conversion in optical fibers"
IEEE J. Quantum Electron., QE-18, pp. 1062-1072 (1982)

[6] N. Blomembergen, "Non-linear optics"
(W.A. Benjamin, Inc., New York, 1965)

[7] F. Zernike and J.E. Midwinter, "Applied non-linear optics", (John Wiley and Sons, New York, 1973)

[8] A. Yariv, "Quantum electronics" Chap. 16-18 (John Wiley and Sons, New York 1975)

[9] J.A. Armstrong, N. Bloembergen, J. Ducuing and P.S. Pershan, "Interactions between light waves in a non-linear dielectric" **Phys. Rev.**, 127, pp. 1918-1939 (1962)

[10] K.O. Hill, D.C. Johnson, B.S. Kawasaki and R.I. MacDonald, "cw three-wave mixing in single-mode optical fibers" **J. Appl. Phys.**, 49, pp. 5098-5106 (1978)

[11] P.D. Maker and R.W. Terhune, "Study of optical effects due to an induced polarization third-order in the electric field strength" **Phys. Rev.**, 137A, pp. A801-A818 (1965)

[12] E.P. Ippen, "Non-linear effects in optical fibers" in Laser Applications to Optics and Spectroscopy, S.F. Jacobs, M.O. Scully and M. Sargent, Eds. pp. 213-244 (Addison-Wesley, Massachusetts, 1975)

[13] W.P. Urquhart and P.J. Laybourn, "Effective core area for stimulated Raman scattering in single-mode optical fibers" **IEE Proc. Pt. J.**, 132, pp. 201-204 (1985)

[14] D.C. Johnson, K.O. Hill and B.S. Kawasaki, "Brillouin optical-fiber ring oscillator design" **Radio Science**, 12, pp. 519-528 (1977).

CHAPTER 5

PHASE-MATCHED PROCESSES

1. Introduction

2. The Phase-Matched Condition

3. Few-Mode Fibers
   - (a) The Divided-Pump Process
   - (b) Other Processes
   - (c) Symmetry Restrictions

4. Single-Mode Fibers
   - (a) Theory
   - (b) Singly-Clad Fibers
   - (c) Doubly-Clad Fibers
   - (d) Discussion

5. Birefringent Fibers
   - (a) Far From Minimum Dispersion
   - (b) Near Minimum Dispersion

6. Appendix
   - (i) Comparison of exact and approximate results

CHAPTER 5

PHASE-MATCHED PROCESSES

1. Introduction

In the previous chapter we found that the stimulated four-photon mixing process occurs strongly when it is phase-matched. In this Chapter we examine how to achieve this phase-matched condition on single- and few-mode optical fibers, and show how the resulting frequency shift depends on fiber properties.

Phase-matching requires that the sum of the wave-vectors involved in the process should equal zero, but because of material dispersion this condition is not automatically satisfied. In bulk material phase-matching can be achieved by the use of birefringent crystals or by mixing beams of light at different angles.

We show that phase-matching can be achieved on optical fibers by using the material and modal properties of the waveguide. The propagation constant of an individual mode consists of a material contribution, due to the bulk medium of which the fiber is made, and a waveguide contribution, due to the geometry of the fiber. On weakly-guiding waveguides these contributions can be separated out (see Section 3-2). The phase mis-match can then also be written as consisting of material and waveguide contributions, and by balancing these two effects so that they cancel, the phase-matched condition can be satisfied.

On few-mode fibers one can use the fact that different modes propagate through the fiber with different velocities. Thus if one mixes the pump and generated waves into different modes, material dispersion can be countered by inter-modal dispersion.

In this work we are only concerned with the divided-pump process. In this process a pump and Stokes wave are in one mode and a pump and anti-Stokes wave are in another. At the phase-matched condition the frequency shift is proportional to the difference in group delays of the two participating modes. These frequency shifts are of the order of 10^2 cm^{-1} .

Frequency shifts of the order of 10^3 - 10^4 cm^{-1} are possible by using a single-pump process, in which the pump propagates in the same mode. However, this process does not occur for all mode combinations because of symmetry conditions imposed by the overlap integral of the process. As explained in Section 4-5 the gain of the frequency shifted light is proportional to the overlap integral. The divided-pump process has no such symmetry restrictions.

A similar technique can be used to phase-match the stimulated four-photon mixing process on birefringent fibers, whereby the two orthogonal fundamental modes are used. Frequency shifts for birefringence matched parametric processes are typically 10^2 - 10^3 cm^{-1} .

Phase-matching can be achieved on truly single-mode fibers by operating the pump at a wavelength near the zero-dispersion frequency. At this frequency the waveguide and material contributions to intra-modal dispersion cancel (see Section 3-6).

We start by reviewing the phase-matched condition that was derived in Chapter 4, and show that because $\Omega\lambda << 1$ the propagation constants can be expanded about the pump frequency, resulting in analytic expressions for the frequency shift. We then concentrate on the divided-pump process in few-mode fibers, and show that the frequency shift is proportional to the difference in group delay of the participating modes. Other phase-matching processes are discussed.

We then turn to single-mode fibers, and show that phase-matching depends only on the propagation constant total dispersion, $d^2\bar{\beta}/d\omega^2$, and that the generated Stokes and anti-Stokes frequencies must be either side of a frequency $\omega_s < \omega_{zd} < \omega_a$, such that $\bar{\beta}''(\omega_{zd}) = 0$. Thus ω_{zd} is the zero-dispersion frequency that is so important in communications fiber design (see Section 3-6). It should be emphasized that the total dispersion is involved, not just the material effects, and thus four-photon mixing results will reflect the delicate balances and properties of that dispersion.

We discuss the application of these results to singly-clad fibers, which have one ω_{zd} , and fibers of more advanced design, such as the W-fiber which can have more than one zero-dispersion frequency. We also discuss phase-matching on birefringent fibers, and in an Appendix we compare exact and approximate frequency shift formulas.

The phase-matched stimulated four-photon mixing process in few-mode fibers was first examined by Stolen [1], and many other studies have followed [2-4]. This form of phase-matching has been used to study the intensity patterns of the participating modes of the process [5]. Phase-matching on birefringent fibers has also received much attention [6-8], particular as a method of investigating various induced biefringences [9-13].

Phase-matching the stimulated four-photon mixing process on single-mode fibers by using the zero-dispersion properties of the fiber has been previously investigated by a number of authors [14-16]. Frequency shifts on depressed inner cladding (W-) fibers has been reported in [17].

2. The Phase-Matched Condition

In the stimulated four-photon mixing process two pump photons, at frequency ω_p, generate a pair of photons at a higher-frequency, ω_a, called the anti-Stokes frequency, and at a lower frequency, ω_s, called the Stokes frequency. Energy conservation requires that

$$2\,\omega_p = \omega_s + \omega_a \quad .$$

The symmetric shift in frequency between the pump and generated frequencies is given by eqn. (4.13), which we write as

$$\Omega = \frac{1}{\lambda_p} - \frac{1}{\lambda_s} = \frac{1}{\lambda_a} - \frac{1}{\lambda_p} \qquad (5.1)$$

This is the conventional definition for Ω, and has units [length^{-1}]. Later we define a true frequency shift $\bar{\Omega}$ (see eqn. (5.17)) with units [time^{-1}]. The phase mis-match between waves is

$$\Delta k(\Omega) = \bar{\beta}_a(\omega_a) + \bar{\beta}_s(\omega_s) - \bar{\beta}_1(\omega_p) - \bar{\beta}_2(\omega_p) \qquad (5.2)$$

where the subscripts on the $\bar{\beta}$'s indicate different modes. The process occurs strongly when the phase-matched condition is satisfied

$$\Delta k(\Omega) = 0 \qquad (5.3)$$

In general we have

$$\Omega\lambda \ll 1 \qquad (5.4)$$

and the propagation constants at frequencies ω_a and ω_s can be Taylor expanded about ω_p [1]:

$$\bar{\beta}_a(\omega_a) = \bar{\beta}_a(\omega_p + 2\pi\Omega c)$$

$$= \bar{\beta}_a(\omega_p) + (2\pi\Omega c)\left.\frac{d\bar{\beta}_a}{d\omega}\right|_{\omega_p} + \frac{1}{2}(2\pi\Omega c)^2\left.\frac{d^2\bar{\beta}_a}{d\omega^2}\right|_{\omega_p} + \ldots \qquad (5.5a)$$

$$\bar{\beta}_s(\omega_s) = \bar{\beta}_s(\omega_p - 2\pi\Omega c)$$

$$= \bar{\beta}_s(\omega_p) - (2\pi\Omega c)\left.\frac{d\bar{\beta}_s}{d\omega}\right|_{\omega_p} + \frac{1}{2}(2\pi\Omega c)^2\left.\frac{d^2\bar{\beta}_s}{d\omega^2}\right|_{\omega_p} - \ldots \qquad (5.5b)$$

The phase-matched condition may then be written as

$$\Delta k(\Omega) = \bar{\beta}_a(\omega_p) + \bar{\beta}_s(\omega_p) - \bar{\beta}_1(\omega_p) - \bar{\beta}_2(\omega_p)$$

$$+ (2\pi\Omega)\left\{\left.\frac{d\bar{\beta}_a}{dk}\right|_{\omega_p} - \left.\frac{d\bar{\beta}_s}{dk}\right|_{\omega_p}\right\}$$

$$+ \frac{1}{2k}(2\pi\Omega)^2\left\{k\left.\frac{d^2\bar{\beta}_a}{dk^2}\right|_{\omega_p} + k\left.\frac{d^2\bar{\beta}_s}{dk^2}\right|_{\omega_p}\right\} = 0 \qquad (5.6)$$

where we have used $k = \omega/c$. The derivatives of the propagation constants with respect to k are now given by eqns. (3.3) and (3.6). Except near the zero-dispersion wavelength the second derivative of $\bar{\beta}$ with respect to k is dominated by the material dispersion (see fig. 3.12), and we may write

$$k \frac{d^2\bar{\beta}_i}{dk^2} \simeq D(\lambda) \quad , \quad \lambda \lesssim 1.1 \ \mu m \tag{5.7}$$

where i represents any mode and $D(\lambda)$ is given by eqn. (3.7).

In the Appendix we comment on the expansion condition eqn. (5.4), and hence the accuracy of eqn. (5.6), by comparing to a numerical solution of the exact phase-matched condition eqn. (5.2).

3. Few-Mode Fibers

(a) The Divided-Pump Process

In the divided-pump process a pump and anti-Stokes wave progates in one mode, which we label 1, and a pump and Stokes wave propagate in another mode, labelled 2. Figure 5.1 represents such a process. The approximate phase matched condition eqn. (5.6) then takes the form

$$\begin{aligned} \Delta k(\Omega) = {} & (2\pi\Omega)\, n\Delta\left(T_1 - T_2\right) \\ & + \frac{1}{k}\,(2\pi\Omega)^2\, D(\lambda) = 0 \end{aligned} \tag{5.8}$$

where eqns. (3.3) and (5.7) have been used and T is given by eqn (3.5). In eqn. (5.8) $n \equiv n_{co}$. Thus the phase mis-match comprises a material term and a modal term. Phase-matching is achieved by having the inter-modal dispersion, due to the fact that different modes have different delays, compensate the material dispersion, due to the bulk material of the fiber.

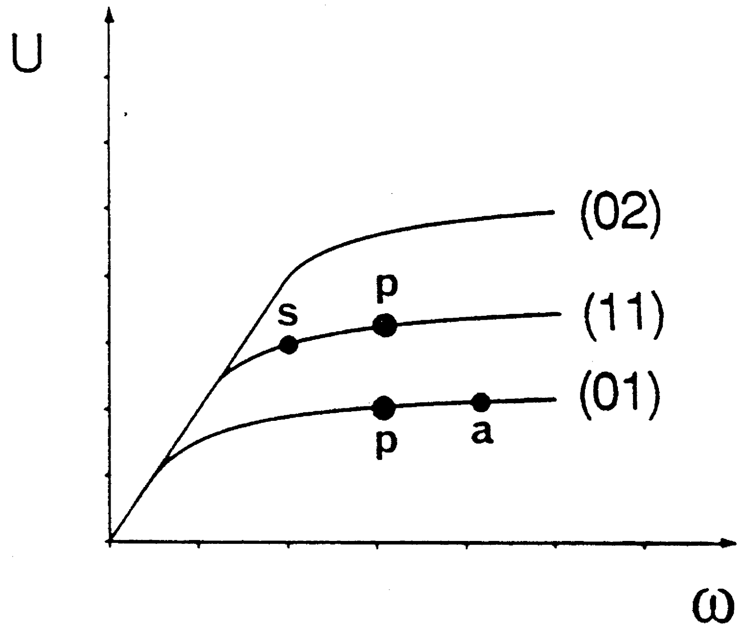

Fig. 5.1 Representation of a divided-pump process showing pump, Stokes and anti-Stokes in various modes. Eigenvalues represent propagation constants.

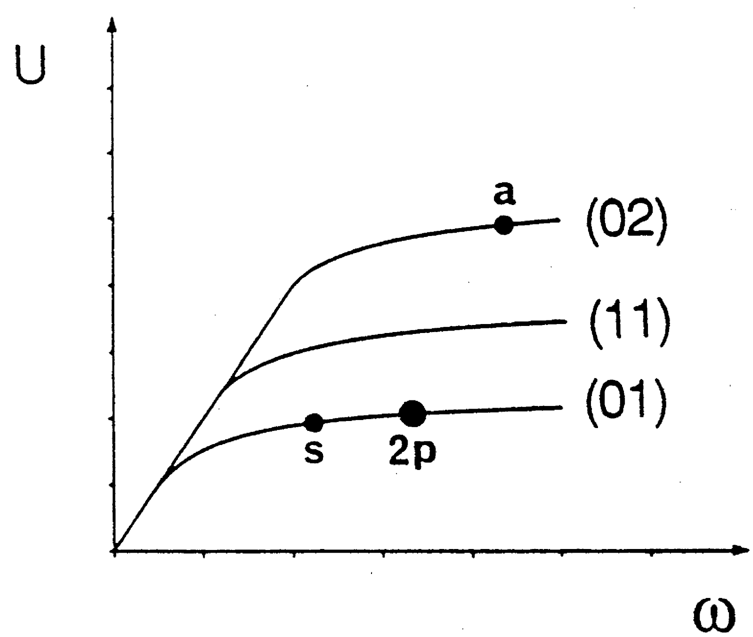

Fig. 5.2 Representation of a single-pump process.

The frequency shift of this process is thus given by

$$\Omega = \frac{n\Delta}{\lambda D(\lambda)} \left(T_2 - T_1\right) \quad . \tag{5.9}$$

That is, the frequency shift of the divided pump process is directly proportional to the inter-modal delay, or difference in group delay. In the Appendix we compare the approximate eqn. (5.9) with numerical solutions of the exact phase-match condition, eqn. (5.2).

If we examine the plots of T vs. V (see figures 3.7 to 3.9) then it is apparent that the Stokes wave (in mode 2) will always be in a higher order mode than the anti-Stokes wave (mode 1) in order that Ω be positive. (Near cut-off the difference in group delays do change sign but we are considering the far-from-cut-off region for good frequency conversion.)

The frequency shift is then only a function of λ and m (the amount of dopant - assumed here to be GeO_2 - in the core), which specifies n, Δ and D; and ρ (fiber core radius) which together with the above quantities specifies V, and hence T. For a singly-clad power-law profile and doubly-clad step profile fiber the diagrams of Chapter 3 can be used to construct Ω for the LP_{01} and LP_{11} mode combination.

(b) Other Processes

A second type of process used to phase-match on few mode fibers is the single pump process, in which both pump photons are in one mode and the Stokes and anti-Stokes waves appear in different modes. Figure 5.2 represents such a process. The approximate phase-matched condition eqn. (5.6) is:

$$\Delta k = \bar{\beta}_a + \bar{\beta}_s - 2\bar{\beta}_p \simeq (2\pi\Omega)\; n\Delta\left(T_a - T_s\right) + 2\pi\lambda D(\lambda)\Omega^2 = 0$$

where the anti-Stokes wave is in mode 1 and the Stokes and pump waves are in mode 2. The frequency shift can be found by solving the quadratic:

$$\Omega = \frac{n\Delta}{2\lambda D}\left(T_a - T_s\right)\left[\pm \left\{1 + \frac{4D\left(U_a^2 + U_s^2 - 2U_p^2\right)}{n\Delta V^2\left(T_a - T_s\right)^2}\right\}^{1/2} - 1\right] \tag{5.10}$$

where we have used eqn. (3.1):

$$\bar{\beta}_i = kn - kn\Delta\; U_i^2/V^2 \quad .$$

In general the term proportional to $1/\Delta$ within the square root in eqn. (5.11) is much greater than unity, and a good approximation for the frequency shift is

$$\dot{\Omega} \simeq \frac{1}{\lambda V}\left(\frac{n\Delta}{D}\right)^{1/2}\left(U_a^2 + U_s^2 - 2U_p^2\right)^{1/2} \tag{5.11}$$

We have now imposed restrictions on which modes may participate in this process:

$$U_a^2 + U_s^2 - 2U_p^2 > 0 \tag{5.12}$$

Figure 2.3 will then specify which modes satisfy this condition for some V. However, there are further restrictions on which mode combinations are possible which we discuss in part (c) of this Section.

The case where the Stokes and pump waves are in the LP_{01} mode and the anti-Stokes wave is in the LP_{02} mode is discussed in reference [1]. Using the same fiber parameters the approximate formula for frequency shift (eqn. (5.11)) is only a few percent different from the value calculated in [1] (see fig. 5.12). This equation represents a simple, approximate formula to evaluate the frequency shift of any single-pump process.

(c) Symmetry Restrictions

In Chapter 4 we saw that at the phase-matched condition the gain of the Stokes and anti-Stokes wave will depend on the overlap integral $\langle S12a \rangle$, defined by eqn. (4.19):

$$\langle S12a \rangle = \frac{\int \psi_s \psi_1 \psi_2 \psi_a \, dA}{\left[\int \psi_s^2 \, dA\right]^{1/2} \left[\int \psi_1^2 \, dA\right]^{1/2} \left[\int \psi_2^2 \, dA\right]^{1/2} \left[\int \psi_a^2 \, dA\right]^{1/2}} \tag{5.13}$$

Because the $\ell \geq 1$ modes consist of functions of r multiplied by $\cos(\ell\phi)$ or $\sin(\ell\phi)$ (see eqn. (2.20)) the numerator of eqn. (5.13) may equal zero depending on the combination of modes. This symmetry restriction does not affect the divided-pump process (see eqn. (4.26)) because we deal with the square of the fields:

$$\int \psi_s \psi_1 \psi_2 \psi_a \, dA = \int \psi_1^2 \psi_2^2 \, dA \quad \text{(divided-pump)} \quad . \tag{5.14}$$

However, the single-pump process will only occur if the symmetry restrictions imposed by eqn. (5.13) are not violated. We have

$$\int \psi_s \psi_1 \psi_2 \psi_a \, dA = \int \psi_p^2 \psi_s \psi_a \, dA \quad \text{(single-pump)} \quad . \tag{5.15}$$

In other words, the process will only occur (subject to the conditions discussed in part (b), see eqn. (5.12)) if

$$\int \psi_s \psi_a \, dA \quad \alpha \quad \int_0^{2\pi} \left\{ \begin{matrix} \cos(s\phi) \\ \sin(s\phi) \end{matrix} \right\} \left\{ \begin{matrix} \cos(a\phi) \\ \sin(a\phi) \end{matrix} \right\} d\phi \neq 0 \quad .$$

That is, both modes must have the same mode number ℓ , although different m numbers are allowed.

4. Single-Mode Fibers

(a) Theory

In this section we show that phase-matching on single-mode fibers depends only on the propagation constant total dispersion, $d^2\bar{\beta}/d\omega^2 \equiv d^2\bar{\beta}/c^2dk^2$ (refer to eqn. (3.6)). Throughout this Chapter, unless otherwise specified, $\bar{\beta}$ will be differentiated with respect to ω .

All the waves propagate in the fundamental mode, and phase-matching will occur when

$$\Delta k(\bar{\Omega}) = \bar{\beta}(\omega_a) + \bar{\beta}(\omega_s) - 2\bar{\beta}(\omega_p) = 0 \tag{5.16}$$

where for convenience we define a true frequency shift $\bar{\Omega}$:

$$\bar{\Omega} = 2\pi\Omega c = \omega_a - \omega_p = \omega_p - \omega_s \quad . \tag{5.17}$$

If we use the exact Taylor expansion expression [18]

$$f(a+h) = f(a) + \sum_{m=1}^{n-1} \frac{h^m}{m!} f^{(m)}(a) + \int_0^1 \frac{h^n(1-t)^{n-1}}{(n-1)!} f^{(n)}(a+th)\, dt \tag{5.18}$$

then we can write the propagation constant at the anti-Stokes frequency ω_a as

$$\begin{aligned} \bar{\beta}(\omega_a) &= \bar{\beta}(\omega_p + \bar{\Omega}) \\ &= \bar{\beta}(\omega_p) + \bar{\Omega}\, \bar{\beta}'(\omega_p) + \\ &\qquad \bar{\Omega}^2 \int_0^1 (1-t)\, \bar{\beta}''(\omega_p + t\, \bar{\Omega})\, dt \end{aligned} \tag{5.19}$$

and similarly for $\bar{\beta}(\omega_s)$. The primes indicate differentiation with respect to ω . Substituting into eqn. (5.16) leads to an integral expression for the phase-matched condition on single-mode fibers:

$$\int_{\omega_s}^{\omega_a} \left\{1 - \left| \frac{\omega_p - f}{\bar{\Omega}} \right| \right\} \bar{\beta}''(f)\, df = 0 \quad . \tag{5.20}$$

Integration by parts checks that eqn. (5.20) is exactly equivalent to $\Delta k(\bar{\Omega}) = 0$.

Since the expression $\{\ldots\}$ is positive for $\omega_p - \bar{\Omega} < f < \omega_p + \bar{\Omega}$, we see that eqn. (5.20) requires $\bar{\beta}''$ to change sign if $\bar{\Omega}$ is to be non-zero. Thus

$$\omega_s < \omega_{zd} < \omega_a \tag{5.21}$$

where $\bar{\beta}''(\omega_{zd}) = 0$ (see Section 3-6). ω_{zd} is the frequency at which the total dispersion of the fiber is zero, and is related to the zero-dispersion wavelength by $\omega_{zd} = 2\pi c/\lambda_{zd}$. As we saw in Section 3-6 $\bar{\beta}''$ may have several sign changes: we return to this point later.

Equation (5.20) indicates that phase-matching in a single-mode fiber actually depends only on the form of the total propagation constant dispersion $\bar{\beta}''$.

To gain insight, we use a full Taylor series expansion of $\bar{\beta}(\omega)$ around ω_p (see eqn. (5.5)). Truncating after the $\bar{\Omega}^4$ terms and applying eqn. (5.16) or (5.20) gives

$$\bar{\Omega} \simeq [- 12\bar{\beta}^{II}(\omega_p)/\bar{\beta}^{IV}(\omega_p)]^{1/2} \tag{5.22}$$

where we now use Roman numerals to indicate the order of differentiation with respect to ω . Thus $\bar{\Omega}$ depends only on values of $\bar{\beta}^{II}(\omega_p)$ versus ω_p curve (i.e. figs. 3.12 and 3.13) and its shape or curvature $\bar{\beta}^{IV}(\omega_p)$. This important formula immediately tells us that $\Omega = 0$ when $\omega_p = \omega_{zd}$ and that $\bar{\beta}^{II}(\omega_p)$ and $\bar{\beta}^{IV}(\omega_p)$ must have opposite signs for the four-photon mixing process to occur. Therefore, if $\bar{\beta}^{IV}(\omega_{zd}) \neq 0$, we expect phase matching on one side of the zero-dispersion point only.

Expression (5.22) should be accurate when ω_p is near ω_{zd} , so that $\bar{\Omega}$ is small and the truncated expansion highly accurate. The exact results confirm this and the accuracy for shifts Ω up to ~ 2000 cm^{-1} . $\bar{\beta}$ and its derivatives can be numerically computed, using the dispersion data of Chapter 3.

(b) Singly-Clad Fibers

We now apply the above phase-matching theory to singly-clad fibers operating at the minimum dispersion frequency (or wavelength).

Figure 5.3 shows the Stokes and anti-Stokes frequencies plotted against pump frequency, all normalized by the appropriate ω_{zd} (see Section 3-6), for a step-index fiber with ρ = 3.5 μm and various profile heights. The equivalent range of wavelength is $1.25\mu m < \lambda_p < 1.32\mu m$. Over this range $\bar{\beta}^{IV}$ is negative, and no phase-matching occurs until ω_{zd}, where $\bar{\beta}^{II}$ changes sign from negative to positive. This is shown in figure 5.4, where the exact numerical solution of eqn. (5.16) is compared with expression (5.22). We observe that the approximation is very good and successfully explains the rapid variation of Ω for ω_p in the region of ω_{zd}.

The grading of the core index profile modifies the fiber dispersion properties [19], and to illustrate the effect on four-photon mixing we use the clad power-law profile (see Section 2-3(b)) and vary q with fixed $\rho = 3.5\mu m$ and $\Delta = 0.006$. The results are displayed in figure 5.5. The experimental results of reference [15], for a fiber stated to be not truly step index, in fact correspond closely to our q = 15 curve.

In figure 5.6 we consider a step-profile fiber with $\Delta = 0.006$ pumped at the 1.319μm Nd:YAG laser line and having different core radii. In this way the material dispersion contribution is fixed but the waveguide contribution varies. The frequency shift at phase-matching varies rapidly on one side ω_{zd}, and is zero on the other. This agrees with the experimental results of [16,17].

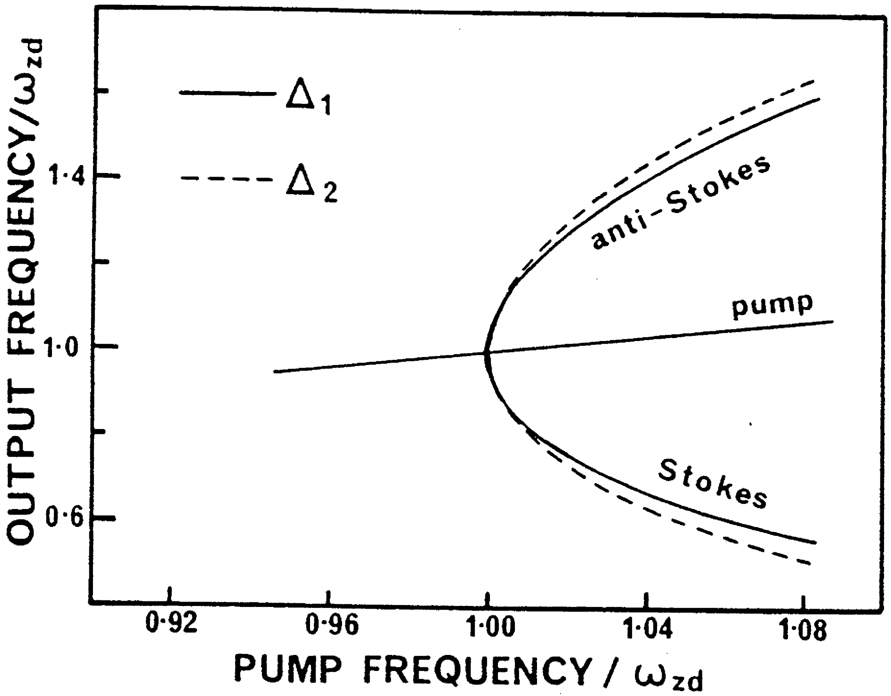

Fig. 5.3 Normalized pump and output frequencies for two different GeO_2-doped step-index fibers with ρ = 3.5 µm . Profile heights are Δ_1 = 0.0035 (m = 3.1%) and Δ_2= 0.0060 (m = 5.8%) .

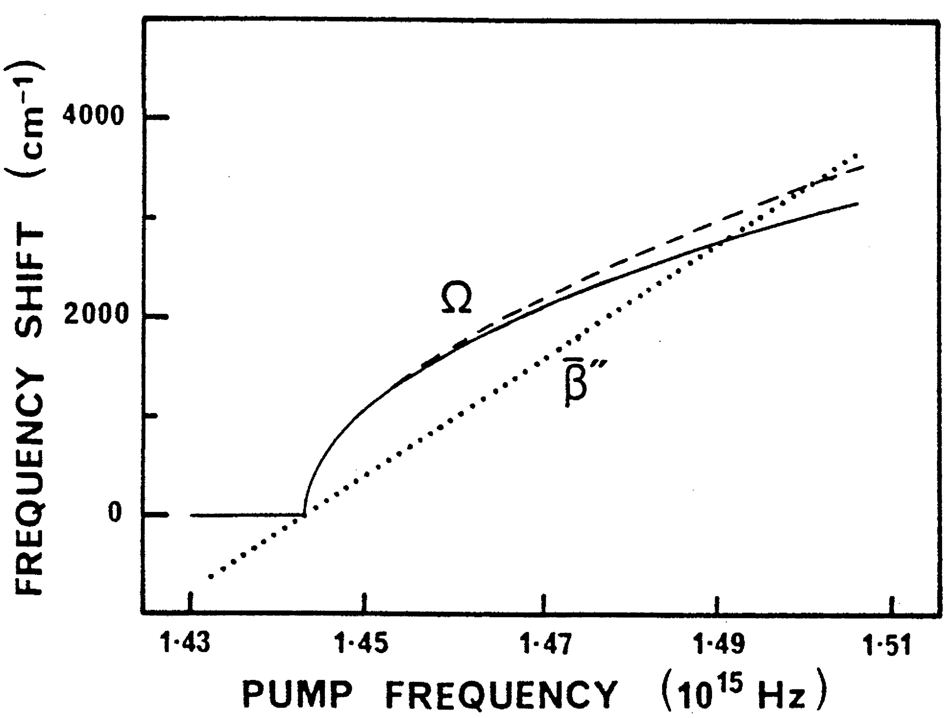

Fig. 5.4 Frequency shift Ω versus pump frequency. The solid curve is the exact result, while the broken curve is the approximation (eqn. (5.22)). The fiber has a 5.8 m% GeO_2-doped step-index core (Δ = 0.0060) with ρ = 3.5 µm . The dotted curve is a suitably scaled $\bar{\beta}^{II}$.

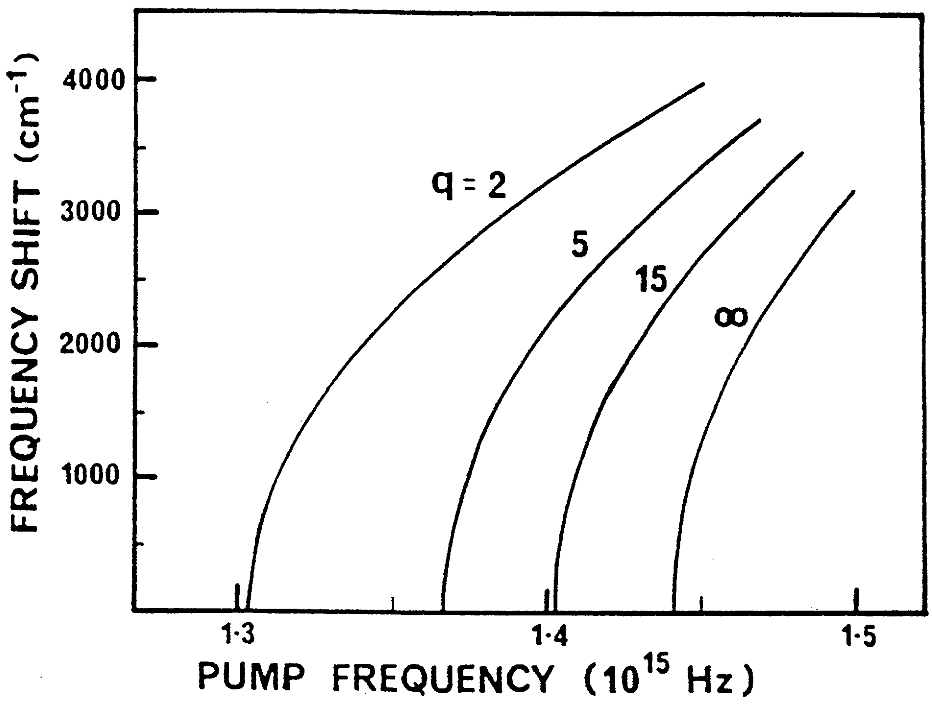

Fig. 5.5 Frequency shift against pump frequency for a clad power-law profile fiber with fixed ρ 3.5 μm and Δ = 0.0060 (m = 5.8 %) . q = ∞ in the step-index profile.

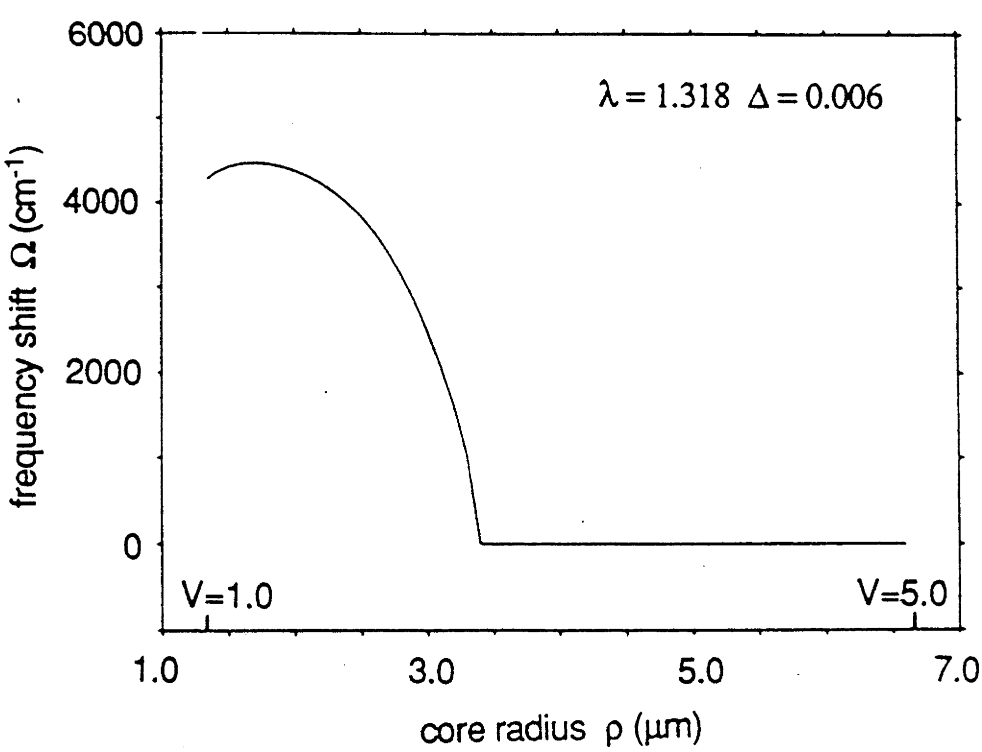

Fig. 5.6 Frequency shift against core radius ρ for a step-index fiber with Δ = 0.0060 (m = 5.8%) and pumped at λ_p = 1.318 μm .

(c) Doubly-Clad Fibers

We have seen that near material dispersion the modal part of $\bar{\beta}$ controls the precise form of $\bar{\beta}''$. Thus we anticipate interesting frequency shifts on fibers that have more than one zero, such as W-fibers.

To anticipate the features of four-photon mixing in such fibers we begin with a parabolic dispersion model as shown in figure 5.7. The zero-dispersion frequencies are ω_1 and ω_2, and the total dispersion is

$$\bar{\beta}''(\omega) = A(\omega - \omega_1)(\omega_2 - \omega) \tag{5.23}$$

where A is a constant. Equation (5.22), which is exact for a $\bar{\beta}''(\omega)$ of this form, is used, and the result is plotted in figure 5.7.

We see that matching occurs only in the positive $\bar{\beta}''$ region. The frequency shift $\bar{\Omega}$ is zero at frequencies ω_1 and ω_2, and the maximum shift, occurring when $\omega_p = (\omega_1 + \omega_2)/2 = \omega_{mid}$, is given by $\bar{\Omega}_{max} = (3/2)^{1/2}(\omega_2 - \omega_1)$. The anti-Stokes and Stokes frequencies still straddle a zero-dispersion point, as required by eqn. (5.20), and obey the rule

$$\begin{aligned}
&\left\{\begin{matrix}\omega_s < \omega_1 \\ \omega_p < \omega_a < \omega_2\end{matrix}\right\} \quad \text{for } \omega_1 < \omega_p < \omega_{mid} \\
&\left\{\begin{matrix}\omega_1 < \omega_s < \omega_p \\ \omega_2 < \omega_a\end{matrix}\right\} \quad \text{for } \omega_{mid} < \omega_p < \omega_2
\end{aligned} \tag{5.24}$$

We now consider frequency shifts on W-fibers that have dispersion curves given by fig. 3.13. In figure 5.8 we plot the frequency shift given by the numerical solution of eqn. (5.16) for a W-fiber with $P = 0.5$, $Q = 1.5$, $\rho = 3.3\ \mu m$, $\Delta = 0.0045$ and $V = 2.2$ (refer to Section 2-3(c) for definitions of the W-fiber parameters). Similar curves will correspond to the particular shape of $\bar{\beta}''$ shown in fig. 3.13. We note that for some values of ω_p there will be two values for Ω. Thus this type of phase-matching may be used to determine the dispersion characteristics of such advanced design fibers.

(d) Discussion

The frequency shifts in four-photon experiments on single-mode fibers are determined solely by the dispersion properties, and great sensitivity is expected for pump frequencies around the zero-dispersion wavelength. We emphasize that this refers to total dispersion, which can be zero for several frequencies in advanced design optical fibers, and that it is not sufficient to consider material dispersion alone.

Equation (5.20) leads to some general, exact result for phase matching, while eqn. (5.22) provides a formula for understanding the structure of Ω versus ω_p curves in terms of the behaviour of the $\bar{\beta}''(\omega_p)$ versus ω_p curves. In particular, we have shown that when $\omega_p = \omega_{zd}$, then $\Omega = 0$ and no new waves are generated.

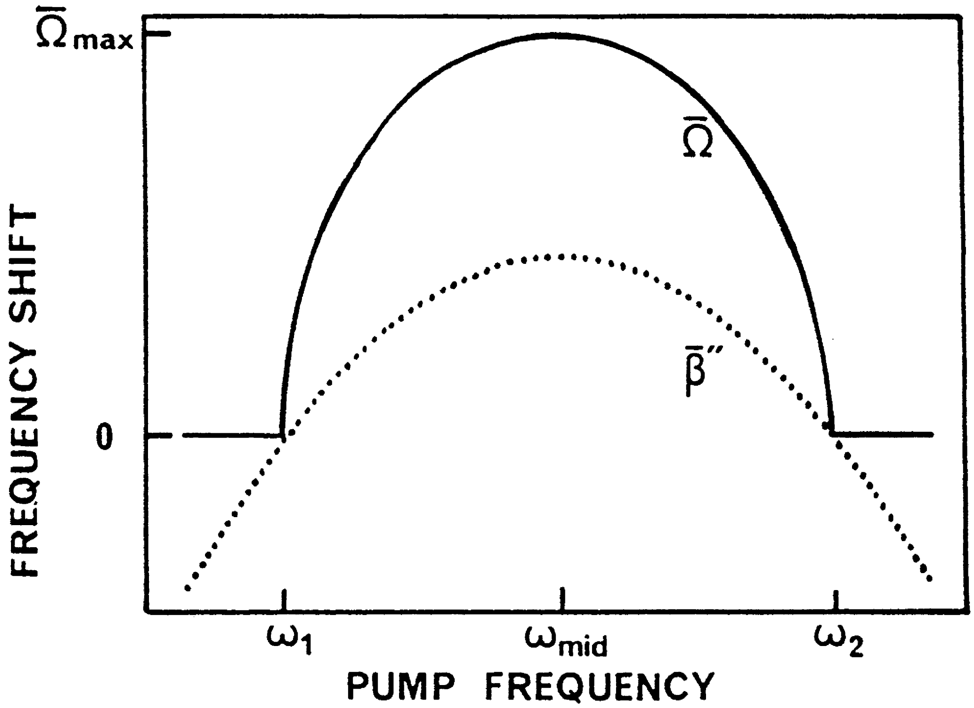

Fig. 5.7 Frequency shift $\bar{\Omega}$ for a parabolic dispersion model. $\bar{\beta}^{II}$, normalized by an arbitrary scale factor, is also included. $\bar{\Omega}_{max} = (3/2)^{1/2}(\omega_2 - \omega_1)$

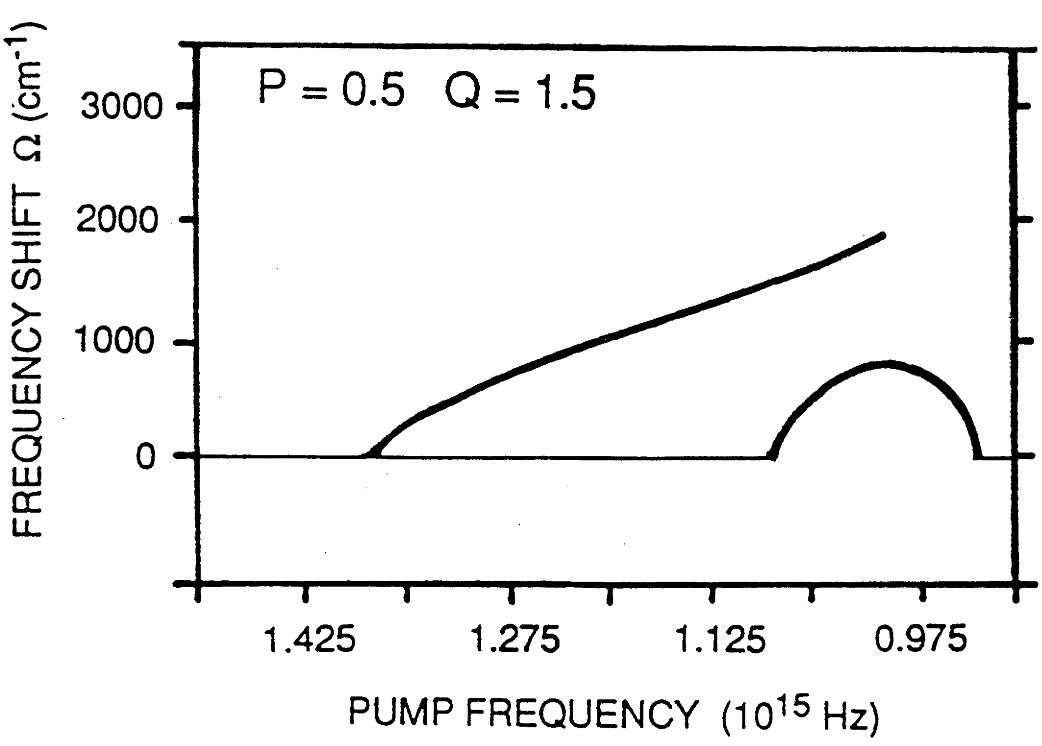

Fig. 5.8 Frequency shift against pump frequency for a W-fiber with $P = 0.5$, $Q = 1.5$, $\Delta = 0.0045$ ($m = 4.2$ %) and $\rho = 3.3$ μm, so that $V = 2.2$.

5. Birefringent Fibers

(a) Far From Minimum Dispersion

When the pump frequency is far from minimum dispersion the four-photon mixing process can be phase-matched by using the two orthogonal fundamental modes, in the same way that a pair of modes are used in few-mode fibers, and the theory of Section 3 applies. Either a divided-pump or single-pump process is possible, and there is no symmetry restriction from the overlap integrals. However, because the difference in propagating constants is much smaller than in the few-mode case (i.e. $\{\bar{\beta}_x - \bar{\beta}_y\} << \{\bar{\beta}_{11} - \bar{\beta}_{01}\}$) practical frequency shifts are best obtained by using the single-pump process. A typical birefringence matching process is shown in fig. 5.9, but many combinations of Stokes, anti-Stokes and pump waves are possible [7].

In all these processes the perpendicular component of the third-order susceptibility is involved. Because this component is only about a third of the parallel susceptability [20] the gain of the birefringent matched process is less than the few mode case. However, the overlap integral of the single-mode process is nearly twice as large as the few-mode process (see eqns. (4.27) and (4.28)) so this loss is compensated.

(b) Near Minimum Dispersion

When the pump frequency is near minimum dispersion the theory of Section 3-3 does not apply, and phase-matching must be done according to Section 3-4. However, in this case both x- and y- modes have total dispersion close to zero $\bar{\beta}''_x \simeq \bar{\beta}''_y \simeq 0$.

In figure 5.10 we vary pump frequency and show the frequency shift on a birefringent fiber. We have chosen a birefringence $B = \beta_x - \beta_y = 5 \times 10^{-5}\ \mu m^{-1}$. This value is fairly typical for a birefringence due to an elliptical core cross-section (see Chapter 6) or a birefringence due to bending stress (see Chapter 7).

Stokes and anti-Stokes waves are generated separately in the two orthogonal modes, with frequency shifts dependent on the pump frequency. Specifically, if the zero-dispersion frequencies of the two orthogonal modes are denoted by ω^x_{zd} and ω^y_{zd} (i.e. $\bar{\beta}''(\omega^x_{zd}) = \bar{\beta}''(\omega^y_{zd}) = 0$) then (i) no new waves are created if $\omega^x_{zd} < \omega_p$ and $\omega^y_{zd} < \omega_p$; and (ii) new waves are created in only one polarization direction if $\omega^x_{zd} < \omega_p < \omega^y_{zd}$.

However, as fig. 5.10 shows, the difference in the two frequency shifts is very small, and it would require precise optical equipment to measure this difference. This method is not practical as a way to measure birefringence.

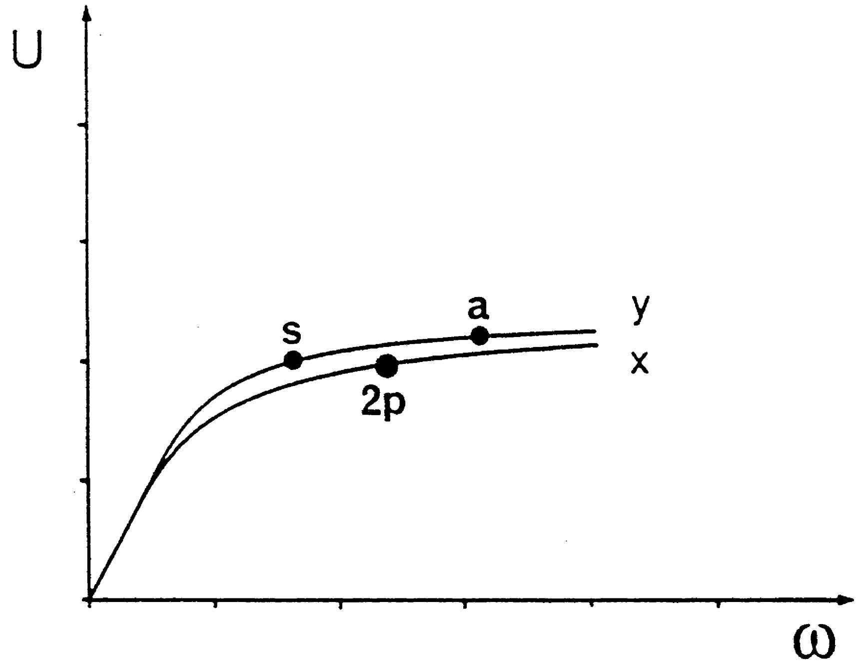

Fig. 5.9 Representation of a birefringent-matched process.

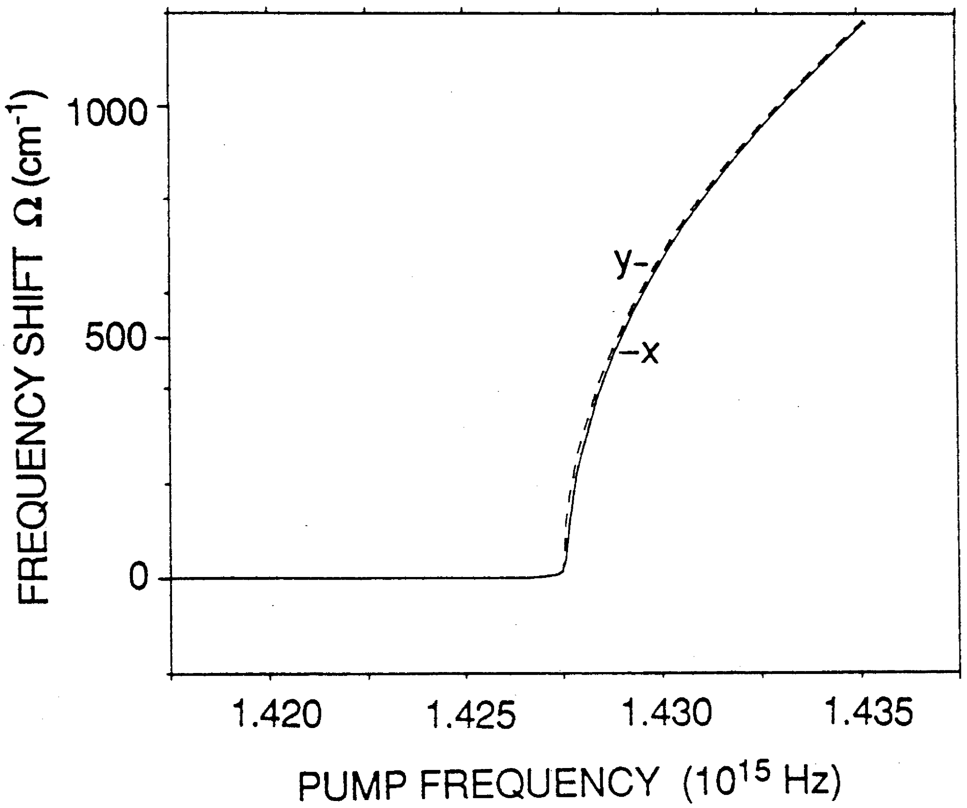

Fig. 5.10 Frequency shift versus pump frequency for a birefringent step-index fiber operating near the zero dispersion frequency. The magnitude of the birefringence is $B \approx 5 \times 10^{-5}\ \mu m^{-1}$.

6. Appendix

(i) Comparison of exact and approximate results

In figure 5.11 we compare the exact phase mismatch eqn. (5.2) against the approximate expression eqn. (5.8) for a divided-pump process on a step-index fiber. In fig. 5.11 (a) we consider phase matching between the LP_{01} and LP_{11} modes and in (b) the LP_{01} and LP_{21} modes. The frequency shift for the processes is at the phase-matched condition $\Delta k = 0$.

In Section 6-2 we commented that the approximation eqn. (5.6) is valid for the condition

$$\Omega\lambda_p << 1$$

In the divided pump processes $\Omega \lesssim 500\ cm^{-1}$ and if we consider a frequency doubled Nd:YAG laser $(\lambda_p = 0.532\ \mu m)$ this condition always holds. In the single pump process we may have $\Omega \simeq 5000\ cm^{-1}$ and the approximation will not be as accurate, although still valid. We are not concerned with this process in this work, although our approximate expression for frequency shift, eqn. (5.11), is the first time (to the author's knowledge) that such an explicit expression has been derived. In figure 5.12 we compare eqn. (5.11) to the exact frequency shift (from $\Delta k = 0$) by plotting Ω against core radius ρ (this is effectively a variation in V, since $\lambda = 0.532\ \mu m$ is fixed). The difference is less than a few percent.

The approximation for phase-matching on single-mode fibers near the longer wavelength minimum dispersion region is discussed in Section 6-4, and shown in figure 5.4

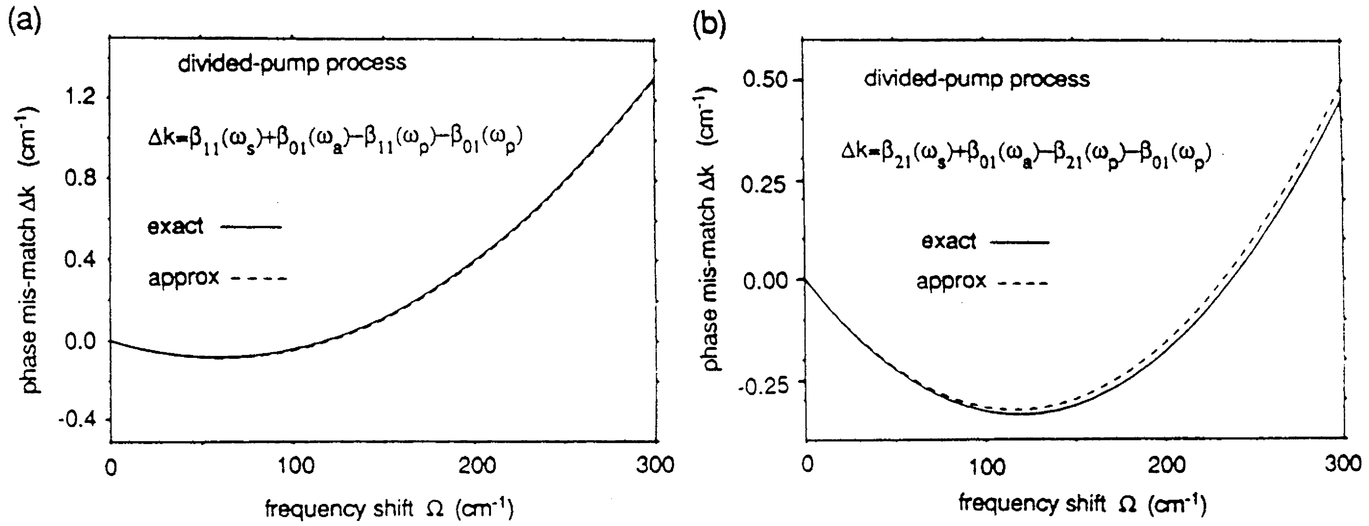

Fig. 5.11 Comparison of exact and approximate solutions of $\Delta k(\Omega)$ versus Ω for a divided-pump process for (a) the LP_{01} and LP_{11} mode combination and (b) the LP_{01} and LP_{21} mode combination.

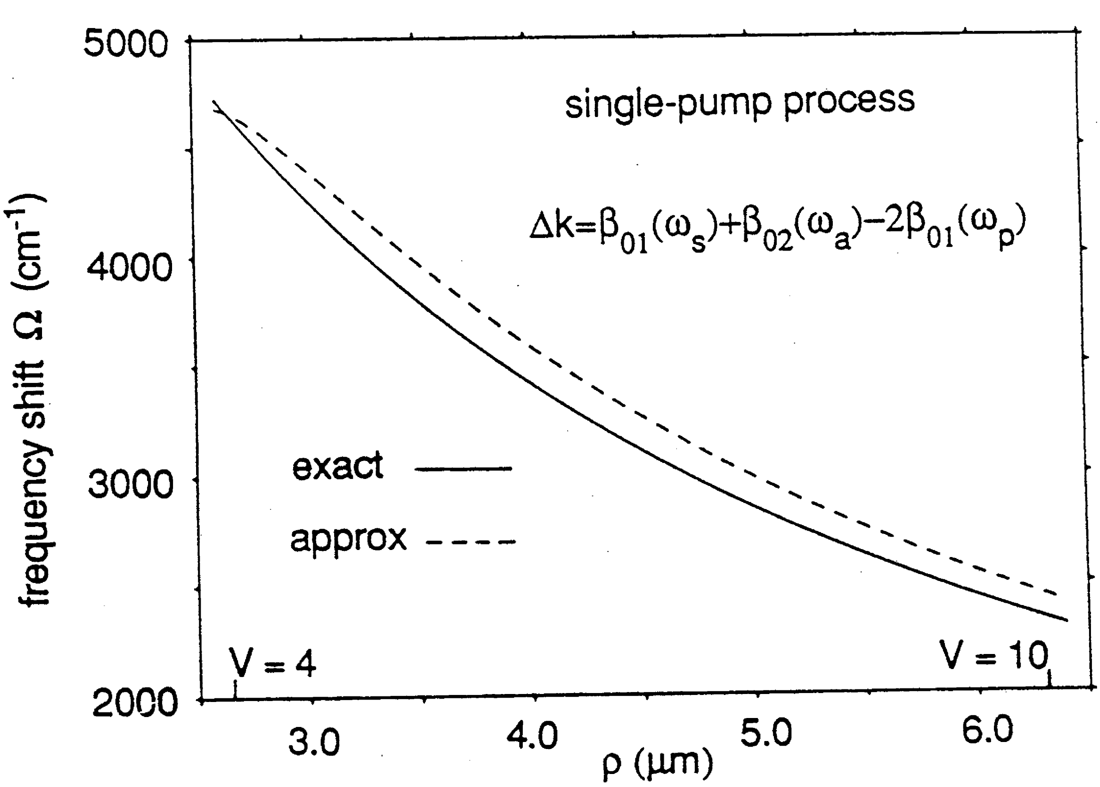

Fig. 5.12 Comparison of exact and approximate frequency shifts for a single-pump process. The frequency shift is plotted against core radius ρ .

References to Chapter 5

[1] R.H. Stolen, "Phase-matched stimulated four-photon mixing in silica-fiber waveguides"
IEEE J. Quantum Electron., QE-11, pp. 100-103 (1975).

[2] E.M. Dianov, E.A. Zakhidov, A. Ya. Karasik, P.V. Mamyshev and A.M. Prokhorov, "Stimulated four-photon non-linear processes in few-mode glass fiber-optic waveguides"
Sov. Phys. JETP, 56, pp. 21-26 (1982).

[3] V.P. Kalosha and A.P. Khapalyuk, "Frequency shift in stimulated four-photon processes in few-mode glass fiber waveguides"
Sov. J. Quantum Electon., 14, pp. 1568-1570 (1984).

[4] K.O. Hill, D.C. Johnson and B.S. Kawasaki, "Efficient conversion of light over a wide spectral range by four-photon mixing in a multi-mode graded-index fibers"
Applied Optics, 20, pp. 1075-1079 (1981).

[5] R.H. Stolen and W.N. Leibolt, "Optical fiber modes using stimulated four-photon mixing"
Applied Optics, 15, pp. 239-243 (1976).

[6] R.H. Stolen, M.A. Bosch and C. Lin, "Phase-matching in birefringent fibers"
Optics Letters, 6, pp. 213-214 (1981).

[7] R.K. Jain and K. Stenerson, "Phase-matched four-photon mixing processes in birefringent fibers"
Appl. Phys., B35, pp. 49-57 (1984).

[8] K. Stenerson and R.K. Jain, "Small Stokes-shift frequency conversion in single-mode birefringent fibers"
Opt. Comm., 51, pp. 121-126 (1984).

[9] K.I. Kitayama, S. Seikai and N. Uchida, "Stress-induced frequency tuning for stimulated four-photon mixing in a birefringent single-mode fiber"
Appl. Phys. Lett., 41, pp. 322-324 (1982).

[10] K.I. Kitayama and M. Ohashi, "Frequency tuning for stimulated four-photon mixing by bending-induced birefringence in a single-mode fiber"
Appl. Phys. Lett., 41, pp. 619-621 (1982).

[11] N. Shibata, M. Ohashi, K.I. Kitayama and S. Seikai, "Evaluation of bending-induced birefringence based on stimulated four-photon mixing"
Optics Letters, 10, pp. 154-156 (1985).

[12] T. Nakashima, N. Shibata, M. Ohashi and S. Seikai, "Evaluation of axial fibre strain based on the stimulated four photon mixing process"
Electron. Letters, 21, pp. 935-936 (1985).

[13] M. Ohashi, K.I. Kitayama, N. Shibata, S. Seika, "Frequency tuning of a Stokes wave for stimulated four-photon mixing by temperature-induced birefringence change"
Optics Letters, 10, pp. 77-79 (1985).

[14] W. Washio, K. Inove and T. Tanigawa, "Efficient generation of near-I.R. stimulated light scattering in optical fibers pumped in low-dispersion region at 1.3 μm "
Electron. Letters, 16, pp. 331-333 (1980).

[15] C. Lin, W.A. Reed, A.D. Pearson and H.-T. Shang, "Phase matching in the minimum chromatic dispersion region of single-mode fibers for stimulated four-photon mixing"
Optics Letters, 10, pp. 493-495 (1981).

[16] C. Lin, W.A. Reed, A.D. Pearson, H.-T. Shang and P.D. Glodis, "Designing single-mode fibers for near-I.R. (1.1-1.7 μm) frequency generation by phase-matched four-photon mixing in the minimum chromatic dispersion region" **Electron. Letters**, 18, pp. 87-88 (1982).

[17] J.P. Pocholle, J Raffy, M. Papuchon and E. Desurvire, "Raman and four-photon mixing amplification in single-mode fibers" **Optical Eng.**, 24, pp. 600-608 (1985).

[18] E.T. Whittaker and G.N. Watson, "A Course of Modern Analysis", 4th Ed. p.95, (Cambridge Uni. Press, Cambridge, 1969).

[19] See ref. [3-3].

[20] See ref. [4-4].

CHAPTER 6

MODES ON A PERTURBED OPTICAL FIBER
and their study by the
FOUR-PHOTON MIXING PROCESS

CHAPTER 6

MODES ON A PERTURBED OPTICAL FIBER

and their study by the

FOUR-PHOTON MIXING PROCESS

1. Introduction

The use of optical waveguides in communication systems or as optical sensing devices requires an understanding of their modal properties. In particular the effect on these properties when the waveguide is perturbed in some manner must be analysed in order that it either be eliminated or incorporated into the design of the optical system. In this Chapter we look at perturbations to the refractive index profile of singly-clad step-profile fibers.

We examine changes to the field and propagation constants of a fiber that has a non-circular core cross-section, and a fiber that has a dip, or depression, on its refractive index profile.

We first consider the case of the non-circular core cross-section, and show that in few-mode fibers the higher-order scalar propagation constants become non-degenerate. The mode splits into odd and even symmetries which propagate through the fiber with different polarization directions and different group delays. We discuss this important point in detail in the next Section.

We then show that in single mode fibers there is a birefringence created by the non-circularity. For perturbations described by a Fourier cosine series this birefringence is equivalent to the birefringence due to an elliptical core cross-section. A Greens function method is used to include first-order corrections to the field.

In order to measure these perturbations a divided-pump four-photon mixing experiment, on which pump waves excite the odd (sine) and even (cosine) symmetries of the $\ell \geq 1$ modes and generate a Stokes and an anti-Stokes wave, is proposed.

We then consider another type of perturbation, the ~~Guassian~~ Gaussian dip in the refactive index profile of the core. In this case the symmetry of the fiber is unaffected, so that there is no mode splitting, but modal properties (cut-off, group delay, dispersion, etc.) will be changed.

We use this perturbed profile to describe the results of a divided-pump four-photon mixing experiment performed on a fiber designed for single-mode operation at 1.3 μm . The experiment was performed with a pump wavelength of 0.532 μm , and five different modes were observed in various combinations. A further experiment involved bending the fiber, so that the symmetry was broken. Mode splitting of the $\ell = 1$ modes was observed; the theory and experimental results for the bent case are presented in Chapter 7.

The modal properties of perturbed optical fibers have been studied using a variety of methods [1,4], but these studies do not discuss the balance between symmetry and polarization effects. Propagation in profiles with various refractive index dips have been investigated previously in the course of work to design optimized fibers for communications systems [10,11].

2. Modes on Fibers with Preferred Axes of Symmetry

Throughout the next two Chapters we consider weakly guiding waveguides, whereby the polarization properties of the modes can be treated separately. Thus the modes are treated as scalar modes multiplied by a polarization term.

Let us first consider the polarization effects. As discussed in Chapter 2, linearly-polarized (LP) modes are nearly correct for a straight fiber and corrections are given by eqn. (2.14). In a straight fiber with a circularly symmetric core there are no uniquely defined polarization axes. However, in a fiber with a deformed core cross-section, two defined axes are defined and the theory in [5] indicates that the modes will become truly linearly polarized - they will have fixed field directions in the fiber and maintain their intial state of polarization.

The effects of polarization are included to derive the birefringnece of the fundamental mode in these perturbed fibers. However, these effects are small, and higher-order modes can be described by a scalar field multiplied by an appropriate polarization unit vector.

The scalar modes have fields and propagation constants that satisfy the scalar wave equation. For the higher-order modes of a straight circularly symmetric fiber there are two solutions to this equation representing an even mode and an odd mode, with the propagation constant being equal for both symmetries. We show that when the symmetry of the waveguide is disturbed the degeneracy of the higher-order modes is broken and the propagation constants are different for the two symmetries.

3. Corrections to the Propagation Constant

We now examine the effect of a perturbation on propagation constants. Scalar theory is sufficient to describe the effects on the $\ell \geq 1$ modes but polarization corrections must be included to describe birefringence. The ratio of symmetry effects to polarization effects gives a quantitive criteria for when the $\ell \geq 1$ modes become truly linearly polarized.

(a) Scalar Theory

Let ψ_0 and $\bar{\beta}_0$ be the field and propagation constant of a mode on a weakly-guiding waveguide with circularly-symmetric refractive index distribution n_0^2 , and let ψ and $\bar{\beta}$ be the field and propagation constant of a mode on a different weakly-guiding waveguide with arbitrary refractive index profile n^2 :

$$\left(\nabla_t^2 + k^2 n_0^2 - \bar{\beta}_0^2\right)\psi_0 = 0 \tag{6.1a}$$

$$\left(\nabla_t^2 + k^2 n^2 - \bar{\beta}^2\right)\psi = 0 \tag{6.1b}$$

Note that eqn. (6.1a) is our normal scalar wave equation with solutions discussed in Section 2-3.

If we multiply eqn. (6.1a) by ψ , and eqn. (6.1b) by ψ_0 , subtract and integrate over the infinite cross-section A_∞ we have [6]

$$\bar{\beta}^2 - \bar{\beta}_0^2 \int_{A_\infty} \psi_0 \psi \, dA = k^2 \int_{A_\infty} \left(n^2 - n_0^2\right) \psi_0 \psi \, dA$$
$$+ \int_{A_\infty} \left\{\psi_0 \nabla_\tau^2 \psi - \psi \nabla_\tau^2 \psi_0\right\} dA \quad . \tag{6.2}$$

The second integral on the right-side can be converted to a line integral at infinity, which will vanish since ψ_0 and ψ and their derivatives decay exponentially to zero for bound modes (see Section 2-2(b)).

We now assume the arbitrary refractive index profile n^2 can be written in terms of n_0^2 :

$$n^2(x,y) = n_0^2(x,y) + \delta n(x,y) \quad . \tag{6.3}$$

This is not a perturbation relation. There is no restriction on the magnitude of δn , only that eqn. (6.3) is valid. Substituting eqn. (6.3) into eqn. (6.2) we have a reciprocal relation between the two different waveguides:

$$\delta\beta^2 \equiv \bar{\beta}^2 - \bar{\beta}_0^2 = k^2 \int_{A_\infty} \delta n \; \psi_0\psi \; dA \Big/ \int_{A_\infty} \psi_0\psi \; dA \tag{6.4}$$

The difference in propagation constants is given by eqn. (2.40):

$$\delta\beta = \bar{\beta} - \bar{\beta}_0 \simeq \left(\bar{\beta}^2 - \bar{\beta}_0^2\right)/2kn_{co} \quad . \tag{6.5}$$

If δn is small, then it may be treated as a perturbation and we can set $\psi \simeq \psi_0$. The difference in propagation constants due to the different waveguides is:

$$\delta\beta = \frac{V}{2\rho(2\Delta)^{1/2}} \int_{A_\infty} \frac{\delta n}{n_{co}^2} \psi_0^2 \; dA \Big/ \int \psi_0^2 \; dA \tag{6.6}$$

where we have used the definition of V (eqn. (2.15)).

(b) Birefringence

The fundamental mode consists of two orthogonal modes which in a circularly-symmetric cross-section are degenerate. If the symmetry is broken there will be a resultant difference between the propagation constants of the two orthogonal modes. This is called birefringence.

Because the fundamental modes are independent of azimuthal angle ϕ the expression (6.6) will, in general, be identical for both x- and y-polarized modes. That is, scalar theory is insufficient to describe birefringence, and we must consider the vector or polarization corrections to the scalar wave equation [5].

In Section 2-2(b) we derived an expression for the correction to the scalar propagation constant due to these polarization effects. The difference between an x-polarized mode and a y-polarized mode on a step-index fiber is given by eqn. (2.42)

$$\delta\beta_x - \delta\beta_y = \frac{\rho(2\Delta)^{3/2}}{2V} \oint_\ell \left(\frac{\partial\psi}{\partial x}\hat{n}_x - \frac{\partial\psi}{\partial y}\hat{n}_y\right)\psi\, d\ell \Big/ \int_{A_\infty} \psi^2\, dA \tag{6.7}$$

where $\underset{\sim}{e}_t \approx \bar{\underset{\sim}{e}}_t = \psi\,\hat{\underset{\sim}{x}},\ \psi\,\hat{\underset{\sim}{y}}$. We can convert the above expression to polar coordinates by using

$$\frac{\partial\psi}{\partial x} = \cos\phi\,\frac{\partial\psi}{\partial r} - \frac{\sin\phi}{r}\frac{\partial\psi}{\partial\phi} \quad ; \quad \frac{\partial\psi}{\partial y} = \sin\phi\,\frac{\partial\psi}{\partial r} + \frac{\cos\phi}{r}\frac{\partial\psi}{\partial\phi}$$

$$\hat{n}_x = |\hat{\underset{\sim}{n}}|\cos\phi \quad ; \quad n_y = |\hat{\underset{\sim}{n}}|\sin\phi$$

where $\hat{\underset{\sim}{n}}$ is the unit outward normal (i.e., in the direction of $\hat{\underset{\sim}{r}}$). Substituting into eqn. (6.7) we obtain the birefringence in an optical fiber:

$$B = \delta\beta_x - \delta\beta_y = \frac{(2\Delta)^{3/2}}{2V\rho} \oint_{\ell} \left(\frac{\partial\psi}{\partial R} \cos 2\phi - \frac{\partial\psi}{\partial\phi} \sin 2\phi\right)\psi|\hat{\underset{\sim}{n}}|d\ell / \int_{A_\infty} \psi^2 \, dA/\rho^2 \quad . \tag{6.8}$$

(c) **Discussion**

When an optical fiber is perturbed in some manner the symmetry may be broken and there will be preferred axes of symmetry, as discussed in Section 6-2. For modes that are described by

$$\psi = F_\ell(R) \left\{ \begin{matrix} \cos\ell\phi \\ \text{or} \\ \sin\ell\phi \end{matrix} \right\}$$

then eqn. (6.6) will describe the difference between the propagation constants of the even (cos) and odd (sin) symmetry modes. On the other hand, the difference between the x-polarized mode and y-polarized mode for the $\ell = 0$ case is given by eqn. (6.8).

If we set $\delta n = \varepsilon$ times {some function describing the perturbation}, with $|\varepsilon| << 1$, then the difference in symmetry modes for $\ell \geq 1$ is obtained from eqn. (6.6), and is proportional to

$$B_{sym} = \delta\beta_e - \delta\beta_o \propto \frac{V \ \varepsilon}{2\rho(2\Delta)^{1/2}} \tag{6.9}$$

where subscripts e and o represent even and odd modes, respectively, and Δ is the profile height.

The difference in propagation constants due to polarization effects is given by eqn. (6.8), and is proportional to

$$B_{pol} = \delta\beta_x - \delta\beta_y \propto \frac{(2\Delta)^{3/2}}{2\rho V} \quad . \tag{6.10}$$

Combining eqns. (6.9) and (6.10) we have

$$\frac{B_{sym}}{B_{pol}} \propto \left(\frac{V}{2\Delta}\right)^2 \varepsilon$$

When a fiber has its symmetry broken by a small perturbation of order ε, polarization effects will be much smaller than symmetry considerations if

$$\varepsilon > \left(\frac{2\Delta}{V}\right)^2 \quad . \tag{6.11}$$

This supports the argument of Section 6-2 that polarization effects are small, and $\ell \geq 1$ modes can be described by scalar theory. Eqn. (6.11) is equivalent to the criteria for $\ell \geq 1$ modes to become truly linearly polarized. The true criteria is found from the ratio of eqn. (6.6) and the general expression for polarization corrections, eqn. (2.42). This is discussed in detail in reference [5], and is used to discuss LP modes on bent fibers in the next Chapter.

4. Arbitrary Cross-Section Fibers

We consider a small but arbitrary change to the core-radius of a circularly-symmetric step-profile fiber, as shown in figure 6.1(a). The perturbed normalized radius is described by

$$R_p(\phi) = \left\{1 + \sum_{j=1}^{\infty} a_j \cos j(\phi - \phi_j)\right\} \tag{6.12}$$

Polar angles ϕ_j and amplitudes a_j are arbitrary, but a_j is assumed small so that we may neglect terms of order a_j^2. The mean radius is $\langle R_p \rangle = 1$, which is equivalent to the normalized radius of the unperturbed fiber.

Axes x_j' and y_j' have unit vectors (see fig. 6.1)

$$\hat{\underset{\sim}{x}}'_j = \hat{\underset{\sim}{y}} \sin\phi_j + \hat{\underset{\sim}{x}} \cos\phi_j$$

$$\hat{\underset{\sim}{y}}'_j = \hat{\underset{\sim}{y}} \cos\phi_j - \hat{\underset{\sim}{x}} \sin \phi_j \qquad (6.13)$$

The perturbation is confined to the core-cladding boundary; the change to the refractive index in this region is given by

$$k^2\delta n = k^2\left(n_{co}^2 - n_{c\ell}^2\right) = V^2/\rho^2 \quad . \qquad (6.14)$$

This perturbation region is built up of elements

$$dA = \frac{1}{2}\left(R_p^2(\phi) - 1\right) d\phi$$

$$\simeq \sum_{j=1}^{\infty} a_j \cos j\phi \, d\phi \qquad (6.15)$$

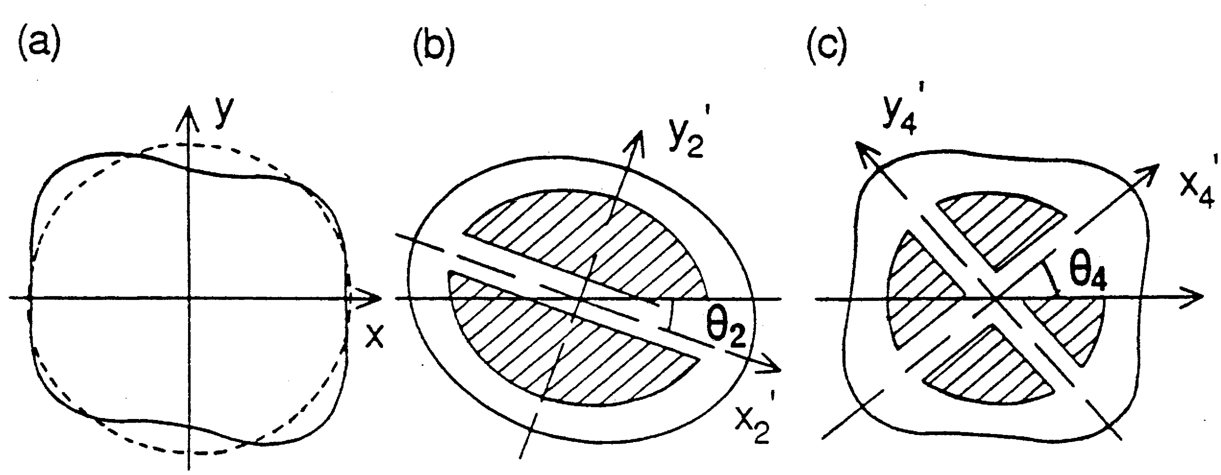

Fig. 6.1 (a) Circular boundary (dashed curve) perturbed with non-zero a_2 and a_4, and $\theta_2 = -20°$, $\theta_4 = 40°$. Optical axes and schematic presentation of sine mode intensity are for (b) the first $\ell = 1$ and (c) the $\ell = 2$ modes. The axes in (b) also apply to the fundamental mode. The perturbations are unrealistically large for illustrative purposes.

(a) **Higher-Order, $\ell \geq 1$ modes**

For the higher-order modes there is an odd and an even mode for every ℓ . The fields are given by

$$\psi = \begin{cases} F_\ell(R)\ \cos\ell\phi & \text{for the even mode} \\ F_\ell(R)\ \sin\ell\phi & \text{for the odd mode} \end{cases} \tag{6.16}$$

and $F_\ell(R)$ is given by eqn. (2.23) for the step-profile. Because the perturbation only exists close to the boundary, and is zero elsewhere, we can set

$$F_\ell(R) \approx F_\ell(1) = 1$$

The difference between $\ell \geq 1$ even and odd modes is then given by eqn. (6.6) and (6.14)-(6.16):

$$\delta\beta_e - \delta\beta_o = \frac{V(2\Delta)^{1/2}}{2\pi\rho\chi_\ell} \sum_{j=1}^{\infty} a_j \int_0^{2\pi} \cos 2\ell\phi\ \cos j\phi\ d\phi \tag{6.17}$$

where χ_ℓ is the normalization integral eqn. (2.25).

Equation (6.17) is only non-zero for the term proportional to $a_{2\ell}$. Thus the modes are

$$\psi_\ell = F_\ell(R) \left\{ \begin{matrix} \cos\ell(\phi - \phi_{2\ell}) \\ \text{or} \\ \sin\ell(\phi - \phi_{2\ell}) \end{matrix} \right\} \{\hat{\underset{\sim}{x}}'_{2\ell} \ \text{ or } \ \hat{\underset{\sim}{y}}'_{2\ell}\} \quad . \tag{6.18}$$

The propagation constant degeneracy between even and odd modes is broken. From eqn. (6.17) we have

$$\bar{\beta}_e - \bar{\beta}_o = \frac{a_{2\ell}}{\rho} \frac{(2\Delta)^{1/2}}{V} \frac{U^2\ K_\ell^2(W)}{K_{\ell-1}(W)\ K_{\ell+1}(W)} \tag{6.19}$$

(b) **Fundamental, $\ell = 0$ modes**

The approximation $\psi \approx \psi_0$ is inadequate for determining the vector corrections to the scalar propagation constant on the arbitrary cross-section fiber (see eqn. (6.8)). In the Appendix we use a Green's function method to show that corrections to the fundamental field of a step-profile fiber are given by

$$\psi = F_0(R) + V^2 \sum_{j=1}^{\infty} F_j(R)\, D_j\, a_j \cos j\phi \tag{6.20a}$$

where

$$D_j = \frac{K_j J_j}{W\, J_j K_{j-1} + U K_j J_{j-1}} \tag{6.20b}$$

$$F_j(R) = \begin{cases} J_j(UR)/J_j & 0 < R \leq 1 \\ K_j(WR)/K_j & R > 0 \end{cases} \tag{6.20c}$$

In eqns. (6.20) we have set $J_n \equiv J_n(U)$ and $K_n \equiv K_n(W)$.

We now substitute eqn. (6.20a) into eqn. (6.8) to obtain the birefringence. The details are left to the Appendix. By symmetry, only the term in ψ proportional to a_2 has any effect, and the birefringence is given by:

$$B = \frac{a_2}{\rho} \frac{(2\Delta)^{3/2}}{V} \frac{W^2}{V^2} \left[(U^2 - W^2)\left(\frac{J_0}{J_1}\right)^2 + UW^2\left(\frac{J_0}{J_1}\right)^3 + U^2 \right] \tag{6.21}$$

where $J_\ell \equiv J_\ell(U)$. Thus the fundamental modes have the form

$$\psi_{01} = \psi\ (\hat{\underset{\sim}{x}}{}_2' \quad \text{or} \quad \hat{\underset{\sim}{y}}{}_2') \tag{6.22}$$

where ψ is given by eqn. (6.20), and the birefringence is given by eqn. (6.21).

(c) Elliptical Core Cross-Section

We compare our results for the arbitrary cross-section fiber (eqn. (6.19) for mode splitting and eqn. (6.21) for birefringence) to known results for the specific case of the elliptical cross-section fiber.

The normalized radius for the elliptical core is

$$R_e(\phi) = \frac{\left(1 - e^2\right)^{1/4}}{\left(1 - e^2 \cos^2\phi\right)^{1/2}} \qquad (6.23)$$

where e is a measure of the ellipticity and is defined by

$$e^2 = 1 \left(\frac{\text{minor axis}}{\text{major axis}}\right)^2$$

since e << 1 one can Taylor expand eqn. (6.13). To first order the result is

$$R_e(\phi) = 1 + \frac{1}{4} e^2 \cos 2\phi \quad . \qquad (6.24)$$

By comparing with eqn. (6.12) one associates

$$a_2 = \frac{1}{4} e^2 \quad . \qquad (6.25)$$

From the results of section (a) only the $\ell = 1$ mode set will split, with a difference in propagation constants given by eqn. (6.19). This agrees with the known results [5,6]. Substituting eqn. (6.25) into (6.21) yields the birefringence due to an elliptical core. This agrees with previous results [4,7].

(d) Discussion

On a circularly symmetric optical fiber the $\ell \geq 1$ modes are called HE and EH modes, whose polarization properties change as they propagate along the fiber. When the cross-section is no longer circular, however, these modes become linearly-polarized (LP) modes.

In single mode fibers the perturbation will create a birefringence. One must take into account polarization effects, and perturbation corrections to the field, in order to describe this birefringence. We have used a Green's function method to derive these field corrections for any mode. However, symmetry effects will dominate polarization effects for only slight perturbations.

We have shown that when the perturbation parameter $a_{2\ell}$ is sufficiently non-zero the ℓ mode set becomes LP with polarization axes

$$\hat{\underset{\sim}{x}}'_{2\ell}\ ,\ \hat{\underset{\sim}{y}}'_{2\ell} \qquad \ell \geq 1$$

$$\hat{\underset{\sim}{x}}'_{2}\ ,\ \hat{\underset{\sim}{y}}'_{2} \qquad \ell = 0$$

Although the fundamental and $\ell = 1$ modes have the same optical axes, higher order modes may have different axes, contrary to the statement in ref. [6]. The ℓ modes "see" a circular fiber perturbed by the $a_{2\ell}$ term (see fig. 6.1).

Only the ℓ set of modes will be degenerate for the $a_{2\ell}$ perturbation; i.e. only the $\ell = 1$ modes will split on an elliptical core cross-section. The higher-order modes will also split, but second-order perturbation theory must be used to describe these smaller effects. In general, for an elliptical core cross-section, the $\ell = k$ propagation constants will be degenerate when one uses e^{2k} perturbation theory, where e is the ellipticity. In order to use terms that have coefficients e^4 one must consider corrections to the modal field which have coefficient e^2 . These can be derived by a Green's function method, and are given in the Appendix for any mode ℓ .

In Section 6-6 we propose the use of a divided-pump four-photon mixing process to investigate these modal splittings due to cross-section shapes, and present theoretical curves for frequency shift.

5. Step-Index Fibers with a Dip in the Profile

Early low-loss fibers fabricated by the chemical vapour deposition (CVD) process, or the modified chemical vapour deposition (MCVD) process, often have a refractive index dip in the core [8]. This is due to the preferential evaporation of the dopant during the high-tempertures of the preform collapsing stage [9].

We consider a Gaussian-shaped dip in the core of a fiber, which we write as

$$\delta n = \gamma \Delta n_{co}^2 \; e^{-R^2/d^2} \tag{6.26}$$

where γ is the dip depth and d the dip width, as shown in figure 6.2.

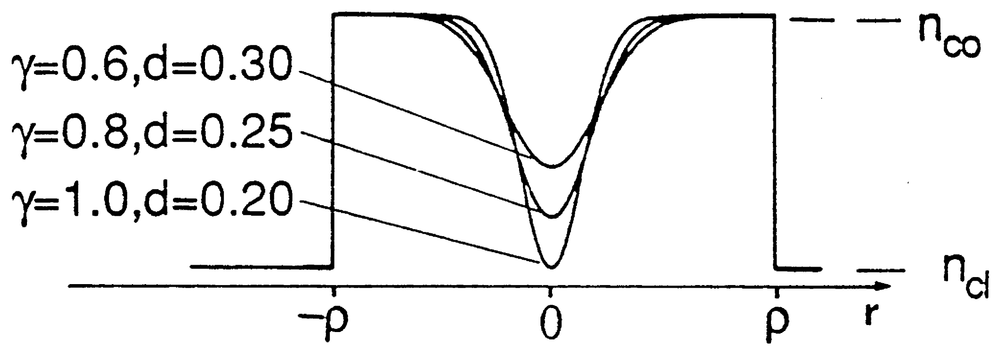

Fig. 6.2 Refractive index profiles for the fiber with a dip in the core.

(a) Perturbation Analysis

For very small dips we may set $\psi \simeq \psi_0 = F_\ell(R)\begin{Bmatrix}\cos\ell\phi\\ \sin\ell\phi\end{Bmatrix}$, where $F_\ell(R)$ is given by eqn. (2.23). The perturbation region is over the core, and the difference in propagation constants is given by eqn.(6.4):

$$\bar{\beta}^2 - \bar{\beta}_0^2 = -\frac{\gamma\Delta k n_{co}^2}{2J_\ell^2(U_0)\chi_\ell}\int_0^1 e^{-R^2/d^2}\, J_\ell^2(U_0R)\, RdR \qquad . \qquad (6.27)$$

where U_0 is the eigenvalue of the unperturbed fiber, eqn.(2.18a), and χ_ℓ is the normalization factor, eqn. (2.25). Because the Gaussian function falls off very rapidly in our examples we replace the integration over the core by integration over the infinite cross-section. The result is

$$\bar{\beta}^2 - \bar{\beta}_0^2 = -\frac{\gamma}{2}\, U_0^2 d^2 \exp\left(-\frac{1}{2}U_0^2d^2\right) I_\ell\left(\frac{1}{2}U_0^2 d^2\right)\frac{\left(K_0(W_0)/J_0(U_0)\right)^2}{K_1^2(W_0)}$$

$$(6.28)$$

From eqn. (2.41) the eigenvalues of a fiber with a dip in the core is

$$U_d^2 = U_0^2 - \rho^2(\bar{\beta}^2 - \bar{\beta}_0^2) \tag{6.29}$$

The $\ell = 0$ modes will be significantly affected, because these modes have their intensity peaks in the centre of the profile. The $\ell \geq 1$ modes, on the other hand, have zero intensity at the centre of the profile and peaks towards the core-cladding boundary, thus they are only slightly affected by the presence of the dip (see fig. 6.4).

(b) Numerical Analysis

Equation (6.28) will be accurate for small dips where the approximation $\psi \simeq \psi_0$ is valid, but in practice dips have a depth [8] $0.6 < \gamma < 1.0$ and the fields, particular the fundamental mode field, will be significantly affected by the dip [10,11].

In this case the fields and propagation constants can be evaluated by a numerical procedure. In terms of eqn. (2.17) the profile shape for the Gaussian dip is

$$f = \frac{1}{2}\gamma e^{-R^2/d^2} \tag{6.30}$$

Substituting eqn. (6.30) into eqn. (2A.2), and employing the numerical procedure outlined in the Appendix of Chapter 2, yields the eigenvalue for this profile.

In figure 6.3 we compare eqn. (6.29) and the eigenvalue obtained numerically for the fundamental mode in the presence of a refractive index dip. We vary the dip width d for $\gamma = 1$ and $\gamma = 0.5$ and a fixed $V = 2.2$.

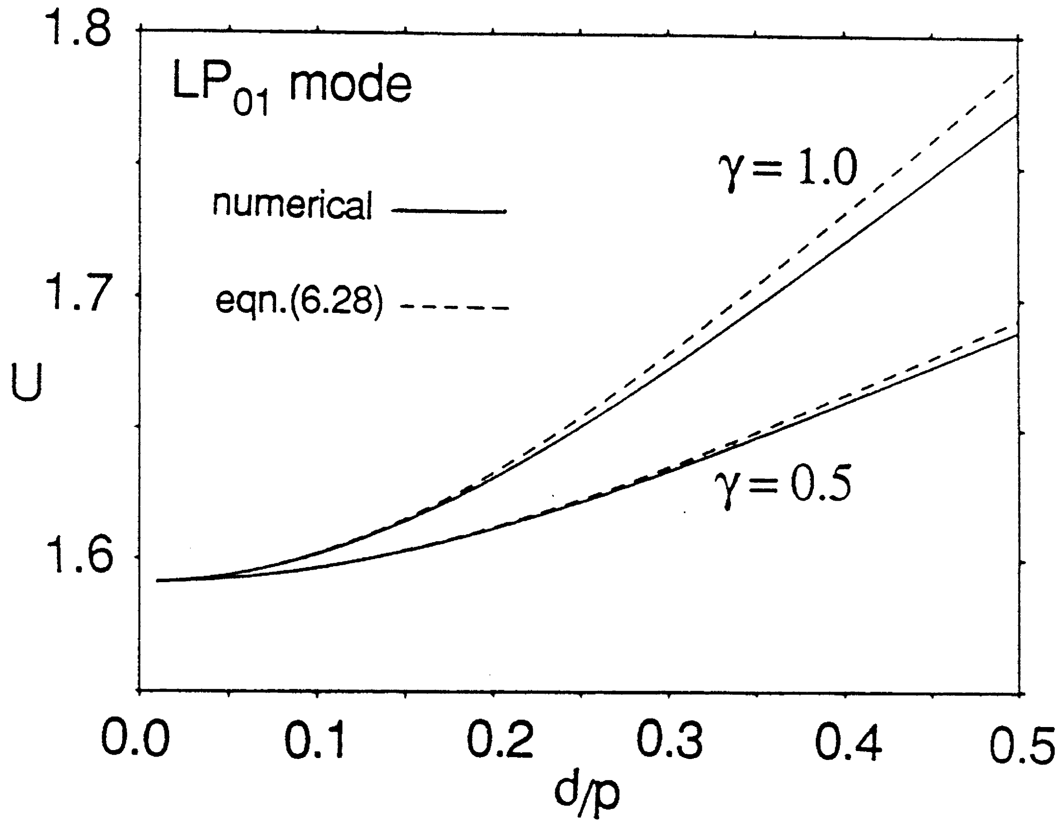

Fig. 6.3 Comparison of the numerical and approximate solutions of the fundamental mode eigenvalue plotted against dip width d/ρ . V is fixed at 2.2.

In figure 6.4 we plot (a) the eigenvalue (from eqn. (2A.2)) and (b) the modal group delay (calculated numerically from the above eigenvalues and eqn. (3.5)) against normalized frequency V. We consider a dip with parameters $\gamma = 0.64$ and $d = 0.30$, and for comparison we include the step-profile (unperturbed) result, $\gamma = 0$.

In figure 6.5 we plot the cut-off value of the $\ell = 1$ mode against d for several values of dip depth γ . The cut-off value of the $\ell = 1$ mode increases with increasing dip size.

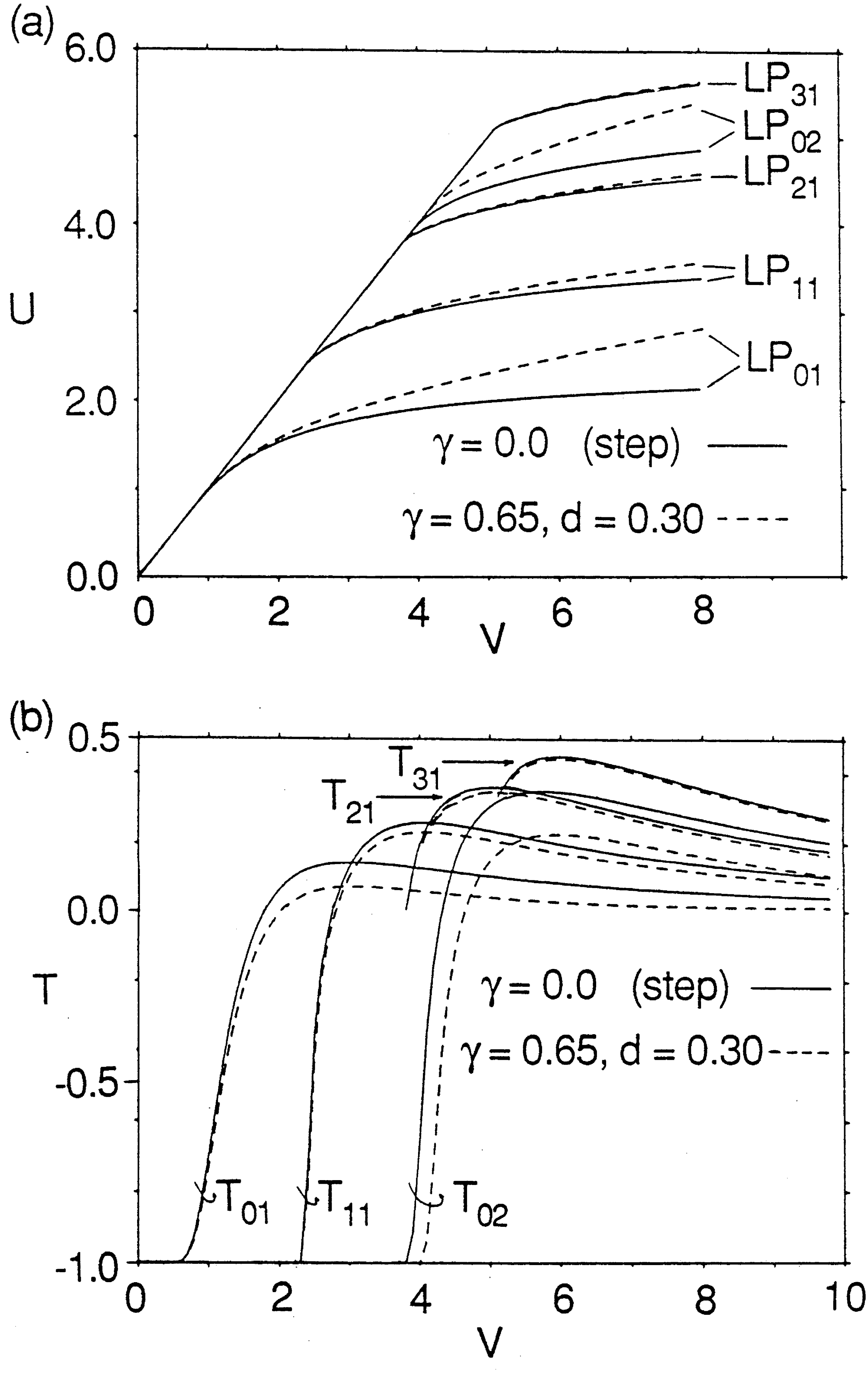

Fig. 6.4 (a) The eigenvalue U and (b) the modal group delay T against normalized frequency V for a dip profile with $\gamma = 0.64$, $d = 0.30$. The unperturbed curves ($\gamma = 0$) are included for comparison.

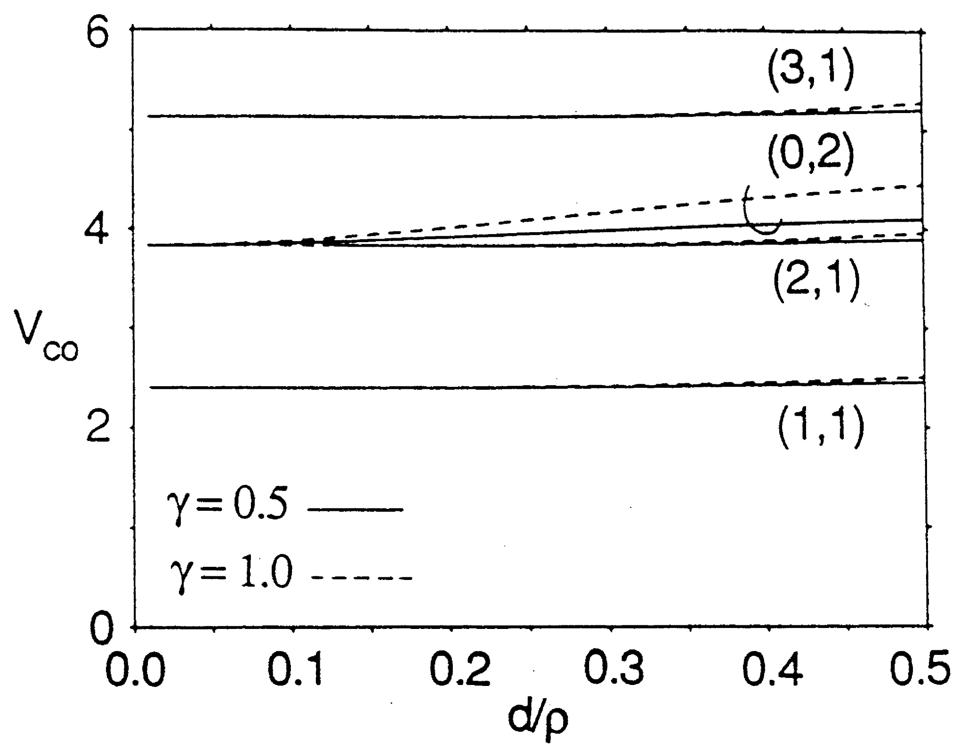

Fig. 6.5 Cut-off values against dip width d/ρ for $\gamma = 1.0$ and $\gamma = 0.5$.

6. Four-Photon Mixing Experiments

We look at measuring the perturbation studied in this Chapter by using the stimulated four-photon mixing process. First we present theoretical frequency shifts for the case of the arbitrary core cross-section fiber, and then we compare theoretical results to experimental frequency shifts on a fiber with a dip in refractive index profile.

(a) Arbitrary Cross-Section Fibers

A divided-pump four photon mixing experiment, in which pump waves excite the odd (sine) and even (cosine) symmetries of the $\ell \geq 1$ modes and generate a Stokes and an anti-Stokes wave, is proposed to measure the mode splitting specified by eqn. (6.19). The phase-matched condition for this process determines the frequency shift Ω_ℓ from pump to generated waves (see Section 5-3). Because the ℓ modes only "see" the $a_{2\ell}$ perturbation term, as explained in Section 6-4(d), Ω_ℓ is proportional to, and hence a measure of, $a_{2\ell}$.

Figure 6.6 gives theoretical curves for the first few modes. Thus a study of frequency shifts using four-photon mixing gives information on fiber perturbations, symmetry and magnitude.

The single-mode process may also be employed, subject to the symmetry restrictions of Section 5-3(c), which will generate larger frequency shifts than those given here, and hence more suitable in practice. The mode splitting of the ℓ = 1 modes on an elliptical core fiber have been observed in such a process [12].

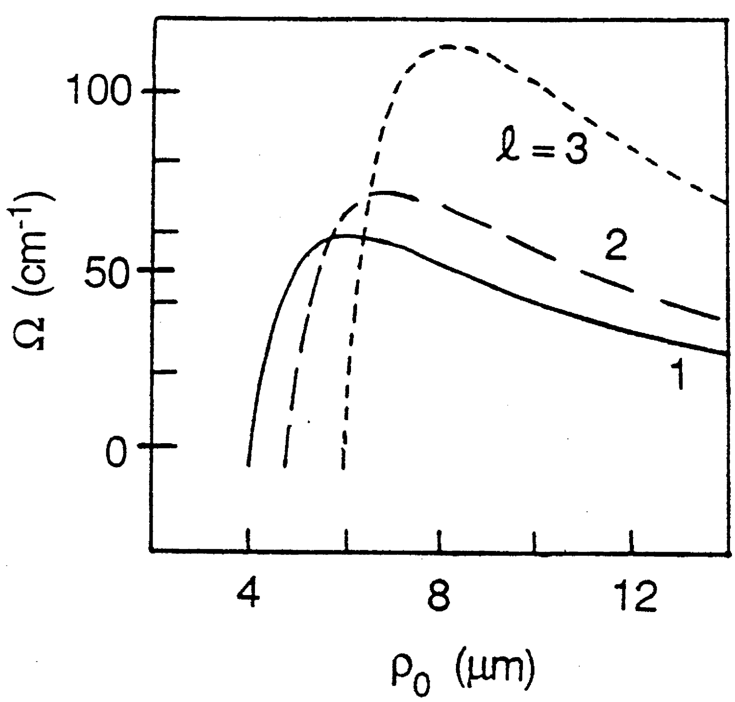

Fig. 6.6 Frequency splitting Ω between the two symmetries of the first few modes against fiber core radius ρ_0 for a divided-pump four-photon mixing experiment. Pump wavelength λ_p = 0.532 μm , Δ = 0.01, and $a_{2\ell}$ = 0.06 .

(b) Experiments on Profiles with a Refractive Index Dip*

Frequency shifts on a few-mode fiber using the stimulated four-photon mixing process have been measured [13]. Experiments were conducted using a Q-switched Nd:YAG laser with intra- ~~inter~~cavity frequency doubling, so that $\lambda_p = 0.532\ \mu m$. The 12 m length of fiber made by Fujikura Densen was coupled through a x20 microscope objective.

The recollimated fiber output was directed to a monochromator and simultaneously through a pair of high-dispersion prisms to a display screen. This arrangement allowed the participating modes to be identified as the spectrum was being recorded. By adjusting the launch conditions a variety of mode combinations could be produced at the phase-matched condition.

Figure 6.7 shows the experimental shifts for various mode combinations. The important observation from this diagram is that the modal group delay of the LP_{02} mode is less than the modal group delay of the LP_{21} , since the difference in group delays is directly proportional to the frequency shift (see eqn. (5.9)). We deduce, therefore, that the fiber cannot be a step-profile (see fig. 3.7 and 3.8), and from the results of Section 6-5, and in particular fig. 6.4(b), we conclude the fiber must have a refractive index dip in the core.

To determine γ and d (assuming the dip can be modelled by eqn. (6.30)) we consider the ratios of the experimental frequency

---

* I would like to thank G.E. Rosman for allowing me to participate in re-creating the original experiment [13], and for many invaluable discussions concerning this experiment and four-photon mixing in general.

shifts. This is equivalent to the ratio of the difference in modal group delays (see eqn. (5.9)) which depends only on V. We define

$$\Omega_{\ell m} = (T_{\ell m} - T_{01})(n_{co}\Delta)/(\lambda D(\lambda)) \equiv \delta T_{\ell m}(V)N(m) \qquad (6.31)$$

where the function variable m is the molar percent of GeO_2 dopant. We thus have

$$\Omega_{\ell m}/\Omega_{11} = \frac{T_{\ell m} - T_{01}}{T_{11} - T_{01}} \equiv \frac{\delta T_{\ell m}(V)}{\delta T_{11}(V)} \quad . \qquad (6.32)$$

The experimental ratios $\Omega_{\ell m}/\Omega_{11}$ are given in Table 6.1 For the Ω_{21}/Ω_{11} ratio there will be a spread of values around 1.98 because of the deviation in measuring Ω_{21} (see fig. 6.7).

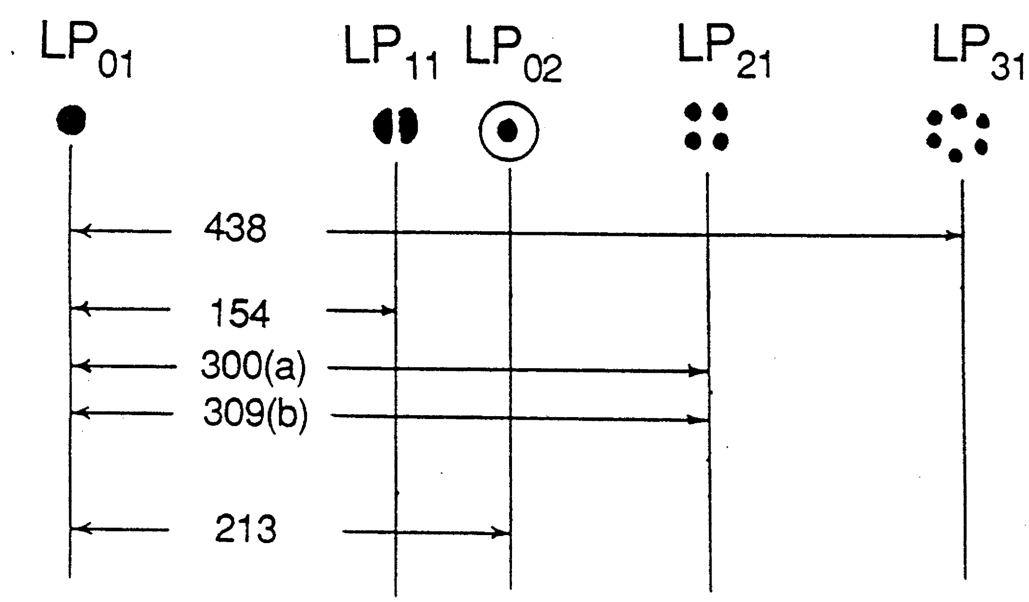

Fig. 6.7 Summary of the experimental results of ref. [13]. For each mode pair the numbers indicate the frequency shift in cm^{-1} units. The biggest discrepancy is between the two readings (a) and (b) of the LP_{21}-LP_{01} pair.

Table 6.1

Ratio of experimental and theoretical frequency shifts

$\Omega_{\ell m}/\Omega_{11}$	$\delta T_{\ell m}/\delta T_{11}$			
	Exp.	Theory (V=6)		
		$\gamma = 0.95$ $d = 0.20$	$\gamma = 0.73$ $d = 0.25$	$\gamma = 0.64$ $d = 0.30$
Ω_{02}/Ω_{11}	1.38	1.38	1.38	1.38
Ω_{21}/Ω_{11}	1.98	1.99	1.99	2.00
Ω_{31}/Ω_{11}	2.84	2.83	2.84	2.85

The ratio $\delta T_{\ell m}/\delta T_{11}$ can be numerically determined as a function of V for various values of γ and d . We find that V must be in the range $5.9 < V < 6.1$ to fit the results of Table 6.1, although γ,d and V are not uniquely defined. As the fiber is specified to be single-moded at 1.3 μm , this value is qualitively what one would expect at 0.532 μm (see fig. 6.5).

If we choose V=6, then the experimental ratios are best fitted by the theoretical dip parameters given in Table 6.1. The value of δT_{11} is included, so that $\delta T_{\ell m}$ can be found.

To find the material composition (assuming GeO_2 dopant) we re-write eqn. (6.31) as

$$N(m) = \frac{n_{co}\Delta}{\lambda\ D(\lambda)} = \frac{154}{\delta T_{11}} \quad (cm^{-1}) \tag{6.33}$$

where $\delta T_{11}(V)$ is found numerically, and $\Omega_{11} = 154\ cm^{-1}$ is found from the experimental results. In figure 6.8 we plot the material function N(m) against m for $\lambda = 0.532\ \mu m$. Eqn. (6.33) specifies N(m), and then fig.6.8 specifies the value of m for some δT_{11}. The material parameters n_{co}, Δ and $D(\lambda)$, which are functions of m, are then given by eqn. (3.11). The results are presented in Table 6.2.

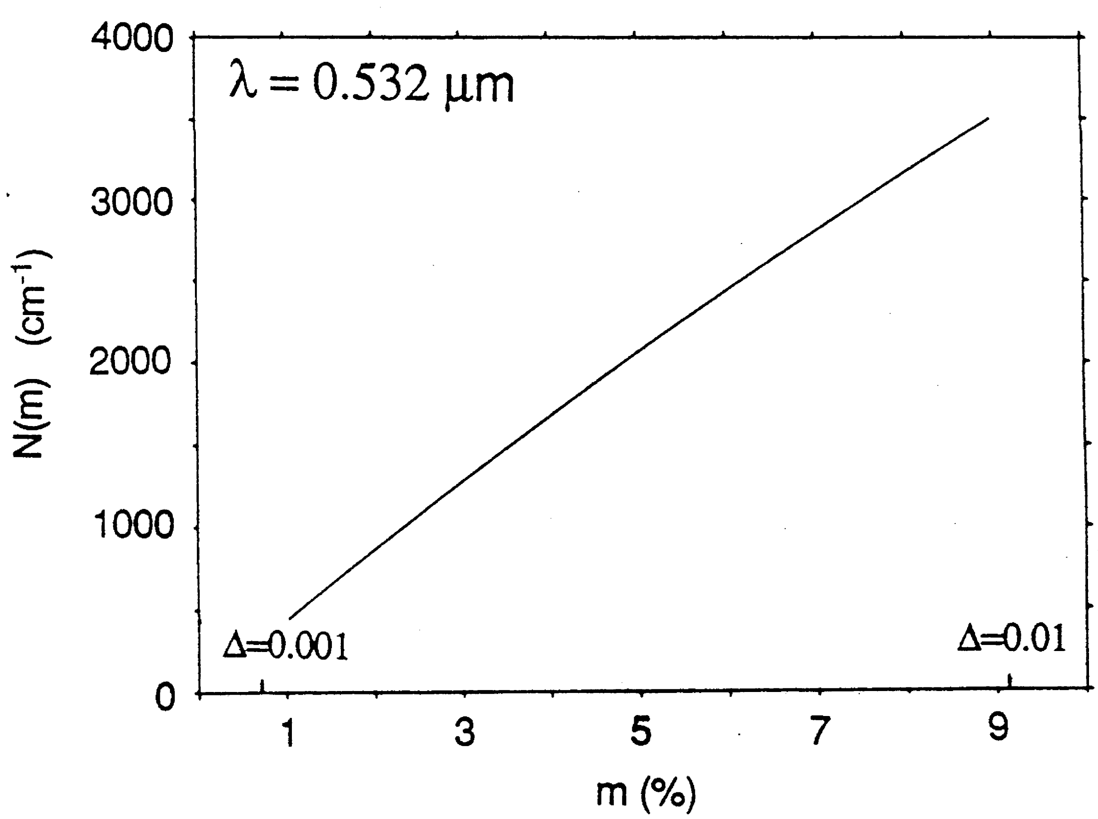

Fig. 6.8 The function N(m) (eqn. (6.33)) plotted against m, the amount of GeO_2 dopant in the core.

Table 6.2 Theoretical Parameters for Frequency Shift

Fiber $V = 6.00$	δT_{11}	$N(m)$ (cm^{-1})	m(%)	Δ	ρ (μm)
γ=0.95,d=0.20	0.1425	1080.7	2.522	0.0028	4.59
γ=0.73,d=0.25	0.1441	1068.7	2.493	0.0028	4.62
γ=0.64,d=0.25	0.1454	1059.1	2.470	0.0028	4.64
		λ = 0.532 μm			

The value of ρ is found by setting the normalized frequency (eqn. (2.15)) to $V = 6.0$ at $\lambda = 0.532$. These values of ρ and Δ are in good agreement with the value given by Fujikura on the specification sheet for this fiber: $\rho = 4.5\ \mu m$, $\Delta = 0.0026$. Theoretical frequency shifts are now given by eqn. (6.31). Comparison with the experimental data is shown in Table 6.3.

Table 6.3 Comparison of Theoretical and Experimental Frequency Shifts (cm^{-1})

Ω	Exp	Theory		
		$\gamma=0.95$, $d=0.20$	$\gamma=0.73$, $d=0.25$	$\gamma=0.64$, $d=0.30$
Ω_{11}	154	154.0	154.0	154.0
Ω_{02}	213	212.4	212.5	211.8
Ω_{21}	305	305.8	307.0	308.5
Ω_{31}	438	435.5	437.1	439.1

The profile of this fiber was measured* by a modified near-field method [14], and the graph is shown in fig. 6.9. Our fiber model with $\gamma=0.64$, $d=0.30$ is overlaid for comparison. The depth of the depression is limited by the resolution of the method [15], and the actual dip most likely has $\gamma \gtrsim 0.6$ [9].

The measured core radius is in good agreement with the theoretical prediction, but the measured profile height is $0.0036 < \Delta < 0.0041$, some 30% larger than our value. Our Δ should be interpreted as an "effective" profile height, taking into account the profile shape of fig. 6.9. Furthermore, we have assumed a pure silica cladding and a GeO_2 doped core. Different material composition may alter the N(m) vs. m curve, and hence our results.

However, further evidence to support the validity of our simple profile shape can be found by examining the dispersion curves. In figure 6.10 we compare the experimental dispersion data to the numerical derivative $k\, d^2\bar{\beta}/dk^2$, where $\bar{\beta}$ is the propagation constant for the dip profile with $\gamma = 0.64$, $d = 0.30$, $\Delta = 0.0028$ and $\rho = 4.64 \mu m$. The difference in the zero-dispersion wavelength ($\lambda_{zd} = 1.3\ \mu m$) between experiment and theory is 0.3%.

---

* The author gratefully acknowledges Professor P.L. Chu, D. Irving, and T. Whitebread for conducting these experiments.

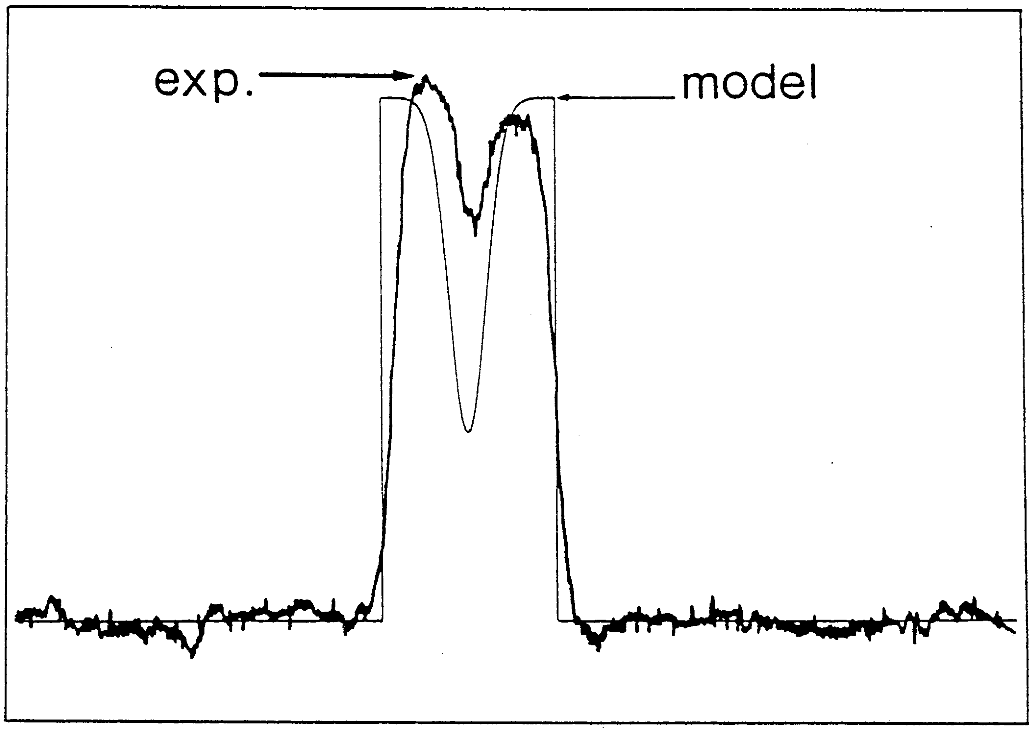

Fig. 6.9 The measured refractive index profile of the Fujikura fiber, superimposed on the profile model with parameters $\gamma = 0.64$, $d = 0.30$, $\Delta = 0.0028$ and $\rho = 4.64\ \mu m$.

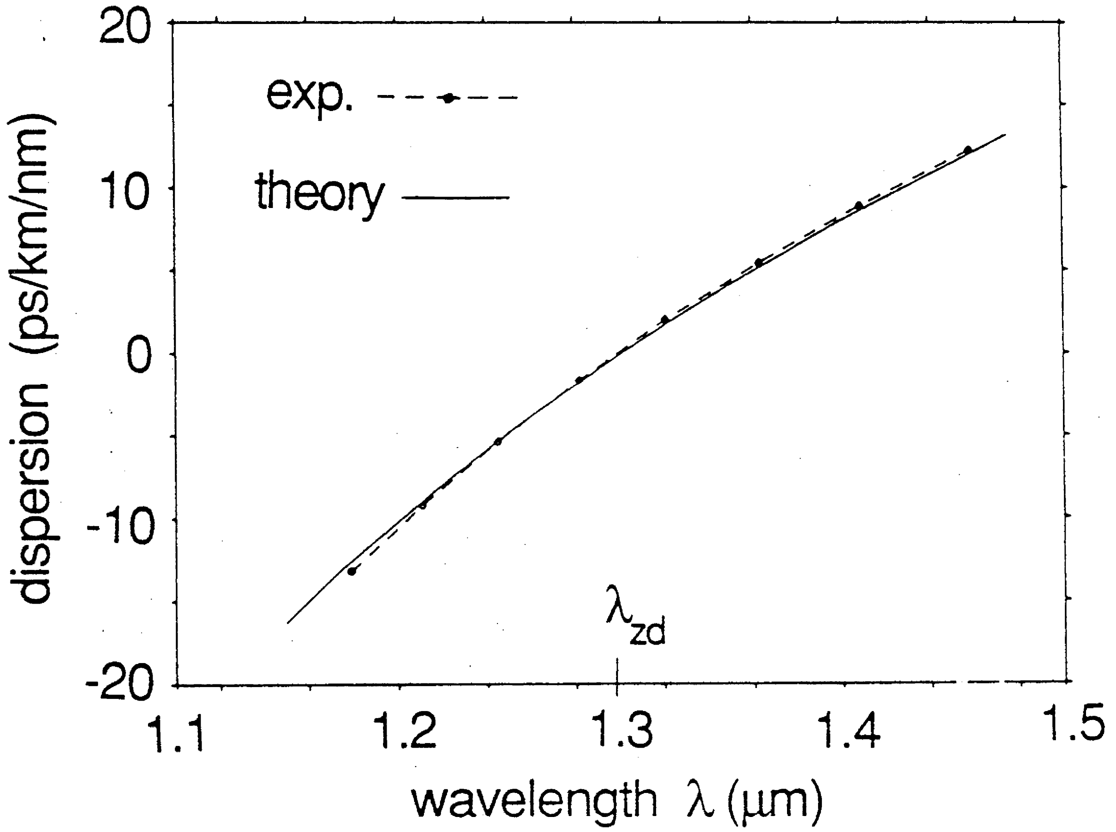

Fig. 6.10 Dispersion properties of the profiles shown in Fig. 6.9. The theoretical curve is the numerical derivative $k\, d^2\bar{\beta}/dk^2$.

7. Appendix

(i) Green's function method

We generalize a Green's function method for determining the field corrections to the fundamental mode of an elliptical core fiber [4,6] to the case of the few mode arbitrary core cross-section fiber. We substitute eqn. (6.3) into eqn. (6.16), and rearrange to obtain

$$\left(\nabla_t^2 + k^2 n_0^2 - \bar{\beta}^2\right)\psi = -k^2\ \delta n\psi \tag{6A.1}$$

where $\bar{\beta}^2$ is given by eqn. (6.4) and $\delta n\psi \equiv \delta n(\underset{\sim}{r})\ \psi(\underset{\sim}{r})$.

The homogeneous solution to this equation, which we denote ψ_h , is the scalar wave equation. A particular solution, which we denote ψ_p , is the integral equation

$$\psi_p(\underset{\sim}{r}) = -k^2 \int_{A'} G(\underset{\sim}{r},\underset{\sim}{r}')\ \delta n(\underset{\sim}{r}')\ \psi(\underset{\sim}{r}')\ dA' \tag{6A.2}$$

where A' is the area in which δn is non-zero, $\underset{\sim}{r}'$ is a fixed position, and $G(\underset{\sim}{r},\underset{\sim}{r}')$ is the Green's function which satisfies the equation

$$\left(\nabla_t^2 + k^2 n_0^2 - \bar{\beta}^2\right) G(\underset{\sim}{r},\underset{\sim}{r}') = \delta(\underset{\sim}{r} - \underset{\sim}{r}') \tag{6A.3}$$

where δ is the Dirac delta function.

$\psi(\underset{\sim}{r}')$ is unknown, but if we assume a small perturbation we can replace $\psi(r')$ by $\psi_0(r')$, where ψ_0 is the solution to the unperturbed scalar wave equation. We then have [16]

$$\psi_p(\underset{\sim}{r}) = -k^2 \int_{A'} G(\underset{\sim}{r},\underset{\sim}{r}')\ \delta n(\underset{\sim}{r}')\ \psi_0(\underset{\sim}{r}')\ dA' \quad . \tag{6A.4}$$

The two-dimensional delta function on the right side of eqn. (6A.2) can be expanded in polar coordinates as

$$\delta(\underset{\sim}{r} - \underset{\sim}{r}') = \frac{1}{r}\,\delta(r - r')\,\delta(\phi - \phi')$$
$$= \frac{1}{r}\,\delta(r - r') \sum_{-\infty}^{\infty} e^{i\ell(\phi - \phi')} \tag{6A.5}$$

We assume a similar expansion for the Green's Function:

$$G(\underset{\sim}{r},\underset{\sim}{r}') = \frac{1}{2\pi} \sum_{-\infty}^{\infty} g_n^r\,(r,r')\,e^{i\ell(\phi - \phi')} \quad . \tag{6A.6}$$

From eqns. (6A.2), (6A.5) and (6A.6), the radial Green's Function $g_n^r(r',r)$ satisfies

$$\left(\frac{\partial^2}{\partial r^2} + \frac{1}{r}\frac{\partial}{\partial r} - \frac{n^2}{r^2} + k^2 n_0^2 - \bar{\beta}^2\right) g_n^r(r,r') = \frac{1}{r}\,\delta(r - r') \tag{6A.7}$$

The complementary solution to eqn. (6A.7), for a step-profile, is

$$g_n^r = \begin{cases} A_n J_n(UR)/J_n(U) & 0 \le R \le 1 \\ B_n K_n(WR)/K_n(W) & R > 1 \end{cases} \tag{6A.8}$$

where the normalized eigenvalues are defined as

$$U^2 = \rho^2\left(k^2 n_{co}^2 - \bar{\beta}^2\right) = U_0^2 - \rho^2\,\delta\beta^2$$
$$W^2 = \rho^2\left(\bar{\beta}^2 - k^2 n_{c\ell}^2\right) = W_0^2 + \rho^2\,\delta\beta^2 \tag{6A.9}$$

where $\delta\beta^2$ is given by eqn. (6.4) and U_0, W_0 are the eigenvalues of the unperturbed fiber, eqn. (2.18).

g_n^r must be continuous at $r = \rho$, so that $A_n = B_n$ at $R = 1$. A_n and B_n are determined from the condition

$$\lim_{\varepsilon \to 0} \left(\frac{\partial g_n^r}{\partial R}\right) \Bigg|_{R - \varepsilon}^{R + \varepsilon} = 1$$

from which we obtain

$$A_n = B_n = - \frac{K_n(W)\, J_n(U)}{WJ_n(U)\, K_{n-1}(W) + UK_n(W)\, J_{n-1}(W)} \equiv -D_n \tag{6A.10}$$

The solution to eqn. (6A.1) is the addition of the homogeneous and particular solutions

$$\psi = \psi_h + \psi_p \tag{6A.11}$$

where ψ_p is given by eqn. (6A.4), with the Green's function given by eqn. (6A.6) and (6A.8).

(ii) Perturbation solution for field corrections

The homogeneous solution to eqn. (6A.1) for a step-profile fiber is

$$\psi_h = F_\ell(R) \begin{Bmatrix} \cos \ell\phi \\ \sin \ell\phi \end{Bmatrix} \tag{6A.12}$$

where $F_\ell(R)$ is given by eqn. (2.23) with eigenvalues U and W given by eqn. (6A.9).

Because the perturbation is zero everywhere but in the region close to the fiber boundary $r = \rho$ (see fig. 6.1), we can approximate the modal fields of the unperturbed fiber by their values at the boundary interface:

$$\psi_0 \simeq \begin{Bmatrix} \cos\ell\phi \\ \sin\ell\phi \end{Bmatrix} \tag{6A.13}$$

for $\begin{Bmatrix} \text{even} \\ \text{odd} \end{Bmatrix}$ modes. The particular solution to eqn. (6A.1) is given by eqn. (6A.4). If we substitute in eqn. (6A.13), (6.14) and (6.15) into (6A.4) we have

$$\psi_p(r,\phi) = -V^2 \sum_{j=1}^{\infty} a_j \int_0^{2\pi} G(R,1,\phi,\phi') \cos j\phi' \cos\ell\phi' \, d\phi' \tag{6A.14}$$

The Green's function is given by eqn. (6A.6), and we rewrite it as

$$G(R,R',\phi,\phi') = \sum_{n=0}^{\infty} g_n^r(R,R') \, g_n^\phi(\phi,\phi') \tag{6A.15}$$

where g_n^r is given by eqn. (6A.8) and

$$g_n^\phi = \begin{cases} \dfrac{1}{2\pi} , & n = 0 \\[2ex] \dfrac{1}{\pi} \cos(\phi - \phi') , & n \geq 1 \end{cases} \tag{6A.16}$$

Substituting eqn. (6A.15) into eqn. (6A.14) yields the particular solution

$$\psi_p = -V^2 \sum_{j=1}^{\infty} \sum_{n=0}^{\infty} a_j g_n^r \int_0^{2\pi} g_n^{\phi} \cos j\phi' \cos \ell\phi' \, d\phi' \tag{6A.17}$$

For the fundamental ($\ell = 0$) mode we have

$$\psi_p = -V^2 \sum_{j=1}^{\infty} a_j \, g_j^r \cos j\phi \quad . \tag{6A.18}$$

The radial Green's function is given by eqn. (6A.8) and (6A.10):

$$g_j^r = - D_j F_j(R) \tag{6A.19}$$

where $F_j(R)$ is given by eqn. (2.23) and D_j is given by eqn. (6A.10).

Furthermore, for the $\ell = 0$ mode $\delta\beta^2 = 0$, so that $U = U_0$ and $W = W_0$, and the eigenvalue equation

$$U_0 \frac{J_1(U_0)}{J_0(U_0)} = W_0 \frac{K_1(W_0)}{K_0(W_0)} \tag{6A.20}$$

can be used to simplify the expression D_j.

The field in the perturbed fiber is $\psi = \psi_h + \psi_p$ with ψ_h given by eqn. (6A.12), and ψ_p given by eqn. (6A.18). This is eqn. (6.20) in the text.

If we have an elliptical core cross-section, with $a_2 = 1/4\ e^2$, then eqn. (6.20) is identical to the result of ref. [4].

(iii) Birefringence on arbitrary cross-section fibers

The birefringence is given by substituting eqn. (6.20) into eqn. (6.8). In order to take into account all contributions of order a_j, ψ and its first derivative must be evaluated at

$$R = 1 + \sum_{j=1}^{\infty} a_j \cos j\phi \equiv 1 + \alpha \tag{6A.21}$$

with $\alpha \ll 1$. We then have

$$F_n(1 + \alpha) = F_n(1) + \alpha F_n'(1) \tag{6A.22a}$$

$$F_n'(1 + \alpha) = F_n'(1) + \alpha F_n''(1) \tag{6A.22b}$$

where $F_n(R)$ is given by eqn. (2.23) for the step-profile fiber. From eqn. (2.23) and Bessel function recurrence relations, $F_n(1)$, $F_n'(1)$ and $F_n''(1)$ are easily evaluated.

The element of length $d\ell$ is

$$d\ell = (1 + \alpha)\, d\phi \tag{6A.23}$$

The unit outward normals in cartesian coordinates is

$$n_x = (\cos\phi - \eta \sin\phi)$$

$$n_y = (\sin\phi + \eta \cos\phi) \tag{6A.24}$$

$$\eta = \sum_{j=0}^{\infty} j\, a_j \sin j\phi$$

Substitution of eqns. (6A.22) - (6A.24) into eqn. (6.7) or (6.8) yields the birefringence on arbitrary cross-section fibers, eqn. (6.21). Because of the $\cos 2\phi$, $\sin 2\phi$ terms in the equation for birefringence (see eqn. (6.8)) only the term proportional to a_2 is non-zero.

References for Chapter 6

[1] M. Miyagi and S. Nishida, "Vector analysis of propagation constants in dielectric optical waveguides with perturbed refractive index-profile"
IEEE Trans. Microwave Theory Tech., MTT-33, pp. 667-673 (1985)

[2] J. Sakai and T. Kimura, "Polarization behaviour in multiply perturbed single-mode fibers"
IEEE J. Quantum Electron., QE-18, pp. 59-65 (1982)

[3] R.A. Sammut, C.D. Hussey, J.D. Love and A.W. Snyder, "Modal analysis of polarization effects in weakly-guiding fibers"
IEE Proc. Pt. H, 128, pp.173-187 (1981)

[4] A.W. Snyder, J.D. Love and R.A. Sammut, "Green's function methods for perturbed optical fibers"
J. Opt. Soc. Am., 72, pp. 1131-1135 (1982)

[5] See ref. [2-7]

[6] See ref. [2-1]

[7] J.D. Love, R.A. Sammut and A.W. Snyder, "Birefringence in elliptically deformed optical fibers"
Electron. Letters, 15, pp. 615-616 (1979)

[8] H.M. Presby, "Axial refractive index depression in preforms and fibers"
Fiber Int. Opt., 2, pp. 111-126 (1979)

[9] D. Marcuse, "Principles of Optical Fiber Measurements", (Academic Press, New York, 1981)

[10] W.A. Gambling, H. Matsumura and C.M. Ragdale, "Wave propagation in a single-mode fibre with dip in the refractive index"
Opt. Quantum Electron., 10, pp. 301-309 (1978).

[11] R.H. Stolen, "Modes in fiber optical waveguides with ring index profiles"
Applied Optics, 14, pp. 1533-1537 (1975)

[12] See ref. [5-2]

[13] G.E. Rosman, "Time-domain Interpretation of Four-Photon Spectra from Optical Fibres"
Electron. Letters, 20, pp. 240-241 (1984).

[14] D. Irving, "The measurement and interpretation of single-mode optical fibre refractive index profiles"
(Ph.D Thesis, University of New South Wales, Australia, 1985)

[15] P.V.H. Sabine personnel communications

[16] P. Morse and H. Feshbach, "Methods of Mathematical Physics", (McGraw-Hill, New York, 1953).

CHAPTER 7

MODES ON A BENT OPTICAL WAVEGUIDE
and their study by the
FOUR-PHOTON MIXING PROCESS

1. Introduction

2. Field Equations

3. Single-Mode Fibers
   (a) Fields of the Fundamental Mode
   (b) Geometrical Birefringence
   (c) Discussion

4. Few-Mode Waveguides

5. The Step-Index Slab Waveguide
   (a) Solutions to the Perturbation Equations
   (b) Deformation of Fields due to Bending
   (c) Exact Solution to the First-Order Wave Equation

6. The Step-Index Optical Fiber
   (a) Fields of the Bent Fiber
   (b) Propagation Constant Corrections
   (c) Discussion

7. Four-Photon Mixing Experiments on Bent Few-Mode Fibers

8. Appendix
   (i) Derivation of field equations
   (ii) The x- and y-polarized fields of the fundamental mode
   (iii) Birefringence due to polarization corrections
   (iv) Fields of the single-layer slab waveguide
   (v) Fields of the step-index fiber
   (vi) Corrections to the propagation constant
   (vii) Stability of LP modes on a bent fiber
   (viii) Some Bessel function integrals

CHAPTER 7

MODES ON A BENT OPTICAL WAVEGUIDE
and their study by the
FOUR-PHOTON MIXING PROCESS

1. Introduction

In this chapter we examine changes to the propagation characteristics occurring when optical waveguides are bent. The literature concerned with bends and micro-bends on waveguides is extensive, but in general these studies have dealt with radiation losses [1 - 3]. We will not be concerned with loss here, although the perturbed fields derived in Section 7-1 may be used to obtain more accurate bending loss results, as reported previously [4 - 6].

When an optical fiber or waveguide is bent it is well known that the modal field will shift towards the outer core-cladding boundary as the bend radius decreases [4,7], but the effect on the modal propagation constants, which dictate the birefringence, dispersion and group delay properties of the fiber, is not widely understood.

We show that in single-mode fibers this field shift creates a geometrical birefringence, in addition to the well known birefringence caused by stress [8,9]. In few-mode fibers, the field shift causes a splitting of the higher-order modal fields.

We present simple formulas describing the perturbations to the field and propagation constant of any mode, of either even or odd symmetry. The field in the bent waveguide is derived by assuming that the bend is slight, so that it's effects may be treated as a perturbation to the field and propagation constant of the straight fiber.

Throughout we consider weakly-guiding waveguides, whereby the polarization properties of the modes can be treated seperately, as formulated in Section 2-4. The bend breaks the symmetry of the fiber, and the modes are treated as scalar modes multiplied by a polarization term. The discussion of polarization effects and symmetry effects on waveguides with preferred axes of symmetry in Section 6-2 is then applicable.

After deriving the field equations a perturbation analysis is employed where the fields and propagation constants of the bent fiber are expanded in an ascending series of (ρ/a), where ρ is the waveguide radius and a is the bending radius. The first term in this series is the unperturbed or straight waveguide solution. Each term in the series for the fields decays quickly to zero in the cladding, regardless of the magnitude of the bending radius. However, physically, modes become radiative when the radius is small enough, so that the perturbation solutions will only be accurate close to and within the core region.

The single-mode step-index optical fiber is examined first, and it is shown that the bend creates a difference between the x- and y- polarized fields of the fundamental mode. However, this difference in scalar modes does not describe the birefringence, as reported previously [10]. In that analysis the authors neglected a term, and in fact the birefringence they calculated is zero to order $(\rho/a)^2$, where ρ is the radius of the fiber and a is the radius of curvature. We show that there is a geometrical birefringence of order $(\rho/a)^2$, and that it is due to the inclusion of vector or polarization corrections to the scalar modal fields.

The case of the step-index slab waveguide is then examined, and more physical solutions, in which the field will no longer be bound for small bend radius, are presented. We determine the radiation point, which is the distance from the waveguide where the phase velocities of the propagating mode reaches the local speed of light and the field becomes radiative.

An analysis of the step-index optical fiber is then presented, where the fields and propagation constants are derived. To first-order, the propagation constant of the $\ell=1$ mode becomes non-degenerate. Numerical results are presented for the clad power-law profile. We show that bending the waveguide causes the higher-order scalar propagation constants to become non-degenerate. As explained in Section 6-2, when the symmetry of the waveguide is disturbed the mode splits into odd and even symmetries which propagate through the fiber with different polarization directions and different group delays.

Finally, we use the theory of phase-matching on few-mode fibers to demonstrate that the mode splitting of the $\ell=1$ modes can be measured by the four-photon mixing process and compare our theory to some experimental results.

Theoretical research on modal fields in a bent waveguide has been widely performed. The perturbation expansion used here has been used to analyse the fields and propagation constants of a single- and multi-layered slab waveguide [12],[13]. Analytic solutions for the fields in a bent step-index fiber have been obtained using a first order perturbation theory to the vector wave equation [14],[15], but the solutions are complicated. Experimental confirmation of the field shift in a bent fiber [16],[17] have been reported.

2. Field Equations

To derive the field equations, the vector wave equation, eqn.(2.10) is written in a cylindrical coordinate system, $(\bar{R}, \Theta, \bar{Y})$, with origin at the centre of curvature, as shown in Figure 7.1

$$(\underset{\sim}{\nabla}^2 + k^2n^2)\underset{\sim}{E} = -\underset{\sim}{\nabla}(\underset{\sim}{E}\cdot\underset{\sim}{\nabla}\ln(n^2)) \qquad (7.1)$$

For a wave propagating along the Θ or z axis, the wave equation can be converted to the local coordinate system (r,ϕ,z) where the following geometric relations are used:

$$\bar{R} = a + r\cos\phi$$

$$\Theta = z/a$$

$$\bar{Y} = r\sin\phi$$

The electric field components in the two coordinate systems are related by

$$E_{\bar{R}} = (1/\bar{R})^{1/2}\, E_x \exp(-i\beta_x z) \quad \text{and} \quad E_{\bar{Y}} = (1/\bar{R})^{1/2}\, E_y \exp(-i\beta_y z)$$

E_x and E_y then satisfy the following equations :

$$(\nabla_t^2 + k^2n^2)E_x + \frac{a^2}{\bar{R}^2}\left(\frac{1}{4a^2} - \beta_x^2\right)E_x = -\frac{2}{\bar{R}}\frac{\partial E_x}{\partial \bar{R}} - \left(\frac{3}{2\bar{R}} + \frac{\partial}{\partial \bar{R}}\right)\left(E_x \frac{\partial}{\partial \bar{R}} \ln(n^2)\right) \qquad (7.2a)$$

$$(\nabla_t^2 + k^2n^2)E_y + \frac{a^2}{\bar{R}^2}\left(\frac{1}{4a^2} - \beta_y^2\right)E_y = -\frac{\partial}{\partial \bar{Y}}\left(E_y \frac{\partial}{\partial \bar{Y}} \ln(n^2)\right) \qquad (7.2b)$$

where $E_y = 0$ for light polarized in the x direction, and $E_x = 0$ for light polarized in the y-direction. In eqn.(7.2)

$$\nabla_t^2 = \frac{\partial^2}{\partial r^2} + \frac{1}{r}\frac{\partial}{\partial r} + \frac{1}{r^2}\frac{\partial^2}{\partial \phi^2} .$$

In order to solve the equations one exploits the fact that $\Delta \simeq 0$, and the weak-guidance approximation can be invoked so that the polarization correction term can be neglected intially. The fields and propagation constants of eqn.(7.2) then satisfy a scalar wave equation, and are denoted by $\bar{E}$ and $\bar{\beta}$.

Using the fact that the quantity (ρ/a) is much less than unity the scalar electric field and scalar propagation constant can be expanded in an ascending series of (ρ/a) such that

$$\begin{aligned} \bar{E} &= \bar{E}_0 + \left(\frac{\rho}{a}\right) \bar{E}_1 + \left(\frac{\rho}{a}\right)^2 \bar{E}_2 + \ldots \\ \bar{\beta}^2 &= \bar{\beta}_0{}^2 + \left(\frac{\rho}{a}\right) \bar{\beta}_1{}^2 + \left(\frac{\rho}{a}\right)^2 \bar{\beta}_2{}^2 + \ldots \end{aligned} \tag{7.3}$$

where $\bar{E}_0$ and $\bar{\beta}_0{}^2$ are the straight waveguide solutions. In the next Chapter we study the accuracy of the perturbations expansions eqn. (7.3).

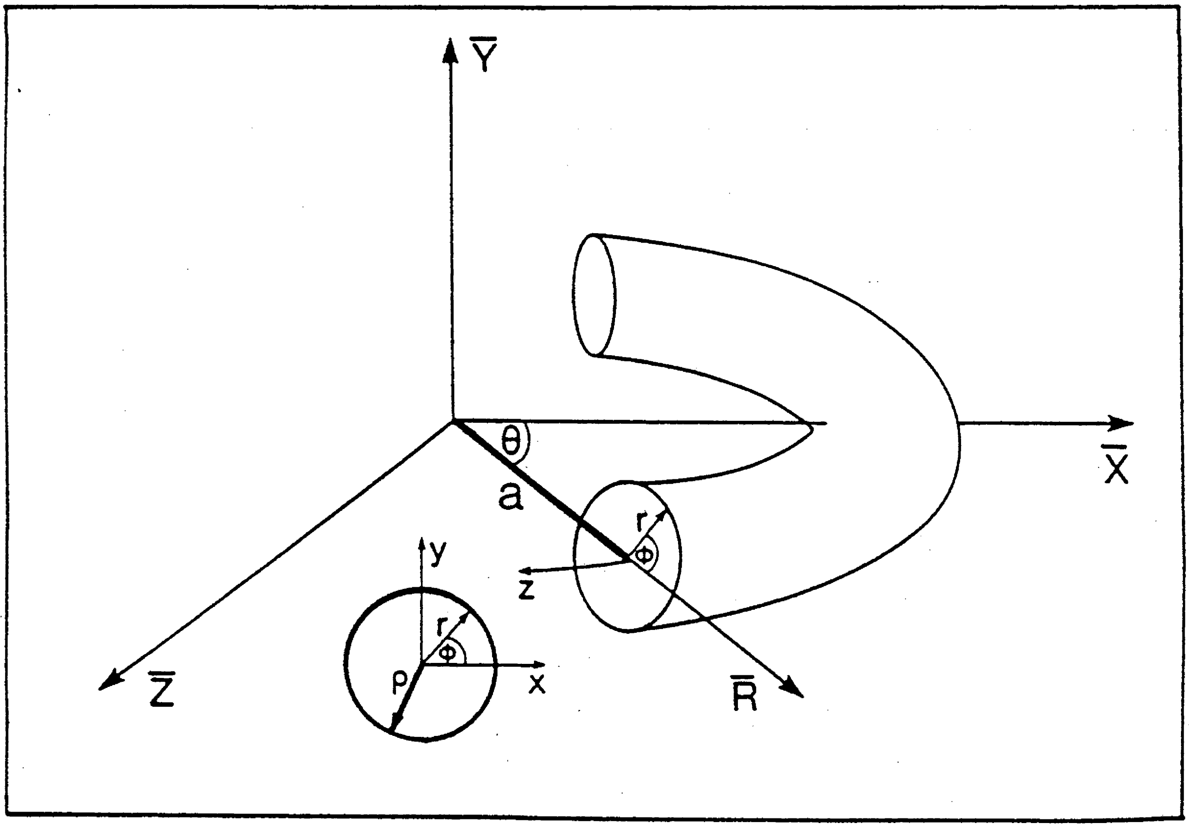

Fig. 7.1 Cylindrical coordinate system $(\bar{R},\theta,\bar{Y})$ and local coordinate system (r,ϕ,z) of the bent fiber.

3. Single-Mode Fibers

We now consider the fundamental mode. Using a Taylor expansion on the second term on the left-side of eqn.(7.2), and then substituting in eqn.(7.3), the following system of equations for $\bar{E}_0$ and $\bar{E}_1$ result to first order:

$$D\bar{E}_{0y} = 0$$

$$D\bar{E}_{1y} = \bar{\beta}_{1y}^2\, \bar{E}_{0y} - 2\, R \cos\phi\, \bar{\beta}_{0y}^2\, \bar{E}_{0y} \qquad (7.4a)$$

$$D\bar{E}_{0x} = 0$$

$$D\bar{E}_{1x} = \bar{\beta}_{1x}^2\, \bar{E}_{0x} - 2\, R \cos\phi\, \bar{\beta}_{0x}^2\, \bar{E}_{0x} - 2 \cos\phi\, \partial\bar{E}_{0x}/\partial R \qquad (7.4b)$$

where $Df = (\nabla_t^2 + k^2n^2 - \bar{\beta}_0^2)f$ is the scalar wave equation for the unperturbed fiber. For the fundamental mode $\bar{E}_0$ is only a function of r. In Section 7-4 we show that by multiplying the first of eqns. (4a) by $\bar{E}_1$,and the second by $\bar{E}_0$, subtracting and integrating over the infinite cross section an expression for $\bar{\beta}_1^2$ results, which is equal to zero for any symmetric fiber. Thus the lowest order correction to the propagation constant behaves as $(\rho/a)^2$.

The method described above to derive the field equations can be extended to include higher-order corrections (see Section 8-3(b)), and dispenses with the need to solve Petermann's auxillary equation [6], which can lead to numerical difficulties when applied to arbitrary profile fibers [18].

(a) Fields of the Fundamental Mode

In the Appendix we show that the solutions to equation (7.4) are given by

$$\bar{E}_{0y} = \begin{cases} J_0(UR)/J_0(U) \\ K_0(WR)/K_0(W) \end{cases}$$

$$\bar{E}_{1y} = \begin{cases} 2(\frac{V^2}{2\Delta})U \frac{J_1(UR)}{J_0(U)} \{A_0 - \frac{R^2}{4U^2}\} \cos\phi \\ 2(\frac{V^2}{2\Delta})W \frac{K_1(WR)}{K_0(W)} \{B_0 + \frac{R^2}{4W^2}\} \cos\phi \end{cases} \tag{7.5a}$$

$$\bar{E}_{0x} = \begin{cases} J_0(UR)/J_0(U) \\ K_0(WR)/K_0(W) \end{cases}$$

$$\bar{E}_{1x} = \begin{cases} 2(\frac{V^2}{2\Delta})U \frac{J_1(UR)}{J_0(U)} \{A_0 - \frac{R^2}{4U^2} - \Delta \frac{R}{UV^2} \frac{J_0(UR)}{J_1(UR)}\} \cos\phi \\ 2(\frac{V^2}{2D})W \frac{K_1(WR)}{K_0(W)} \{B_0 + \frac{R^2}{4W^2} - \Delta \frac{R}{WV^2} \frac{K_0(WR)}{K_1(WR)}\} \cos\phi \end{cases} \tag{7.5b}$$

The constants A_0 and B_0 are found by matching the field and its derivative at the boundary $R = 1$ and are given explicitly in Table 7.2.

The third term in brackets for $\bar{E}_{1x}$ is of order Δ , and we may write $\bar{E}_{1y} \simeq \bar{E}_{1x}$. More generally

$$\bar{E}_y \simeq \bar{E}_x \tag{7.6}$$

Thus when analysing bent fibers the scalar equation for $\bar{E}_y$ (see eqn. (7.2)) is adequate to describe the fields and propagation constants.

(b) Geometrical Birefringence

The birefringence is the difference in the fundamental mode propagation constants of the x-polarized field and the y-polarized field. These may be calculated directly from the scalar wave equation, but in general scalar theory will not be sufficient to account for the subtle field corrections that manifest as a birefringence, and a more precise theory must be employed. We show here that birefringence due to bending is a consequence of the vector terms in Maxwells equations.

Previously the geometrical birefringence was found by essentially calculating $\bar{\beta}_{2x}^2$ and $\bar{\beta}_{2y}^2$ which result from the differential equation for $\bar{E}_2$ [10]. However, the authors neglected two terms in the equation for $\bar{E}_{2x}$, which occur from the expansion of the wave equation for $\bar{E}_x$ (eqn. (7.2)). Inclusion of these terms exactly cancels their result, and to order $(\rho/a)^2$ their birefringence is zero.*

In order to account for birefringence in the fundamental mode the scalar wave equation is no longer adequate, and polarization properties must be included in Maxwell's equations. As in Chapter 2, we use perturbation methods to incorporate the polarization effects, which manifest as corrections to the scalar propagation constant. In the Appendix we show that, to lowest order, the geometrical birefringence in a bent single-mode fiber is given by

$$B_g = \beta_x - \beta_y = \frac{(2\Delta)^{3/2}}{2V\rho}\left\{ \int_{A_\infty} \left\{\cos 2\phi \frac{\partial\psi}{\partial R} - \frac{\sin 2\phi}{R}\frac{\partial\psi}{\partial\phi}\right\} \psi \frac{df}{dR}\, dA - \frac{3}{2}\left(\frac{\rho}{a}\right)\int_{A_\infty}\left(1 - \left(\frac{\rho}{a}\right)R\cos\phi\right)\psi^2 \frac{df}{dR}\, dA \right\} \Big/ \int_{A_\infty} \psi^2\, dA \qquad (7.7)$$

---

* I would like to thank Professor Zong-Qi Lin and Xi-Sheng Fang of Shanghai Jiao Tong University, China, for their kind response to my communications with them.

where $\psi = \bar{E}_y \approx \bar{E}_x$ and f(R) specifies the profile shape. The integration is performed over the infinite cross section of the fiber.

Substituting the electric field expansion (eqn.(7.3)), with $\bar{E}_0 \equiv \bar{E}_0(R)$, $\bar{E}_1 \equiv \bar{E}_1(R)\cos\phi$, into eqn.(7.7) yields the geometrical birefringence in a bent fiber to lowest order:

$$B_g = \frac{(2\Delta)^{3/2}}{8V\rho}\left(\frac{\rho}{a}\right)^2 \int_0^\infty \frac{df}{dR}\left(\bar{E}_1(R)\,\frac{d\bar{E}_1(R)}{dR} + \frac{\bar{E}_1^2(R)}{R}\right) RdR \Big/ \int_0^\infty \bar{E}_0^2(R)\; RdR \tag{7.8}$$

The second integral of eqn.(7.7) is an order of $V^2/2\Delta$ smaller than the first term, and can be neglected, since $V^2/2\Delta$ is always a large quantity.

Substituting eqn.(7.5a) into eqn.(7.8), and using $df/dR = \delta(R-1)$, the geometrical birefringence in a step-index fiber is obtained;

$$B_g = \frac{1}{4}\left(\frac{\rho}{a}\right)^2 kn_{co}\, g(V) \tag{7.9a}$$

$$g(V) = U\,\frac{J_1(U)}{J_0(U)}\left(\frac{1}{W^2} - \frac{1}{U^2}\right) \tag{7.9b}$$

where $\rho kn_{co} = V/\surd(2\Delta)$.

In the next chapter we compare eqn.(7.9) to a Gaussian approximation, and plot the function g(V) against normalized frequency V. (See figure 8.3))

(c) Discussion

The geometrical birefringence due to bending is given by eqn(7.9). The birefringence due to stress has a dominant term given by [8]

$$B_s = -0.25\ (b/a)^2\ kn_{co}\left(\ n_{co}^2\ (p_{11} - p_{12})(1 + \nu)\ \right)$$

where b is the fiber outer radius, p_{ij} are the strain optical coefficients and ν is Poisson's ratio. At $\lambda = 0.633\ \mu m$ the ratio between the two birefringences is $B_g / B_s = -2.67\ g(V)\ (\rho/b)^2$, where g(V) is given by eqn.(7.9b).

The geometrical birefringence behaves as $B_g \sim kn_{co}(\rho/a)^2$, where ρ is the fiber radius and a is the radius of the bend. The ratio between the two birefringences for practical purposes is $B_g / B_s \sim 10^{-3}$. Thus the geometrical birefringence is several orders of magnitude smaller than the bending induced birefringence due to stress, and can be ignored for all practical purposes.

In conclusion, we have found that the geometrical birefringence is due to the inclusion of vector or polarization corrections to the scalar wave eqation. We have shown that the two orthogonally polarized scalar fields, $\bar{E}_y$ and $\bar{E}_x$, are approximately equal, and it is only neccesary to determine $\bar{E}_y$ (given by eqns. (7.3) and (7.4)) to analyse the modal properties of a bent fiber.

4. Few-Mode Waveguides

Following the above discussion we only consider the y-polarized field, and from here on drop the y-subscript. We consider the scalar form of eqn.(7.2b), and after Taylor expanding the second term on the left-side and substituting in the perturbation expansions (eqn.(7.3)) a system of simultaneous differential equations for $\bar{E}_0$, $\bar{E}_1$ and $\bar{E}_2$ is obtained;

$$D\bar{E}_0 = 0 \tag{7.10a}$$

$$D\bar{E}_1 = \bar{\beta}_1^2 \bar{E}_0 - 2\frac{r}{\rho}\cos\phi\, \bar{\beta}_0^2 \bar{E}_0 \tag{7.10b}$$

$$\begin{aligned} D\bar{E}_2 = {} & \bar{\beta}_1^2 \bar{E}_1 + \bar{\beta}_2^2 \bar{E}_0 \\ & - 2\frac{r}{\rho}\cos\phi\, \bar{\beta}_0^2 \bar{E}_1 - 2\frac{r}{\rho}\cos\phi\, \bar{\beta}_1^2 \bar{E}_0 \\ & + 3\left(\frac{r}{\rho}\right)^2 \cos^2\phi\, \bar{\beta}_0^2 \bar{E}_0 - \frac{1}{4\rho^2} \bar{E}_0 \end{aligned} \tag{7.10c}$$

where Df is the wave equation of the unperturbed fiber:

$$Df = \left(\frac{\partial^2}{\partial r^2} + \frac{1}{r}\frac{\partial}{\partial r} + \frac{1}{r^2}\frac{\partial^2}{\partial\phi^2} + \left(k^2 n^2 - \bar{\beta}_0^2\right)\right) f \quad .$$

Multiplying eqn.(7.10a) by $\bar{E}_1$ and eqn.(7.10b) by $\bar{E}_0$, subtracting and integrating over the infinte cross-section, yields the propagation constant correction $\bar{\beta}_1^2$:

$$\bar{\beta}_1^2 = 2\bar{\beta}_0^2 \int_{A_\infty} (r/\rho)\cos\phi\, \bar{E}_0^2\, dA \Big/ \int_{A_\infty} \bar{E}_0^2\, dA \quad .$$

It is seen that $\bar{\beta}_1^2 = 0$ for any symmetric fiber, hence the lowest order correction to $\bar{\beta}_0^2$ behaves as $(\rho/a)^2$. Applying a similar operation between eqns.(7.10a) and (7.10c) yields the next higher order term, $\bar{\beta}_2^2$:

$$\bar{\beta}_2^2 = 2\,\bar{\beta}_0^2 \int_{A_\infty} (r/\rho)\cos\phi\,\bar{E}_0\bar{E}_1\,dA \Big/ \int_{A_\infty} \bar{E}_0^2$$
$$- 3\,\bar{\beta}_0^2 \int_{A_\infty} (r/\rho)^2 \cos^2\phi\,\bar{E}_0^2\,dA \Big/ \int_{A_\infty} \bar{E}_0^2\,dA + \frac{1}{4\rho^2} \qquad (7.11)$$

If we use the approximation $\bar{\beta}_0^2 \approx k^2 n_{co}^2 = V^2/\rho^2(2\Delta)$ then we see from eqn. (7.10b) that $\bar{E}_1 \sim V^2/(2\Delta)\,\bar{E}_0 \gg \bar{E}_0$ and the second and third terms of eqn. (7.11) can be neglected. The equation for the lowest order correction to the propagation constant is then given by

$$\bar{\beta}_2^2 = \frac{2}{\rho^2}\frac{V^2}{2\Delta}\int_{A_\infty} R\cos\phi\,\bar{E}_1\bar{E}_0\,dA \Big/ \int_{A_\infty} \bar{E}_0^2\,dA \qquad (7.12)$$

5. The Step-Index Slab Waveguide

To appreciate and gain an understanding of bending effects on optical fibers we first consider the simpler problem of the bent slab waveguide.

(a) Solutions to the Perturbation Equations

We consider a bent slab waveguide, unbounded in the y-direction, as shown in figure 7.2. The field equations (7.4) can then be written as

$$D\bar{E}_0 = 0$$
$$D\bar{E}_1 = -\frac{2}{\rho^2}\frac{V^2}{2\Delta}\,X\,\bar{E}_0 \qquad (7.13)$$

where X is the dimensionless coordinate, $X = x/\rho$, and ρ is the half width of the guide.

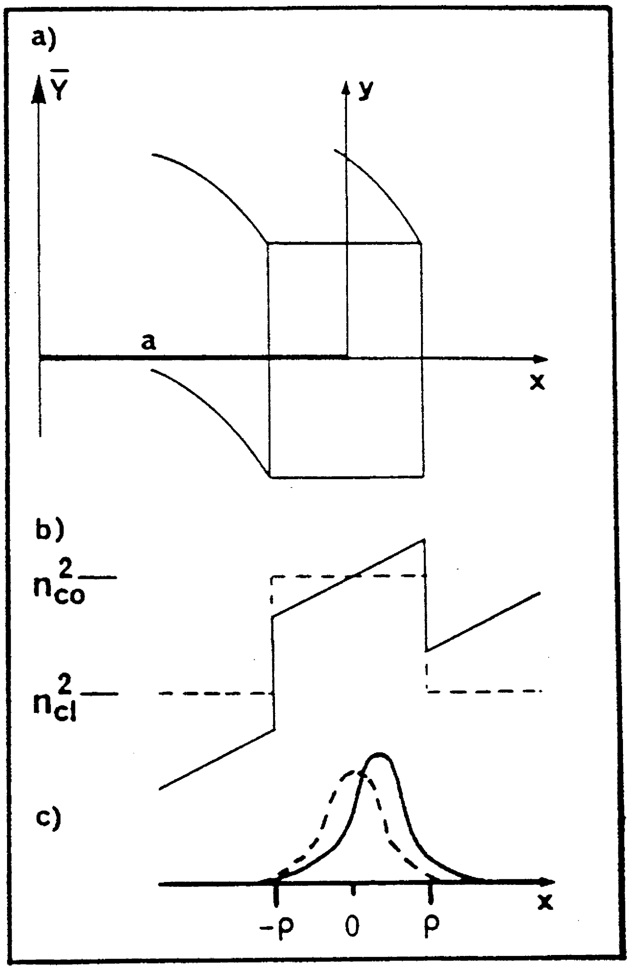

Fig. 7.2

(a) Coordinate system for the bent slab waveguide; (b) the effective refractive index due to the bend; and (c) the shift of the field intensity towards the outer core-cladding boundary.

The fields for a step profile slab waveguide are specified by

$$\bar{E}_0 = \left\{ \begin{array}{c} \cos(UX)/\cos(U) \\ \sin(UX)/\sin(U) \end{array} \right\} \qquad 0 < |X| \le 1$$

$$= \left\{ \begin{array}{c} \exp(-W|X|)/\exp(-W) \\ (X/|X|).\exp(-W|X|)/\exp(-W) \end{array} \right\} \qquad |X| > 1 \quad . \tag{7.14}$$

for $\left\{ \begin{array}{c} \text{even} \\ \text{odd} \end{array} \right\}$ modes.

The method of solution of equation (7.13) is left to the Appendix. The fields, for both odd and even symmetries, are given in Table 7.1. The results agree with those in reference [12] and [13]. Figure 7.3 shows the bent fields for the first odd and even modes of a bent slab waveguide, where the guide is bent with a constant curvature radius of 1 cm. We consider a waveguide with half-width $\rho = 4.1$ μm , profile height $\Delta = 0.0035$, and an operating wavelength of $\lambda = 0.633$μm , so that $V = 5.0$.

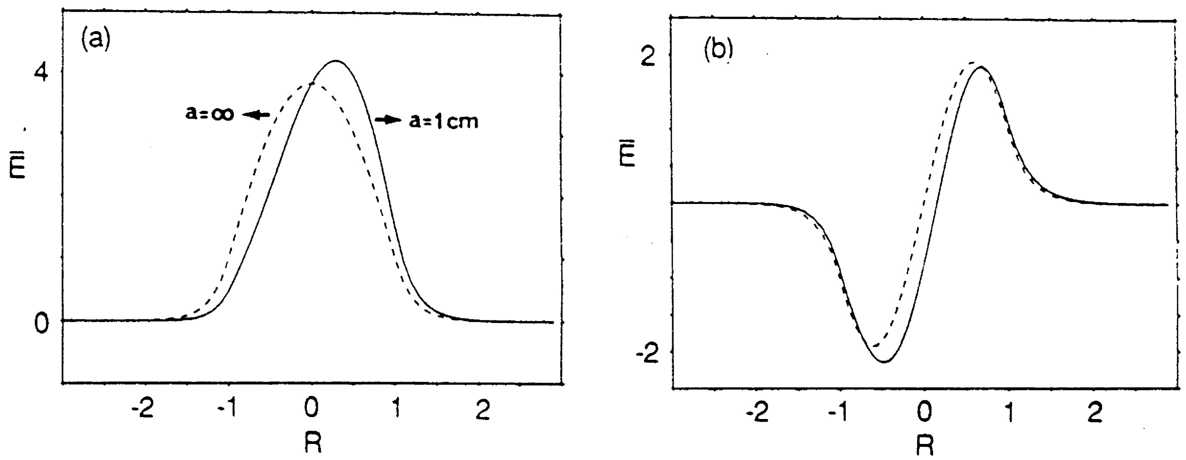

Fig. 7.3 Bent fields of the slab waveguide for (a) the first even mode; and (b) the first odd mode, for a waveguide with characteristics $\rho = 4.1$ μm, $\Delta = 0.0035$ and $\lambda = 0.633$ so that $V = 5.0$. The dashed line is for radius of curvature $a = \infty$ (the straight fiber) and the unbroken line is for $a = 1$ cm.

(b) Deformation of Fields due to Bending

The shift of the field can be written down approximately. The shift in the origin for the even mode occurs when $\partial E/\partial X = 0$. Assuming a small shift, the trigonometric functions of Table 7.1 can be expanded to second order to give

$$\Delta X_{even} = \left(\frac{\rho}{a}\right)\left(\frac{V^2}{2\Delta}\right)\left(\left(1 + \frac{1}{W}\right)^2 - \frac{1}{U^2}\right)\frac{1}{U^2} \quad .$$

For the odd fields the shift in the origin occurs when $E = 0$; expansion of the trigonometric functions of Table 7.1 yields

$$\Delta X_{odd} = \frac{1}{2}\left(\frac{\rho}{a}\right)\left(\frac{V^2}{2\Delta}\right)\left(1 + \frac{1}{W}\right)^2 \frac{1}{U^2} \quad .$$

From a physical standpoint, the shift in the field can be viewed with a ray model [19], shown in fig. 7.4. A ray propagates along the straight section of fiber with ray invariant $\beta = n_{co} \cos\theta_z$ where θ_z is less than the complement of the critical angle θ_c. As the ray enters the curved section, it will still reflect off both the outer and inner core-cladding interface. However, as the radius of curvature becomes smaller, the ray may only be guided by the outer core-cladding boundary. This ray representation indicates a shift in the intensity of the field.

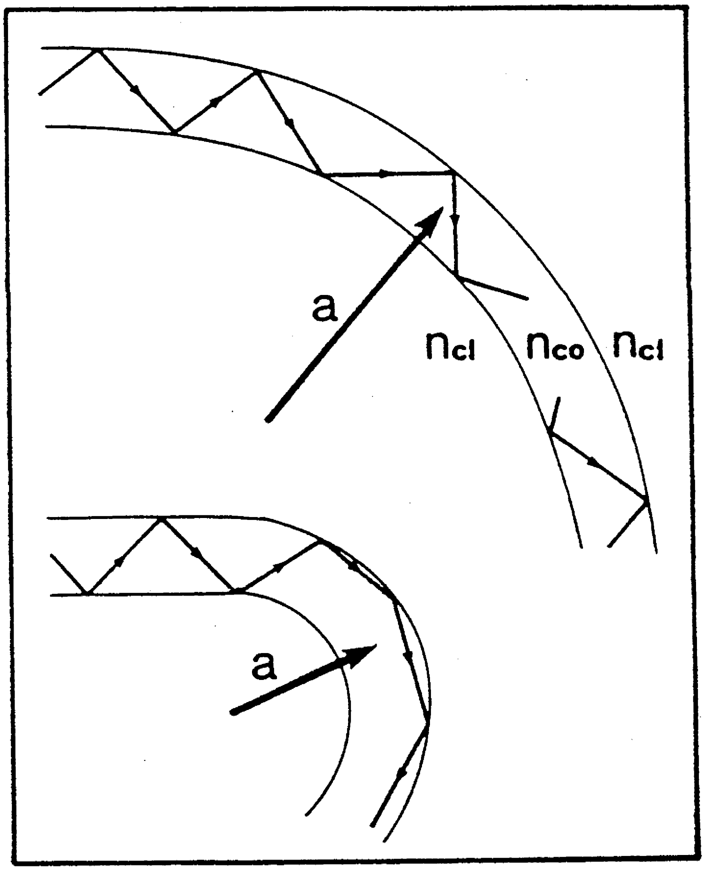

Fig. 7.4 Ray model for the bent slab waveguide showing the shift in the field.

(c) **Exact Solution to the First-Order Wave Equation**

This field shift can also be shown by re-writing the scalar form of eqn.(7.2b) to first-order in (ρ/a) as

$$\left\{\frac{\partial^2}{\partial X^2} + \rho^2\left(k^2 n_e^2 - \bar{\beta}^2\right)\right\} \bar{E}(X) = 0 \tag{7.15}$$

where n_e^2 is an effective refractive index which takes into account the bend of the waveguide:

$$n_e^2 = n^2 + 2n_{co}^2 \left(\frac{\rho}{a}\right) X \quad . \tag{7.16}$$

The approximation $\bar{\beta}^2 \approx k^2 n_{co}^2$ has been used in eqn. (7.15).

The effective refractive index indicates a shift in the field intensity towards the outer core-cladding boundary, as shown in Figure 7.2b and 7.2c. As the radius of curvature becomes less, the guiding power (the refractive index of the core) of the waveguide shifts away from the centre.

The perturbation solutions are given by Table 7.1 and illustrated in Figure 7.3. They are the so-called "straight waveguide solutions" for the effective index of eqn. (7.16) - the fields in the cladding exponentially decay to zero and never become radiative, regardless of the magnitude of the radius of curvature. However, as figure 7.5 indicates, the fields do become radiative; that is the wave is no longer guided, at some distance x_R from the centre of the core when $\bar{\beta} = kn_{c\ell}$.

Equation (7.15) can be solved exactly, remembering that this is a first-order approximation to eqn. (7.2b) Considering a step-profile waveguide we write eqn. (7.15) as

$$\left\{\frac{\partial^2}{\partial X^2} + U^2 + \left(\frac{\rho}{a}\right)\frac{V^2}{\Delta}\; X\right\}\bar{E} = 0 \qquad \text{CORE}$$

$$\left\{\frac{\partial^2}{\partial X^2} - W^2 + \left(\frac{\rho}{a}\right)\frac{V^2}{\Delta}\; X\right\}\bar{E} = 0 \qquad \text{CLADDING .} \qquad (7.17)$$

These equations can be solved in terms of Airy functions, and are given by

$$\bar{E} = Ai(-\,z_1) \quad , \quad z_1 = (AX + U^2)/A^{2/3} \qquad \text{CORE}$$

$$\bar{E} = Ai(-z_2) + iBi(-z_2) \quad , \quad z_2 = (AX - W^2)/A^{2/3} \qquad \text{CLADDING} \qquad (7.18)$$

where $A = 2\left(\frac{\rho}{a}\right)\frac{V^2}{2\Delta}$. The eigenvalues of eqn. (7.18) are found by matching the core and cladding fields and their first derivatives at the boundary X=1. Eqn. (7.18) is shown qualitavely in figure 7.5.

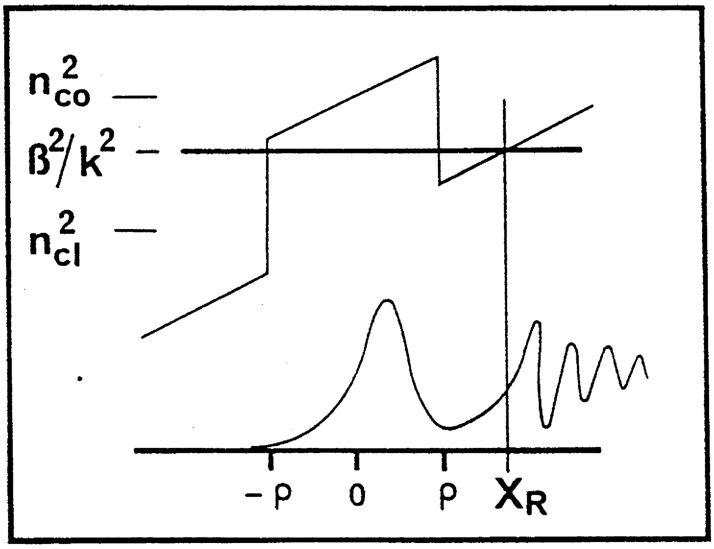

Fig. 7.5 A schematic representation of the first mode of eqn. (7.18). The normalized radiation point, X_R/ρ , is the point in the cladding where the propagation constant satisfies $\bar{\beta} = kn_{cl}$, and the field becomes radiative.

The normalized radiation point, x_R/ρ , is found when the propagation constant $\beta^2/k^2 = W^2/\rho^2k^2 + n_{cl}^2$ is equal to the effective refractive index n_e^2 of eqn. (7.16)

$$X_R \equiv \frac{x_R}{\rho} = \left(\frac{a}{\rho}\right) \frac{\Delta}{V^2} W^2 \quad . \tag{7.19}$$

Substituting this into the field for the cladding gives $E_{CLAD} = A_i\ (0)$. The radiation point is shown in figure 7.5.

4. The Step-Index Optical Fiber

(a) Fields of the Bent Fiber

The $\bar{E}_0$ fields of the (ℓ,m) straight circularly symmetric fiber in the "weakly-guiding" approximation are given by eqn.(2.26)

The method of solution of the perturbation equations (7.10) is left to the appendix. The fields for the first few modes, with both odd and even symmetry, for the bent step-profile fiber are presented in Table 7.2. The equation for the bent field for the $\ell = 0$ mode agrees with the result of references [16] and [20]. The method of solution outlined in the Appendix can be applied to any mode, for either odd or even symmetry.

The modal fields for the $\ell=0$ and $\ell=1$ odd and even modes are shown in Figure 7.6, where as an example we have chosen a few mode fiber with V=5 ($\Delta=0.0035$, $\rho=4.1$ µm, $\lambda=0.632$ µm) and fixed bending radius of a=1 cm.

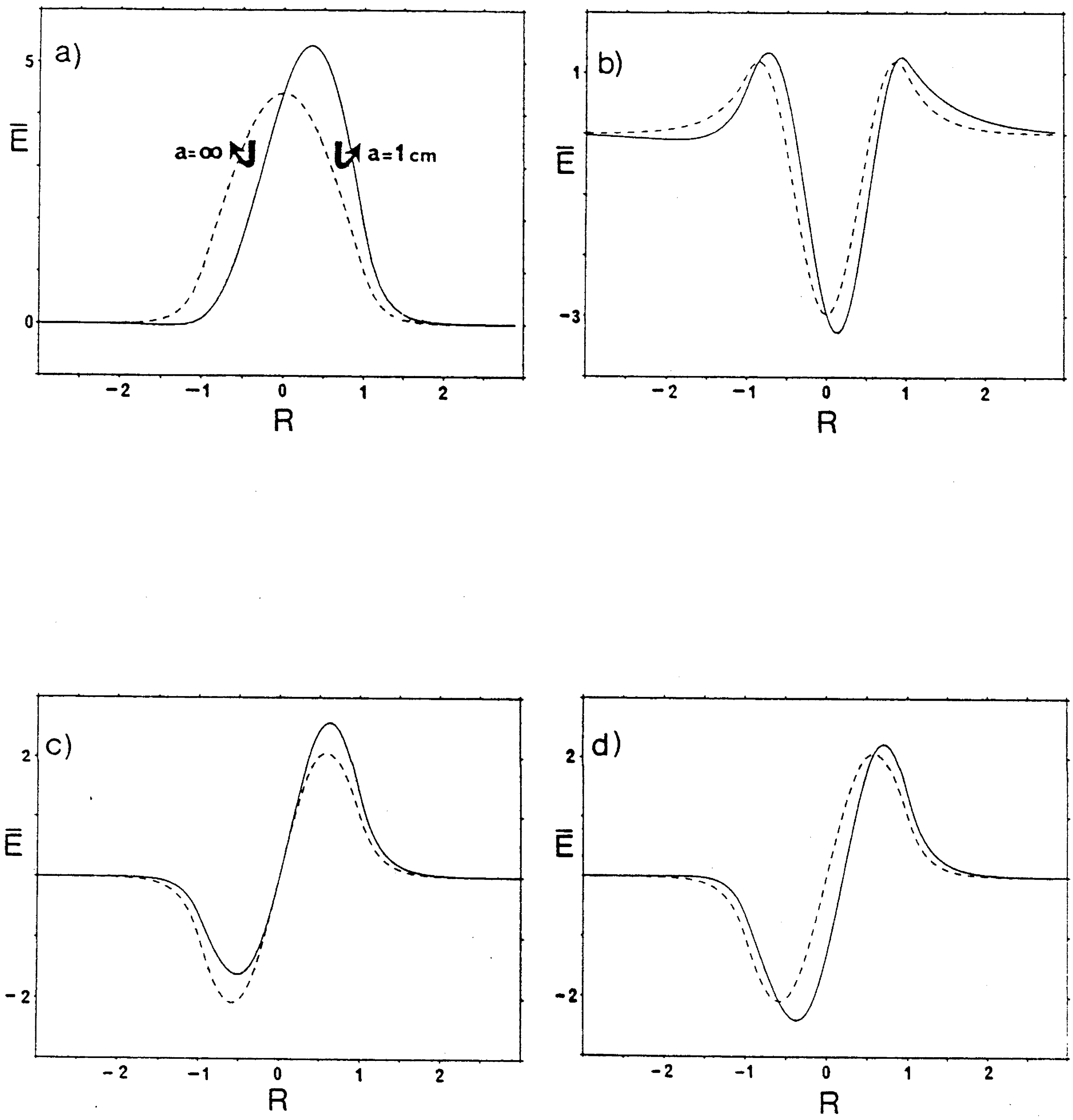

Fig. 7.6 (a) The fundamental (LP_{01}) mode; (b) the LP_{02} mode; (c) the LP_{11} odd mode; and (d) the LP_{11} even mode of a bent fiber with characteristics ρ = 4.1 μm, Δ = 0.0035, and λ = 0.633 μm so that V = 5.0. The dashed line is for radius of curvature a = ∞ (the straight fiber) and the unbroken line is for a = 1 cm.

(b) Propagation Constant Corrections

The correction to the propagation constant, $\bar{\beta}_2^2$, is found by substituting the fields of Table 7.2 into eqn. (7.12). The general solution is given in the appendix, and the results are summarized in Table 7.3.

The difference in the propagation constants for the $\ell=1$ mode is

$$\delta\beta = \beta_e - \beta_o = \frac{1}{4\rho}\left(\frac{V^2}{2\Delta}\right)^{3/2} B(V) . \left(\frac{\rho}{a}\right)^2$$
$$B(V) = \frac{1}{U^2}\left(\frac{1}{W^2}\frac{J_2(U)}{J_0(U)}(W^2 - U^2) - \frac{J_1{}^2(U)}{J_0{}^2(U)}\right) \tag{7.20}$$

where subscripts e and o represent the even and odd mode, respectively, and the eigenvalue eqn. (2.26) has been used. In figure 7.7 we plot the function B(V) against normalized frequency V.

The group delay is specified by $d\bar{\beta}/dk$ (see Chapter 3), and thus in the bent fiber the $\ell=1$ mode will seperate into linearly polarized odd and even modes, where the sep~~e~~aration varies as $(\rho/a)^2$. In the appendix it is shown that only the $\ell=1$ mode will split when first-order perturbation terms are used.

The effect of profile variation on the mode splitting can be examined by considering the clad-power law profile, described by the profile given in Section 2-3(b). Figure 7.7 shows the variation of the mode splitting as a function of V for two values of q. As V gets large, or q small, the splitting becomes smaller.

Figure 7.7 indicates that maximum splitting occurs for the largest profile volume, which is the step-profile. The larger the profile volume, the better the guiding power of the fiber. Thus for small profile volumes, or in the case of the clad power-law profile, small values of q, the fiber does not guide the higher-order modes as efficiently, and the non-degeneracy of the ℓ = 1 modes become less pronounced. This is because the ℓ = 1 mode, as compared to the fundamental modes, has most of its intensity near the core-cladding boundary and so its guidance is very sensitive to profile changes. As q becomes small, the intensity peaks of the ℓ = 1 mode almost lie in the cladding and the mode loses its guiding power. Thus the subtle effects of mode splitting decreases as the ℓ = 1 mode loses its power to the cladding as the grading of the profile increases. The effects of grading are schematically demonstrated in fig. 7.8.

Near cut-off the propagation constants vary rapidly with respect to V (see Section 2-3(b)) and the rate of change approaches infinity. It is in this region that the difference between the two propagation constants changes sign and becomes very large, as shown in figure 7.7. However, the modes are not strongly guided in this region, and the above discussion concerning the effect of profile variation does not apply.

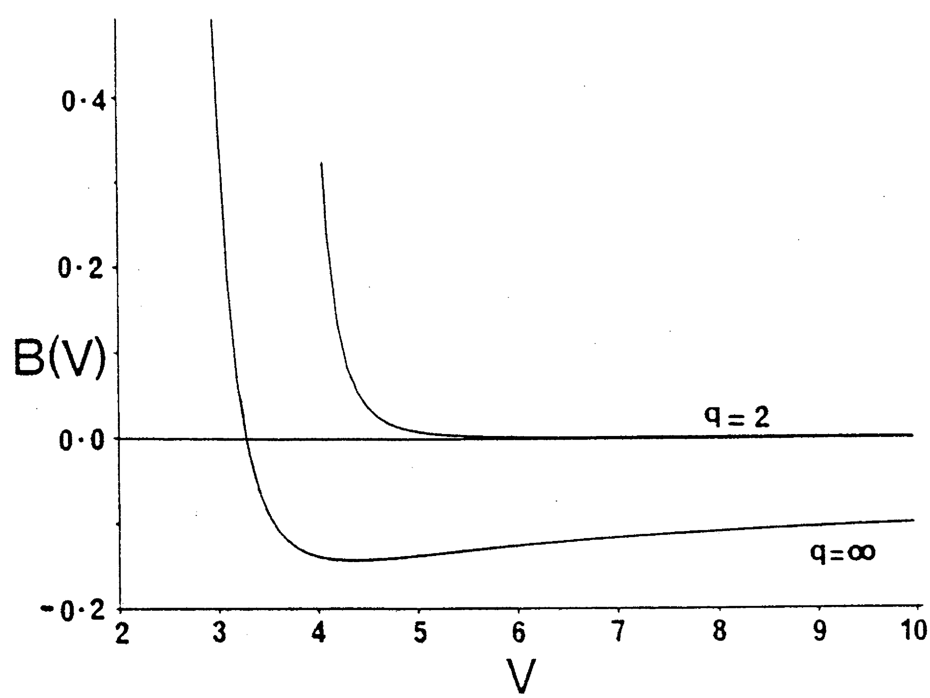

Fig. 7.7 The normalized difference in propagation constants for the ℓ = 1 odd and even mode for a clad power-law profile against normalized frequency V. $q = \infty$ is the step profile.

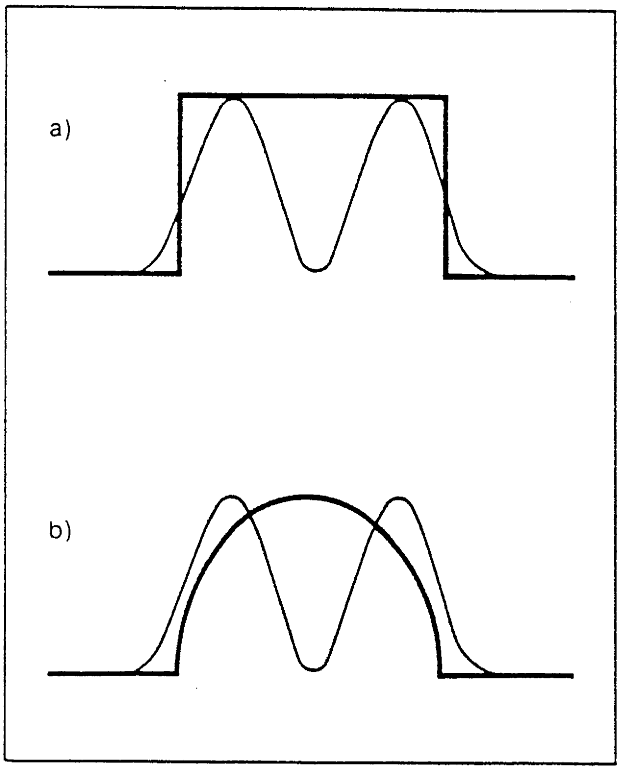

Fig. 7.8

Schematic representation showing the effects of grading on the $\ell \geq 1$ modes.

(c) **Discussion**

Using first-order perturbation theory, simple analytic expressions for the fields and propagation constants of a bent step-index optical waveguide have been obtained. The bend breaks the symmetry of the waveguide, and the scalar propagation constants of the higher-order modes become non-degenerate. The $\ell = n$ mode set will become non-degenerate when the n^{th} - order term in the perturbation expansion is included in the analysis. For example, using first-order perturbation theory only the $\ell = 1$ scalar mode set splits, with a difference in propagation constants given by eqn. (7.20), whereas to that order the scalar $\ell \geq 2$ mode set remains degenerate. The accuracy of first-order perturbation theory is dicussed in Chapter 8.

The perturbation solutions are unphysical in that the fields in the cladding always decay to zero, regardless of the magnitude of the bend. We have shown, by still using first-order perturbation theory, that solutions can be obtained for the step-index slab waveguide which give the point in the cladding at which the field becomes radiative.

7. Four-Photon Mixing Experiments on Bent Few-Mode Fibers*

In order to experimentally investigate the theoretical mode splitting described by eqn. (7.20) we use the same fiber as that used in the divided-pump four-photon mixing experiment detailed in section 6-6.

Recall that there were several theotetical dip-profiles that fitted the experimental results for the straight fiber case. When the theory was applied to mode splitting due to bends all three profile models gave similar results. However, the profile with dip depth $\gamma = 0.64$ and dip width $d = 0.30$ gave the best results. This is the profile shown in fig. 6.9. From Section 6-6 the effective fiber parameters were estimated to be: $\rho = 4.6\ \mu m$ and $\Delta = 0.0028$, so that at $\lambda = 0.523\ \mu m$ (wavelength of the frequency-doubled Nd:YAG laser) the normalized frequency was $V = 6.0$.

The propagation constant corrections β_2^2 for the $\ell = 0$ and (11) odd and even modes can be found by numerically solving eqn. (7.12). The perturbation fields $\bar{E}_1$ are given by the numerical solution of eqn. (7A.25) in the Appendix.

The modal parameter U in a bent fiber is found by substituting the perturbation expansion of $\bar{\beta}$ (eqn. (7.3)) into the definition of the scalar eigenvalue, eqn. (2.18a). The result is

$$U^2 = U_0^2 - \left(\frac{\rho}{a}\right)^2 \bar{\beta}_2^2 \tag{7.21}$$

where U_0 is the scalar eigenvalue of the straight fiber, and $\bar{\beta}_2^2$ is given in Table 7.3 for the first few modes.

---

* These experiments were conducted by G.E. Rosman at the Telecom Research Labs, Melbourne, Australia.

The modal group delay in the bent fiber is then given by $T = U^2/V^2 - 2(U/V)\, dU/dV$. Substituting this expression into the equation for frequency shift, eqn. (5.9), yields the frequency shift for the following pair of modes: (02) - (01), (11 odd) - (01) and (11 even) - (01).

The experimental set-up is described in Section 6-6. The fiber was wound around cylinders of different diameters, taking care not to twist the fiber or apply undue tensile strain. As in experiments on the straight fiber, by adjusting the launch conditions it was possible to divide the pump wave between the fundamental mode and the odd and even (11) modes of the bent fiber.

Figure 7.9 shows the measured frequency shift (small circles) and theoretical frequency shift (solid line) plotted against bend radius. The effect of stress due to bending on the refractive index has been included by using an effective (20% larger) bend radius [21,22].

Figure 7.10 is the difference in frequency shift, $\delta\Omega$, between the two LP_{11} symmetry modes plotted against bend radius. The experimental results (small circles) are generated by taking the lines of best fit through the data of fig. 7.9 and subtracting.

In conclusion, the theoretical prediction that the LP_{11} mode will separate into odd and even modes, which propagate along a fiber with different group delays and different fixed directions of polarization, has been experimentally confirmed by using a divided-pump four-photon mixing process.

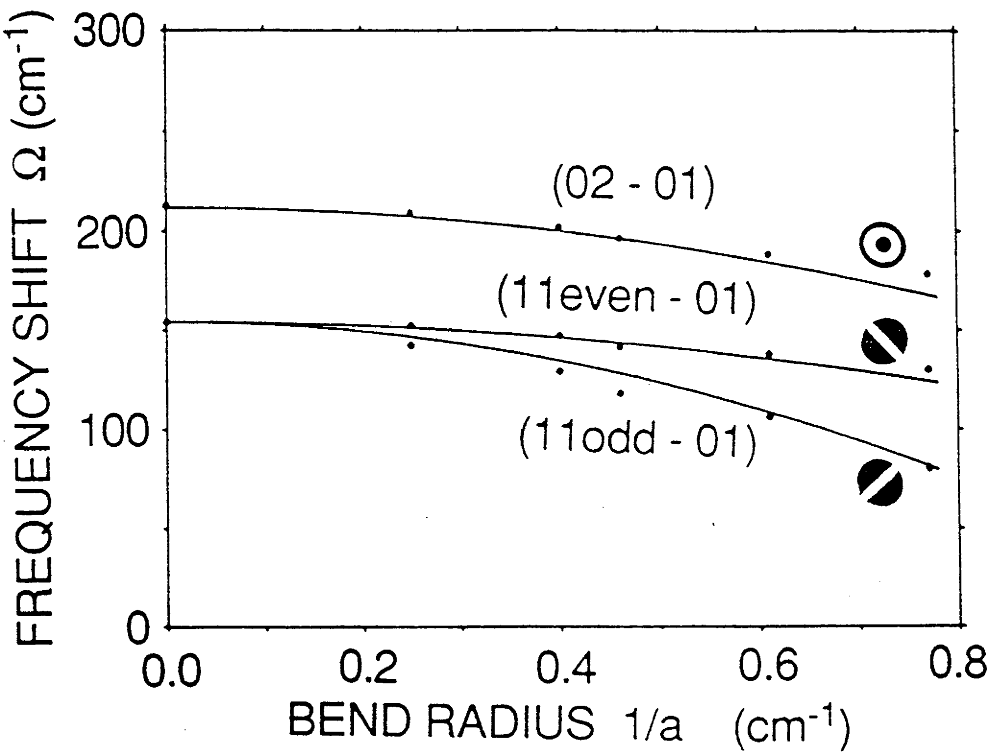

Fig. 7.9 Measured frequency shift (small circles) and theoretical frequency shift (solid line) plotted against bend radius. The intensity patterns indicate the Stokes mode seen at the output. The anti-Stokes mode was always the (01) mode.

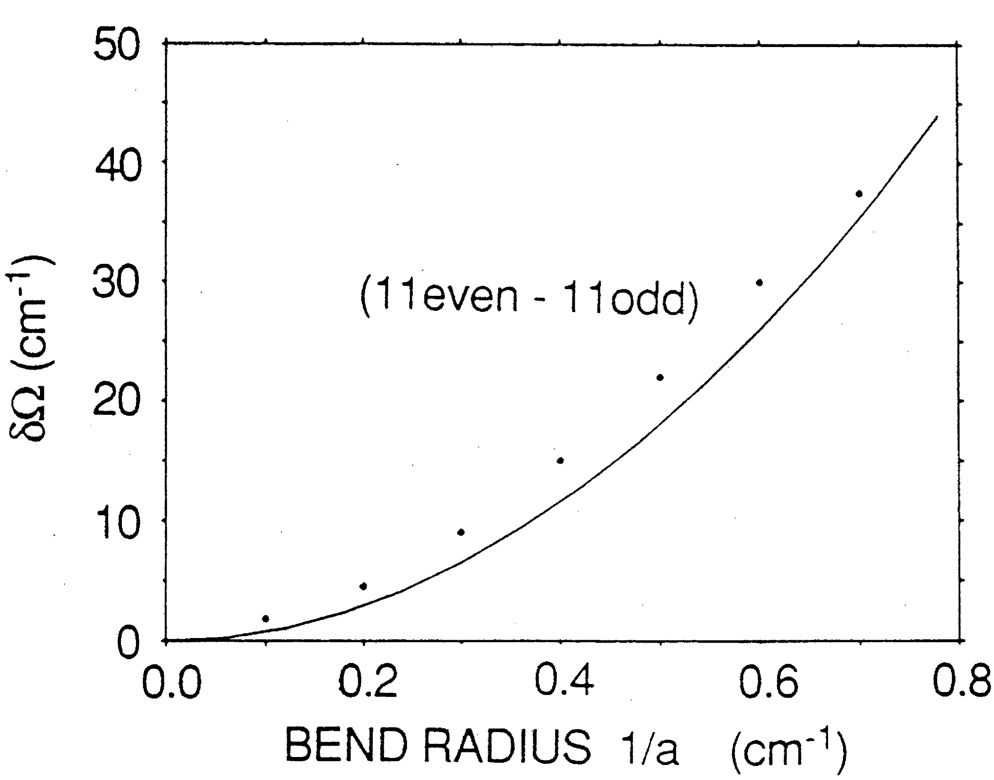

Fig. 7.10 The difference in frequency shift, $\delta\Omega$, between the two LP_{11} symmetry modes plotted against bend radius.

Table 7.1: Fields of the bent slab waveguide $\bar{E}_y = \left(1 + \left(\frac{\rho}{a}\right) X\right)^{-1/2} \left(\bar{E}_0 + \left(\frac{\rho}{a}\right) \bar{E}_1\right)$

$\bar{E}_0$	$\bar{E}_1$	REGION
$\cos(UX) / \cos U$ (even)	$-\left(\frac{V^2}{2\Delta}\right)\left(\frac{1}{2U}\right) \left\{\sin(UX)\left(X^2 - \frac{1}{2U^2} - C_{co}\right) + \cos(UX)\left(\frac{X}{U}\right)\right\}/\cos(U)$	CORE
$\sin(UX) / \sin U$ (odd)	$\left(\frac{V^2}{2\Delta}\right)\left(\frac{1}{2U}\right) \left\{\cos(UX)\left(X^2 - \frac{1}{2U^2} - C_{co}\right) - \sin(UX)\left(\frac{X}{U}\right)\right\}/\sin(U)$	
$e^{-W\|X\|} / e^{-W}$ (even)	$\left(\frac{V^2}{2\Delta}\right)\left(\frac{1}{2W}\right) \left(\|X\|X + \frac{X}{W} + \frac{\|X\|}{X} C_{cl}\right) e^{-W\|X\|}/e^{-W}$	CLAD
$\frac{X}{\|X\|} e^{-W\|X\|} / e^{-W}$ (odd)	$\left(\frac{V^2}{2\Delta}\right)\left(\frac{1}{2W}\right) \left(X^2 + \frac{\|X\|}{W} + C_{cl}\right) e^{-W\|X\|}/e^{-W}$	

$$C_{co} = \left(1 + \frac{1}{W}\right)^2 - \frac{1}{2U^2} \quad ; \quad C_{cl} = \left(1 + \frac{1}{W}\right)\left(\frac{W}{U^2} - 1\right)$$

Table 7.2: Electic Field of the bent fiber $\bar{E} = \left(1 + \left(\frac{\rho}{a}\right) R \cos\phi\right)^{-1/2}\left(\bar{E}_0 + \left(\frac{\rho}{a}\right) \bar{E}_1\right)$

mode	$\bar{E}_0$	$\bar{E}_1$	Region
$\ell = 0$	$J_0(UR)/J_0(U)$	$f^0_{co}(R) \cos\phi \; ; \; f^0_{co} = 2\left(\frac{V^2}{2\Delta}\right) UR^2 \frac{J_1(UR)}{J_0(U)} \left\{\frac{A_0}{R^2} - \frac{1}{4U^2}\right\}$	CORE
	$K_0(WR)/K_0(W)$	$f^0_{cl}(R) \cos\phi \; ; \; f^0_{cl} = 2\left(\frac{V^2}{2\Delta}\right) WR^2 \frac{K_1(WR)}{K_0(W)} \left\{\frac{B_0}{R^2} + \frac{1}{4W^2}\right\}$	CLAD
$\ell = 1$ odd	$\frac{J_1(UR)}{J_1(U)} \sin\phi$	$f^{odd}_{co}(R) \sin 2\phi \; ; \; f^{odd}_{co} = \left(\frac{V^2}{2\Delta}\right) UR^2 \frac{J_2(UR)}{J_1(U)} \left\{\frac{A_1}{R^2} + \frac{1}{4U^2} \frac{J_0(UR)}{J_2(UR)}\right\}$	CORE
	$\frac{K_1(WR)}{K_1(W)} \sin\phi$	$f^{odd}_{cl}(R) \sin 2\phi \; ; \; f^{odd}_{cl} = \left(\frac{V^2}{2\Delta}\right) WR^2 \frac{K_2(WR)}{K_1(W)} \left\{\frac{B_1}{R^2} + \frac{1}{4W^2} \frac{K_0(WR)}{K_2(WR)}\right\}$	CLAD

Table 7.2. continued

mode	$\bar{E}_0$	$\bar{E}_1$	Region
$\ell = 1$ even	$\frac{J_1(UR)}{J_1(U)} \cos\phi$	$f_{co}^{even}(R) \cos 2\phi + g_{co}^{even}(R)$ $f_{co}^{even} = f_{co}^{odd}$ $g_{co}^{even} = \left(\frac{V^2}{2\Delta}\right) UR^2 \frac{J_0(UR)}{J_1(U)} \left\{\frac{C_1}{R^2} - \frac{1}{4U^2} \frac{J_2(UR)}{J_0(UR)}\right\}$	CORE
	$\frac{K_1(WR)}{K_1(W)} \cos\phi$	$f_{cl}^{even}(R) \cos 2\phi + g_{cl}^{even}(R)$ $f_{cl}^{even} = f_{cl}^{odd}$ $g_{cl}^{even} = \left(\frac{V^2}{2\Delta}\right) WR^2 \frac{K_0(WR)}{K_1(W)} \left\{\frac{D_1}{R^2} + \frac{1}{4W^2} \frac{K_2(WR)}{K_0(WR)}\right\}$	CLAD

Table 7.2 continued

Matching Constants for the fields

$C_1 = \{ - \frac{K_2}{K_0} \} / 4U^2$	$D_1 = \{ + \frac{J_2}{J_0} \} / 4W^2$
$A_0 = \{ \frac{2}{W} \frac{K_1}{K_0} + 1 \} / 4U^2$	$B_0 = \{ \frac{2}{U} \frac{J_1}{J_0} - 1 \} / 4W^2$
$A_1 = \{ \frac{4}{W} \frac{K_0}{K_1} + \frac{K_0}{K_2} \} / 4U^2$	$B_1 = \{ - \frac{4}{U} \frac{J_0}{J_1} + \frac{J_0}{J_2} \} / 4W^2$
$K_\ell \equiv K_\ell(W)$	$J_\ell \equiv J_\ell(U)$

Table 7.3: Correction to the propagation constant: $\bar{\beta}^2_{bend} = \bar{\beta}^2_0 + (\frac{\rho}{a})^2\, \bar{\beta}^2_2/\rho^2$

Mode	$\bar{\beta}^2_2$
$\ell = 0$	$(\frac{V^2}{2\Delta})^2 \frac{1}{V^2} \{ 2A_0W^2 - \frac{W^2}{6U^2} (2 - \frac{J_2^2}{J_1^2}) + 2B_0U^2 + \frac{U^2}{6W^2} (2 + \frac{K_2^2}{K_1^2}) \}$
$\ell = 1$ odd	$(\frac{V^2}{2\Delta})^2 \frac{1}{2V^2} \{ 2A_1 (2 - \frac{J_1^2}{J_0J_2}) W^2 - \frac{1}{6} \frac{W^2}{U^2} (2 \frac{J_1^2}{J_0J_1} - \frac{J_2}{J_0})$ $+ 2B_1U^2 (2 - \frac{K_1^2}{K_0K_2}) + \frac{1}{6} \frac{U^2}{W^2} (2 \frac{K_1^2}{K_0K_2} + \frac{K_2}{K_0}) \}$
$\ell = 1$ even	$\beta^2_2\binom{\ell=1}{odd} + (\frac{V^2}{2\Delta})^2 \frac{1}{V^2} \{- 2C_1 W^2 \frac{J_1^2}{J_0J_2} + \frac{1}{2} \frac{W^2}{U^2} \frac{J_2}{J_0}$ $+ 2D_1 U^2 \frac{K_1^2}{K_0K_2} + \frac{1}{2} \frac{U^2}{W^2} \frac{K_2}{K_0} \}$

Appendix

(i) Derivation of the field equations

The vector wave equation is

$$\left(\underset{\sim}{\nabla}^2 + k^2n^2\right)\underset{\sim}{E} = -\underset{\sim}{\nabla}\left(\underset{\sim}{E}\cdot\underset{\sim}{\nabla}\,\ell n(n^2)\right) \quad . \tag{7A.1}$$

In the coordinate system $(\bar{R},\theta,\bar{Y})$ of figure 7.1 is the electric field components $E_{\bar{R}}$ and $E_{\bar{Y}}$ will then satisfy the equations

$$\begin{aligned}(\nabla^2 + k^2n^2)E_{\bar{Y}} &= -\frac{\partial}{\partial\bar{Y}}\left(\underset{\sim}{E}\cdot\underset{\sim}{\nabla}\,\ell n(n^2)\right)\\(\nabla^2 + k^2n^2)E_{\bar{R}} &= \frac{1}{\bar{R}^2}\left(E_{\bar{R}} + 2\frac{\partial E_\Theta}{\partial\Theta}\right) - \frac{\partial}{\partial\bar{R}}\left(\underset{\sim}{E}\cdot\underset{\sim}{\nabla}\,\ell n(n^2)\right)\end{aligned} \tag{7A.2}$$

where

$$\nabla^2 = \frac{\partial^2}{\partial\bar{R}^2} + \frac{1}{\bar{R}}\frac{\partial}{\partial\bar{R}} + \frac{1}{\bar{R}^2}\frac{\partial^2}{\partial\Theta^2} + \frac{\partial^2}{\partial\bar{Y}^2} .$$

Using the Maxwell equation $\underset{\sim}{\nabla}\cdot n^2\underset{\sim}{E} = 0$ in the cylindrical coordinate system we have

$$\underset{\sim}{\nabla}\cdot\underset{\sim}{E} = -\left(\underset{\sim}{E}\cdot\underset{\sim}{\nabla}\,\ell n(n^2)\right) = \frac{E_{\bar{R}}}{\bar{R}} + \frac{\partial E_{\bar{R}}}{\partial\bar{R}} + \frac{\partial E_{\bar{Y}}}{\partial\bar{Y}} + \frac{1}{\bar{R}}\frac{\partial E_\Theta}{\partial\Theta} \tag{7A.3}$$

and the wave equation for $E_{\bar{R}}$ becomes

$$\begin{aligned}(\nabla^2 + k^2n^2)E_{\bar{R}} = &-\frac{E_{\bar{R}}}{\bar{R}^2} - \frac{2}{\bar{R}}\left(\frac{\partial E_{\bar{R}}}{\partial\bar{R}} + \frac{\partial E_{\bar{Y}}}{\partial\bar{Y}}\right)\\&-\left(\frac{2}{\bar{R}} + \frac{\partial}{\partial\bar{R}}\right)\left(\underset{\sim}{E}\cdot\underset{\sim}{\nabla}\,\ell n(n^2)\right)\end{aligned} \tag{7A.4}$$

The coordinate system $(\bar{R},\Theta,\bar{Y})$ and (r,ϕ,z) are related by

$$\bar{R} = a + r\cos\phi$$

$$\Theta = z/a$$

$$\bar{Y} = r\sin\phi$$

The field equations for $E_{\bar{Y}}$ and $E_{\bar{R}}$ can now be converted to the local coordinate system:

$$\left(\nabla_t^2 + k^2n^2 + \frac{a^2}{\bar{R}^2}\left(\frac{1}{4a^2} - \beta_y^2\right)\right)E_y = -\frac{\partial}{\partial\bar{Y}}\left(E_y\frac{\partial}{\partial\bar{Y}} + E_x\frac{\partial}{\partial\bar{R}}\right)\ln(n^2) \qquad (7A.5a)$$

$$\left(\nabla_t^2 + k^2n^2 + \frac{a^2}{\bar{R}^2}\left(\frac{1}{4a^2} - \beta_x^2\right)\right)E_x = -\frac{2}{\bar{R}}\left(\frac{\partial E_y}{\partial\bar{Y}} + \frac{\partial E_x}{\partial\bar{R}}\right)$$
$$- \left(\frac{3}{2\bar{R}} + \frac{\partial}{\partial\bar{R}}\right)\left(E_y\frac{\partial}{\partial\bar{Y}} + E_x\frac{\partial}{\partial\bar{R}}\right)\ln(n^2) \qquad (7A.5b)$$

where

$$\nabla_t^2 = \frac{\partial^2}{\partial r^2} + \frac{1}{r}\frac{\partial}{\partial r} + \frac{1}{r^2}\frac{\partial^2}{\partial\phi^2}$$

$$\frac{\partial}{\partial\bar{Y}} = \sin\phi\frac{\partial}{\partial r} + \frac{\cos\phi}{r}\frac{\partial}{\partial\phi} \qquad (7A.6)$$

$$\frac{\partial}{\partial\bar{R}} = \cos\phi\frac{\partial}{\partial r} - \frac{\sin\phi}{r}\frac{\partial}{\partial\phi}$$

and the electric field components between the two coordinate systems are related by

$$E_{\bar{R}} = (a+r\cos\phi)^{-1/2}\, E_x\, e^{-i\beta_x z} \quad , \quad E_{\bar{Y}} = (a+r\cos\phi)^{-1/2}\, E_y\, e^{-i\beta_y z} \tag{7A.7}$$

If light is polarized along the x- direction then $E_y = 0$, and similarly if light is polarized along the y-direction $E_x = 0$, and eqn. (7.2) results. The refractive index profile n^2 is assumed to depend only on r.

The scalar wave equation results when terms involving $\ell n(n^2)$ are set equal to zero, and we denote scalar quantities by $\bar{E}_x$, $\bar{\beta}_x^2$, $\bar{E}_y$ and $\bar{\beta}_y^2$. To first order in ρ/a , the scalar fields $\bar{E}_x$ and $\bar{E}_y$ are determined from the differential equations (7.4).

(ii) The x- and y- polarized fields of the fundamental mode

The field equations for x- and y-polarized fields of the fundamental mode are given by eqn. (7.4), where $\bar{\beta}_1^2 = 0$. Here we present explicit solutions for a step-profile fiber. In part (v) of the Appendix we generalize these solutions to any $LP_{\ell m}$ mode. If we assume a solution of the form:

$$\begin{aligned} \bar{E}_{1y} &= f_y \cos\phi \\ \bar{E}_{1x} &= f_x \cos\phi \end{aligned} \tag{7A.8}$$

then eqns. (7.4) become

$$\begin{aligned} &\left(f_y'' + \frac{1}{R} f_y' - \frac{1}{R^2} f_y + \rho^2(k^2n^2 - \beta_0^2)f_y\right) = -2\rho^2 R\, \bar{\beta}_0^2\, \bar{E}_{0y} \\ &\left(f_x'' + \frac{1}{R} f_x' - \frac{1}{R^2} f_x + \rho^2(k^2n^2 - \beta_0^2)f_x\right) = -2\rho^2 R\, \bar{\beta}_0^2\, \bar{E}_{0x} - 2\rho\, \bar{E}_{0x}' \end{aligned} \tag{7A.9}$$

where the primes indicates differentiation with respect to R, and since there is no correction to $\bar{\beta}^2$ to first order we have set $\bar{\beta}^2_{0y} = \bar{\beta}^2_{0x} = \bar{\beta}^2_0$. The homogeneous solution to these equations are

$$f_h = \begin{cases} \bar{A}_0 J_1(UR) & 0 \le R \le 1 \\ \bar{B}_0 K_1(WR) & R > 1 \end{cases} \tag{7A.10}$$

A particular solution can be found by assuming

$$f_p = p\, f_h \tag{7A.11}$$

resulting in a first order differential equation for p':

$$\begin{aligned} p''_y + p'_y\left(\frac{2f'_h}{f_h} + \frac{1}{R}\right) &= -\,2\rho^2\, \bar{\beta}^2_0\, R\, E_{0y}/f_h \\ p''_x + p'_x\left(\frac{2f'_h}{f_h} + \frac{1}{R}\right) &= -\,2\rho^2\, \bar{\beta}^2_0\, R\, \bar{E}_{0x}/f_h - 2\rho^2\, \bar{E}'_{0x}/f_h \end{aligned} \tag{7A.12}$$

Equation (7A.12) can be solved by using the integrals in part (viii) of the Appendix and with integrating factors

$$\begin{array}{ll} R\, J_1^2(UR) & 0 \le R \le 1 \\ R\, K_1^2(WR) & R > 1 \end{array} \tag{7A.13}$$

The result is

$$\begin{aligned} p_y^{co} &= -\,\frac{\rho^2}{2U\bar{A}_0}\,\{\bar{\beta}^2_0\, R^2\}/J_0(U) \\ p_y^{c\ell} &= \frac{\rho^2}{2W\bar{B}_0}\,\{\bar{\beta}^2_0\, R^2\}/K_0(W) \end{aligned} \tag{7A.14a}$$

and

$$p_x^{co} = -\frac{\rho^2}{2U\bar{A}_0}\{\bar{\beta}_0^2 R^2 + \frac{2UR}{\rho^2}\frac{J_0(UR)}{J_1(UR)}\}/J_0(U)$$

$$p_x^{c\ell} = \frac{\rho^2}{2W\bar{B}_0}\{\bar{\beta}_0^2 R^2 - \frac{2WR}{\rho^2}\frac{K_0(WR)}{K_1(WR)}\}/K_0(W) \qquad (7A.14b)$$

The radial field distribution for $\bar{E}_1$ is then given by

$$f = f_h + f_p = f_h(1 + p)$$

so that

$$f_y^{co} = 2\rho^2\bar{\beta}_0^2\, U\,\frac{J_1(UR)}{J_0(U)}\{A_0 - \frac{R^2}{4U^2}\}$$

$$f_y^{c\ell} = 2\rho^2\bar{\beta}_0^2\, W\,\frac{K_1(WR)}{K_0(W)}\{B_0 + \frac{R^2}{4W^2}\} \qquad (7A.15a)$$

and

$$f_x^{co} = 2\rho^2\bar{\beta}_0^2\, U\,\frac{J_1(UR)}{J_0(U)}\{A_0 - \frac{R^2}{4U^2} - \frac{R}{2\rho^2\bar{\beta}_0^2 U}\frac{J_0(UR)}{J_1(UR)}\}$$

$$f_x^{c\ell} = 2\rho^2\bar{\beta}_0^2\, W\,\frac{K_1(WR)}{K_0(W)}\{B_0 + \frac{R^2}{4W^2} - \frac{R}{2\rho^2\bar{\beta}_0^2 W}\frac{K_0(WR)}{K_1(WR)}\} \qquad (7A.15b)$$

Equations (7.5) are given by eqn. (7A.8) and (7A.15), with the approximation $\rho^2\bar{\beta}_0^2 = V^2/2\Delta$. The constants in eqn. (7A.15) are given in part (v) of the Appendix.

(iii) Birefringence due to polarization corrections

Following the approach of Section 2-2(b) we multiply the first of equations (7A.5) by $\bar{E}_y$, and multiply the scalar wave equation for $\bar{E}_y$ by E_y. Subtracting and integrating over the infinite cross-section yields

$$\beta_y^2 - \bar{\beta}_y^2 = \int_{A_\infty} \bar{E}_y \frac{\partial}{\partial \bar{Y}} \left(E_y \frac{\partial \ln n^2}{\partial \bar{Y}}\right) dA \bigg/ \int_{A_\infty} \frac{a^2}{\bar{R}^2} \bar{E}_y E_y \, dA \tag{7A.16}$$

where

$$\int_{A_\infty} \left(\bar{E}_y \nabla_t^2 E_y - E_y \nabla_t^2 \bar{E}_y\right) dA$$

can be converted to a line integral, which will vanish since the fields of bound modes and their first derivative decay exponentially to zero at large distances from the waveguide.

Furthermore, the numerator of the right-hand side can be written as

$$\int_{A_\infty} \bar{E}_y \frac{\partial}{\partial \bar{Y}} \left(E_y \frac{\partial \ln n^2}{\partial \bar{Y}}\right) dA = \int_{A_\infty} \frac{\partial}{\partial \bar{Y}} \left(\bar{E}_y E_y \frac{\partial \ln n^2}{\partial \bar{Y}}\right) dA - \int_{A_\infty} \left(E_y \frac{\partial \ln n^2}{\partial \bar{Y}}\right) \frac{\partial \bar{E}_y}{\partial \bar{Y}} \, dA \quad .$$

The first term on the right-hand side can be converted to a line integral which vanishes. We have

$$\beta_y^2 - \bar{\beta}_y^2 = - \int_{A_\infty} \left(E_y \frac{\partial \ln n^2}{\partial \bar{Y}}\right) \frac{\partial E_y}{\partial \bar{Y}} \, dA \bigg/ \int_{A_\infty} \frac{a^2}{\bar{R}^2} \bar{E}_y E_y \, dA \quad . \tag{7A.17}$$

Applying a similar operation between the vector equation for E_x and the scalar equation for $\bar{E}_x$ we obtain

$$\beta_x^2 - \bar{\beta}_x^2 = \{-\int_{A_\infty} (E_x \frac{\partial \ell n\ n^2}{\partial \bar{R}}) \frac{\partial \bar{E}_x}{\partial \bar{R}} dA + \frac{3}{2} \int_{A_\infty} \frac{\bar{E}_x E_x}{\bar{R}} \frac{\partial \ell n\ n^2}{\partial \bar{R}} dA$$
$$+ 2 \int_{A_\infty} (\frac{\bar{E}_x}{\bar{R}} \frac{\partial E_x}{\partial \bar{R}} - \frac{E_x}{\bar{R}} \frac{\partial \bar{E}_x}{\partial \bar{R}}) dA\} \,/ \int_{A_\infty} \frac{a^2}{\bar{R}^2} E_x \bar{E}_x \, dA \quad . \tag{7A.18}$$

Because the vector correction is small we assume that $\bar{E} \simeq E$, and by eqn.(7.5) the x- and y-polarized fields of the scalar wave equation are approximately equal, so that $\bar{E}_y \simeq \bar{E}_x$ and $\bar{\beta}_y^2 \simeq \bar{\beta}_x^2$. We then have from eqns. (7A.17) and (7A.18)

$$\beta_x^2 - \beta_y^2 = -\{ \int_{A_\infty} (\Psi \frac{\partial \Psi}{\partial \bar{R}} \frac{\partial \ell n\ n^2}{\partial \bar{R}} - \Psi \frac{\partial \Psi}{\partial \bar{Y}} \frac{\partial \ell n\ n^2}{\partial \bar{Y}}) dA$$
$$- \frac{3}{2} \int_{A_\infty} \Psi^2 \frac{\partial \ell n\ n^2}{\bar{R} \partial \bar{R}} dA\} \,/ \int_{A_\infty} \frac{a^2}{\bar{R}^2} \Psi^2 \, dA$$

where

$$\Psi = \bar{E}_y \simeq \bar{E}_x \quad .$$

By Taylor expanding $\bar{R} = a(1 + \frac{r}{a} \cos\theta)$ and using eqn.(7A.6) we have to lowest order in (ρ/a)

$$\beta_x^2 - \beta_y^2 = -\{ \int_{A_\infty} \Psi \frac{\partial \ell n\ n^2}{\partial r} (\cos 2\phi \frac{\partial \Psi}{\partial r} - \frac{\sin 2\phi}{r} \frac{\partial \Psi}{d\phi}) dA$$
$$- \frac{3}{2} \int_{A_\infty} (1 - \frac{r}{a} \cos\phi) \frac{r}{a} \cos\phi \, \Psi^2 \frac{\partial \ell n\ n^2}{r\ \partial r} dA\} \,/ \int_{A_\infty} \Psi^2 \, dA \quad . \tag{7A.19}$$

If we make the substitutions

$$\frac{\partial \ell n\ n^2}{\partial r} \simeq -2\Delta \frac{df}{dr}$$

where $f(r)$ specifies the profile shape, $n^2 = n_{co}^2(1 - 2\Delta f)$, and

$$B = \beta_x - \beta_y = \frac{\rho(2\Delta)^{1/2}}{2V}\left(\beta_x^2 - \beta_y^2\right) \qquad (7A.20)$$

then eqn. (7.7) in the text results (refer to Section 2-2).

(iv) Fields of the single-layer slab waveguide

For a step-profile single-layer slab waveguide the field in the straight (unperturbed) waveguide is given by eqn. (7.14). Assuming a solution to eqn. (7.13) is given by

$$\bar{E}_1 = \Phi \bar{E}_0 \qquad (7A.21)$$

the resulting first-order differential equation for Φ' is

$$\Phi'' + \Phi'\left(\frac{2\bar{E}_0'}{\bar{E}_0}\right) = -2\rho^2\bar{\beta}_0^2 X \qquad (7A.22)$$

This can be solved with the help of integrating factors

$$\left\{\begin{matrix}\cos^2(UX)\\ \sin^2(UX)\end{matrix}\right\} \quad , \quad e^{-2W|X|}$$

for the $\left\{\begin{matrix}\text{even}\\ \text{odd}\end{matrix}\right\}$ modes in the core, cladding region. The solutions are given in Table 7.1 where the matching constants are determined by matching Φ_{co} and Φ_{cl} and their first derivatives at the boundary $X = 1$, and using the eigenvalue equations $U \tan U = W$ for the even mode, and $U \cot U = -W$ for the odd mode [23].

(v) Fields of the step-index fiber

Here we generalize the solution to the field equations outlined in part (ii) of the Appendix. The field in the straight (unperturbed) fiber is

$$\bar{E}_0 = F_\ell(R) \begin{Bmatrix} \cos\ell\phi \\ \sin\ell\phi \end{Bmatrix} \tag{7A.23}$$

where $F_\ell(R)$ is given by eqn. (2.26) and the solution for the first order correction to the field is of the form

$$\bar{E}_1 = f_\ell(R) \begin{Bmatrix} \cos(\ell+1)\phi \\ \sin(\ell+1)\phi \end{Bmatrix} + g_\ell(R) \begin{Bmatrix} \cos(\ell-1)\phi \\ \sin(\ell-1)\phi \end{Bmatrix} \tag{7A.24}$$

for $\begin{Bmatrix} \text{even} \\ \text{odd} \end{Bmatrix}$ modes. Upon substitution into eqn. (7.10b) the resulting differential equations for f(R) and g(R) are

$$\begin{aligned} f'' + \frac{1}{R} f' + \gamma^2 f - \frac{(\ell+1)^2}{R^2} f &= -\rho^2 \bar{\beta}_0^2 \, R \, F_\ell(R) \\ g'' + \frac{1}{R} g' + \gamma^2 g - \frac{(\ell-1)^2}{R^2} g &= -\rho^2 \bar{\beta}_0^2 \, R \, F_\ell(R) \end{aligned} \tag{7A.25}$$

where $\gamma^2 = \rho^2(k^2n^2 - \bar{\beta}_0^2) = +U^2, -W^2$ for the core, cladding region of a step-profile fiber. The homogeneous solutions to the above equations are

$$f_h = \begin{cases} \bar{A}_\ell \, J_{\ell+1}(UR) & \text{CORE} \\ \bar{B}_\ell \, K_{\ell+1}(WR) & \text{CLAD} \end{cases}$$

$$g_h = \begin{cases} \bar{C}_\ell \, J_{\ell-1}(UR) & \text{CORE} \\ \bar{B}_\ell \, K_{\ell-1}(WR) & \text{CLAD} \end{cases} \tag{7A.26}$$

A particular solution can be found by assuming $f_p = p_f f_h$ and $g_p = p_g g_h$ resulting in a first order differential equation for p'

$$p_f'' + p_f' \left(\frac{2f_h'}{f_h} + \frac{1}{R}\right) = -\rho^2 \bar{\beta}_0^2 \; R \; F_\ell / f_h \qquad (7A.27)$$

A similar equation results for p_g. Eqn.(7A.27) can be solved with the integrals in part (viii) of the Appendix and with integrating factors

$$R\, J_{\ell+1}^2(UR) \quad , \quad R\, K_{\ell+1}^2(WR) \qquad \text{for } p_f$$

and

$$R\, J_{\ell-1}^2(UR) \quad , \quad R\, K_{\ell-1}^2(WR) \qquad \text{for } p_g$$

for core, cladding regions. The solution to equations (7A.25) is

$$f_\ell = f_h(1 + p_f) \quad , \quad g_\ell = g_h(1 + p_g)$$

and can be written as

$$f_\ell^{co}(R) = \rho^2 \bar{\beta}_0^2 \; U \; \frac{J_{\ell+1}(UR)}{J_\ell(U)} \left(A_\ell + \frac{R^2}{4U^2} \frac{J_{\ell-1}(UR)}{J_{\ell+1}(UR)}\right) \qquad \text{CORE}$$

$$f_\ell^{cl}(R) = \rho^2 \bar{\beta}_0^2 \; W \; \frac{K_{\ell+1}(WR)}{K_\ell(W)} \left(B_\ell + \frac{R^2}{4W^2} \frac{K_{\ell-1}(WR)}{K_{\ell+1}(WR)}\right) \qquad \text{CLAD}$$

$$(7A.28)$$

$$g_\ell^{co}(R) = \rho^2 \bar{\beta}_0^2 \; U \; \frac{J_{\ell-1}(UR)}{J_\ell(U)} \left(C_\ell - \frac{R^2}{4U^2} \frac{J_{\ell+1}(UR)}{J_{\ell-1}(UR)}\right) \qquad \text{CORE}$$

$$g_\ell^{cl}(R) = \rho^2 \bar{\beta}_0^2 \; W \; \frac{K_{\ell-1}(WR)}{K_\ell(W)} \left(D_\ell + \frac{R^2}{4W^2} \frac{K_{\ell+1}(WR)}{K_{\ell-1}(WR)}\right) \qquad \text{CLAD}$$

where the matching constant A_ℓ is related to $\bar{A}_\ell$ of eqn. (7A.26) by

$A_\ell = \bar{A}_\ell \; J_\ell(U)/\rho^2\bar{\beta}_0^2 \; U$

and similarly for the other constants.

The constants are determined by matching the functions $f_\ell^{co}(R)$, $g_\ell^{co}(R)$ and $f_\ell^{cl}(R)$, $g_\ell^{cl}(R)$ and their first derivatives at the fibre boundary $R = 1$, and using the eigenvalue equation (2.24):

$$A_\ell = \left(\frac{2}{W} (\ell+1) \frac{K_{\ell-1}(W)}{K_\ell(W)} + \frac{K_{\ell-1}(W)}{K_{\ell+1}(W)} \right) \frac{1}{4U^2}$$

$$B_\ell = \left(- \frac{2}{U} (\ell+1) \frac{J_{\ell-1}(U)}{J_\ell(U)} + \frac{J_{\ell-1}(U)}{J_{\ell+1}(U)} \right) \frac{1}{4W^2}$$

(7A.29)

$$C_\ell = \left(\frac{2}{W} (\ell-1) \frac{K_{\ell+1}(W)}{K_\ell(W)} - \frac{K_{\ell+1}(W)}{K_{\ell-1}(W)} \right) \frac{1}{4U^2}$$

$$D_\ell = \left(- \frac{2}{U} (\ell-1) \frac{J_{\ell+1}(U)}{J_\ell(U)} + \frac{J_{\ell+1}(U)}{J_{\ell-1}(U)} \right) \frac{1}{4W^2}$$

and $A_0 = - C_0$, $B_0 = D_0$.

(vi) Correction to the propagation constants

Substituting eqn. (7A.23) and (7A.24) into eqn. (7.12) yields

$$\delta\beta_0 = \frac{2\,\bar{\beta}_0^2}{\chi_0} \int_0^\infty F_0(R)\, f_0(R)\, R^2\, dR \quad , \quad \ell = 0$$

$$\delta\beta_1 = \frac{\bar{\beta}_0^2}{\chi_1} \left[\int_0^\infty F_1(R) f_1(R)\, R^2 dR + 2\int_0^\infty F_1(R) g_1(R)\, R^2 dR \left\{\begin{matrix}1\\0\end{matrix}\right\}\right] \quad , \quad \left\{\begin{matrix}\text{even}\\\text{odd}\end{matrix}\right\}\ \ell = 1$$

$$\delta\beta_\ell = \frac{\bar{\beta}_0^2}{\chi_\ell} \int_0^\infty F_\ell(R) \left(f_\ell(R) + g_\ell(R)\right) R^2\, dR \quad , \quad \ell > 1$$

where $\delta\beta \equiv \bar{\beta}_2^2$ and

$$\chi_\ell = \int_0^\infty F_\ell^2(R)\, R\, dR = \frac{V^2}{2U^2}\ \frac{K_{\ell-1}(W)\ K_{\ell+1}(W)}{K_\ell^2(W)}$$

With the help of the integrals in part (viii) of the Appendix the results presented in Table 7.3 are obtained. The difference in the even and odd propagation constants of the higher order modes are

$$\bar{\beta}_e^2 - \bar{\beta}_o^2 = \delta\beta_e - \delta\beta_o = \begin{cases} \dfrac{2\bar{\beta}_0^2}{\chi_1} \displaystyle\int_0^\infty F_1(R)\, g_1(R)\, R^2\, dR & \ell = 1, \\ 0 & \ell > 1. \end{cases}$$

Using the approximation $\bar{\beta}_e - \bar{\beta}_o \simeq 2\,\bar{\beta}_0\,(\bar{\beta}_e - \bar{\beta}_o)$ we obtain eqn. (7.20) for the $\ell = 1$ case.

(vii) Stability of LP modes on a bent fiber

The criterion that modes are linearly polarized on optical fibers is [11]

$$\Lambda = (\bar{\beta}_e - \bar{\beta}_o)/(\beta_1 - \beta_2) \gg 1 \qquad (7A.30)$$

where $\bar{\beta}_e$ and $\bar{\beta}_o$ are the even and odd propagation constants of the bent scalar equation and β_1 and β_2 are the exact modes (i.e., scalar modes plus polarization corrections) of the circularly symmetric straight fiber. $\bar{\beta}_e - \bar{\beta}_o$ is given by eqn. (7.20) and $\beta_1 - \beta_2$ is given in Table 2.1. Substituting into eqn. (7A.30) we have

$$\Lambda \sim \left(\frac{V^2}{2\Delta}\right)^3 \left(\frac{\rho}{a}\right)^2 \gg 1 \qquad (7A.31)$$

For the few-mode fiber of figure 7.6 ($V = 5$, $\rho = 4.1\ \mu m$, $\Delta = 0.0035$) the $\ell = 1$ modes will be linearly polarized for curvature radius $a < 80$ cm.

(viii) Some Bessel function integrals

$$\int x\, Z_\ell^2\, dx = \frac{1}{2} x^2 \left(Z_\ell^2 - Z_{\ell-1} Z_{\ell+1}\right) \tag{7A.32}$$

$$\int x^2\, Z_\ell Z_{\ell\pm1} dx = \pm \frac{1}{2} x^2\, Z_\ell^2 + (\ell \mp 1) \int x\, Z_\ell^2\, dx \tag{7A.33}$$

$$\begin{aligned} 3 \int x^3\, Z_\ell^2\, dx = {} & 2\left(\ell^2 - 1\right) \int x\, Z_\ell^2\, dx \\ & - x^2(\ell - 1)\, Z_\ell\left(Z_\ell + x\, Z_{\ell+1}\right) \\ & + \frac{1}{2} x^4 \left(Z_\ell^2 + Z_{\ell+1}^2\right) \end{aligned} \tag{7A.34}$$

$$\int x^4\, Z_\ell Z_{\ell\pm1}\, dx = \mp \frac{1}{2} x^4 Z_\ell^2 + \left(\ell \pm 2\right) \int x^3\, Z_\ell^2\, dx \tag{7A.35}$$

$$\begin{aligned} & \int \frac{x}{Z_{\ell\pm1}^2} \left(\ell\, Z_\ell^2 - (\ell \pm 1)\, Z_{\ell-1} Z_{\ell+1}\right) dx \\ & = \mp x^2 \frac{Z_{\ell\mp1}}{Z_{\ell\pm1}} \end{aligned} \tag{7A.36}$$

where $Z_\ell = J_\ell(x) = K_\ell(-ix)/i^{\ell+1}$.

Integrals (7A.32) and (7A.34) are obtained from Schafheitlin's reduction formula [24].

8. References

[1] E.A.J. Marcatili, "Bends in optical dielectric guides"
Bell Syst. Tech. J., 48, pp.2013-2132 (1969)

[2] E.F. Kuester and D.C. Chang, "Surface-wave radiation loss from curved dielectric slabs and fibres"
IEEE J. Quantum Electron., QE-11, pp.903-907 (1975)

[3] I.A. White, "Radiation from bends in optical waveguides: The volume-current method"
Microwaves, Opt. and Acoust., 3, pp.186-188 (1979)

[4] D. Marcuse, "Field deformation and loss caused by curvature of optical fibres"
J. Opt. Soc. Am., 66, pp.311-320 (1976)

[5] K. Peterman, "Theory of microbending loss in monomode fibres with arbitrary refractive index profiles"
AEU, 30, pp.337-342 (1976)

[6] K. Peterman, "Microbending loss in monomode fibres"
Electron. Letters, 12, pp.107-109 (1976)

[7] W.A. Gambling, H. Matsumura and R.A. Sammut "Mode shift at bends in single-mode fibers"
Electron. Letters, 13, pp.695-697 (1977)

[8] R. Ulrich, S.C. Rashleigh and W. Eickhoff, "Bending induced birefringence in single mode fibers"
Optics Letters, 5, pp.273-275 (1980)

[9] N. Shibata, M. Tsubokawa and S. Seika, "Polarization mode dispersion in a coil of single mode fiber"
Optics Letters, 10, pp.92-94 (1985)

[10] X-S. Fang and Z-Q. Lin, "Birefringence in curved single mode optical fibers due to waveguide geometry effect - perturbation analysis"
IEEE J. Lightwave Tech., LT-3, pp.789-794 (1985)

[11] See ref. [2-7]

[12] S. Kawakami, M. Miyagi and S. Nishida, "Bending losses of dielectric slab optical waveguide with double or multiple claddings: theory"
Applied Optics, 14, pp.2588-2597 (1975).

[13] Y. Takuma, M. Miyagi and S. Kawakami, "Bent asymmetric dielectric slab waveguides: a detailed analysis"
Applied Optics, 20, pp.2291-2298 (1981)

[14] M. Miyagi and G.L. Yip, "Field deformation and polarization change in a step-index optical fibre due to bending"
Opt. Quantum Electron., 8, pp.335-341 (1976)

[15] J.J. Sakai and T. Kimura, "Fields in a Curved optical fibre"
IEEE J. Quantum Electron., QE-17, pp.29-34 (1981)

[16] Z.W. Bao, M. Miyagi and S. Kawakami, "Measurements of field deformations caused by bends in a single mode optical fibre",
Applied Optics, 22, pp.3678-3680 (1983)

[17] W.A. Gambling, H. Matsumura and C.M. Ragdale, "Field deformation in a curved single-mode fiber"
Electron. Letters, 13, pp.130-132 (1978)

[18] S. Sarkar, A. Kumar, I.C. Goyal, E.K. Sharma and R. Tewari, "On microbending loss calculations in single mode fibers with arbitrary index profiles"
Opt. Comm., 53, pp.91-94 (1985)

[19] I.A. White, "Radiation losses in dielectric optical waveguides",
(Ph.D Thesis, Australian National University, 1977)

[20] J.V. Wright, "Microbending loss in monomode fibres: Solutions of Peterman's Auxillary function",
Electron. Letters, 19, pp.1067-1068 (1983)

[21] K. Nagano, S. Kawakami, and S. Nishida, "Change of the refractive index in an optical fiber due to external forces"
Applied Optics, 17, pp. 2080-2085 (1978)

[22] J.H. Hannay, "Mode coupling in an elastically deformed optical fiber"
Electron. Letters, 12, pp.173-174 (1976)

[23] See ref. [2-1]

[24] G.N. Watson, "A treatise on the theory of Bessel functions"
(Cambridge University Press, 1958)

CHAPTER 8

THE GAUSSIAN APPROXIMATION FOR BENT FIBERS

CHAPTER 8

THE GAUSSIAN APPROXIMATION FOR BENT FIBERS.

1. Introduction

In Chapter 2 we presented a Gaussian approximation for the low-order modes of a circularly-symmetric step-profile fiber. In this Chapter we wish to capitalize on the simple analytic forms of the approximation to gain some insight into the effect of bending on modal characteristics.

The simple forms of the Gaussian approximation allow an investigation of the higher-order solution of the field equations of the bent fiber. This reveals information about the expansion parameter used in the perturbation analysis in Chapter 7. We give results which show that for a range of bending radii and V-values the expansion parameter can be of order unity, thus invalidating first-order perturbation theory.

We start by examining the single-mode case, and first derive the first-order field corrections for the x- and y- polarized modes. We show that, in general, the difference between these two modes is negligible. Later we use these first-order fields to write down a simple expression for the geometric birefringence due to bending, a problem that was formalised in the previous Chapter. We compare the simple formula to the more rigorous step-index solution derived in Chapter 7.

We then derive complete expressions (within the Gaussian approximation) for the field and propagation constant of the bent fiber. These expressions are not restricted by the magnitude of the peturbation, and reduce to the usual first-order corrections when the perturbation parameter is small. They give simple expressions for the field shift and 3-db field width of the fundamental mode. We compare our results for the field shift and field width with some experimental data, and find excellent agreement.

Assuming that the perturbation parameter is sufficiently small, we derive simple expressions for the first-order field correction $\bar{E}_1$ for the $\ell = 1$ odd and even modes, in order to examine the mode splitting predicted in Chapter 7. However, we find that the Gaussian approximation is not suited to describing the subtle effects of mode splitting.

Finally, we return to four-photon mixing on bent few mode fibers and investigate the overlap integrals that participate in the mode splitting experiment of Section 7-7. These overlap integrals are related to the relative gain of the process (see Section 4-5), and we show that the two $\ell = 1$ symmetry modes participating in the experiment should have different gains.

2. The Expansion Parameter for Bends

In the next section we show that the perturbation expansion parameter is not (ρ/a), but $\varepsilon = (\rho/a)C$, where $C = \rho^2 \bar{\beta}_0^2 R_0{}^2 = \left(V^2/2\Delta\right) R_0^2$. The parameter C is quite large ($C \sim 10^3$), thus ε may become unreasonably large for quite moderate bending radii, thus invalidating the perturbation theory.

In figure 8.1 C is plotted against V for several values of profile height Δ . If the operating wavelength λ and fiber radius ρ are specified, then the value of C for any fiber can be found from figure 8.1. The minimum bend radius for the perturbation theory to remain valid is then given by $a_{min} = \rho C/\varepsilon_{max}$, where ε_{max} is the maximum tolerable size of the expansion parameter, and its value will dictate the accuracy of the perturbation theory. For example, if $\varepsilon \le 0.5$ then for the few mode fiber of figure 8.5 (V=5) $a_{min} \ge 1.5$ cm , and for the same fiber operating at 1.3 μm (V=2.35) $a_{min} \ge 0.5$ cm . For values of bend radius smaller than a_{min} the mode characteristics described by first-order perturbation theory will be invalidated.

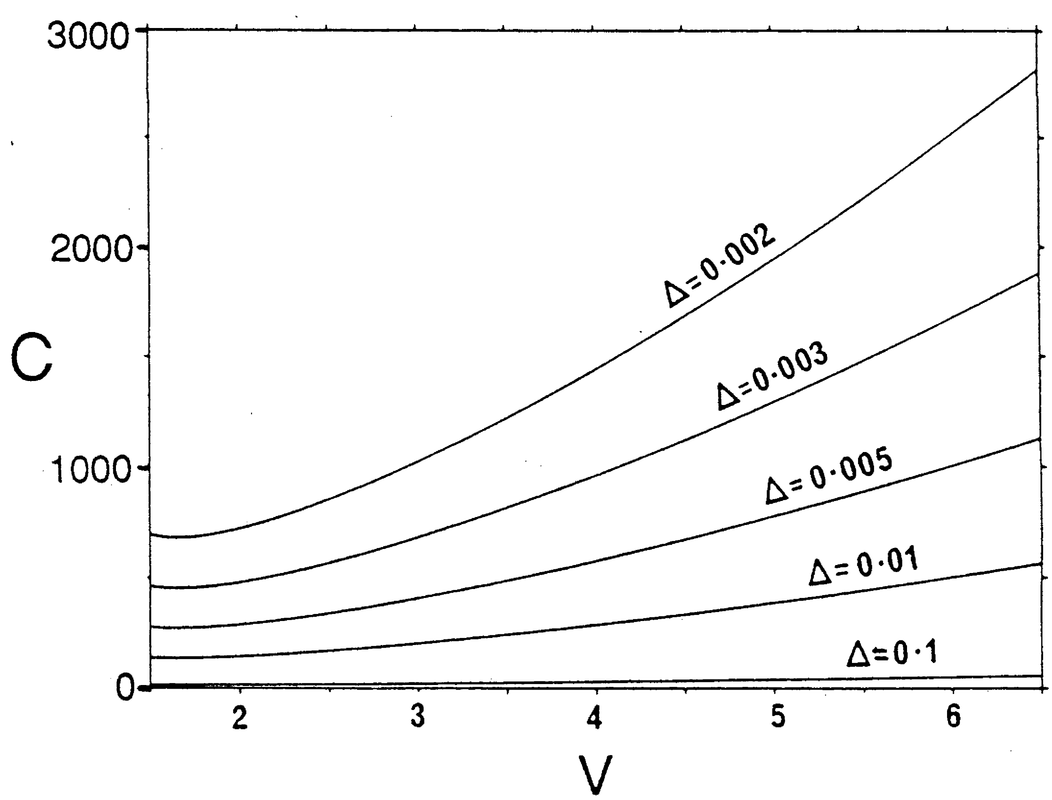

Fig. 8.1 The perturbation parameter C against normalized frequency V for a range of profile heights Δ .

2. Single-Mode Fibers

(a) First-Order Field Corrections

We have shown that for a step-profile fiber eqn. (7.4) can be solved exactly in terms of Bessel functions (see eqn. (7.5)), however the expressions are complicated and it is not easy to extract the physics. It is well known that the Gaussian approximation is useful when describing the modal fields of the unpertubed fiber, as the simple analytic forms of the approximation explicitly show the dependence of parameters on field changes. We consider a Gaussian modal field

$$\bar{E}_{0x} = \bar{E}_{0y} = \exp(-R^2/2R_0{}^2) \tag{8.1}$$

In the Appendix it is shown that substituting eqn. (8.1) into eqn. (7.4) yields the field in the bent fiber to first-order:

$$\begin{aligned} \bar{E}_y &= \left(1 + \frac{\rho}{a}\, C\, R \cos\phi\right) \exp(-R^2/2R_0{}^2) \\ \bar{E}_x &= \left(1 + \frac{\rho}{a}\,(C-1)\, R \cos\phi\right) \exp(-R^2/2R_0{}^2) \end{aligned} \tag{8.2}$$

where $C = (V^2/2\Delta)\, R_0{}^2$. Because Δ is small the quantity C is always large, and $\bar{E}_y \approx \bar{E}_x$. This supports the argument of Chapter 7 that the difference between the orthogonally polarized modes is negligible, and the field $\bar{E}_y$ is suitable for describing the field in the bent fiber.

From eqn. (8.2) the shift in maximum intensity r_d , to lowest order in $\left(\frac{\rho}{a}\right)$, is given by

$$\frac{r_d}{\rho} = \left(\frac{\rho}{a}\right) \frac{V^2}{(2\Delta)} R_0{}^4 \equiv \varepsilon R_0^2 \tag{8.3}$$

This agrees with refs. [1,2]

(b) Field Corrections Summed to all Orders

We want to investigate higher-order perturbation terms of the field equations using the simple Gaussian function eqn. (8.1). The motivation for this study derives from the fact that eqn. (8.3) explains experimental results [3] in regions where simple first-order perturbation theory (i.e. eqn. (8.2)) is invalid.

The electric field in the bent fiber is assumed to be linearly polarized. The full scalar wave equation for the bent fiber is thus given by setting $\ell n(n^2)$ equal to zero in eqn. (7.2b) In terms of the local coordinate system (r,ϕ,z) (refer to fig. 7.1) we have

$$\left\{\frac{\partial^2}{\partial r^2} + \frac{1}{r}\frac{\partial}{\partial r} + \frac{1}{r^2}\frac{\partial^2}{\partial\phi^2} + k^2n^2\right\}\bar{E} + \left(1 + \frac{r}{a}\cos\phi\right)^{-2}\left\{\frac{1}{4a^2} - \bar{\beta}^2\right\}\bar{E} = 0 \tag{8.4}$$

where $\bar{E}$ and $\bar{\beta}$ are the scalar field and propagation constants of the bent fiber.

To solve eqn. (8.4) we note that $\rho/a \ll 1$, and Taylor expand the second term and substitute in the series

$$\bar{E} = \sum_{n=0}^{\infty} \left(\frac{\rho}{a}\right)^n \bar{E}_n \tag{8.5a}$$

$$\bar{\beta}^2 = \sum_{n=0}^{\infty} \left(\frac{\rho}{a}\right)^n \bar{\beta}_n^2 \tag{8.5b}$$

The result of this substitution is a set of simultaneous differential equations for $\bar{E}_n$, the first three terms of which are given by eqn. (7.10).

It was noted in Section 7-4 that each term in the differential equations is proportional to some power of C. If only the largest terms in C are kept, then we show in the Appendix that the field and propagation constant are given by

$$\bar{E} = \sum_{n=0}^{\infty} \frac{1}{n!} \left[\varepsilon(r/\rho)\cos\phi\right]^n \bar{E}_0 = e^{\varepsilon(r/\rho)\cos\phi}\, \bar{E}_0 \tag{8.6a}$$

$$\bar{\beta}^2 = \bar{\beta}_0^2 + (\rho/a)^2\, \bar{\beta}_2^2 = \bar{\beta}_0^2 + \varepsilon^2/\rho^2 \tag{8.6b}$$

where $\varepsilon = (\rho/a)\, C$. Eqns. (8.6a) and (8.6b) do not depend on the mangitude of ε : They are solved assuming only that $(\rho/a) \ll 1$. Eqn. (8.6a) is the solution to the differential equation

$$\left\{\frac{\partial^2}{\partial r^2} + \frac{1}{r}\frac{\partial}{\partial r} + \frac{1}{r^2}\frac{\partial^2}{\partial\phi^2} + k^2n^2 - \bar{\beta}_0^2 + 2\bar{\beta}_0^2\left(\frac{r}{a}\right)\cos\phi - \left(\frac{\rho}{a}\right)^2 \bar{\beta}_2^2\right\}\bar{E} = 0 \tag{8.7}$$

which is equivalent to eqn. (8.4) after substitution of eqn. (8.6b) and neglecting one term which is smaller in magnitude than other terms by a factor (ρ/a) . We emphasize that we are using this Gaussian scheme to investigate perturbation procedures and to obtain useful results, but we are not generating an exact solution to the original non-approximate problem.

The shift in the intensity of the electric field is found from eqn. (8.6a), and is identical to eqn. (8.3). Thus eqn. (8.3) is valid for any ε . From eqn. (8.6a) the 3-dB full-width of the bent field is

$$w/\rho = R_0\, (\ell n 2)^{1/2} \tag{8.8}$$

This is the width of the straight (unperturbed) fiber. Thus, according to eqn. (8.6a), there is no change to the field width when the fiber is bent.

(c) Numerical Results

We use the the spot-size for the fundamental mode of a step-profile fiber defined by eqn. (2.45). Figure 8.2 shows the field shift and 3-db full width, given by eqns. (8.3) and (8.8), plotted against bend radius. The experimental results of [3] are provided for comparison. The effect of stress on the refractive index has been included in the standard way by using an effective bend radius [4].

Note that for this fiber $\varepsilon \sim 1$ at $(a/\rho) \sim 10^3$, thus the first-order perturbation theory presented in [3] is not valid in this region. On the other hand, our simple formula for field shift, eqn. (8.3), which is valid for large ε , is in excellent agreement with the experimental results. Eqn. (8.6a) predicts no change in field width with respect to bend radius (see eqn. (8.8)), which also agrees with the experimental results except for very tight bends. In that case the field has shifted markedly onto the core-cladding interface, a region where properties of the field are not rigoursly dealt with by the Gaussian approximation.

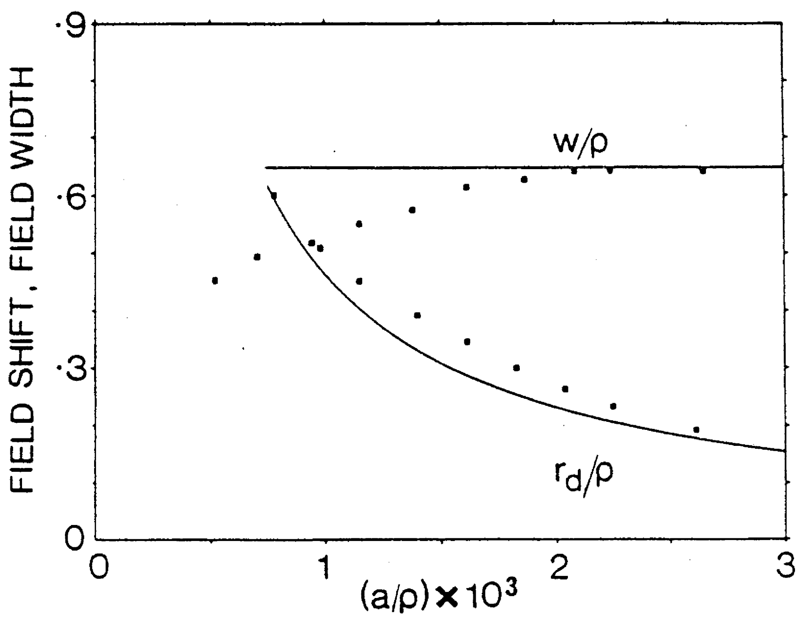

Fig. 8.2 The field shift and 3-dB full-width of the fundamental mode plotted against normalized bend radius a/ρ . The experimental points are from reference [3]. The fiber parameters are: $\lambda = 0.633\ \mu m$, $\rho = 2.4\ \mu m$, and $\Delta = 0.002$ so that $V = 2.26$.

4. Birefringence

We now return to the problem of the geometrical birefringence induced by bends, which is formalised in Section 7-3(c). We assume that ε is small, and substitute the first-order field $\bar{E}_y$ of eqn.(8.2) into eqn. (7.8). The Gaussian approximation to the geometrical birefringence is then given by

$$B_g = \frac{1}{4} \left(\frac{\rho}{a}\right)^2 kn_{co}\, g(V) \tag{8.9a}$$

$$g(V) = V^2 \left(2R_0{}^2 - 1\right) e^{-1/R_0{}^2} \tag{8.9b}$$

In figure 8.3 we compare the Gaussian solution with the step-index fiber solution for the geometrical birefringence. We plot the function g(V), given by eqns. (8.9b) and (7.9b), against normalized frequency V. We emphasize that these are the solutions obtained from first-order corrections to the field.

The approximation predicts the correct behaviour of the function g(V). The difference between the two solutions is due to the fact that birefringence is sensitive to boundary conditions at the core - cladding interface, and this is the region where the Gaussian approximation is not rigorous.

Figure 8.4 shows the variation of the geometrical birefringence, eqn. (8.9), against bend radius for a fiber with parameters $\rho = 2.5$ µm , $\Delta = 0.009$ and operating at $\lambda = 1.32$ µm so that $V = 2.3$. We have included the well-known birefringence due to stress (see Section 7-3(c)), but note that it has been scaled by a factor of 10^{-3} to fit on this figure. The birefringence due to stress depends only on the fiber outer-radius, b (=62.5 µm in figure 8.4) and the wavelength of light used. We note that the stress contribution to the birefringence dominates.

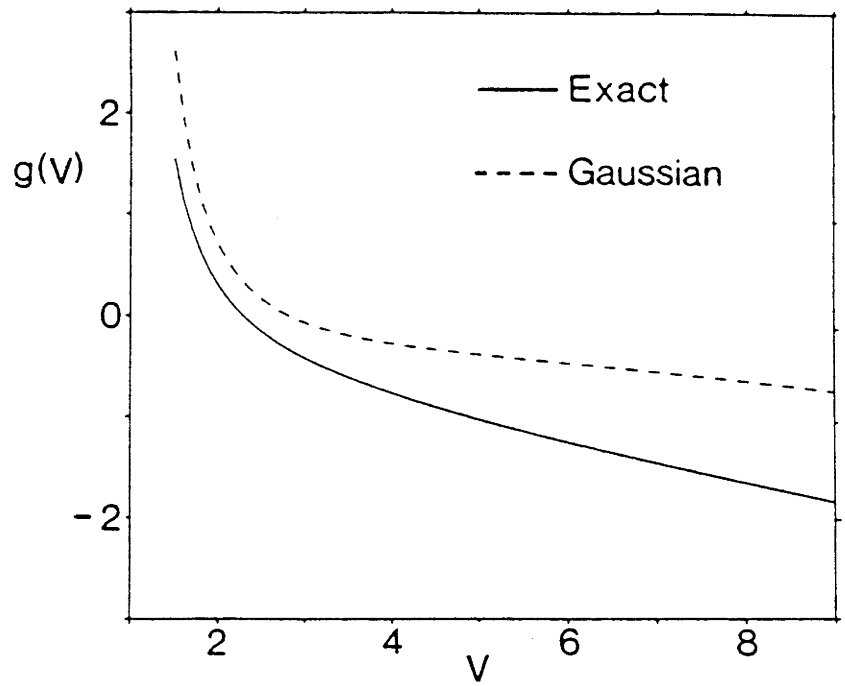

Fig. 8.3 The birefringence function g(V) plotted against normalized frequency V. The unbroken curve is the exact step-index solution eqn. (7.9b) and the dashed curve is the Gaussian approximation (eqn. (8.9b)).

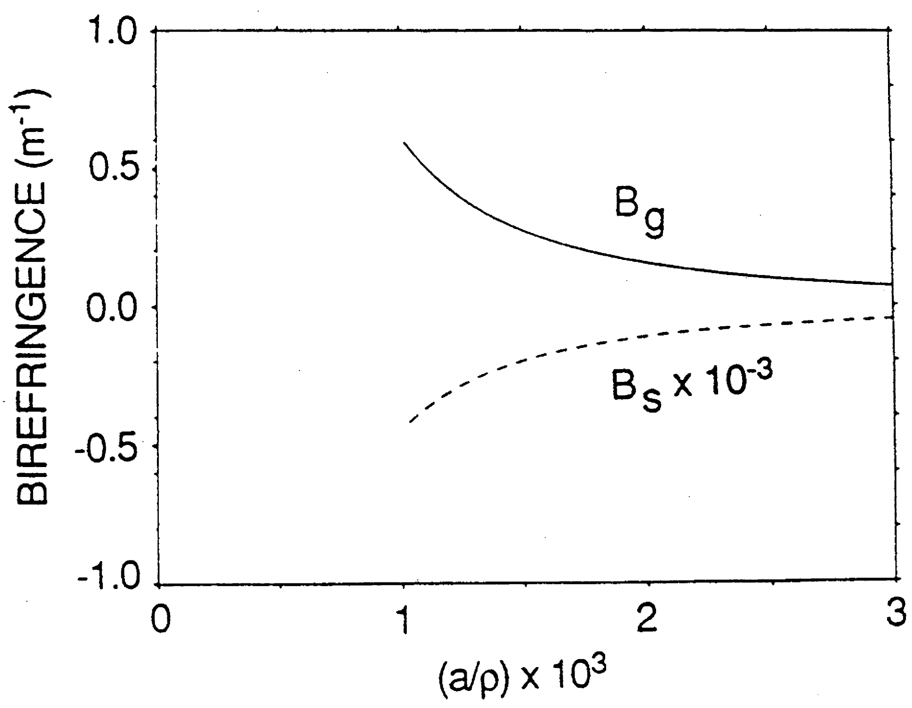

Fig. 8.4 The geometrical bending birefringence (eqn. (8.10)) plotted against normalized bend radius (a/ρ) . The fiber parameters are ρ = 2.5 μm, Δ = 0.009 and λ = 1.32 μm so that V = 2.30. The dashed line curve is the bending birefringence due to stress (see Section 7-3(c)), scaled by a factor of 10^{-3}. The outer radius of the fiber is b = 62.5 μm .

5. Few-Mode Fibers

The Gaussian approximation is useful when describing the modal fields of a straight fiber, so the simple analytic forms of the approximation should offer some insight into the effect on modal characteristics due to bending. Here we present simple analytic forms for the perturbed field $\bar{E}_1$, which allow an evaluation of the shift in the intensity peaks, and propagation constant correction $\bar{\beta}_2^2$ for the $\ell = 1$ odd and even modes.

The fields in the straight fiber are specified by the Gaussian approximation of Table 2.2, with spot-size notation defined by eqn. (2.52). The perturbation equations (7.10) are easily solved for $\bar{E}_1$ (see Appendix), and the integrals in eqn.(7.12) are then trivial. The results are summarized in Table 8.1.

Figure 8.5 is a comparison of the field corrections $\bar{E}_1$ for the exact solutions (Table 7.2) and Gaussian solutions (Table 8.1) of the (01), (11 odd) and (11 even) modes. The Gaussian fields have been normalized to have the same modal power as the exact fields in the straight fiber. We see that the approximations are in excellent agreement, with the largest discrepancies occurring at the boundary R = 1.

From Table 8.1 we see that the Gaussian approximation correction to the propagation constant is the same for the odd and even $\ell = 1$ modes, and thus no splitting is predicted. This is because the subtle effects of mode splitting are strongly dependent on boudary effects, such as profile shape (see Section 7-6(b) and figure 7.8), and as mentioned before this is the region where the approximation is not rigorous. The difference between the exact and approximate value of $\bar{\beta}_2^2$ for the $\ell = 0$ mode is 17% and 13% at V=2.2 and V=5, respectively. The optimum V is V=3.3, where the percentage difference between exact and approximate values is 5%.

Table 8.1: Gaussian Approximation to Fields of the Bent Fiber

MODE	(01)	(11) odd	(11) even
$\bar{E}_0$	$e^{-R^2/2M_{01}^2}$	$\frac{R}{M_{11}}\, e^{-R^2/2M_{11}^2} \sin\phi$	$\frac{R}{M_{11}}\, e^{-R^2/2M_{11}^2} \cos\phi$
$\bar{E}_1$	$C_{01} R\cos\phi$ $\times\ e^{-R^2/2M_{01}^2}$	$C_{11} R\sin\phi\cos\phi$ $\times\ \frac{R}{M_{11}}\, e^{-R^2/2M_{11}^2}$	$C_{11} R\left(\cos^2\phi - \frac{M_{11}^2}{R^2}\right)$ $\times\ \frac{R}{M_{11}}\, e^{-R^2/2M_{11}^2}$
$\bar{\beta}_2^2$	C_{01}^2/ρ^2	C_{11}^2/ρ^2	C_{11}^2/ρ^2
$C_{\ell m} = \rho^2\, \bar{\beta}_0^2\, M_{\ell m}^2 \approx \frac{V^2}{2\Delta}\, M_{\ell m}^2$			

In Table 8.1 the spot-sizes $M_{\ell m}$ are defined by eqn. (2.52), and we have introduced a new parameter $C_{\ell m}$, which we note is different for different spot-sizes.

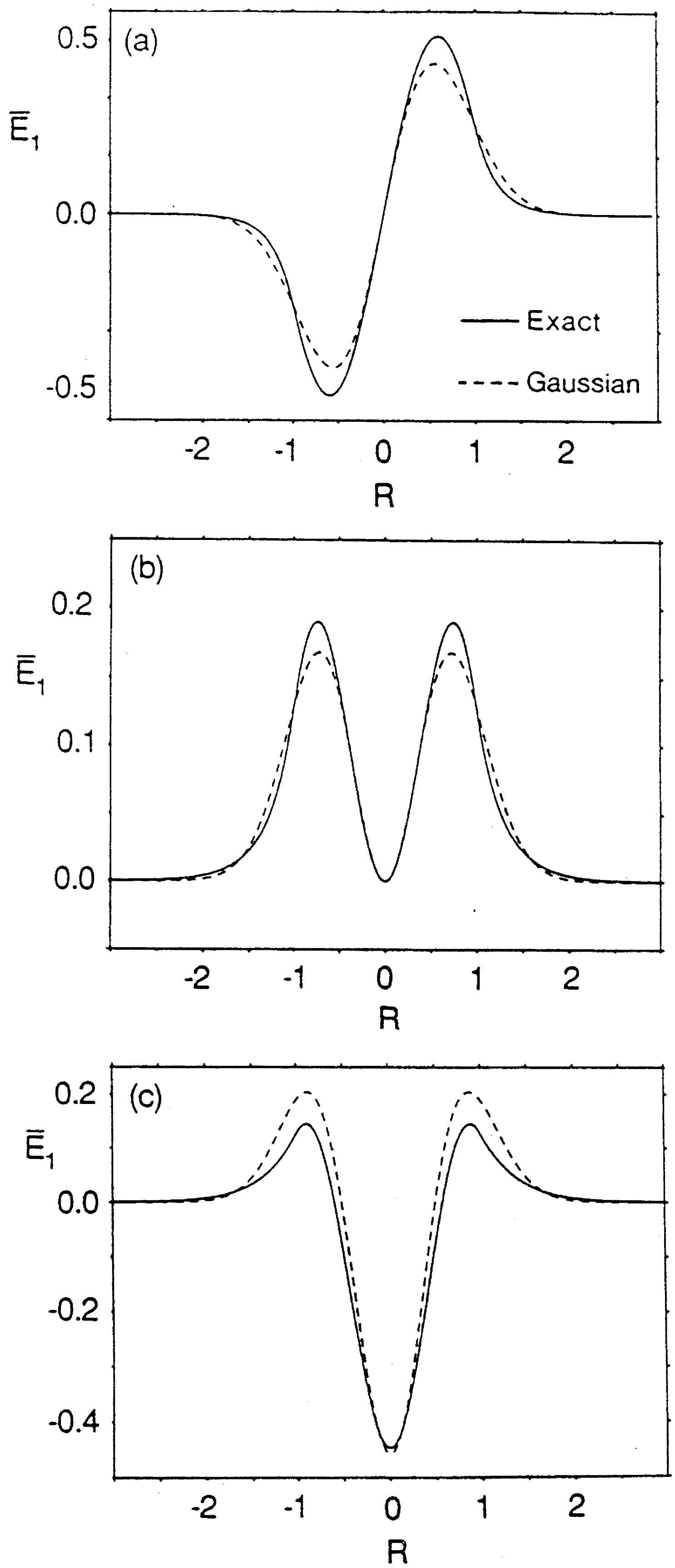

Fig. 8.5 Comparison of the Gaussian approximation and exact step-index solutions of the field correction $\bar{E}_1$ for (a) the (01) (fundamental) mode, (b) the (11 odd) mode, and (c) the (11 even) mode. The Gaussian fields have been normalized to have the same modal power as the exact fields in the straight fiber.

6. Overlap Integrals for Bent Fibers

In Section 4-5 we showed that the gain of the Stokes or anti-Stokes waves was proportional to the overlap integral of the particular four-photon process, and gave examples by using Gaussian fields for various mode combinations. We now return to the divided-pump four-photon mixing process, which have overlap integrals defined by eqn. (4.26)

$$\langle 1|2\rangle = \frac{\int \psi_1^2 \ \psi_2^2 \ dA}{\int \psi_1^2 \ dA \int \psi_2^2 \ dA} \tag{8.10}$$

Where ψ now represents the bent field $\bar{E} = \bar{E}_0 + (\rho/a)\bar{E}_1$, and subscripts on the ψ's are for mode 1 and mode 2.

(a) Single-Mode Processes

For four-photon mixing on bent single-mode fibers all three waves propagate in the (01) mode. Substituting the bent fields of Table 8.1 into eqn. (8.10) yields

$$\langle 01|01\rangle = \frac{1}{2\pi} \frac{1}{M_{01}^2} \left(1 + \frac{1}{2} (\rho/a)^2 \ C_{01}^2 \ M_{01}^2\right) \quad . \tag{8.11}$$

where M_{01} and C_{01} are defined in Table 8.1. Thus the overlap integral can be separated into the straight fiber overlap integral, I_0 , plus a perturbation correction due to the bend:

$$\langle 01|01\rangle = I = I_0 + (\rho/a)^2 \ I_2 \tag{8.12}$$

where I_0 is given by eqn. (4.27).

There is a proportional increase in gain due to the bend, which for the single mode process is equal to

$$\delta g = (\rho/a)^2 \, I_2/I_0 = \frac{1}{2} (\rho/a)^2 \, c_{01}^2 \, M_{01}^2 \qquad (8.13)$$

This increase in gain is very small, $\delta g/g \ll 1$.

(b) Few-Mode Processes

Expressions for <01|11o> and <01|11e> processes in a bent fiber can be found by substituting the Gaussian fields of Table 8.1 into eqn. (8.10). The expressions are complicated, as they involve both spot-sizes M_{01} and M_{11} , but the essential result is that the overlap integral can be split into two parts:

$$\begin{aligned} \langle 01|11o\rangle &= I_0 + (\rho/a)^2 \, I_{2o} \\ \langle 01|11e\rangle &= I_0 + (\rho/a)^2 \, I_{2e} \end{aligned} \qquad (8.14)$$

where $I_0 = \langle 01|11\rangle$ is given by eqn. (4.28), and we find that $I_2 \simeq I_{2o} > I_{2e}$.

In conclusion, the effect of bending is to increase the overlap integral of the relevant process, and hence the gain. In the process where the degeneracy of the LP_{11} modes is split there is a larger proportional increase in the gain of (11 odd) mode than the (11 even) mode.

7. Discussion

It is apparent that the usual perturbation expansion for the field in a bent fiber results in coefficients in powers of $\varepsilon = (\rho/a)\,\frac{V^2}{2\Delta}\,R_0^2$, which may become large, invalidating the perturbation theory, for quite moderate bending radii. Using a Gaussian function to approximate the field in a straight fiber we have derived analytic expressions for the field and propagation constant in a bent fiber that are independent of the size of ε . Within this approximate scheme, we have explained experimental field shifts due to the bend in regions where the perturbation parameter $\varepsilon \sim 1$.

The Gaussian approximation appears to be sufficient for describing the field shift and 3-dB full width of the field in the bent fiber, as validated by figure 8.2. However, the Gaussian approximation appears inadequate to successfully describe the geometrical birefringence and the $\ell = 1$ mode splitting due to bends. These effects are sensitive to boundary conditions at the core - cladding interface, such as grading, and it is in this region that the field properties are not rigorously dealt with by the Gaussian approximation.

7. Appendix

(i) Fundamental mode solution

The differential equation to be solved is given by eqn. (7.4a), with $\bar{\beta}_1^2$ set to zero and the y-subscript dropped:

$$\bar{E}_1'' + \frac{1}{R}\bar{E}_1' + \rho^2\left(k^2n^2 - \bar{\beta}_0^2\right)\bar{E}_1 = \bar{c}\ R\cos\phi\ \bar{E}_0 \qquad (8A.1)$$

where $\bar{c} = -2\rho^2\bar{\beta}_0^2 = -V^2/2\Delta$, and primes indicates differentiation with respect to R. The Gaussian approximation to the fundamental mode is given by eqn.(8.1):

$$\bar{E}_0 = e^{-R^2/2R_0^2} \qquad (8A.2)$$

The basis for our scheme to approximately solve the bending field equations is the assumption that $\bar{E}_0$ approximately satisfies the differential equation

$$\bar{E}_0'' + \frac{1}{R}\bar{E}_0' + \rho^2\left(k^2n^2 - \bar{\beta}_0^2\right)\bar{E}_0 = 0 \qquad (8A.3)$$

We assume a solution of the form

$$\bar{E}_1 = f(R)\ \bar{E}_0\cos\phi \qquad (8A.4)$$

then substitution of eqn. (8A.4) and (8A.2) into (8A.1) yields the auxillary differential equation for the radial function f:

$$f'' + \frac{1}{R}f'\left(1 - 2R\ \bar{E}_0'/\bar{E}_0\right) - \frac{1}{R^2}f = \bar{c}\ R \qquad (8A.5)$$

A solution to eqn. (8A.5) is

$$f = -\frac{1}{2}\bar{c}\,R_0^2\,R \;\equiv\; CR \qquad (8A.6)$$

$\bar{E}_1$ is given by eqn. (8A.4) and (8A.6), and is given in the text in Table 8.1 or by eqn. (8.2a). The correction to the propagation constant is given by eqn. (7.12):

$$\bar{\beta}_2^2 = \frac{2C}{\rho^2 R_0^2}\int R\cos\phi\;\bar{E}_1\bar{E}_0\,dA \Big/ \int \bar{E}_0^2\,dA \;=\; C^2/\rho^2 \qquad (8A.7)$$

In a similar manner one can progressively solve all the terms in the infinite series expansion of $\bar{E}$ and $\bar{\beta}^2$ (eqn. (8.5)). It becomes apparent that all terms $\bar{\beta}_n^2$ $(n \geq 1)$ are equal to zero except for the $n = 2$ term, and eqn. (8.6) results. Using eqn. (8A.7) the simultaneous differential equations that describe the field on the bent fiber can be written as (compare to eqn. (7.10)):

$$D\,\bar{E}_0 = 0$$

$$D\,\bar{E}_1 = -\frac{2}{R_0^2}\,C\,R\cos\phi\;\bar{E}_0 \qquad (8A.8)$$

$$D\,\bar{E}_n = -\frac{2}{R_0^2}\,C\,R\cos\phi\;\bar{E}_{n-1} + C^2\,\bar{E}_{n-2} \quad , \quad n \geq 2$$

When the solutions to these equations are summed eqn. (8.6a) results.

(ii) $\ell = 1$ mode solution

We consider the $\ell = 1$ even mode;

$$\bar{E}_0 = \frac{R}{M_{11}}\,e^{-R^2/2M_{11}^2}\cos\phi \qquad (8A.9)$$

The method of solution that follows can be applied to the $\ell = 1$ odd mode as well. Analogously to eqn. (8A.3), we assume $\bar{E}_0$ approximately satisfies the differential equation

$$\bar{E}_0'' + \frac{1}{R}\bar{E}_0' - \frac{1}{R^2}\bar{E}_0 + \rho^2\left(k^2n^2 - \bar{\beta}_0^2\right)\bar{E}_0 = 0 \tag{8A.10}$$

We assume a solution of the form

$$\bar{E}_1 = f\bar{E}_0 + g\bar{E}_0 \cos 2\phi \tag{8A.11}$$

where f and g are functions of the radial coordinate only. Substituting eqn. (8A.11) into (8A.10) yields the auxillary differential equations for the functions f and g:

$$f'' + \frac{1}{2} f'\left(3 - \frac{2R^2}{M_{11}^2}\right) + \frac{1}{R^2} f = \bar{c}R \tag{8A.12a}$$

$$g'' + \frac{1}{R} g'\left(3 - \frac{2R^2}{M_{11}^2}\right) - \frac{3}{R^2} g = \bar{c}R \tag{8A.12b}$$

Solutions to eqns. (8A.12) are

$$f = AR + B/R \quad , \qquad g = DR \tag{8A.13}$$

where

$$A = -\frac{\bar{c}}{2} M_{11}^2 \quad , \quad B = \frac{\bar{c}}{2} M_{11}^4 \quad , \quad D = A \tag{8A.14}$$

The $\bar{E}_1$ field of the $\ell = 1$ even mode is then given by eqn. (8A.11) which is the expression in Table 8.1 where

$$C_{\ell m} = -\frac{1}{2}\bar{c}\, M_{\ell m}^2$$

References

[1] W.A. Gambling, H. Matsumura, and C.M. Ragdale, "Field deformations in a curved single-mode fibre"
Electron. Letters, 14, pp. 130-132 (1978)

[2] See ref. [2-1]

[3] Z.W. Bao, M. Miyagi and S. Kawakami, "Measurements of field deformation caused by bends in single mode optical fiber"
Applied Optics, 22, pp. 3678-3680 (1983)

[4] See ref. [7-21] and ref. [7-22].

CHAPTER 9

CONCLUSION

The development of long lengths of low-loss optical fibers have opened a new era in the study of non-linear processes. These non-linear optical effects maybe detrimental to the fiber system, but on the other hand, these same effects are potentially useful in various fiber-optical devices, and also for investigations of the fiber itself.

In this thesis we have seen how the stimulated four-photon mixing process maybe used to investigate the subtle effects that occur when fibers are perturbed, and also when more advanced design fibers are used. The knowledge of such perturbation effects could be important in the design of future high-sensitivity fiber systems.

In conclusion, the potential of non-linear processes in optical fibers is only just becoming apparent, and as in other areas of fiber research there is the promise of close interaction between theory and experiment. Continuing investigations in this field will lead to the development of optical systems of great finesse and sensitivity, and enable the further study of interesting optical phenomena.